Thiopolymers

Applications in water remediation and development

Samuel Petcher

Supervisor: Dr. Thomas Hasell

Secondary Supervisor: Dr. Thomas McDonald

A thesis presented for the degree of

Doctor of Philosophy

Department of Chemistry

University of Liverpool

United Kingdom

May 2021

Acknowledgements

When I was a child, I always wanted to be a scientist. That aspiration most likely developed from watching Dexter's Laboratory. Anyway, it seemed that the older I got, the more I disliked science, I found it boring, dry, and honestly quite easy. After this I fell into the trap of thinking science *was* easy and promptly failed two years of A-Levels and had to repeat them. After this I started my undergraduate degree and I learned that science was boring, dry, and hard.

After nearly failing out of my undergraduate degree, I managed to scrape the requirements to finish my masters. At this point in time I met Tom Hasell. I would like to give Tom the credit for being probably the most positive academic influence I have ever experienced. Tom, thank you for all your help and support over the years. I genuinely mean that.

Naturally, there are many other people that I would like to thank. So I'll start by thanking my parents and grandparents for supporting me during all the rough moments of my late teenage years, I wouldn't be here without you. I'd like to thank Monika Lisauskaitė, my lovely partner, who has changed me for the better.

Continuing this list, I'd like to thank Robin Longfield, who gave me the conviction I needed to make it through 4 years of A-Levels. I'd also like to thank Paul Barrie and Mark Rawson-Gill for being a early role models. I'd like to thank all members of the Hasell group for their help and guidance and providing a positive environment to work in.

I'd like to extend my thanks to the whole of the Chemistry Department at the University of Liverpool. We might not all get along, but it's a great place to do your PhD.

Every person you meet makes a small footprint on your personality, attitudes, and habits. So how could I have written this document without these footprints? I probably couldn't. It's just a shame that Tom couldn't footprint unit space errors out of my personality.

I've probably forgotten a lot of people. But please know I genuinely appreciated your efforts in helping my get to where I am now. *Thank you.*

Publications

1. Mesoporous knitted inverse vulcanised polymers, **Samuel Petcher**, Bowen Zhang, Thomas Hasell, Chemical Communications, 2021, *10.1039/D1CC01152A*

2. Inverse Vulcanized Polymers with Shape Memory, Enhanced Mechanical, Properties, and Vitrimer Behavior, Peiyao Yan, Wei Zhao, Bowen Zhang, Liang Jiang, **Samuel Petcher**, Jessica A. Smith, Douglas J. Parker, Prof. Andrew I. Cooper, Prof. Jingxin Lei, Dr. Tom Hasell, Angewandte Chemie, 2020, *10.1002/ange.202004311*

3. Inverse vulcanization below the melting point of sulfur, Bowen Zhang, Hui Gao, Peiyao Yang, **Samuel Petcher**, Thomas Hasell, Materials Chemistry Frontiers, 2020, *10.1039/C9QM00606K*

4. Catalytic inverse vulcanization, Xiaofeng Wu, Jessica A. Smith, **Samuel Petcher**, Bowen Zhang, Douglas J. Parker, John M. Griffin & Tom Hasell, Nature Communications, 2019, *10.1038/s41467-019-08430-8*

5. Crosslinker Copolymerization for Property Control in Inverse Vulcanization, Jessica A. Smith, Sarah J. Green, **Samuel Petcher**, Douglas J. Parker, Bowen Zhang, Max J. H. Worthington, Dr. Xiaofeng Wu, Dr. Catherine A. Kelly, Thomas Baker, Dr. Christopher T. Gibson, Dr. Jonathan A. Campbell, Prof. David A. Lewis, Dr. Mike J. Jenkins, Dr. Helen Willcock, Dr. Justin M. Chalker, Dr. Tom Hasell, Chemistry - A European Journal, 2019, *10.1002/chem.201901619*

6. A ternary system for delayed curing inverse vulcanisation, Bowen Zhang, **Samuel Petcher**, Thomas Hasell, Chemical Communications, 2019, *10.1039/C9CC04380B*

7. Macroporous sulfur polymers from a sodium chloride porogen—a low cost, versatile remediation material, **Samuel Petcher**, Douglas Parker, Thomas Hasell, Environmental Science: Water Research and Technology, 2019, *10.1039/C9EW00477G*

8. Low cost and renewable sulfur-polymers by inverse vulcanisation, and their potential for mercury capture, D. J. Parker, H. A. Jones, **Samuel Petcher**, L. Cervini, J. M. Griffin, R. Akhtar, T. Hasell, Journal of Materials Chemistry A, 2017, *10.1039/c6ta09862b*

Abstract

Elemental sulfur is produced as part of the hydrodesulfurisation process in the refining of crude oil. All crude oil contains a small fraction of sulfur, and this sulfur is usually found in the form of heteroatomic alkanes. Unfortunately, the supply of elemental sulfur far exceeds the anthropological demands.

As a result of this there is an abundance of elemental sulfur. This elemental sulfur is usually stored as large monolithic piles. The effects and hazards of storing mega-tonne quantities of elemental sulfur have not yet been studied. What is clear, however, is that new uses for this chemical element should be discovered.

Currently, it is possible to generate sulfuric acid and fertilisers from elemental sulfur. However, the needs for these chemical derivatives are saturated and no more is needed. In 2013, Jeffrey Pyun and coworkers discovered that it is possible to generate stable polymers from elemental sulfur and small molecule dienes. This polymerisation process was termed 'inverse vulcanisation'.

As a result of this technological leap, there has been a slew of discoveries in the field of inverse vulcanisation. Applications of these polymers include, but are not limited to: ion-exchange, battery materials, fertiliser composites, water purification materials, and antibacterial materials.

One of the key applications of sulfur polymers that are to be discussed in the content of this thesis are ion-exchange materials. Sulfur polymers have demonstrable applications in the removal of ionic mercury from solution. Mercury is a potent and environmentally present neurotoxin.

The research presented in this thesis concerns the generation of porous sulfur polymers and their application in the removal of mercury from aqueous solution. This body of research makes up chapters 2 and 3 of the thesis, whilst chapter 4 explores the development and application of catalysts for inverse vulcanisation.

It was found that it is possible to generate macroporous and mesoporous polymers from elemental sulfur and both materials have applications in mercury removal.

Furthermore, several catalysts were developed for the inverse vulcanisation process that considerably reduced the time of reaction.

Contents

Chapter 1

Introduction

1.1 Prelude

These following pages exist in the hope that they can provide some background for the reader before they delve into the more content dense and technically written pages that follow. The intention is to "set the scene" and present a brief overview of the topics, problems, and questions that will be tackled in this thesis.

This thesis in a broad sense attempts to develop and understand improvements in the generation of polymers from elemental sulfur. The first chapter is a summary of current work in the field of sulfur polymers. The middle chapters (2,3) focus on the incorporation of porosity into sulfur polymers. The 2nd chapter explores the use of a sacrificial sodium chloride porogen to produce porosity. The 3rd chapter explores the applicability of the 'hypercrosslinking' reaction to linear sulfur polymers.

The final chapter (4) explores the application of novel catalysts in the inverse vulcanisation process.

Elemental Sulfur, Production and Properties

Sulfur is an element with an atomic number of 16, and occurs in nature as a yellow crystal.[1,2] One of the main uses of sulfur is as an industrial precursor for the production of sulfuric acid.[3] Another application is found in industry as carbon disulfide: an important industrial solvent and chemical precursor.[4] Further but diminishing (<10 %) uses of sulfur include but are not limited to: agrochemicals, pesticides, antimicrobial agents, dye feedstocks, and pharmaceuticals.[5,6] Interestingly, the majority of these applications of sulfur do not require large molar equivalents of sulfur in itself.

The basis of the work in this thesis is rooted in one of the newer (>1830 A.D) applications of sulfur: vulcanisation.[7] There are many accounts detailing the discovery of vulcanisation, however, the chemistry that was discovered is more important; sulfur may react with natural rubber.[2,6] The products of this reaction are a mechanically improved, insoluble polymeric network. These properties are imbued upon the polymer by the formation of sulfur cross-links amongst the individual polymer chains (Scheme 1.1). Vulcanisation was a revolutionary process and resulted in the production of materials used almost ubiquitously. Despite the revolutionary aspect of the process, little information regarding the mechanism is available other than speculation.[8] Industrially speaking, one of the largest consumers of this produced vulcanised rubber is the car tyre industry.[9]

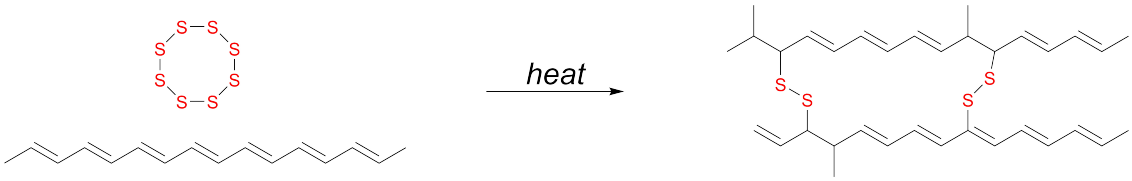

Scheme 1.1: Reaction scheme illustrating the concept of cross-linking long chain polyenes with elemental sulfur. The process is now more commonly known as the vulcanisation process and is used to produce materials used ubiquitously throughout the world

Whilst there are an abundance of uses for elemental sulfur, there is a greater supply than demand. Historically, sulfur was mined in its elemental form found in deposits near areas of volcanic activity.[10] In these times' sulfur was considered a commodity product and was actively sought out. One of the key uses of elemental sulfur in medieval times was as a part of gunpowder.[11] Since then, the position of sulfur has changed; the advent of the oil-refining industry and development of the petrochemical industry has improved sulfur supply.

Crude oil is a naturally occurring mixture of hydrocarbons that results when large amounts of dead organisms are subjected to heat and pressure for an extended time.[12] It is one of the most important commodities in the modern world, and while not free from controversy it is agreed to be completely necessary for modern societal function. Large fractions of naturally occurring crude oil are contaminated with sulfur; anything above 0.5% sulfur is categorised as 'sour'.[13] This sour oil is always purified before it is further used in industry in a process that is known as hydrodesulfurisation.[14,15] Without purification the 'sour' oil can poison catalysts that are used in reformation of petroleum distillate. Sour crude oil also releases SO_2 upon complete combustion; this gas is responsible for acid rain.[16–19]

Traditionally, elemental sulfur was produced as a result of the Frasch process.[20] In this process, elemental sulfur deposits are melted using super-heated water. The deposit is then collected in its elemental state when cool. However, most implementations of the Frasch process have been superseded by the hydrodesulfurization process.

One of the results of the large scale introduction of the hydrodesulfurisation process was the shift in value of sulfur, from an important commodity to a waste product. Prior to hydrodesulfurisation sulfur was a valuable chemical, worth fighting over.[21] Hydrodesulfurisation produces more sulfur than is used, supply now outstrips demand. A result of this is that large open stores of elemental sulfur have been constructed.(Figure 1.1) The long-term effects of storage of vast amounts of sulfur have not yet been studied. There is also potential for fire, which would be catastrophic considering the complete combustion products of elemental sulfur. (Equation 1.1) It becomes apparent that finding uses for this excess sulfur is an important, and relevant task.

$$\frac{1}{8}S_{8(s)} + O_{2(g)} \rightarrow SO_{2(g)} \tag{1.1}$$

Given that in this section some of the uses, sources and properties of elemental sulfur have been explored, it is important to note that a slight deviation will be taken in the following subsection before we arrive at the final key concept that underpins the research area that will be explored in this thesis: polymers. It is possible to form polymers from elemental sulfur alone, but they are unstable. Furthermore, there is no use for them.

Figure 1.1: A large monolithic pile of elemental sulfur that is stored out on the Alberta oil sands, CA

1.2 Polymers

1.2.1 Polymerisation mechanisms

Polymers are an important subclass of materials alongside metals, ceramics, and composites. Most people are familiar with the physical characteristics of polymers, whether they consciously know it or not. On the molecular level, polymers are comprised of repeat subunits and in this sense they are macromolecules. As demonstrated in Figure 1.2a, the increase of molecular weight(M_w) of ethene when it is polymerised has an effect on the physical properties.[22]

The formation of polymers may proceed through a variety of mechanisms: step, radical, ionic, and ring-opening are a few of the major polymerisation mechanisms.[22] The two mechanisms that are of particular relevance to this body of work are radical and ionic.
In the case of sulfur polymers, much debate is placed onto the specific mechanism, but this will be discussed in detail later. Conventional radical polymerisation fits into a scheme of 4 steps:

1. initiation
2. propagation
3. termination
4. chain transfer

In the first step of polymerisation a molecule containing a bond that may undergo homolytic fission dissociates into two radicals species. This is illustrated in (Figure 1.2b), in which benzoyl peroxide homolytically splits into two benzoyl radicals. There are many types of radical initiator, and they often work by the homolytic fission of the C-C, N-N, or O-O bond. These radicals may then react with an initial monomer, to form an initiator-monomer active species that may participate in propagation steps. The propagation steps are simply the radical addition of an active chain to another monomer unit. This step may continue indefinitely unless termination or chain transfer occur. In termination, two active chains may combine to form an inactive chain. For a more in depth discussion, the reader may be directed to the 'Handbook of radical polymerization', Matyjaszewski *et al.*[23]

Chain transfer was intentionally left out of the diagram because it is more variable in nature. Chain transfer involves the radical attack of an active species on something that is not another polymer active site (termination). This could be any manner of things: the solvent, gaseous contaminants, reactive functional groups on the monomer, or even purposefully designed chain-transfer agents (CTAs). These types of molecules have become increasingly used in polymer science over the past half a century, championed by techniques such as reversible addition-fragmentation polymerisation (RAFT).[24,25] The current state-of-the-art techniques can produce polymers with variety in functionality, architecture, and physical properties; by careful selection of reaction conditions even solid-state morphology can be influenced.[26]

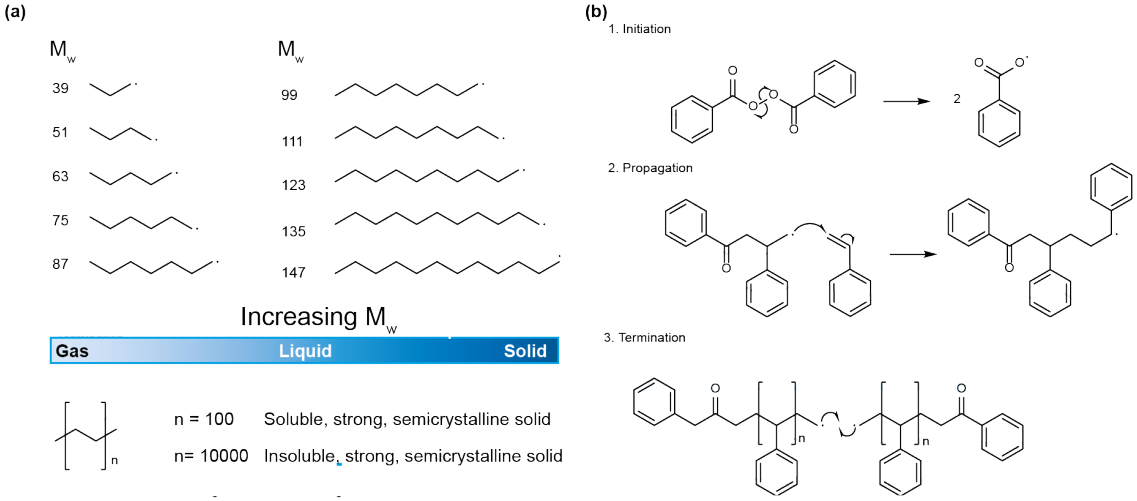

Figure 1.2: (a) A demonstration of three of the principle steps involved in a radical polymerisation reaction mechanism: initiation, propagation, and termination steps involving benzoyl peroxide and styrene (b) Schematic illustrating the effect of increasing M_w on the properties of ethene, demonstrating the increase in solidity as M_w increases

The Glass Transition (T_g)

The T_g of a polymer is defined by the IUPAC Goldbook as follows:

> *"A second-order transition in which a supercooled melt yields, on cooling, a glassy structure. Below the glass-transition temperature the physical properties vary in a manner similar to those of the crystalline phase."*
>
> **-IUPAC Goldbook, Definitions of terms relating to phase transitions of the solid state (IUPAC Recommendations 1994)**

To the layman, however, this definition can be somewhat complex. There are essentially two parts to this definition, the first being the description of the term "phase transition". This is analogous to the solid-liquid transition, more formally termed the melting transition (T_m). In this transition we go from a solid like ice, to a liquid like water. The same thing is observed for the T_g, except in polymers the transition is from a rubbery state to a hard, brittle state. The second part of the definition is merely a description of the two phases in question. An example of a first order transition would be a melting transition, and a second order would be a T_g. Qualitatively speaking, the second order transition resembles the mathematical derivative of the first order transition.

When the T_g is required to be determined for a material, a differential scanning calorimeter (DSC) is used. This machine measures the heat capacity of a material as a function of its temperature. The produced data is plotted into a thermogram. (Figure 1.3a) demonstrates the appearance of a T_g and a T_m in a thermogram.

Furthermore, in (Figure 1.3b) it is possible to see the effect of deformation on a material above and below its T_g. Above the T_g the material will elastically deform, and below it will not. In the case demonstrated in the schematic, the material undergoes a brittle fracture when stressed above its limit of deformation when below it's T_g.[27]

To explain the origin of the T_g at a molecular level, one must consider the vibrations, rotations, and translations of the polymer chains. Above the T_g there is a long-range motion available to the polymer chains; this has previously been referred to as 'segmental' motion.[28] A result of this motion is that the polymer chains are able to slide over one another, resulting in a 'rubbery' state. When they don't move, they behave more like a glass.

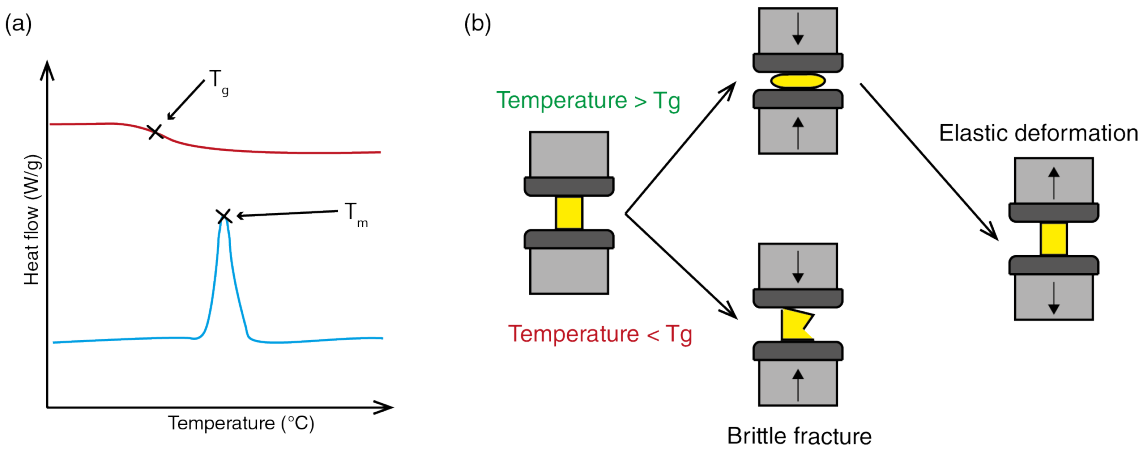

Figure 1.3: (a) A simulated DSC thermogram for two imaginary materials, one displaying a glass transition (T_g)and the other displaying a melting transition (T_m) (b) Schematic demonstrating the effect of deformation of a polymeric sample above and below its T_g. Above the T_g the polymer will elastically deform, below it will fracture

Molecular Weight, Number Average Molecular Weight and Dispersity

$M_W$is another key attribute in the properties of a polymer. M_w is a property all chemists should be familiar with, and its usage is no different when applied to polymers. As previously mentioned in (Figure 1.2) the mechanical properties of the polymers are usually a result of their high value of M_w, sometimes in combination with other electronic effects. The mechanical strength of polymers increases with increasing values of M_w, and for polymers with intended application in the solid state, an appreciable degree of mechanical strength is desirable. It is also important to consider that in any polymer sample there will be no single, M_w and that a variety of masses will be represented in the sample.

Considering this information, we may want to represent this distribution of weights of polymers in a statistical fashion. The way that this is achieved is in a two-fold fashion. The first of which is 'number average molecular weight' $\overline{M}_n$: the total M_w of polymer divided by the number of molecules present in the sample. Expressed as an equation where (N_x is the number of polymer chains, M_x is the molecular mass of the chains):

$$\overline{M}_n = \frac{\sum_{x=1}^{\infty} N_x M_x}{\sum_{x=1}^{\infty} N_x} \tag{1.2}$$

It is important to note the 'bar' above M in $\overline{M}_n$, as it is this bar that mathematically defines the variable as an average. This can lead to confusion when interpreting the meaning of

$\overline{M}_w$; the weight average molecular weight. Mathematically speaking, this is the number average molecular weight but also accounting for the number of molecules at a particular weight. Expressed as an equation where (N_x is the number of polymer chains, M_x is the molecular mass of the chains):

$$\overline{M}_w = \frac{\sum_{x=1}^{\infty} N_x M_x^2}{\sum_{x=1}^{\infty} N_x M_x} \tag{1.3}$$

While this may give some preliminary understanding as to the physical interpretation of the $\overline{M}_w$ and $\overline{M}_n$ of a sample, it is best understood in terms of a case study. Referring to (Figure 1.4) we have an imaginary sample of polyethylene. In this sample, there is a slight bias to the higher molecular weights, and as such while the $\overline{M}_n$ is quite close to the 'centre' of the peak the value for the M_w is skewed away due to the weighting of the higher $\overline{M}_w$ chains.

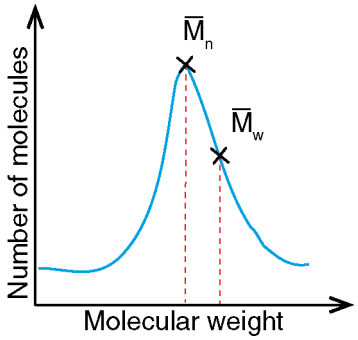

Figure 1.4: Figure illustrating the difference in the obtained value of $\overline{M}_n$, and $\overline{M}_w$ on a graph that is a plot of the different molecular weights vs their number in a given sample of polymer

Finally, there is one final related property of polymers that is relevant when discussing molar mass distributions, and that is polydispersity. Polydispersity is often referred to as dispersity and is represented by the symbol Đ. The value of polydispersity is obtained *via* the following equation:

$$Đ = \frac{\overline{M}_w}{\overline{M}_n} \tag{1.4}$$

Often, it is easy to become lost in the physical interpretation of formulae; especially when the user is not actually using them. The physical interpretation of polydispersity is just a measure of the homogeneity of the system. A $Đ$ value of 1 would indicate a highly homogeneous system wherein all polymer chains are the same length. This is characteristic of living polymerisations. Anything over 2 is usually characteristic of a step-growth mechanism. Free-radical polymerisation is between 1.5–2.0. However, as with most rules — there are exceptions.

1.3 Sulfur polymers

Vulcanisation

Vulcanisation has been previously mentioned, however, in order to fully describe the life-cycle of the material from tree to tyre it is important to consider Latex. Latex is an emulsion of polyunsaturated polymers dispersed in water that are obtained from the aptly named 'rubber tree'.[29] Vulcanisation has been practised in one form or another for hundreds of years, and many claims have been put forth for the "discovery" - although it is debatable that this is merely a tactic of marketing.[30]

In the process of vulcanisation, chemical cross-links are formed amongst the individual polymeric chains through an addition process across the double bonds (Figure 1.1). Mono, di, and polysulfide units can bridge the indivdual polymer chains.[31] Interestingly, one could consider the result of this process to be a giant molecule. A car tyre itself is a giant molecule. Vulcanisation imbudes the material with several unique key properties: the material becomes insoluble, more physically resistant, and even more chemically resistant.[32] These properties are all a result of the chemical cross-linking that has occured.

The formation of these crosslinks is irreversible, and as a result the recycling of rubber is often full of compromises.[33] Large volumes of waste tyres are often stored in landfill, sometimes catching fire and filling the landscape with clouds of acrid smoke. A study performed by the Health Protection Agency, UK on a tyre fire in Swansea, UK estimated that over 25,000 people were negatively effected.[34] Volumes of polyaromatic hydrocarbons, particulate matter, SO_2 and more were released into the environment.[35]

Despite these downsides, vulcanisation is here to stay. Rubber is an enabling technology that is used in almost every consumer device in the world. Vulcanisation produces materials that are tough, chemically resistant, modifiable and cost-effective. Finally, they are able to be produced on a mass scale with ease.

Inverse Vulcanisation

If vulcanisation is the chemical crosslinking of polyenes with elemental sulfur, it leads that the inverse of this would be the chemical crosslinking of polymeric sulfur with small molecule dienes. Regardless, this is an apt description of the process. Generally speaking, the process of inverse vulcanisation involves the mixing of elemental sulfur and a small molecule diene such as divinylbenzene (DVB) and heating. After heating, a solid will form and this is the polymerisation product.

As previously discussed, sulfur is a highly underutilised and interesting chemical element. With over 30 known allotropes, it becomes difficult to interpret and use the complicated phase diagram of sulfur. It is difficult to even determine which form of sulfur is reacting at a given temperature.[36–38] As is visible in Figure 1.5, there are many allotropes of sulfur.

With regard to the many allotropes of sulfur there are two that are of particular importance in the field of inverse vulcanisation. The first of these is monoclinic sulfur, which is the sulfur that most people are familiar with. However, as previously mentioned, upon heating to temperatures above 159 °C the sulfur begins to form long polymeric chains. However, upon cooling, these chains revert to the monoclinic form. In the following paragraphs, a demonstration of an application of 1,3-DIB to stabilise these chains is described.

Recently, work by Chung *et al.* demonstrated the use of elemental sulfur as a feedstock in the polymerisation of 1,3-diisopropenylbenzene (DIB) to form poly[S-(ran)-1,3-diisopropenylbenzene] (S-DIB)[39] (Figure 1.6)

In terms of the mechanism of polymerisation, there has been a large amount of debate surrounding this topic. The initial paper suggested that the sulfur ring homolytically splits into a di-radical species *via* thermal action. This radical species could then propagate from there as a free-radical polymerisation process. This *a priori* theory however is slightly hindered by the observation that use of a radical inhibitor does not significantly alter the onset of the polymerisation process.[40,41]

In the following subsections, there will be in depth discussions surrounding the literature of applications of sulfur polymers. Most of these papers are for a new, and developing field and therefore are not comprehensive in any way, shape, or form. It is my hope that they provide a brief, but comprehensive overview of the area with a focus on water purification.

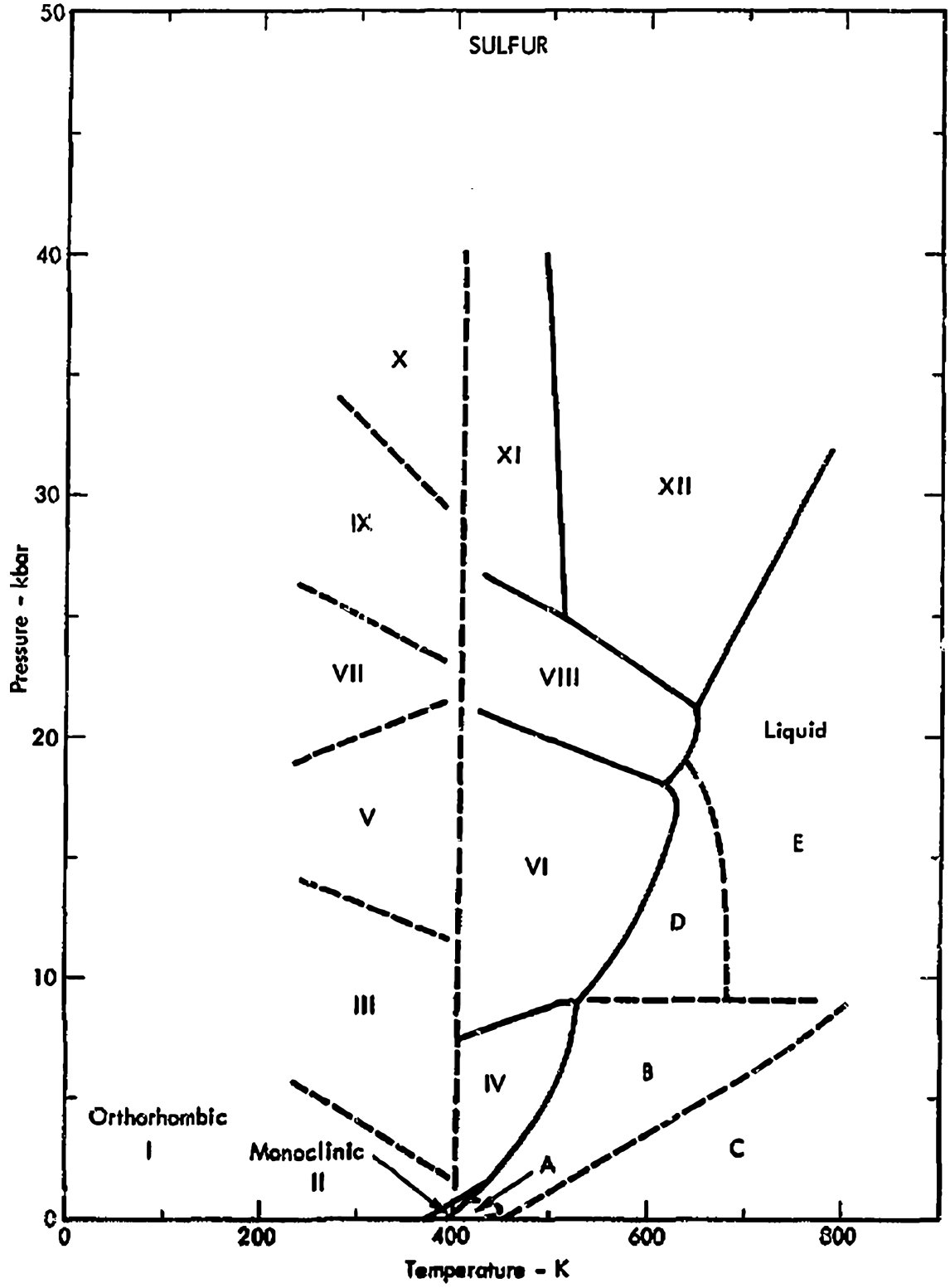

Figure 1.5: Phase diagram of sulfur, published in 1975. Adapted from[38]

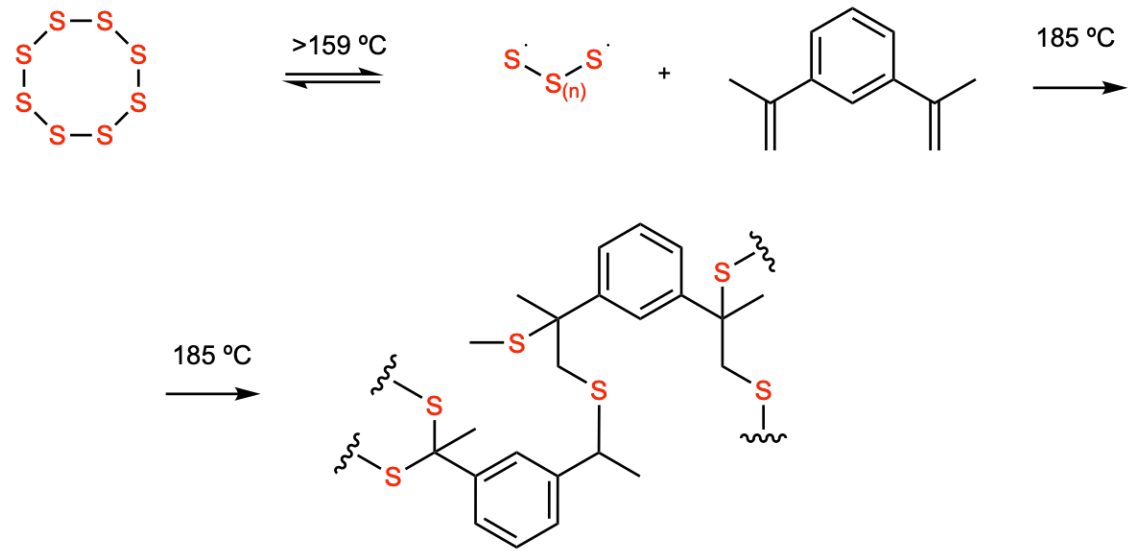

Figure 1.6: The process that has been termed 'inverse vulcanisation' in recent research. Elemental sulfur is heated in the presence of a diene to form cross-linked/hyperbranched polymers. This is dependent on the temperature and molecule used in the formation of the polymer.

1.4 Applied Sulfur Polymers

In his seminal paper, Chung *et al.* explored a series of applications for inverse vulcanised polymers.[39] Said applications have since been further expounded in other bodies of work, demonstrating uses in optics, energy materials, antimicrobial surfaces, gas separation, and finally water purification. Herein, we will explore the applications of sulfur polymers in greater detail.

1.4.1 Antimicrobial Surfaces

The antimicrobial properties of sulfur are known, however, specific mechanisms of activity are not well reported.[42–46] It seems that sulfur has taken on somewhat of a 'presumed' antimicrobial effect in the scientific community. Searches of journals find literature on the subject to be sparse, especially that with discussions of the underlying mechanisms of antimicrobial activity. However, Lin *et al.* discuss the potential of cysteine-containing biological systems interacting with sulfur to produce H_2S, a particularly cytotoxic molecule[47].

Libenson *et al.* demonstrated the positive relationship between the particle size of elemental sulfur aggregates and the antimicrobial activity, hinting at the heterogeneous effects that are in play[42]. This would support the hypothesis of a Cys-S_8 reaction, as no solution effects are observed. The previously mentioned article by Lin *et al.* also notes that

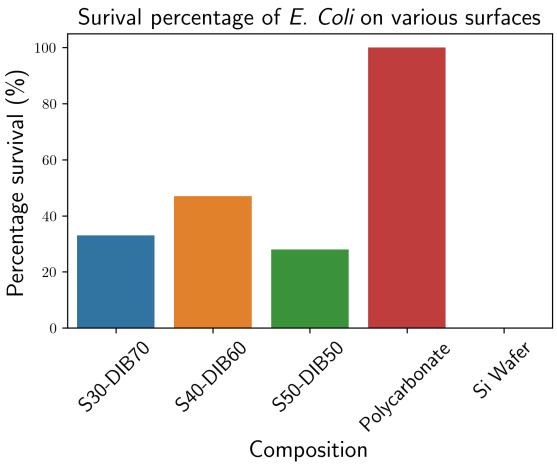

Figure 1.7: Survival % of E. Coli on silicon wafers coated with three different sulfur polymers, polycarbonate, and a silicon wafer control, adapted from work performed by Deng et al.[49]

elemental colloidal sulfur can cause skin irritation, which could be resultant of exposure to corrosive H_2S gas. Naturally, these are mere hypotheses and should not be taken as fact. What we do know for sure is that sulfur is indeed antimicrobial, and this is likely due to the S-S bond contained within the molecule.[47]

Presumably, polymers made from sulfur would actually inherit a degree of this antimicrobial activity. The S-S bonds present in the polymer chains would be amenable to scission, and able to generate a hydropolysulfide. These hydropolysulfides could potentially decay to $H_2S_{(g)}$ which is cytotoxic. The cytotoxicity of $H_2S_{(g)}$ is a result of its depolarising effect on the mitochrondria.[48].

Initially, this idea was explored by Deng *et al.* and they found that the S-DIB surfaces were moderately active for the biocide of *Escherichia coli* (*E. Coli*), killing a maximum of 53% of bacteria on the surface.[49] However, it is important to note that they employed soluble thiopolymers coated onto a silicon wafer substrate. (Figure 1.7) The sample coding in Figure 1.7 is expressed as a weight percentage. For example, S30-DIB70 is 30% weight sulfur, 70% weight 1,3-diisopropenylbenzene.

Further work performed by Smith *et al.* investigated the potential of the pure un-coated sulfur polymer as an antibacterial surface[50]. The work investigated the same bacteria, and another, *Staphylococcus aureus* (*S. Aureus*).

Despite a sparse literature content, it seems that the antibacterial properties of thiopolymers are an interesting and promising field that has the potential to be further expanded upon in the coming years.

1.4.2 Catalysis, Acceleration and Activation

It is important to note that there is a difference in the definition of the three words that are contained in the title, all three of these terms are used in the literature. However, the terms will group them together as there is no evidence for any single of the three terms to be used.

Whilst not an application of thiopolymers, catalysis, acceleration, and activation have become an active area of research within the research community in general. For the sake of brevity, we shall refer to the three under the umbrella term of catalysis. Owing to the high reaction temperatures and extended cure times, and even the impossibility of reaction with certain alkenes, much research has been performed into rate enhancement of sulfur polymer formation.

In 2019 Zhang *et al.* demonstrated that it is possible to synthesise thiopolymers from 4-aminostyrene; they also noted that a marked increase in reaction rate was observed.[51] Furthermore, it was noted that even use of free hindered amines such as *N*-methylimidizole could further enhance the rate of reaction.

In the same year Wu *et al.* published a research article centred around the introduction of rate accelerating agents such as metal dithiocarbamates.[52] They discovered that it was possible to increase the rate of reaction, thermomechanical properties, yields, number of available alkenes, and even to reduce the unwanted side reactions by simple addition of these types of accelerant. They also suggested a reaction pathway for this process .(Figure 1.8) In the process a radical site is generated by the abstraction of a hydrogen atom alpha to an alkene, this may then undergo propagation steps for the formation of a polymer, in the sense of a "classical" inverse vulcanisation reaction. However, they propose that in the catalysed version of the reaction, there are two key processes underway. The first is the coordination of the metal centre to the alkene which would allow for the increased rate of radical addition to the alkene, and secondly the effect of a "sulfurphilic" phase transfer action. In 2020 Zhang *et al.* demonstrated that it is possible to perform inverse vulcanisation *below* the melting point of sulfur, by inclusion of the prior reported metal dithiocarbamate accelerants.[53] However, it is important to note that this was only possible for several alkenes, not all.

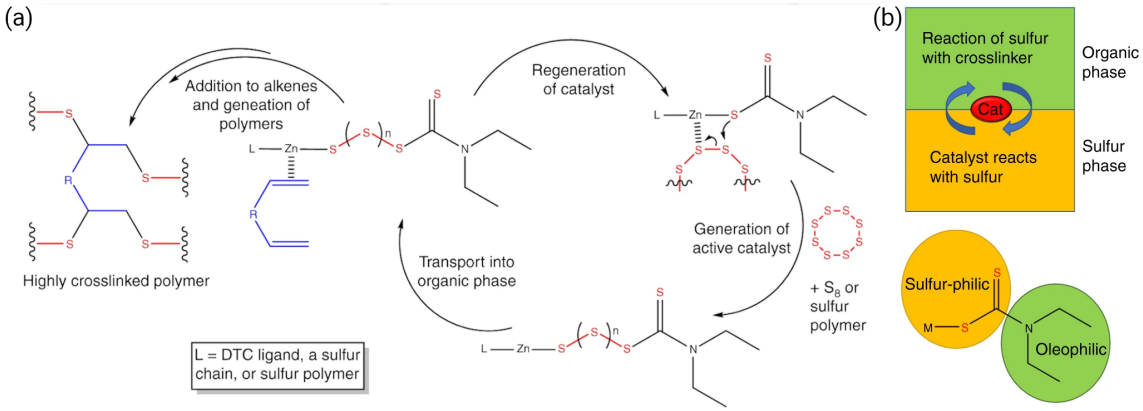

Figure 1.8: ***(a)*** *Scheme illustrating the proposed catalytic cycle in the work performed by Wu et al.* ***(b)*** *One of the keystone properties of the catalyst discovered by Wu et al., the surface-active nature of the catalytic molecule, adapted from* **Wu_2019**

1.4.3 Cathodes

One of the most active areas of research in the application of thiopolymers is in the energy sector. Due to the cost-effective nature of production of thiopolymers, and the desire that exists for the creation of next-generation batteries, a large amount of research is performed. Li-S batteries are the most desirable implementation of this idea, with a theoretical specific energy of 1.8 MJ $Kg^{-}1$.[54] To bring this into context, a general range of specific energy for a traditional Li-ion battery sets around 0.1-0.3 MJ Kg^{-1}.[55]

However, Li-S batteries are not without their problems. Diao *et al.* reported one of the major losses of capacity in Li-S batteries due to the 'shuttle effect'. This irreversible process results in the loss of specific energy of the battery material.[56] The pioneering work in this area was however performed by Mikhaylik *et al.*[57]

When long chain polysulfides are produced in the discharging process they become soluble in the electrolyte, and are able to diffuse to the anode and react directly with the Li metal. These then form shorter chain Li-polysulfides. These polysulfides are then able to diffuse back to the cathode to regenerate the longer chain polysulfides, and deposit LiS/Li_2S in the cathode. This shuttling of Li rapidly diminishes the capacity of the battery in charge-discharge cycles and hence makes the batteries, as yet, impractical to implement.(Figure 1.9) Mitigation of this effect is one of the largest research challenges in the area.[58] Chung *et al.* published what is considered to be the seminal paper in the field in 2013.[39] In this work they demonstrated first the inverse vulcanisation of sulfur to produce thiopolymers, and secondly its application to cathode materials production. They reported a capacity of 823 mA h g^{-1}, and also a diminished capacity fade compared to a pure Li-S battery. However, there was no investigation as to why this fading had diminished and was observed as being "intriguing". Regarding the rate of publication of materials designed for use in cathodes from inverse vulcanised polymers, it would be prohibitive to perform a comprehensive review. Therefore, the following section has attempted to perform a review of some key papers in the field.

In 2015 Kim *et al.* described a synthesis of a sulfur polymer from trithiocyanuric acid. The resultant material had a degree of porosity, and performed well as a cathode material. Since then, others have attempted to limit diffusion of polysulfides by careful selection of charge centres.[59] Others have attempted encapsulation.[60]

In 2018 Hoefling *et al.* published a piece of work concerning solid-state NMR of

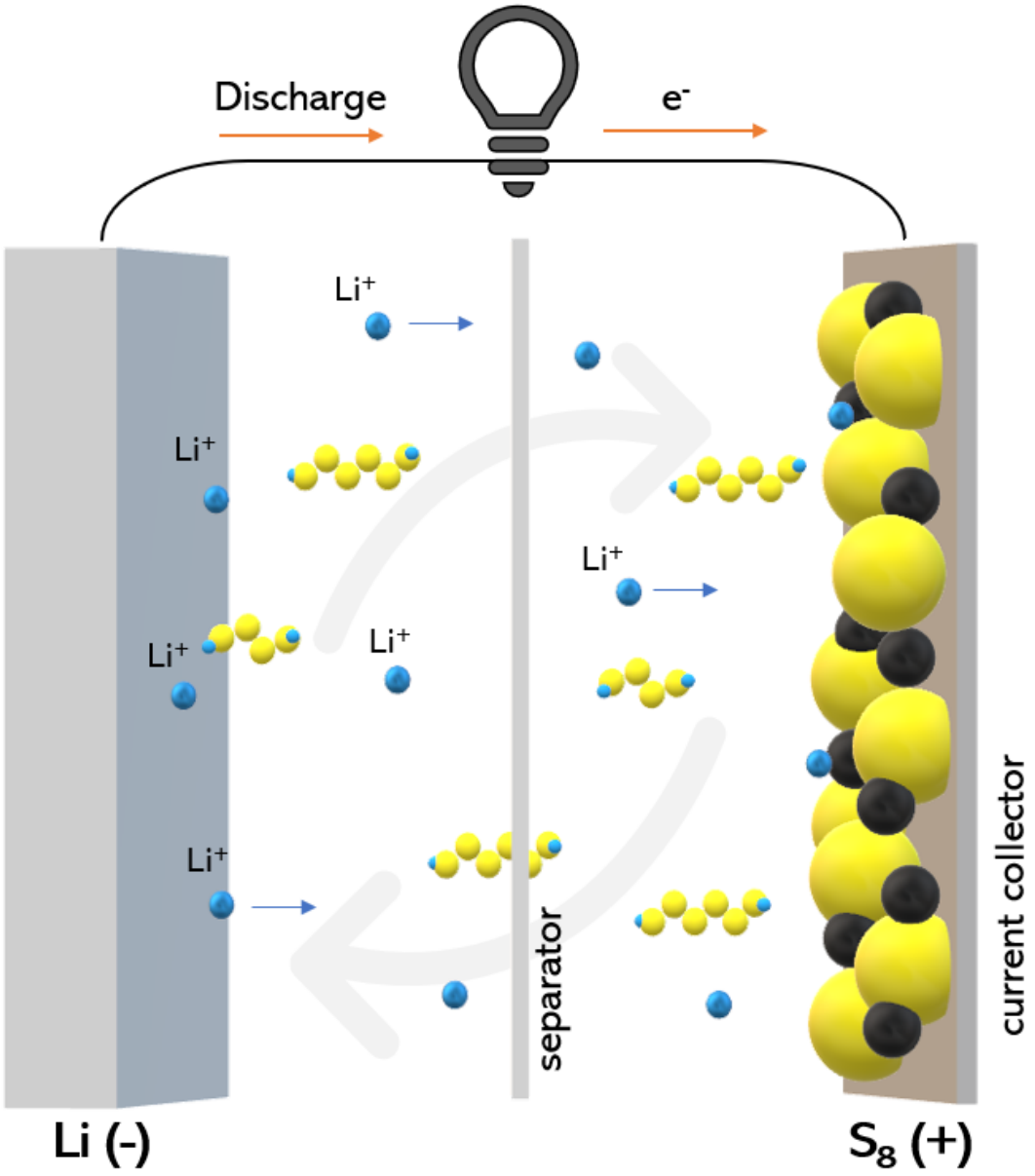

Figure 1.9: Simple diagram to demonstrate the working principle of a lithium sulfur battery, highlighting the issue of the 'shuttle effect', distributed under lisense: CC BY-SA 4.0, author unknown

thiopolymers used in batteries.[61] In what is considered to be common knowledge among the thiopolymer research area they state that the materials are difficult to characterise, owing to their amorphous structures, especially when framed in the context of energy materials. However, despite this they had significant success in the characterisation of the redox process. They were able to observe several key, fundamental processes that occur in the lithium-sulfur redox reaction.

Firstly, they were able to observe the reduction of sulfur and growth of polysulfide chains. Further to this, they observed the transition of the polysulfide chains to different phases also. They also demonstrated that this phase change could further be applied in the deduction of the binding state of the polysulfide (organic vs. inorganic binding). Finally, they demonstrated for the first time a direct observance of the relationship between the composition of the final material and the in-built polysulfide chain lengths. Work set out in the article will potentially pave the way to higher quality research in the future.

With regard to the field of cathode materials that is burgeoning from thiopolymers, and particularly those produced with using the inverse vulcanisation technique, it seems the future is promising. With careful and directed attention to the research of these polymers, it is almost certain that great advancements for science should be possible.

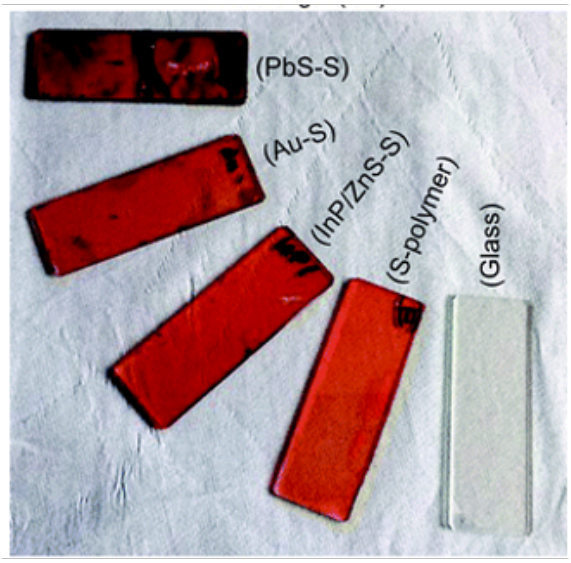

Figure 1.10: Work demonstrated by Bear et al. *demonstrating the incorporation of metal nanoparticles into inverse vulcanised polymer matrices*[62]

1.4.4 Nanocomposites

Polymer nanocomposites are a popular area of research centred around the inclusion of nanoscale objects possessing at least one dimension on the sub-micron scale.[63] Incorporation of nanoparticles into polymers in this regard can have striking effects on the material property. Usually, these dual phases in materials will give properties that come from both materials in that regard. However, when one of the materials is nanosized the effects can be startling as the material will take on a unified property.[64] Nanofillers can affect the mechanical strength, colour, thermomechanical, electrochemical, and even the magnetic properties of the 'mother' substance.

In the field of sulfur polymers, however, only a small amount of research has been performed. Initial research by Bear *et al.* demonstrated it was possible to produce inverse vulcanised polymers with metal nanoparticles incorporated into the polymer matrix.[65,66] Work performed here was quite large in scope, and they were able to incorporate Au, ZnS, PbS, CoO and Fe_3O_4 into a S-DIB matrix. (Figure 1.10) No application was sought or suggested in the article, and it is a shame that this area has not seen any further investigation.

1.4.5 Optics

Elemental sulfur possesses a high refractive-index, and IR transparency. This has been reported and discussed in detail, both because of its interest and use in fields like astronomy for the optical observation of planets, moons, and other celestial bodies contained within the solar system.[67,68]

It is important to note that there is a desire for the improvement of IR transparent materials, particularly those that find application in lenses for thermal imaging optical sensors. Current technology revolves around the use of chalcogenide glasses (Ge, Te) to get the desired combined properties of both IR wavelength light transparency and high refractive index. However, these materials are easily scratched and broken. They are also expensive to manufacture.[67] The refractive index of an object is obtained by taking the measurement displayed in Figure 1.11. A high refractive index is required for the fabrication of lenses.

Snell's law provides an appropriate description of the relationship between the angle of incidence, and the angle of transmission as displayed below in (Equation 1.5), relating to the diagram depicted in Figure 1.11. In the figure and equation n_1 and n_2 are the respective refractive indices of the materials.

$$\frac{Sin\theta_2}{Sin\theta_1} = \frac{n_2}{n_1} = \frac{\theta_1}{\theta_2} \tag{1.5}$$

One of the first investigations of thiopolymers into the area of optics was performed by Griebel *et al.*[69] In their research they determined that a 10 μm film of S-DIB cast onto a glass slide retained 85% optical transparency. The material also was found to have a refractive index of 1.8, which is considered to be very high. Table 1 demonstrates the refractive indices of different materials.

Material	**Refractive index** ($\lambda = 600 \pm 50nm$)
Quartz (s)	1.458[70]
Diamond (s)	2.417[71]
Sodium Chloride (s)	1.544[72]
poly(S-*ran*-(1,3-diisopropenylbenzene)](s)	1.84[69]
poly(S-*ran*-(tetravinyltin)](s)	1.97[73]

Table 1.1: Table displaying several common materials and their refractive indices

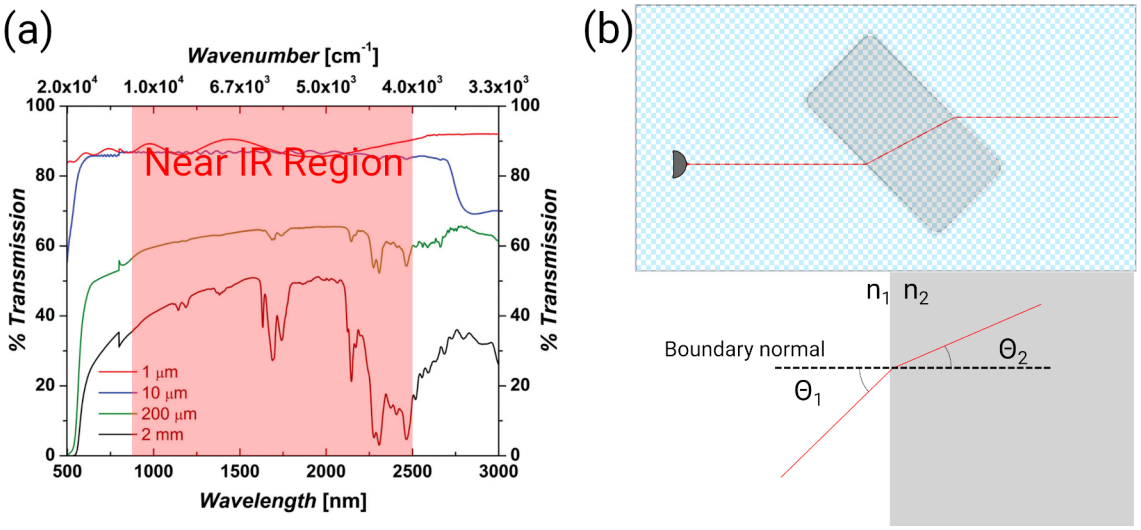

Figure 1.11: (a) A UV-VIS/Near-IR spectrograph of S-DIB at various thicknesses, demonstrating the transmission of the polymer. Adapted from[69] (b) Schematic illustrating the working principle of the refractive index of a phase (top) a schematic representation of how the refractive index is obtained (bottom)

In a following paper Griebel *et al.* demonstrated that these formed lenses could be scratched, and then "self-heal" *via* thermal annealing.[74] In this paper much investigation was performed into the quantification of the mechanical properties of the produced polymers, and this "self-healing" property that was exhibited. However, they did demonstrate that after the phenomenon, the material was able to again be used as an IR-Camera lens.

Klein *et al.* synthesised triisopropenylbenzene from 1,3,5-tribromobenzene using the popular Suzuki coupling reaction.[75] The material, however, did not improve the optical properties of its predecessor. It did improve the thermomechanical properties.

Anderson *et al.* demonstrated that by inclusion of small amounts of Se (10 % w/w), which reacts similarly to sulfur, in an inverse vulcanisation reaction, it is possible to generate a material with an even higher refractive index. (>2.0) They termed this polymer a 'CHIP'.[76]

CHIP is an acronym for 'chalcogenic hybrid inorganic/organic polymer', seemingly shortening a more systematic name for sulfur polymer. Sulfur is thought of as an inorganic element, and is part of the chalcogenides. Hence, when a polymer is formed from elemental sulfur and an organic molecule, a CHIP is produced.

Boyd *et al.* demonstrated a particularly novel route to a polymer in their search for a material with desirable optical properties. They demonstrated that it was possible to

inverse vulcanise tetra-allyl tin.[73] The produced material they termed an 'ORMOCHALC' - an organically modified chalcogenide. They found that it was possible to produce a material that was composed of large amounts of sulfur (>50% w/w), and also had a high refractive index. The research was, however, subject to one issue: gasses generated during the polymerisation process filled the material with occluded pores.

Overall, there is a large scope for the production of polymers of this type. However, much research remains to be completed in this area. For a review article that is related to this work, I would like to refer the reader to an article authored by Griebel *et al.*[77]

1.4.6 Reprocessability

Another key application of thiopolymers, reprocessability, is more concerned with a particular property that is exhibited by the polymers. It has been reported that sulfur polymers are able to display "vitrimeric" properties. These properties are fairly unique and newly reported in the literature (2010). Ludwik Leibler coined the term initially, and his work was centred around epoxy-based thermosetting polymers.[78] Traditional thermoset polymers will not liquefy upon heating. This is owing to their crosslinked nature. However, in a vitrimer there is a degree of reversibility to this bonding, therefore desirable properties of thermosetting polymers such as high solvent resistance, and chemical resistance can be combined with the melt processability that is found in thermoplastic polymers.

Parker *et al.* first demonstrated this vitrimer-like behavior in sulfur polymers.[79] By first forming a polymer from sulfur and squalene, a polyene that is found in the brain of sharks, then subsequently crushing and remoulding it they demonstrated these effects. They performed the same process for perilyl alcohol, a diene that is found in plant matter. This reprocessability was attributed to the reversible behaviour that S-S bonds have been shown to exhibit. (Figure 1.12a) demonstrates this process schematically.

In a related area Tonkin *et al.* demonstrated that it is possible to chemically initiate a form of reversibility in these polymers. By use of organic bases such as phosphines or amines, S-S bonds can be opened and coordinated to, and used to repair the surfaces of the polymers. Figure 1.12b demonstrates this process schematically.[80]

In conclusion, despite reprocesseability being a new area of investigation of thiopolymers it seems that high quality research is being performed. Particularly, the discovery of using a base to 'activate' the S-S linkage seems to be one that could be further exploited.

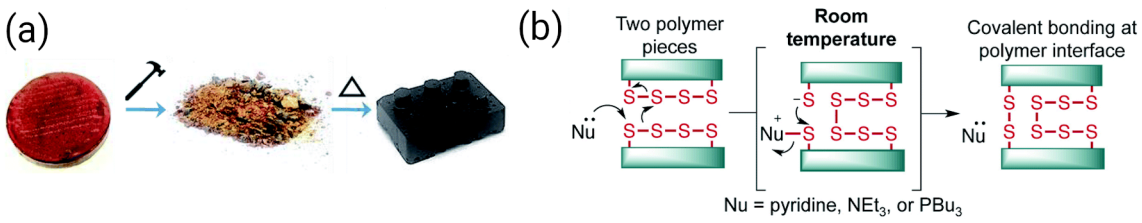

Figure 1.12: (a) Schematic demonstrating the process of inducing S-S bond thermal reorganisation as reported by Parker et al[79] *(b) Schematic demonstrating the process of inducing S-S bond chemical reorganisation as reported by Tonkin et al.*[80]

1.4.7 Water Remediation

There are all manner of reasons water remediation is a well researched topic, in industry but one of the main driving forces for water remediation is pollution. Adverse changes in the environment can be directly attributed to the death of 9 million people in 2015 alone.[81] Water pollution is often discussed in terms of the ocean, riverbeds, and other surface features of the earth. However, the problem literally runs deeper than mere surface pollution. Surface pollution can accumulate and spread to the water table, aquifers, groundwater.

Water pollution is categorised as coming from two different sources: point sources and non-point sources. An example of a point source would be a manufacturing plant, or a sewage treatment facility. These are sources that are attributable to a single point source, and are easily defined. Non-point sources refer to a less concentrated source of pollution, and often do not possess a 'point' origin. A classic example of this would be the knock-on effects of salting roads — alteration of microbial communities at the roadside soils.[82] These alterations can include the promotion of growth of bacteria that produce toxins that may end up in neighbouring human settlements.[83–86]

Filtration and catalytic conversion are technologies that can be used to mitigate the effects of point-source water pollution. For example, the "sour" crude oil is often refined *via* the use of catalytic hydrodesulfurisation, therefore preventing ocean acidification by sulfates.[87] It is obvious how chemistry is able to solve these problems by careful implementation of catalytic processes or ion-exchange facilities.

Of particular relevance to thiopolymers is filtration. A useful property of sulfur is its 'soft' electron donor capability. The Hard-Soft-Acid-Base principle (HSAB principle) was first introduced by Ralph G. Pearson in 1963 in an attempt to unify the reaction behaviour of inorganic and organic chemistry, and is used to this day to qualify the behaviour of several

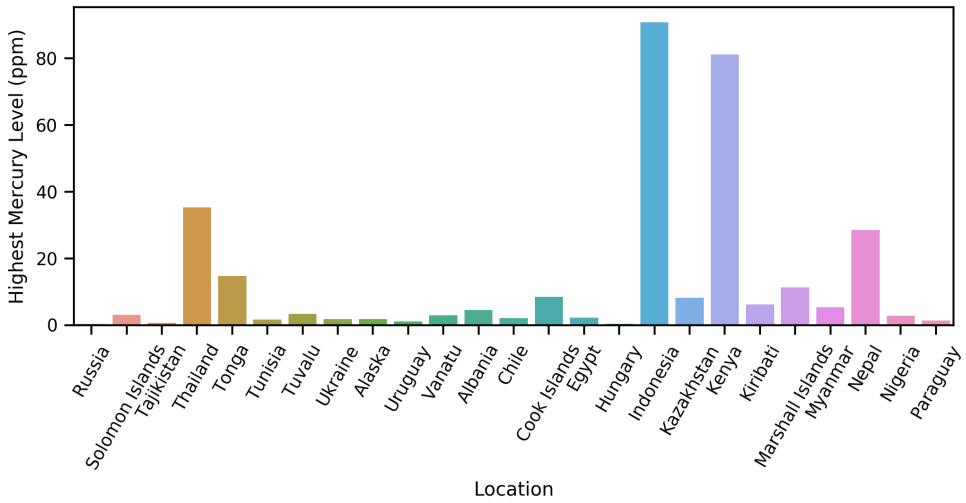

Figure 1.13: Bar chart that demonstrating the level of mercury found in hair of women of child bearing age across the West-Indian isles. It can be seen that mercury contamination in the human body is both pervasion, and unacceptably high. Adapted from[81]

chemical processes.[88] One of the results of this theory is that "soft" Lewis acids will tend to form adducts with "soft" Lewis bases. The specific result which is relevant to thiopolymers is that they will have favourable interactions with metal ions such as Hg^{2+}. Mercury is a persistent and sinister threat to global health.[89] The scale of contamination of humans is demonstrated in Figure 1.13. Any level of mercury contamination is unacceptable, and can contribute to an almost dizzying list of unwanted effects on human health.[90,91]

Water remediation using thiopolymers is a topic that is almost as old as the field itself. Prior to 2016, however, no one had attempted this with inverse vulcanised thiopolymers. In 2016, Crockett *et al.* demonstrated the use of an inverse vulcanised polymer for removal of Hg^{2+} from solution.[92] Co-polymerisation of limonene, an industrial by-product, with sulfur produced a tacky, thermoplastic: poly[S-*ran*-limonene] (S-Limonene). At room temperature, S-Limonene was a very slow-flowing, viscous tar. It was found that this material could reduce the concentration of mercury in solution from 5 ppm to 0 ppm. This improved upon the capacity of elemental sulfur. A chromogenic response was also displayed.

In 2016 Hasell *et al.* demonstrated that it is possible to generate a porous structure from S-DIB by first swelling the polymer in supercritical CO_2 (sCO_2), and then rapidly venting the autoclave, causing the (sCO_2) to undergo a phase transition to a gas.[93] This

has the effect of 'foaming' the polymer, giving it a morphology of occluded bubbles in the polymer. (Figure 1.14 a). It was found that by foaming the polymer, there was an increase in the amount of mercury that the polymer was able to remove from solution. It improved upon the only previously reported material S-Limonene. This was attributed to the creation of a porous structure.

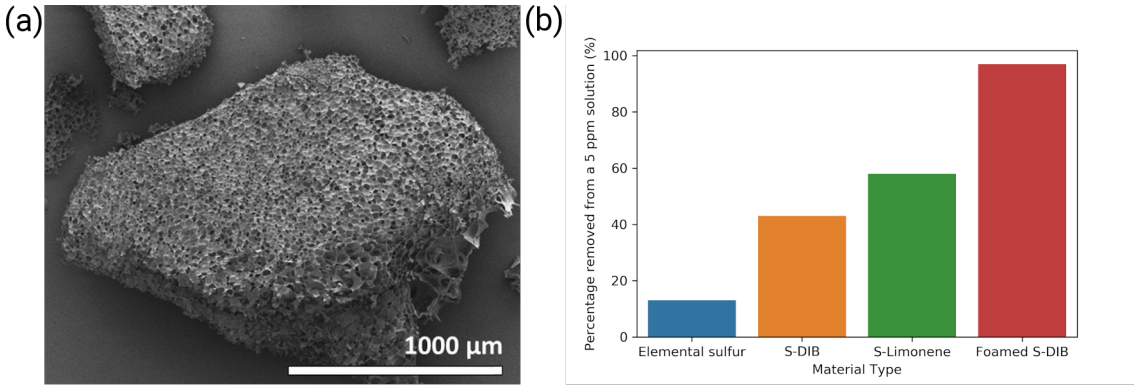

Figure 1.14: (a) Scanning electron micrograph demonstrating the morphology produced when supercritical carbon dioxide is used to foam S-DIB. It is important to note that the porosity is 'closed cell' and has a poor interconnectivity (b) Comparison of the mercury removal from a 5 ppm solution for some polymers made from sulfur, and elemental sulfur itself. Reproduced from[93]

In the following year results were published in a paper which was authored by Parker *et al.* in which they demonstrated that it was possible to generate a polymer with interconnected porosity by the use of the 'salt templating' process.[94] This process required the use of a sacrificial pore generating template. However, despite the apparent improvement in morphology, it was found that the mercury uptake was poor.

This work was expanded upon in 2019 by Petcher *et al.* who demonstrated that the low mercury absorption could be attributed to the incomplete removal of sodium chloride from the composite.[95] It was found that complete removal of the template achieved a mercury capacity of 2.27 mg $g^{-}1$. As this publication was a major component contributing to this thesis formation, it will be reviewed in greater depth in Chapter 2.

In 2017 Worthington *et al.* expanded upon the work performed by Parker *et al.* by demonstrating the use of a sacrificial sodium chloride template to produce a polymer from canola oil.[96] They then tested the effectiveness of the material in the removal of mercury chloride. An interesting aspect of this research was their investigation into the removal of mercury chloride from a matrix that contained loam. They found that despite the inclusion of loam, a particulate soil, the material was still able to effectively remove mercury chloride

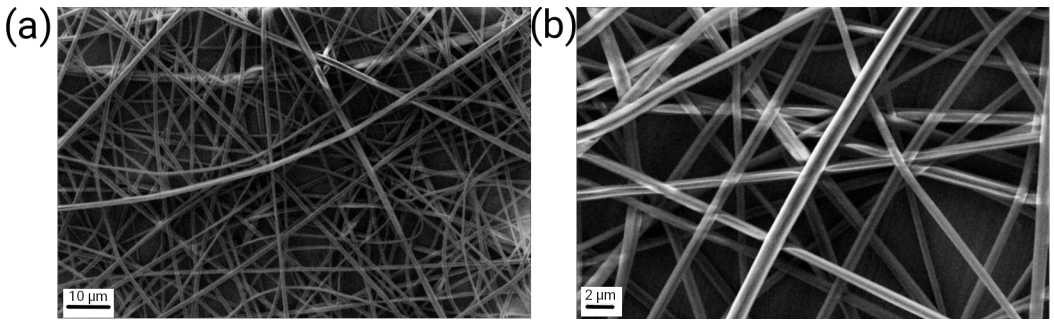

Figure 1.15: The morphology of nanofibres produced by electrospinning a solution of polymethylmethacrylate and S-DIB, adapted from[99]

from solution. It is a well documented phenomenon that competitive absorption can inhibit removal of metal-ions from solution.[97,98]

A particularly interesting application of sulfur polymers in the removal of mercury chloride from solution was performed by Thielke *et al.*.[99] They discovered that by electrospinning a mixture of S-DIB and poly(methyl methacrylate) they could produce a mesh of nanofibres. When these nanofibres were then placed into a solution of mercury chloride, the saturation capacity of the material was found to be 327.6 mg g^{-1}, an incredibly high number when compared to previous reports.[99] The morphology of the produced nanofibres is illustrated in (Figure 1.15).

In 2019 Wu *et al.* demonstrated that by coating a solution of S-Limonene onto a high surface area silica support, it would be possible to then use this composite material to absorb mercury from solution.[52] They found that by coating the material onto silica they were able to achieve absorption capacities of up to 716 mg g^{-1} of polymer. This was actually the highest capacity that has been achieved by a sulfur polymer to date. However, with the mass of the support included, the capacity was reported at 65 mg g^{-1} of polymer. Interestingly, the material was also explored for the removal of Au^{3+} from solution. It was reported that the supported polymers were able to remove up to approximately 40 mg g^{-1} from solution (Inclusive of support weight).

Lundquist *et al.* also investigated the use of sulfur polymers as a coating agent.[100] The work that was performed was centred around the idea of lowering the amount of dust that is generated in the use of activated carbon. If activated carbon containing pollutants are aerosolised and inhaled, it has potential health implications. They coated activated carbon with sulfur polymers to test the ability of the resultant material for the removal of polyfluorooctantoic acid (PFOA) and polyfluorosulfonic acid (PFOS) from water. They are

persistent organic pollutants, with terrible effects on the health of living organisms.[101–103] However, the key result in this study was not the improvement in uptake capacity, but the lowering of dust. So in this sense, the sulfur polymer was more acting as an adhesive than a chemical additive to improve the absorption capacity of the material. They found that the material barely improved the effectiveness of absorption. It did, however, induce particle adhesion, which in turn eases separation of the sorbent from the solvent.

Tikolau *et al.* investigated the effect of structure on the mercury sequestration from solution.[104] They found that hydroxylated oleic acid was able to improve the mercury uptake from solution. They attributed this to the improved wetting of the material.

So far, all the applications of the polymers for mercury removal have been either as pure polymer, supported polymer, or as a polymer blend as demonstrated by Thielke *et al.* The possibility of performing a chemical transformation on the polymer was demonstrated by Lee *et al.*[105] They reported that by heating a thiopolymer alongside an activating agent (KOH) under an inert atmosphere (N_2) at high temperatures (>500 ºC), it was possible to form a type of activated carbon with a high percentage of covalently bound sulfur. They found the produced materials to have a high specific surface area (>2200 m^2 g^{-1}), and an impressively high uptake for both mercury chloride (Q_e = 850 mg g^{-1}) and gold chloroaurate (1497 mg g^{-1}). To my knowledge, no material has outperformed this particular material in regard to sulfur polymers.

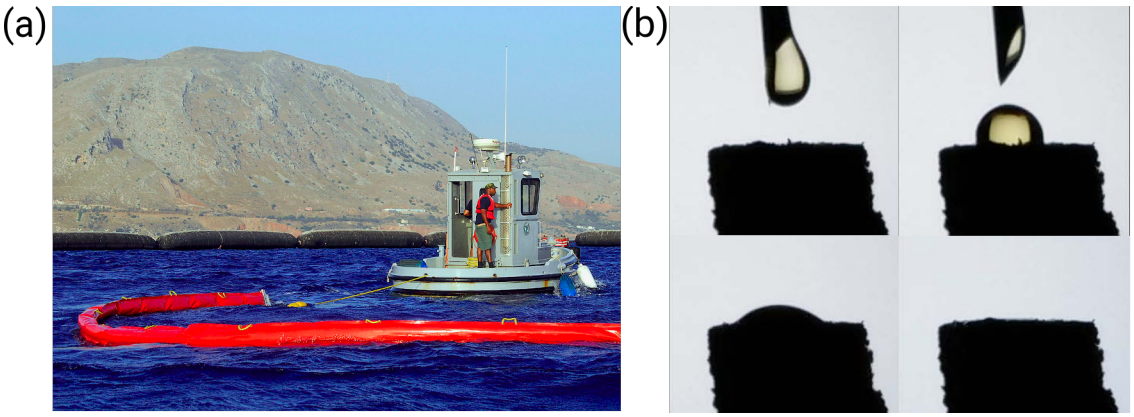

Figure 1.16: (a) Photograph demonstrating an oil trap, that is commonly deployed after an industrial oil spill to prevent the oil-layer from freely spreading across the ocean (b) Demonstration of technology developed by Worthington et al. showing an oil droplet penetrating into the porous network of the polymer. Figure adapted from[106]

Another potential application for sulfur polymers in water remediation was investigated

by Lundquist *et al.*[107] They investigated the use of thiopolymers for the removal of Fe^{3+} from aqueous solution. This particular metal ion is undesirable to have in water because it can cause discolouration of plumbing fixtures and can clog pipes. Fe^{3+} also poor tasting.[108–110] Furthermore, it can promote growth of bacteria when concentrations are high enough.[111] Therefore, they decided to explore the potential of sulfur polymers in removal of this ion from solution. However, it was found that the material was not particularly effective and required up to 20 % weight loading of sorbent to become effective in the removal of iron from solution. To place this in context for the reader, imagine needing 11 thousand kg of filtration media for a household (the average UK household water consumption is 55 thousand L per year)[112].

One more potential application for porous sulfur polymers in water remediation was investigated by Worthington *et al.*[106] (Figure 1.16**a**) demonstrates the entrapment of an oil layer after an oil spill. This technique would then be generally followed by the use of an oil 'sponge' like the technology developed by Worthington. They demonstrated that the hydrophobic nature of the produced materials allowed them to be purposed as oil-water separation agents. (Figure 1.16b) They found that the materials were effective for the absorption of oil layers on water surfaces.This is of particular interest in current research because of events like the BP Gulf of Mexico oil spill, or the Arctic diesel spill.[113,114]

To conclude, it would be apt to note that a wide body of research has been performed into the area of water remediation by using sulfur polymers and their derivatives. There is a degree of creativity in this area that is particularly commendable, with a wide range of efforts at correcting various environmental issues.

1.4.8 Other works of interest

Of course, there are other works of interest concerning sulfur polymers that cannot be placed into a category without having one of their own. One such application was explored by Mann *et al.* In this work, they explored the potential of sulfur polymers as matrices for the loading of amounts of NPK fertiliser.[115] The sulfur polymer slowed the release of NPK fertiliser allowing for a more sustained release, which was demonstrated to improve the growth of tomato plants.

Smith *et al.* also demonstrated the possibility that more than one crosslinking agent being used in the synthesis of thiopolymers. By judicious selection of crosslinking components they were able to demonstrate that it is possible to tune properties such as the (T_g), M_w, solubility or colour of the produced polymers.

1.4.9 Project overview

The work set out in this thesis began as an investigation of sulfur polymers for uses in filtration, water remediation and most specifically mercury capture. However, given that the initial project in the formation of a macro-porous polymer was completed, it became prudent to investigate several related but dissimilar questions:

1. Can we go *smaller* - is mesoporosity possible?
2. Can we alter the chemistry of the polymer to alter the selectivity?
3. Can we understand the mechanism of binding?

Naturally, during the investigation of these topics of interest, many interesting and fruitful courses of study developed. During the course of the project I was able to investigate areas including but not limited to: catalysis, porosity, wettability, synthetic methods, mechanical property investigation, and a litany of other areas.

Bibliography

(1) R. Steudel, *Elemental Sulfur and Sulfur-Rich Compounds I*, Springer, Berlin, Heidelberg, 2003, p. 166.

(2) A. Y. Coran, *Science and Technology of Rubber*, 2005, **17**, 321–366.

(3) D. Phineas, *Oxidation of sulphur dioxide to sulphur trioxide and catalysts*, US2799560A, 1956.

(4) N. Wiberg, *Inorganic Chemistry*, Academic Press, Cambridge, Massachusetts, United States, 2001, p. 817.

(5) Y. Teng, Q. Zhou and P. Gao, *Critical Reviews in Environmental Science and Technology*, 2019, **49**, 2314–2358.

(6) M. Akiba and A. S. Hashim, *Progress in Polymer Science (Oxford)*, 1997, **22**, 475–521.

(7) Q. Lian, Y. Li, K. Li, J. Cheng and J. Zhang, *Macromolecules*, 2017, **50**, 803–810.

(8) M. Smith, *Handbook of Rubber Technology: Natural, Synthetic Rubber and Technology of Vulcanisation Vol. I (HB)*, CBS Publishers & Distributors, 2004.

(9) *Sulfur Market - Growth, Trends, COVID-19 Impact, and Forecasts (2021 - 2026)*, Mordor Intelligence, `https://www.mordorintelligence.com/industry-reports/sulfur-market` (visited on 2021).

(10) G. S. Pointdexter, Y. Pendri, L. B. Snyder, J. P. Yevich and M. Deshpande, in *Kent and Riegel's Handbook of Industrial Chemistry and Biotechnology: Chemistry in the Pharmaceutical Industry*, ed. J. A. Kent, Springer US, Boston, MA, 2007, pp. 404–430.

(11) B. Buchanan, *Gunpowder, Explosives and the State: A Technological History*, Ashgate, 2006.

(12) K. A. Kvenvolden, Organic Geochemistry, Pergamon, 2006, vol. 37, pp. 1–11.

(13) Q. Bozhang, *Petroleum Planning & Engineering*, 2005, **3**.

(14) S. C. Schuman and H. Shalit, *Catalysis Reviews*, 1971, **4**, 245–318.

(15) P. Grange, *Catalysis Reviews–Science and Engineering*, 1980, **21**, 135–181.

(16) G. E. Likens, R. F. Wright, J. N. Galloway and T. J. Butler, *Scientific American*, 1979, **241**, 43–51.

(17) D. W. Schindler, *Science*, 1988, **239**, 149–157.

(18) G. E. Likens and F. H. Bormann, *Science*, 1974, **184**, 1176–1179.

(19) A. G. Clarke and M. Radojevic, *Atmospheric Environment (1967)*, 1987, **21**, 1115–1123.

(20) S. H. Lebowitz, *Journal of Chemical Education*, 1931, **8**, 1630.

(21) L. Riall, *Sicily and the Unification of Italy : Liberal Policy and Local Power, 1859-1866.* Oxford University Press, UK, 1998, p. 401.

(22) R. J. Young and P. A. Lovell, *Introduction to polymers*, CRC press, 2011.

(23) K. Matyjaszewski and T. P. Davis, *Handbook of radical polymerization*, John Wiley & Sons, 2003.

(24) G. Moad, Y. K. Chong, A. Postma, E. Rizzardo and S. H. Thang, *Polymer*, 2005, **46**, 8458–8468.

(25) J. Chiefari, Y. K. (Chong, F. Ercole, J. Krstina, J. Jeffery, T. P. T. Le, R. T. A. Mayadunne, G. F. Meijs, C. L. Moad, G. Moad, E. Rizzardo and S. H. Thang, *Macromolecules*, 1998, **31**, 5559–5562.

(26) W. L. Sederel and G. J. De Jong, *Journal of Applied Polymer Science*, 1973, **17**, 2835–2846.

(27) P. G. Debenedetti and F. H. Stillinger, *Nature*, 2001, **410**, 259–267.

(28) G. Odian, *Principles of Polymerization*, John Wiley & Sons, Inc., 2004.

(29) J. d'Auzac, *Physiology of Rubber Tree Latex: The Laticiferous Cell and Latex- A Model of Cytoplasm*, CRC Press, 2018.

(30) P. W. Barker, *Rubber: History, Production, and Manufacture*, US Government Printing Office, 1940.

(31) D. S. Pearson and W. W. Graessley, *Macromolecules*, 1978, **11**, 528–533.

(32) L. E. Nielsen, *Journal of Macromolecular Science, Part C*, 1969, **3**, 69–103.

(33) K. Fukumori and M. Matsushita, *R&D Review of Toyota CRDL*, 2003, **38**, 39–47.

(34) H. Protection Agency, *Chemical Hazards and Poisons Report - Issue 21, June 2012*, tech. rep., 2012.

(35) L. May and L. Evans, *International Journal of Population Data Science*, 2019, **4**.

(36) A. G. Ferreira and L. Q. Lobo, *Journal of Chemical Thermodynamics*, 2011, **43**, 95–104.

(37) G. C. Vezzoli and R. J. Zeto, *Inorganic Chemistry*, 1970, **9**, 2478–2484.

(38) D. A. Young, *Phase diagrams of the elements*, Livermore, CA (United States), 1975, p. 64.

(39) W. J. Chung, J. J. Griebel, E. T. Kim, H. Yoon, A. G. Simmonds, H. J. Ji, P. T. Dirlam, R. S. Glass, J. J. Wie, N. A. Nguyen, B. W. Guralnick, J. Park, Á. Somogyi, P. Theato, M. E. Mackay, Y. E. Sung, K. Char and J. Pyun, *Nature Chemistry*, 2013, **5**, 518–524.

(40) J. J. Griebel, N. A. Nguyen, A. V. Astashkin, R. S. Glass, M. E. Mackay, K. Char and J. Pyun, *ACS Macro Letters*, 2014, **3**, 1258–1261.

(41) M. M. Coleman, J. R. Shelton and J. L. Koenig, *Industrial and Engineering Chemistry Product Research and Development*, 1974, **13**, 154–166.

(42) L. Libenson, F. P. Hadley, A. P. McIlroy, V. M. Wetzel and R. R. Mellon, *Journal of Infectious Diseases*, 1953, **93**, 28–35.

(43) K. H. Kyung and H. P. Fleming, *Journal of Food Protection*, 1997, **60**, 67–71.

(44) T. Schneider, A. Baldauf, L. A. Ba, V. Jamier, K. Khairan, M. B. Sarakbi, N. Reum, M. Schneider, A. Röseler, K. Becker, T. Burkholz, P. G. Winyard, M. Kelkel, M. Diederich and C. Jacob, *Journal of Biomedical Nanotechnology*, 2011, **7**, 395–405.

(45) S. Shankar and J. W. Rhim, *Food Hydrocolloids*, 2018, **82**, 116–123.

(46) B. R. Dekić, N. S. Radulović, V. S. Dekić, R. D. Vukićević and R. M. Palić, *Molecules*, 2010, **15**, 2246–2256.

(47) A. N. Lin, R. J. Reimer and D. M. Carter, *Journal of the American Academy of Dermatology*, 1988, **18**, 553–558.

(48) M. A. Eghbal, P. S. Pennefather and P. J. O'Brien, *Toxicology*, 2004, **203**, 69–76.

(49) Z. Deng, A. Hoefling, P. Theato and K. Lienkamp, *Macromolecular Chemistry and Physics*, 2018, **219**, 1700497.

(50) J. A. Smith, R. Mulhall, S. Goodman, G. Fleming, H. Allison, R. Raval and T. Hasell, *ACS Omega*, 2020, **5**, 5229–5234.

(51) Y. Zhang, N. G. Pavlopoulos, T. S. Kleine, M. Karayilan, R. S. Glass, K. Char and J. Pyun, *Journal of Polymer Science, Part A: Polymer Chemistry*, 2019, **57**, 7–12.

(52) X. Wu, J. A. Smith, S. Petcher, B. Zhang, D. J. Parker, J. M. Griffin and T. Hasell, *Nature Communications*, 2019, **10**, 647.

(53) B. Zhang, H. Gao, P. Yan, S. Petcher and T. Hasell, *Materials Chemistry Frontiers*, 2020, **4**, 669–675.

(54) P. G. Bruce, S. A. Freunberger, L. J. Hardwick and J. M. Tarascon, *LigO_2 and LigS batteries with high energy storage*, 2012.

(55) N. Nitta, F. Wu, J. T. Lee and G. Yushin, *Materials today*, 2015, **18**, 252–264.

(56) Y. Diao, K. Xie, S. Xiong and X. Hong, *Journal of Power Sources*, 2013, **235**, 181–186.

(57) Y. V. Mikhaylik and J. R. Akridge, *Journal of The Electrochemical Society*, 2004, **151**, A1969–A1976.

(58) J.-M. Tarascon, *Philosophical Transactions of the Royal Society A: Mathematical, Physical and Engineering Sciences*, 2010, **368**, 3227–3241.

(59) H. Kang, H. Kim and M. J. Park, *Advanced Energy Materials*, 2018, **8**, 1–9.

(60) F. Wu, S. Chen, V. Srot, Y. Huang, S. K. Sinha, P. A. van Aken, J. Maier and Y. Yu, *Advanced Materials*, 2018, **30**, 1–8.

(61) A. Hoefling, D. T. Nguyen, P. Partovi-Azar, D. Sebastiani, P. Theato, S. W. Song and Y. J. Lee, *Chemistry of Materials*, 2018, **30**, 2915–2923.

(62) J. C. Bear, W. J. Peveler, P. D. McNaughter, I. P. Parkin, P. O'Brien and C. W. Dunnill, *Chemical Communications*, 2015, **51**, 10467–10470.

(63) A. Kausar, *Journal of Plastic Film & Sheeting*, 1177/8756087919849459, **2020;36(1):94-112**.

(64) P. M. Visakh, in *Nanomaterials and Nanocomposites*, 2016, pp. 1–20.

(65) J. C. Bear, W. J. Peveler, P. D. McNaughter, I. P. Parkin, P. O'Brien and C. W. Dunnill, *Chemical Communications*, 2015, **51**, 10467–10470.

(66) P. D. McNaughter, J. C. Bear, A. G. Mayes, I. P. Parkin and P. O'Brien, *Royal Society Open Science*, 2017, **4**, 170383.

(67) S. Namnabat, J. J. Gabriel, J. Pyun and R. A. Norwood, Organic Photonic Materials and Devices XVI, ed. C. E. Tabor, F. Kajzar, T. Kaino and Y. Koike, SPIE, 2014, vol. 8983, p. 89830D.

(68) K. A. Fuller, H. D. Downing and M. R. Querry, *Applied Optics*, 1991, **30**, 4081.

(69) J. J. Griebel, S. Namnabat, E. T. Kim, R. Himmelhuber, D. H. Moronta, W. J. Chung, A. G. Simmonds, K.-J. Kim, J. van der Laan, N. A. Nguyen, E. L. Dereniak, M. E. Mackay, K. Char, R. S. Glass, R. A. Norwood and J. Pyun, *Advanced Materials*, 2014, **26**, 3014–3018.

(70) G. L. Tan, M. F. Lemon, D. J. Jones and R. H. French, DOI: `10.1103/PhysRevB.72.205117`.

(71) E. Hecht, *Optics*, Addison-Wesley, 2002, pp. 11–12.

(72) R. A. Serway, J. S. Faughn and C. J. Moses, *College Physics*, Brooks/Cole, 2003.

(73) D. A. Boyd, V. Q. Nguyen, C. C. McClain, F. H. Kung, C. C. Baker, J. D. Myers, M. P. Hunt, W. Kim and J. S. Sanghera, *ACS Macro Letters*, 2019, **8**, 113–116.

(74) J. J. Griebel, N. A. Nguyen, S. Namnabat, L. E. Anderson, R. S. Glass, R. A. Norwood, M. E. Mackay, K. Char and J. Pyun, *ACS Macro Letters*, 2015, **4**, 862–866.

(75) T. S. Kleine, N. A. Nguyen, L. E. Anderson, S. Namnabat, E. A. Lavilla, S. A. Showghi, P. T. Dirlam, C. B. Arrington, M. S. Manchester, J. Schwiegerling, R. S. Glass, K. Char, R. A. Norwood, M. E. Mackay and J. Pyun, *ACS Macro Letters*, 2016, **5**, 1152–1156.

(76) L. E. Anderson, T. S. Kleine, Y. Zhang, D. D. Phan, S. Namnabat, E. A. LaVilla, K. M. Konopka, L. Ruiz Diaz, M. S. Manchester, J. Schwiegerling, R. S. Glass, M. E. Mackay, K. Char, R. A. Norwood and J. Pyun, *ACS Macro Letters*, 2017, **6**, 500–504.

(77) J. J. Griebel, R. S. Glass, K. Char and J. Pyun, *Progress in Polymer Science*, 2016, **58**, 90–125.

(78) M. Capelot, M. M. Unterlass, F. Tournilhac and L. Leibler, *ACS Macro Letters*, 2012, **1**, 789–792.

(79) D. J. Parker, S. T. Chong and T. Hasell, *RSC Advances*, 2018, **8**, 27892–27899.

(80) S. J. Tonkin, C. T. Gibson, J. Campbell, D. A. Lewis, A. Karton, T. Hasell and J. M. Chalker, *Chemical Science*, 2020, DOI: `10.1039/d0sc00855a`.

(81) P. J. Landrigan, R. Fuller, N. J. Acosta, O. Adeyi, R. Arnold, N. (Basu, A. B. Baldé, R. Bertollini, S. Bose-O'Reilly, J. I. Boufford, P. N. Breysse, T. Chiles, C. Mahidol, A. M. Coll-Seck, M. L. Cropper, J. Fobil, V. Fuster, M. Greenstone, A. Haines, D. Hanrahan, D. Hunter, M. Khare, A. Krupnick, B. Lanphear, B. Lohani, K. Martin, K. V. Mathiasen, M. A. McTeer, C. J. Murray, J. D. Ndahimananjara, F. Perera, J. Potočnik, A. S. Preker, J. Ramesh, J. Rockström, C. Salinas, L. D. Samson, K. Sandilya, P. D. Sly, K. R. Smith, A. Steiner, R. B. Stewart, W. A. Suk, O. C. van Schayck, G. N. Yadama, K. Yumkella and M. Zhong, *The Lancet*, 2018, **391**, 462–512.

(82) W. T. Pecher, M. Emad Al Madadha, P. DasSarma, F. Ekulona, E. J. Schott, K. Crowe, B. S. Gut and S. DasSarma, *PLoS ONE*, 2019, **14**, 1–15.

(83) D. M. Ramakrishna and T. Viraraghavan, *Water, Air, and Soil Pollution*, 2005, **166**, 49–63.

(84) J. M. O'Neil, T. W. Davis, M. A. Burford and C. J. Gobler, *Harmful algae*, 2012, **14**, 313–334.

(85) L. Tonk, K. Bosch, P. M. Visser and J. Huisman, *Aquatic Microbial Ecology*, 2007, **46**, 117–123.

(86) R. P. Rastogi, D. Madamwar and A. Incharoensakdi, *Frontiers in microbiology*, 2015, **6**, 1254.

(87) S. C. Doney, N. Mahowald, I. Lima, R. A. Feely, F. T. Mackenzie, J. F. Lamarque and P. J. Rasch, *Proceedings of the National Academy of Sciences of the United States of America*, 2007, **104**, 14580–14585.

(88) R. G. Pearson, *Journal of the American Chemical Society*, 1963, **85**, 3533–3539.

(89) P. B. Tchounwou, W. K. Ayensu, N. Ninashvili and D. Sutton, *Environmental Toxicology*, 2003, **18**, 149–175.

(90) T. W. Clarkson and L. Magos, *Critical Reviews in Toxicology*, 2006, **36**, 609–662.

(91) L. Järup, *British Medical Bulletin*, 2003, **68**, 167–182.

(92) M. P. Crockett, A. M. Evans, M. J. Worthington, I. S. Albuquerque, A. D. Slattery, C. T. Gibson, J. A. Campbell, D. A. Lewis, G. J. Bernardes and J. M. Chalker, *Angewandte Chemie - International Edition*, 2016, **55**, 1714–1718.

(93) T. Hasell, D. J. Parker, H. A. Jones, T. McAllister and S. M. Howdle, *Chemical Communications*, 2016, **52**, 5383–5386.

(94) D. J. Parker, H. A. Jones, S. Petcher, L. Cervini, J. M. Griffin, R. Akhtar and T. Hasell, *Journal of Materials Chemistry A*, 2017, **5**, 11682–11692.

(95) S. Petcher, D. J. Parker and T. Hasell, *Environmental Science: Water Research & Technology*, 2019, DOI: 10.1039/c9ew00477g.

(96) M. J. Worthington, R. L. Kucera, I. S. Albuquerque, C. T. Gibson, A. Sibley, A. D. Slattery, J. A. Campbell, S. F. Alboaiji, K. A. Muller, J. Young, N. Adamson, J. R. Gascooke, D. Jampaiah, Y. M. Sabri, S. K. Bhargava, S. J. Ippolito, D. A. Lewis, J. S. Quinton, A. V. Ellis, A. Johs, G. J. Bernardes and J. M. Chalker, *Chemistry - A European Journal*, 2017, **23**, 16219–16230.

(97) A. C. Queiroz Santos, A. Maria de Aguiar Accioly, C. W. Araújo do Nascimento, N. Machado dos Santos, É. E. Chaves de Melo and B. T. de Lima Xavier, *Communications in Soil Science and Plant Analysis*, 2014, **45**, 1499–1510.

(98) J. L. Gardea-Torresdey, K. J. Tiemann, G. Gamez and K. Dokken, *Journal of Hazardous Materials*, 1999, **69**, 41–51.

(99) M. Thielke, L. Bultema, D. Brauer, B. Richter, M. Fischer, P. Theato, M. W. Thielke, L. A. Bultema, D. D. Brauer, B. Richter, M. Fischer and P. Theato, *Polymers*, 2016, **8**, 266.

(100) N. A. Lundquist, M. J. Sweetman, K. R. Scroggie, M. J. Worthington, L. J. Esdaile, S. F. Alboaiji, S. E. Plush, J. D. Hayball and J. M. Chalker, *ACS Sustainable Chemistry and Engineering*, 2019, **7**, 11044–11049.

(101) S. Saikat, I. Kreis, B. Davies, S. Bridgman and R. Kamanyire, *Environmental Science: Processes & Impacts*, 2013, **15**, 329–335.

(102) K. Inoue, F. Okada, R. Ito, S. Kato, S. Sasaki, S. Nakajima, A. Uno, Y. Saijo, F. Sata and Y. Yoshimura, *Environmental health perspectives*, 2004, **112**, 1204–1207.

(103) F. Oliaei, D. Kriens, R. Weber and A. Watson, *Environmental Science and Pollution Research*, 2013, **20**, 1977–1992.

(104) A. D. Tikoalu, N. A. Lundquist and J. M. Chalker, *Advanced Sustainable Systems*, 2020, **4**, 1–9.

(105) J. S. M. Lee, D. J. Parker, A. I. Cooper and T. Hasell, *Journal of Materials Chemistry A*, 2017, **5**, 18603–18609.

(106) M. J. H. Worthington, C. J. Shearer, L. J. Esdaile, J. A. Campbell, C. T. Gibson, S. K. Legg, Y. Yin, N. A. Lundquist, J. R. Gascooke, I. S. Albuquerque, J. G. Shapter, G. G. Andersson, D. A. Lewis, G. J. L. Bernardes and J. M. Chalker, *Advanced Sustainable Systems*, 2018, **2**, 1800024.

(107) N. A. Lundquist, M. J. Worthington, N. Adamson, C. T. Gibson, M. R. Johnston, A. V. Ellis and J. M. Chalker, *RSC Advances*, 2018, **8**, 1232–1236.

(108) J. M. Cohen, L. J. Kamphake, E. K. Harris and R. L. Woodward, *Journal-American Water Works Association*, 1960, **52**, 660–670.

(109) K. Hoehl, G. U. Schoenberger and M. Busch-Stockfisch, *Food Quality and preference*, 2010, **21**, 243–249.

(110) J. E. Dutra-De-Oliveira, J. S. Marchini, J. Lamounier and C. A. Almeida, *Iron-fortified drinking water studies for the prevention of children's anemia in developing countries*, 2011.

(111) N. A. Kinsei, *Journal of bacteriology*, 1960, **80**, 628.

(112) M. J. Hackett and N. F. Gray, *Carbon Dioxide Emission Savings Potential of Household Water Use Reduction in the UK*, tech. rep. 1.

(113) P. W. Sammarco, S. R. Kolian, R. A. Warby, J. L. Bouldin, W. A. Subra and S. A. Porter, *Marine Pollution Bulletin*, 2013, **73**, 129–143.

(114) I. Nechepurenko, *https://www.nytimes.com/2020/06/04/world/europe/russia-oil-spill-arctic.html*, 2020.

(115) M. Mann, J. E. Kruger, F. Andari, J. McErlean, J. R. Gascooke, J. A. Smith, M. J. Worthington, C. C. McKinley, J. A. Campbell, D. A. Lewis, T. Hasell, M. V. Perkins and J. M. Chalker, *Organic and Biomolecular Chemistry*, 2019, **17**, 1929.

Chapter 2

Macroporous Thiopolymers

2.1 Abstract

Much of the work presented in this chapter has been adapted from: 'Macroporous sulfur polymers from a sodium chloride porogen — a low cost, versatile remediation material'[1]

Recent research has demonstrated that it is possible to generate polymers from elemental sulfur and a variety of organic cross linkers using the so called 'inverse vulcanisation' process. The polymerisation is solvent free, self-initiating and has a high atom economy (>90%). A variety of applications have been demonstrated, but the most pertinent is the sequestration of heavy metals. Effective sorbents usually possess a degree of porosity, herein, the generation of a macroporous thiopolymer matrix is demonstrated and tested for its ability to remove aqueous mercury chloride from solution. It was found that the macroporous polymer possessed a capacity of 2.27 mg g^{-1} *(Langmuir fitting) and a surface area of over 15* $m^2 g^{-1}$.

2.2 Introduction

2.2.1 Heavy metal contamination

Heavy metal contamination exists in the waste streams of many industries, such as chemical manufacturing[2], mining operations[3,4], waste incineration[5,6], agriculture[7,8] and fossil fuel fired power stations[9,10]. The emitted heavy metals are extremely harmful environmental pollutants.

Mercury is of particular concern for human health because of its solubility in water and tendency to bioaccumulate and cause adverse reactions in the body.[11] Sources of mercury can be either anthropogenic or natural[12]. The form in which these sources are introduced to the environment are irrelevant, as almost all forms of mercury are harmful and accumulate in sediment, fish, and the groundwater table.

Minimata, Japan is a place in which there are over 2000 registered casualties of dimethylmercury pollution from a local chemical plant.[2] The scale of the incident pushed mercury poisoning to the public eye and as a result the 'Minimata convention' – a global effort to reduce anthropogenic sources of mercury has been signed by over 120 countries.[13]

Mercury is a significant global health hazard, with growing research efforts focused on its remediation from wastewater streams[14]. The ease of application of mercury in small scale gold mining has led to prolific use and now over 25% of global mercury emissions result from this process.[15] Other anthropogenic sources include burning of fossil fuels[16], waste incineration[17], and chemical plants[16]. An important question to consider is that given the widespread pollution, and negative effects on human health, is: should there be a research focus on the remediation of mercury?

2.2.2 Sulfur

The modern petrochemical manufacturing process includes desulfurisation processes.[18] This is because sulfur is contained within crude oil mixtures and can cause acid rain when combusted[19], and other derivative issues such as metal corrosion. The quantity of extracted sulfur results in a large volume of waste material (Figure 2.1). Current industrial uses of sulfur include fertilisers[20], sulfuric acid[21], and carbon disulfide manufacture[22], but the production of sulfur still exceeds demand. The cost of this waste product is approximately the price of shipping. Recently, significant volumes of research have begun to focus

Figure 2.1: A monolithic pile of sulfur, resultant of the hydrodesulfurisation process. Located outside the Alberta oil sands, Canada

on the formation of functional materials from elemental sulfur. One question remains: how are sulfur and mercury intertwined?

Sulfur is a soft Lewis acid, and as such will favourably to donate electron pairs to soft Lewis bases. This idea has come from the HSAB theory, first constructed by Pearson in 1953[23]. 'Softness' and 'hardness' are the extent of polarisability of the electron cloud that surrounds the positive centre of the ion. Therefore, a large, low charge metal ion such as Hg^{2+} would be considered a 'soft' Lewis base. Sulfur in this same sense is considered to be a 'soft' Lewis acid, and the two form favourable adducts. By careful consideration of this idea, it may be possible to form materials that can take advantage of this property. Sulfur in itself is, however, a poorly processable crystalline powder.

Polymeric sulfur is produced *via* the homolysis of sulfur at elevated temperatures and is observable at 159 °C the 'floor temperature' of molten sulfur.[24] At this temperature the S_8 ring undergoes ring opening polymerisation (ROP). Polymeric sulfur is difficult to use, however, because it is thermodynamically unstable and degrades *via* a backbiting mechanism back to S_8 (Figure 2.2). Because of this, so far, uses for polymeric sulfur have been limited.

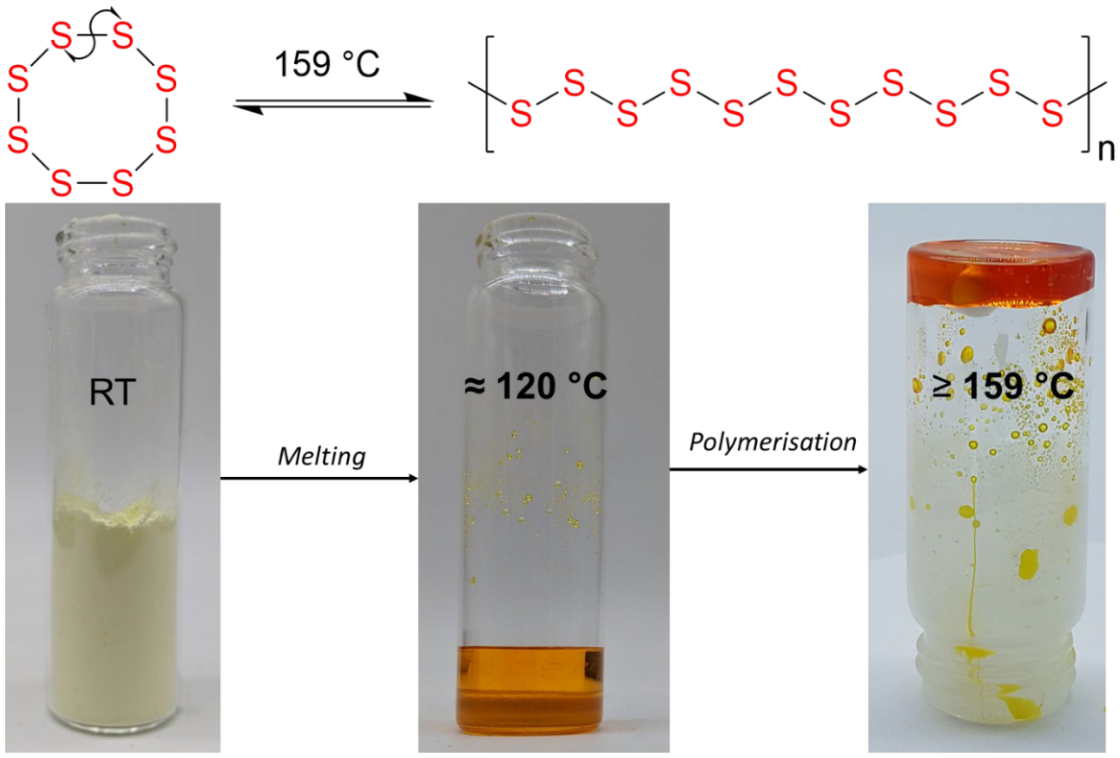

Figure 2.2: Schematic illustrating the melting of elemental sulfur, and subsequent ring opening polymerisation that occurs above the floor temperature, to polymeric sulfur. It is important to note that these processes are fully reversible

2.2.3 Porous Sulfur polymers

Inverse vulcanised polymers are a new class of polymeric materials produced from sulfur and unsaturated organic small molecules. The process was pioneered in the group of Jeffrey Pyun.[25,26] These small molecules, usually dienes, can cross-link and stabilise chains of polymeric sulfur. It is important to note that this process has existed subtly in the literature for many years. Whilst recently, the interest in sulfur polymers is increasing it is, however, possible to trace reactions of this kind back as far as 1975.[27] Through this process enhanced properties are observed such as improved ion sorption[28], processability[29] and stability[30].

Up to 90 wt.% sulfur loading has been demonstrated and yields demonstrated above 90% are regularly achieved.[31] The process is also solvent free, which fulfils one of the principles of green chemistry, alongside the excellent atom economy of the process.[32] As a result of the recent emergence of this class of materials many properties are currently being discovered. Uses that have thus far been demonstrated are: antimicrobial surfaces[33,34], cathode materials[35–37], lens materials[**Griebel2014**, 38–41], novel carbonisation precursors[42],

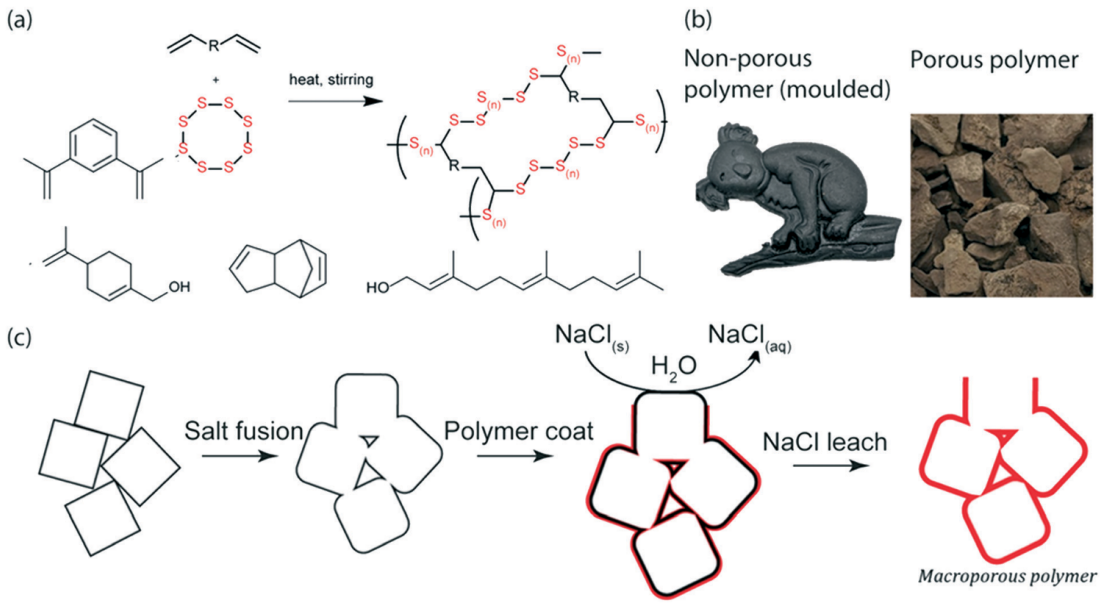

Figure 2.3: (a) Reaction scheme for the research that is described in this chapter (b) Photographs of the non-porous, and porous polymers (c) Schematic illustrating the process of using a sodium chloride porogen to produce a polymer matrix

controlled release media[43], metal ion sorbents[1,44,45], vitrimers[30] and insulation materials[46]. A recent review by Chalker *et al.* detailed many of the applications of inverse vulcanised polymers.[47]

Applications such as those in insulation, controlled release and ion sorption would benefit from porosity. For example, closed cell porosity would benefit applications in insulation and open cell in controlled release and sorption.

Hasell *et al.* first demonstrated the use of supercritical carbon dioxide as a foaming agent, producing a material with a significant fraction of closed cell porosity.[48] However, despite the nature of the porosity the sample still outperformed non-porous samples ground to a powder, and more importantly: elemental sulfur, for mercury uptake.

Thielke *et al.* demonstrated that it was possible to form nanofibres of sulfur polymer mixed with poly(methyl methacrylate) using electrospinning.[44] The fibres were then tested as a mercury sorbent, demonstrating a significant uptake capacity of 327.7 mg g^{-1}. In the wider area of generating macro-porosity in non-sulfur based polymers, there are examples in the literature making use of a technique first reported by Murphy *et al.* in which sodium chloride crystals are used as a template media.[49] This technique was first adapted to sulfur polymers in research by Parker *et al.*[50], as shown in (Figure2.3) Since the Parker *et al.* publication this method has been adapted by several researchers also working on sulfur

polymers. Abraham *et al.* reported a porous sulfur divinylbenzene copolymer produced in this fashion.[46] The produced material was tested for gaseous mercury absorption and performed within the range of commercially activated materials. Furthermore, the material was thermally insulating at levels comparable to commercially available materials. The Chalker research group at Flinders University, Adelaide have demonstrated multiple applications for salt templated porous sulfur polymers: iron sequestration[51], mercury sequestration[28] and oil-water separation.[52] Also, the same research group has explored sulfur polymers as potential controlled release agents for fertiliser.[43]

Herein, the salt template process was investigated and its control of pore size *via* the antisolvent precipitation method. The effect of solvent:antisolvent ratio was investigated and how this effected the subsequent pore size produced in the porous polymer. Further investigations into the versatility of the process were performed by varying the crosslinking agent to both biorenewable and low cost industrial feedstocks.

2.3 Aims

In order to limit the scope of the research to that which is attainable and sensible, the following research aims were set at the beginning of the research:

- Generate a macroporous S-Polymer
- Characterise the textural and morphological properties of the produced material
- Characterise the interactions of the materials with $HgCl_2$ in solution

2.4 Approaches

In this section, an attempt into describing the approaches taken into the formation of porous thiopolymers *via* the use of a solid porogen.

Figure 2.4 demonstrates the process of using a solid-phase template to generate a porous polymeric material. Generally speaking, all that is required is a polymer that may be in the liquid state — solution or melt — that can then be solidified, and the solid-phase template removed. Removal of the template then leaves behind a porous polymer. The porous polymer will have properties that are significantly different from the pure polymer.

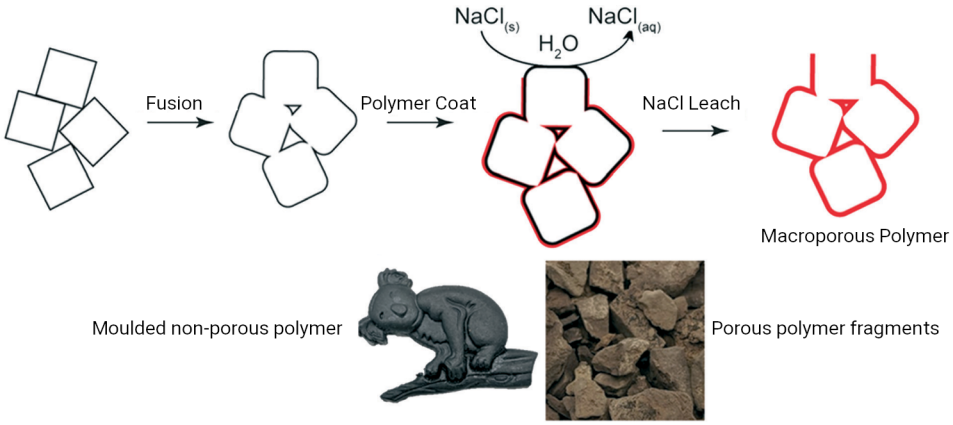

Figure 2.4: Schematic illustrating the process of salt templating to produce a porous polymer. In the scheme the stages of the formation of the porous polymer are demonstrated with first the fusion of NaCl crystals, the subsequent coating with prepolymer and the final stage of porogen leaching. Following this, two images demonstrate the visible difference that is observed at the macroscale when porosity is incorporated into the polymer

However, there are a multitude of variables that can affect the outcome of the process. They include but are not limited to: viscosity of solution, interconnectivity of scaffold, interfacial tension, and extent of intrusion. The viscosity of the solution is simply how 'thick' the resultant liquid is. The interconnectivity is how the pores within the sample are connected, a high interconnectivity would represent a sample where the pores are highly connected and a low interconnectivity would represent a sample with isolated pores. The interfacial tension of the sample represents the interaction of the sample with water, a low interfacial tension would mean that the sample will readily interact with water. The extent of intrusion represents how well water penetrated into the sample. As with most system designs not every variable was important in every system, however it is important to consider them, to ensure that reasons for failure can be investigated.

In the following section, a small discussion around the considerations that were taken into account has been formed. This introduces some reasons for the choices that were made in the experimental method.

2.4.1 Considerations

There are a large variety of solid-phase porogens employed in the literature: paraffin wax[53], polyethyleneglycol[54], glucose[55], and many more[56]. It is important to note, however, that selection of the correct solid-phase porogen is important.

It has been discussed previously that the polymerisation reactions of elemental sulfur often occur at temperatures above 100 °C.[57] This rules out the use of glucose and paraffin wax, as they are liquids at the temperatures that the polymerisation reaction occurs. Furthermore, sugar would react with sulfur unpredictably. Silica would also be out of the question, as it is etched away with basic media; under these conditions, sulfur polymers will degrade.

One potential candidate that has been previously mentioned however is sodium chloride, a high melting point solid that is insoluble in liquid sulfur and conventional hydrocarbons. It is impervious to molten sulfur as well. Furthermore, it is soluble in water. This is important because the leaching process, that is, the process that removes the sodium chloride, requires large volumes of solvent; it would be environmentally inconsiderate to choose an organic solvent in this situation. Sodium chloride is also non-toxic and environmentally benign when disposed of in appropriate places.

To summarise, sodium chloride is an adequate choice for a solid-phase porogen in the synthesis of sulfur polymers due to its chemically inert nature, high melting point, and ease of removal. Hence, in the following chapter it will be investigated in great detail.

Another consideration that must be taken into account for the development of a system for incorporating porosity into the sulfur polymers is the reaction itself. Sulfur is an uncompromisable reagent in the reaction, however the cross-linking alkene is not.

It is well known that in solution polymerisations, and bulk polymerisations that the viscosity of the solution increases as the extent of reaction increases. This can lead to problems; for instance: auto-acceleration. This is a catastrophic increase of rate of reaction that leads to large temperature spikes, and overall system decomposition. This decomposition can be hazardous, in the case of inverse vulcanisation large volumes of H_2S are released.[58]

Inverse vulcanisation reactions suffer from autoacceleration effects. This is because as the reaction progresses, the viscosity of the reaction increases because of the growing polymer chains. At low polymer chain length, termination reactions are highly frequent as the concentration of terminal radicals is high. However, when the conversion levels are

high, these terminal radicals can be considered to be surrounded by a large volume of radically inert polymer. This in turn causes the rapid consumption of monomer, resulting in areas of extremely rapid monomer consumption. This can in turn lead to potentially dangerous thermal runaway. Autoacceleration is easily avoided by adequate stirring, and lower heating. As the viscosity of the reaction medium increases, it will less effectively penetrate into the porous scaffold. Poor penetrations could be avoided by careful selection of a crosslinking agent that produces a reaction profile that allows for the oligomer melt to intrude the porous scaffold.

Prior literature has demonstrated a multitude of reactions with elemental sulfur. Among the fastest of the reactions to progress is 1,3-diisopropenylbenzene. This reaction progresses to completion in ten minutes, according to work performed by Chung *et al.* However, this reaction was performed at 185 °C. It was found in our study that by polymerising 1,3-diisopropenylbenzene at 159 °C the reaction profile slowed down, taking up to 3 hours to gel.

Gelation time is important, when a cross-linked polymer reaches its gel point the polymer will no longer flow. Therefore, all polymers chosen were intruded into the salt porogen prior to the gel point being achieved. The crosslinkers that were chosen for this work were: 1,3-diisopropenylbenzene, farnesol, perillyl alcohol, and cyclopentadiene. The resultant polymers: poly[1,3-diisopropenylbenzene-(*ran*)-sulfur] (S-DIB), poly[farnesol-(*ran*)-sulfur] (S-FSOL), poly[perrilyl alcohol-(*ran*)-sulfur] (S-PA) and poly[dicyclopentadiene-(*ran*)-sulfur] (S-DCPD) were investigated in this body of work.(Figure 2.5) In summary,

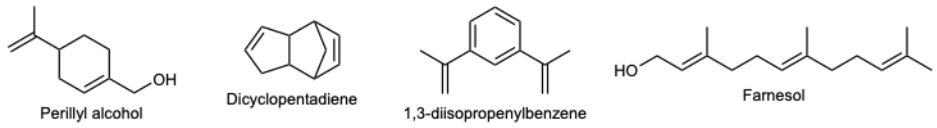

Figure 2.5: Crosslinkers that were chosen for this study: perrilyl alcohol, dicyclopentadiene, 1,3-diisopropenylbenzene, and farnesol

crosslinking agents that had relatively slow reaction profile were chosen. The reactions profiles were investigated in separate bodies of work, such as 'Catalytic Inverse Vulcansation' reported by Wu *et al.*[58] Furthermore, a lack of gel state in the crosslinking agent was another criteria, as this would also prevent intrusion into the porous scaffold. Therefore, crosslinking agents were selected carefully and tailored for the intrusion of the polymerisation mixture into the scaffold.

2.4.2 Sodium Chloride Porogens

A porogen is best defined as an agent that can impart a degree of porosity onto an object.[59] Usually, porogens are a solid scaffold that a liquid polymer is able to form around which is then in turn transformed into a solid, whether by evaporation or solvent or curing. Upon forming a composite, it is then subjected to a leaching process in which the original porogen is removed, leaving behind a porous structure of the desired material. (Figure 2.3) Since the inception of this idea many methods of intrusion into the porous scaffold have been explored, such as: chemical vapour deposition[60], solvent intrusion[61], melt intrusion[46] and others.[62]

In a general sense there are several key requirements for a porogen to successfully form a porous monolith in the process, and they are as follows:

1. The porogenic material must have a shape-persistency and chemically inert nature when it is subjected to the reaction conditions. Without these properties, the structure that is used to form the porous network will collapse and fail to impart porosity on the final object.

2. The porogenic material must have a suitable solubility in something that is not solubilising or chemically reactive with the produced material, if this condition is not met the material will simply degrade in the leaching process.

Therefore, for the formation of a porous network in inverse vulcanised polymers the porogen should have a suitably high thermal stability (>200 °C, in order to cover the range of reported polymerisation temperatures) and naturally be chemically inert to the curing process of the polymers.

A common porogen that has been explored in the literature is sugar, but this porogen would not be appropriate as decomposition temperatures are low (180 °C), and some groups may be amenable to attack by the species present during the polymerisation reaction. However, water solubility is a preferable characteristic for the leaching process.

One of the first materials considered for this process was sodium chloride (NaCl), NaCl has high water solubility, is chemically inert to the reaction process and melts at 801 °C.[63] Because of this NaCl was chosen as a pore forming agent for the research.

Initially, the porogen process inspiration was drawn from a paper published by Murphy *et al.* in which they fused sodium chloride crystals in a humidity oven to form a continuous

object comprised of sodium chloride[49].

When using this NaCl fusion process, it was found that the object formed a solid white monolith that was clearly visually made up of fused NaCl crystals. Having formed the monolithic porogen the next stage was to develop a way of coating the porogen with the polymer.

Most sulfur polymers are known for their lack of solubility in all solvents, due to their cross-linked and thermoset nature.[50] This lack of solubility limited the options for the coating of polymer onto porogen, making the most practical route melt intrusion. To accomplish this, the monolith simply was immersed in prepolymer, and then placed into an oven for curing. To define prepolymer in more specific terms, it can be regarded as a homogeneous mixture of sulfur, oligomers, and cross linker that has begun to react but is not at the stage that it is solid. As conversion increases a gel state is formed and in this stage the mixture can be considered to lie further on the polymer spectrum and away from the oligomer, sulfur and cross linker side. After the sodium chloride matrix absorbed the prepolymer melt, it was placed in an oven and allowed to cure at 140 °C for 12 hours. When removed, the polymer-porogen composite was placed into a beaker of distilled water and the sodium chloride allowed to dissolve into solution. As can be seen in Figure 2.6 the resulting morphology was indicative of an open, interconnected porosity. Due to lack of equipment, no information regarding the specific surface area was ever acquired. Despite this, it is certain that the materials' porosity was interconnected to an extent because water could flow through it, as confirmed by laboratory testing. It was also found by Archimedes principle that the material had a porosity of 95%.

Given that the process worked for sodium chloride as provided, it was decided to next explore the possibility of miniaturising the pores, which would have the effect of increasing the specific surface area of the produced porous material. Initially, this was accomplished by decreasing the size of the produced sodium chloride crystals, then fusing them to produce a monolith with smaller crystals. The resulting monolith could then produce a polymer matrix with a smaller pore size.

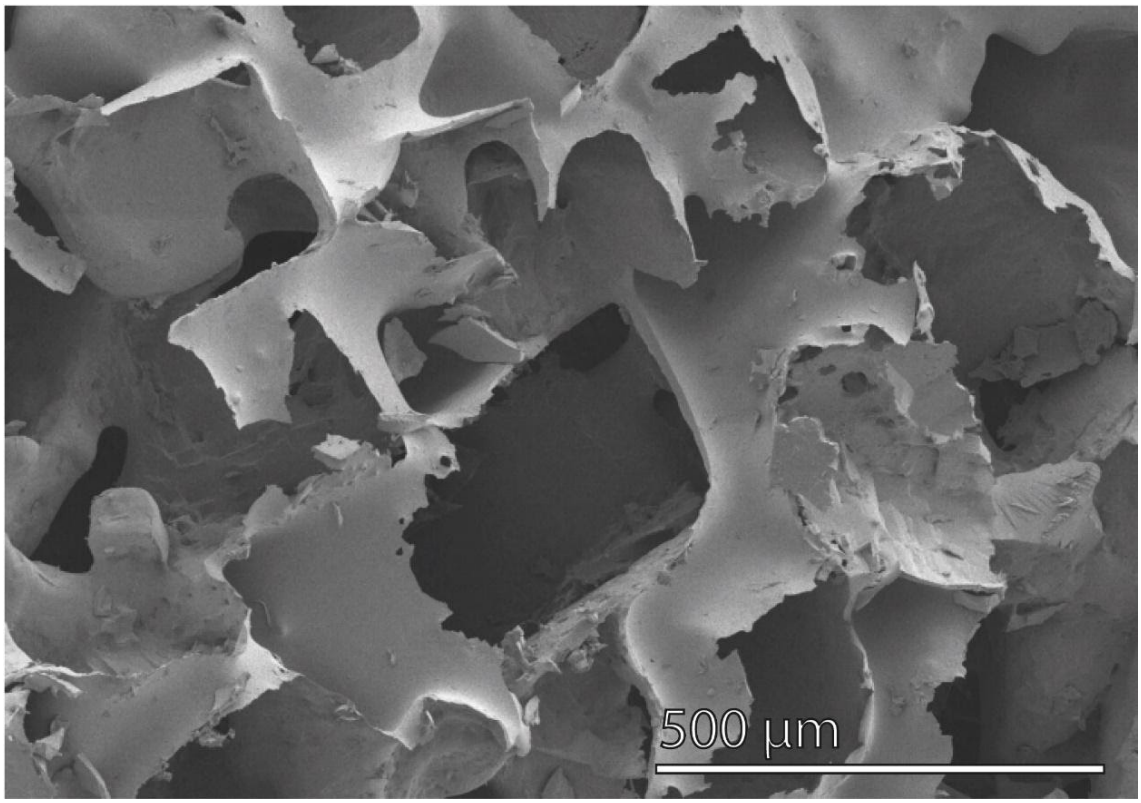

Figure 2.6: SEM micrograph demonstrating the morphology produced when using sodium chloride as a porogen to generate a porous polymer

2.4.3 Miniaturising Sodium Chloride Porogens

Temperature induced precipitation

When designing the experiment that intended to decrease the size of the sodium chloride crystals, it was intended to make use of the fact that sodium chloride can precipitate from solution. Initially, it was decided to employ temperature induced precipitation, wherein, a hot saturated solution of sodium chloride will precipitate when cooled. However, when attempting this process for the first time, we discovered that the process was lacking in several areas:

1. Percentage recoveries were less than 1%, this made the applicability of the process for large scale production incredibly poor
2. The morphology of the produced sodium chloride crystals was not regular
3. It was almost impossible to exert a degree of control over the process, due to the fluctuating temperature of the equipment used

An example of the morphology produced is demonstrated below in Figure 2.7, from a

lower magnification (top) it appears that there is actually a complete lack of crystillinity. This would, however, be a very unlikely situation as solid sodium chloride has never been demonstrated to have an amorphous polymorph.

At a greater magnification, Figure 2.7 reveals the crystal habit of the sodium chloride that precipitated from solution. Whilst the size of the precipitant crystals were small, they show a low degree of apparent porosity. It was important that the produced scaffold possessed a degree of porosity in order to subsequently produce porosity after removal from the produced composite. Because of this, it would be safe to assume that the particles that were produced in this way would be poor for use a porogen. In work published by Tran *et al.* they do not publish a value for the yield that was observed in their experiment. Therefore, it is impossible to compare.[64]

Therefore, it was decided to explore an alternative avenue of research when looking to find a method for the generation of a sodium chloride porogen with smaller pore sizes. The next method considered for the further miniaturisation of the sodium chloride crystals was using an antisolvent to precipitate the sodium chloride from solution.

Antisolvent Precipitation

Firstly, a saturated solution of sodium chloride was formed, then from this solution an aliquot was taken. This aliquot was then poured into ethanol, with stirring. Immediately, a white precipitate of sodium chloride was observed.

The sodium chloride precipitate was then separated from the filtrate and dried in an oven. Upon drying, a monolith immediately formed. By careful variation of the amount of ethanol that was used to precipitate the sodium chloride from solution, several effects were observed. The effects will be discussed in the following sections.

2.4.4 Morphology of antisolvent precipitated sodium chloride

Figure 2.8 contains three micrographs produced using SEM. These micrographs illustrate the dependency of sodium chloride crystal size on the amount of ethanol used in the precipitation process.

When the ratio is 50 : 50 ethanol:brine, such that a 100 mL saturated solution of sodium chloride in water is added into 100 mL of ethanol, the precipitant sodium chloride crystal size is much larger than that for a ratio of 90 : 10 ethanol:brine. This is evident in

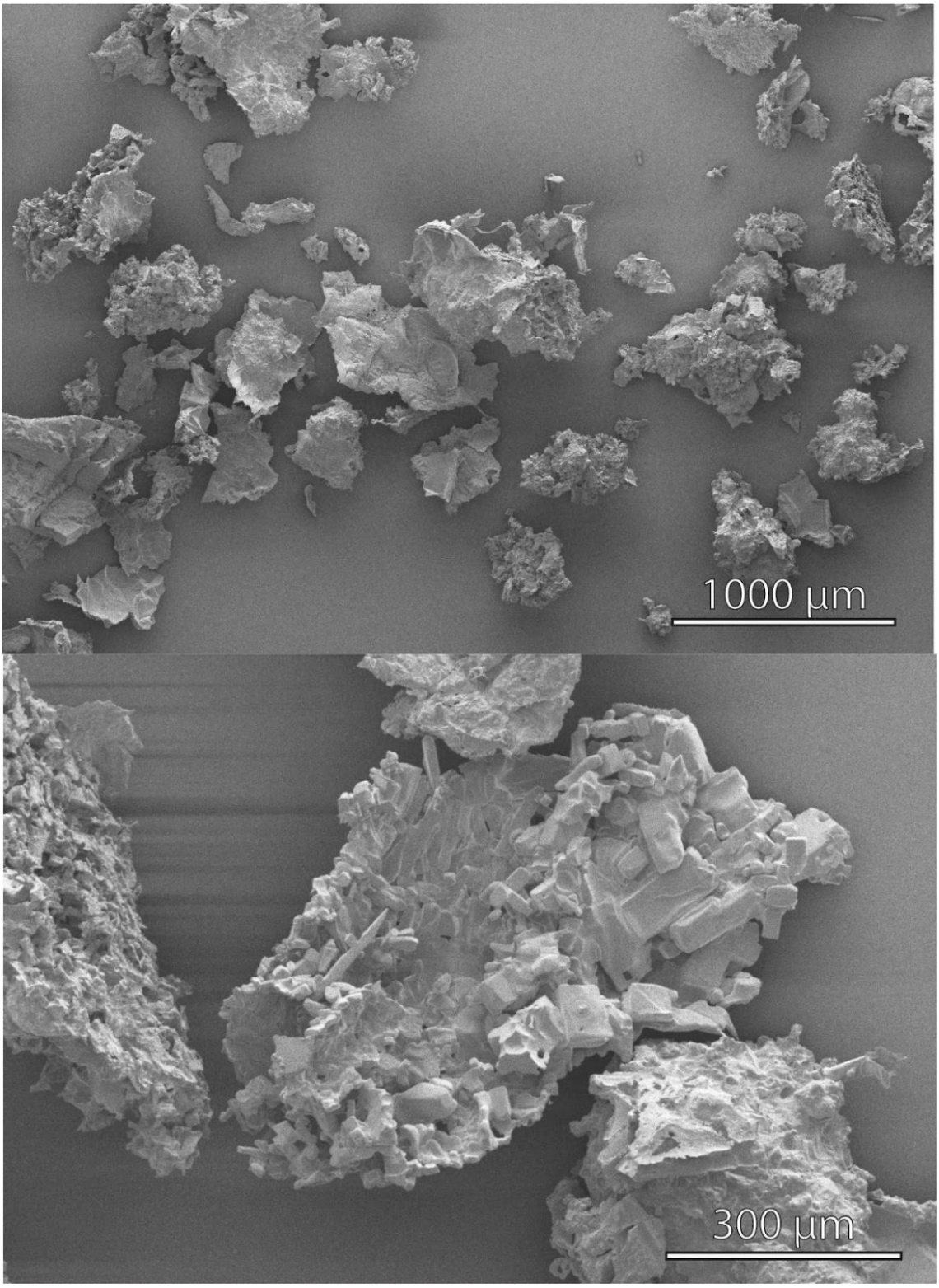

Figure 2.7: SEM Micrograph of the sodium chloride crystals produced in temperature induced crystallisation. At a lower magnification (top) there is no apparent cubic crystal habit, but this becomes visible as the field of view is decreased in size (bottom)

the micrographs.

A facet that is of particular interest, and relevance, is the edges of the cubes. Careful observation reveals that the edges of the crystals of sodium chloride are fused. This fusion allows for an open, interconnected structure. Usually, solid porogens employ the results of percolation theory, which is a mathematical theory that can be applied to geometric objects arrayed randomly in space and the resultant void spaces that they produce[65]. This is inherently complicated, and can be avoided when the porogen is fused.

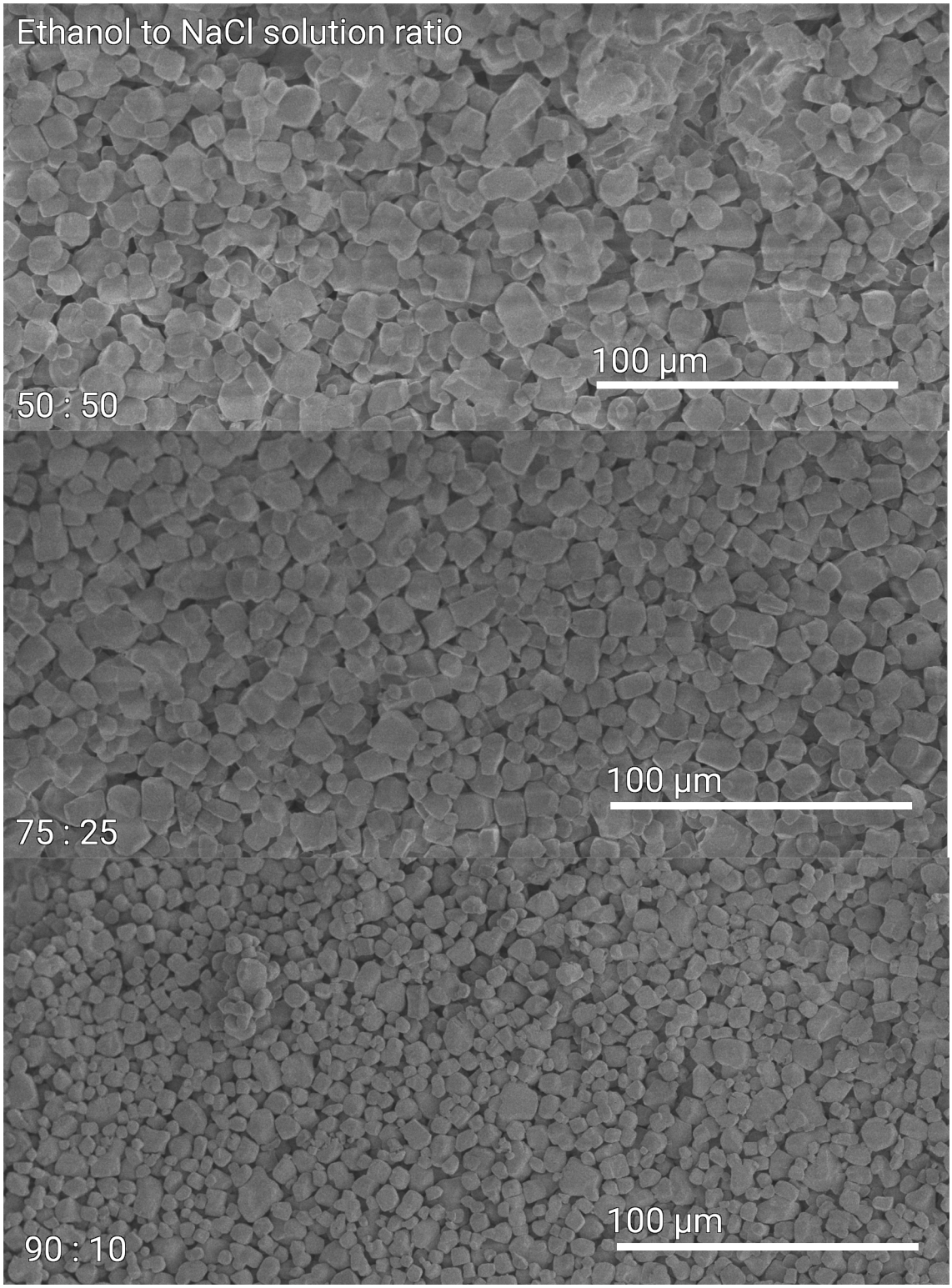

Figure 2.8: Three micrographs produced through the use of SEM (labelled) demonstrating the effect of varying the sodium chloride solution:ethanol ratio (volume) in the final mixture.

Particle sizing

Particle sizing was a somewhat complicated matter. The produced materials would be a poor candidate for dynamic light scattering when in their dispersed state, as they are too large. Furthermore, use of laser diffraction to analyse the particle was impossible as the loading of the particles was too great, and the particles lacked a spherical morphology.[66]

Therefore, it was decided to opt for a method that is more laborious. Several micrographs were taken from each sample, and from each micrograph 100 crystals were measured using the scale bar as a reference point. 300 particles were sized per sample, they were used to generate a histogram.

It turns out that the effect miniaturising the pores was also serendipitous with the effect on the size of the precipitant sodium chloride crystals. Both properties are desirable, a higher yield and smaller pores. As can be seen below, in Figure 2.9 the transition between a 50 : 50 (ethanol : NaCl solution) precipitation and a 75 : 25 is much smaller than that of a 75 : 25 and a 90 : 10 precipitation mixture is much larger.[67]

Looking at the distribution plots that were obtained for the generated materials, it can be observed that as the percentage ethanol is increased in the final mixture, a smaller particle size precipitates from the mixture. This does not eliminate the generation of larger particles. It is important to note that in the case of the 90:10 sample, the size of the particles appears to be negative. This is not the actual case, as it is physically impossible. The nature of the calculation for the distribution of the curve that is displayed is centred around a median value. The plot was a more visual way of displaying the bins of data that were generated.

As demonstrated in (Figure 2.9) a smaller particle size results as the proportion of ethanol in the final mixture is increased. This is likely explained by the fact that as the sodium chloride solution is added into the ethanol, a metastable supersaturated sodium chloride solution is produced. A lower solubility in the resultant mixture increases the rate of crystallisation and this increased rapid crystallisation results in the formation of smaller crystals.

Sodium chloride is highly soluble in water (360 g L^{-1}).[68] However, its solubility in Ethanol is very low (0.513 g L^{-1}).[68] When the saturated solution of sodium chloride in water is added to the ethanol it is found that a precipitate of sodium chloride is formed. It has been shown that in mixtures of ethanol and sodium chloride the solubility decreases

as the amount of ethanol added is increased.[68] Therefore, when the solution of sodium chloride in water is added to the ethanol a metastable solution results. The metastability of the solution collapses almost immediately, and the sodium chloride precipitates from the solution. How quickly the precipitation occurs determines the size of the produced crystals. A quick precipitation will produce smaller crystal sizes and a slow precipitation will produce smaller crystal sizes.[67]

Yields

The effect of precipitant ethanol on the percentage recovery of sodium chloride is demonstrated in Figure 2.10, in which a positive linear relationship between the amount of added ethanol and the precipitant sodium chloride was demonstrated. This is most simply attributed to the insolubility of sodium chloride in ethanol. As brine is added to ethanol, the solubility of the sodium chloride in the resultant solution will lower. The result of this is the sodium chloride will then precipitate from solution.

Given that it had previously been observed that at a higher ethanol concentration more porogen was produced and that a smaller particle size was produced, it was decided that this was to be the chosen formulation. It followed that smaller porogen morphology would produce smaller pores, and hence, a higher specific surface area. Therefore, for applications where specific surface areas are required to be high, the 90 : 10 ratios of ethanol to sodium chloride solution would be ideal.

2.4.5 Generating a porous polymer

Generation of the porous polymer is achieved *via* removal of the sacrificial template. Polymers generated from sulfur are generally not soluble in water bar a few examples in the literature.[69] Sodium chloride is soluble in water.[68] Therefore, by dissolving the sodium chloride in water, the remaining polymer will have the imprint of the sodium chloride crystals left behind. This residual porous polymer is referred to as the polymer 'matrix'.

The polymer matrices were generated from 50 wt% polymer and 50 wt% sodium chloride. This was an arbitrary choice made as because investigation of these ratios has been performed before in the literature, and was beyond the scope of the research being performed. The formed composite material was analysed *via* energy-disperive X-ray spectroscopy (EDS).

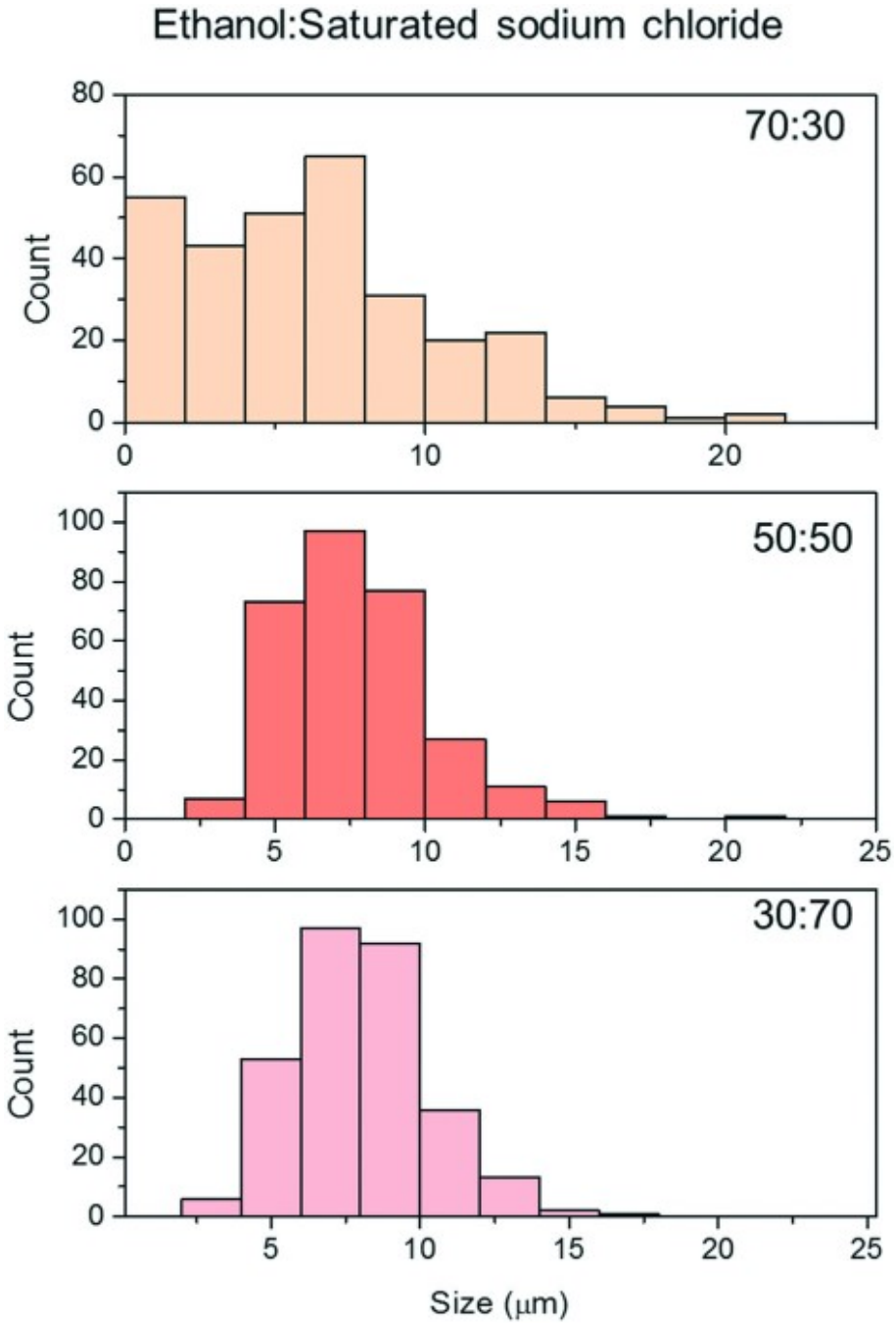

Figure 2.9: Set of histograms demonstrating the result of counting the longest exposed face of 200 sodium chloride crystals from micrographs of precipitant sodium chloride. Demonstrates that as the proportion of ethanol is increased in the final mixture the size of the crystals produced decreases.

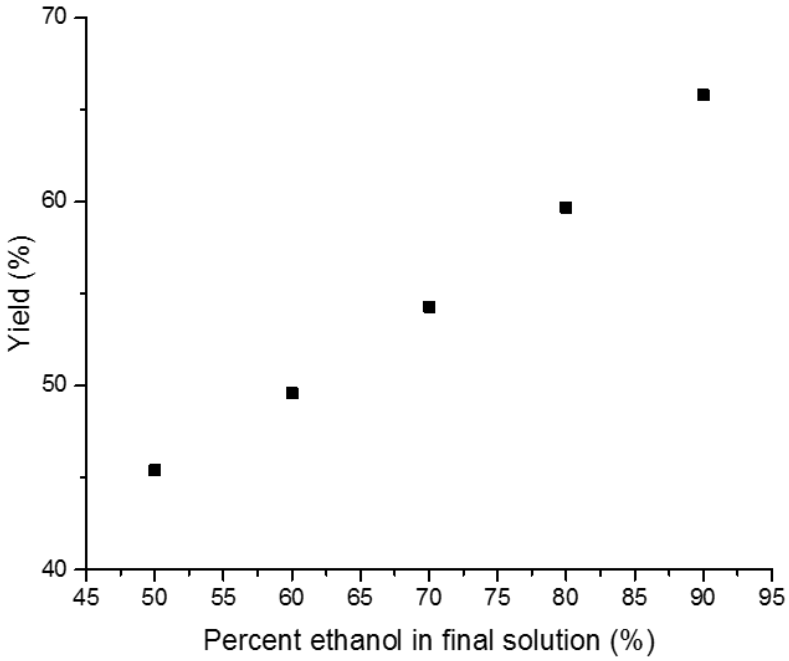

Figure 2.10: Graph demonstrating the percentage recovery of sodium chloride from aqueous solution as a function of percentage of ethanol present in the final mixture

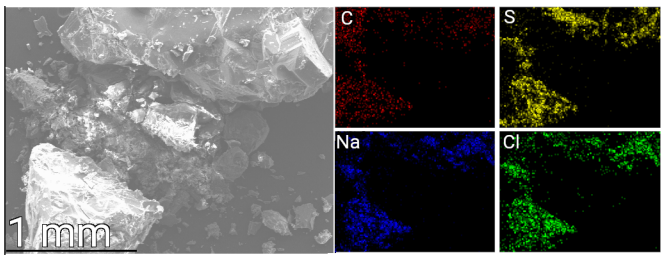

Figure 2.11: (Left) SEM Micrograph demonstrating a particle of the composite sulfur polymer and sodium chloride material (Right) EDX mapping of the same particle demonstrating the inclusion of Na, Cl, S, and C.

EDS revealed the inclusion of sodium, sulfur, carbon, and chlorine in the sample. The morphological separation of the phases is evident and is confirmed by pXRD patterns.

Removal of the sodium chloride template was first achieved *via* soaking in distilled water. This was not very successful, removal of sodium chloride was slow and incomplete. It transpired that produced polymers (S-DIB, S-DCPD, S-PA, S-FSOL) were quite hydrophobic. Whilst no study into the residual sodium chloride was performed, Na and Cl were detected in the ICP-OES spectra when performing mercury sorption experiments. Penetration of the water into the sample was problematic at the outset of the research. Several methods were implemented for the removal of sodium chloride for the polymer.

The first of which was to evacuate the composite material comprised of polymer and NaCl in a round bottom flask with distilled water. This appeared to help the removal of sodium chloride, but did not entirely remove it from the composite. Utilising solvent combinations such as methanol and water to lower the polarity of the solvent was also attempted. This, however, had the unintended effect of partially dissolving some lesser cross-linked polymers. In the interest of keeping the methodology general, it was decided to try a different technique to remove the NaCl.

Attempts were made to remove the sodium chloride from heated water. The surface tension of water decreases linearly — to an extent — as a function of temperature.[70] It was hypothesised that by soaking in boiling water, the water would more effectively penetrate into the porous network and removal a greater amount of sodium chloride. Unfortunately, this boiling water and action of stirring also broke the porous sulfur polymer into pieces.

It was hypothesised that the action of the movement of the template against its containing vessel was the cause of the fragmentation. Sulfur polymers are hard and brittle. These mechanical properties combined with the porous nature of the material make them easy to break. To test this hypothesis, a more gentle approach was considered: Soxhlet extraction. The use of this technique proved invaluable, removal rates of sodium chloride were generally above 95%. Other techniques were considered such as: use of surfactants, solvent mixtures, and even reduced pressure soaking. Overall, Soxhlet extraction proved the most effective technique for the removal of the sodium chloride from the composite formed of sodium chloride and polymer.

Verification of removal of sodium chloride from the polymer composites was achieved *via* several means. The first of which is thermogravimetric analysis. Previously, it has

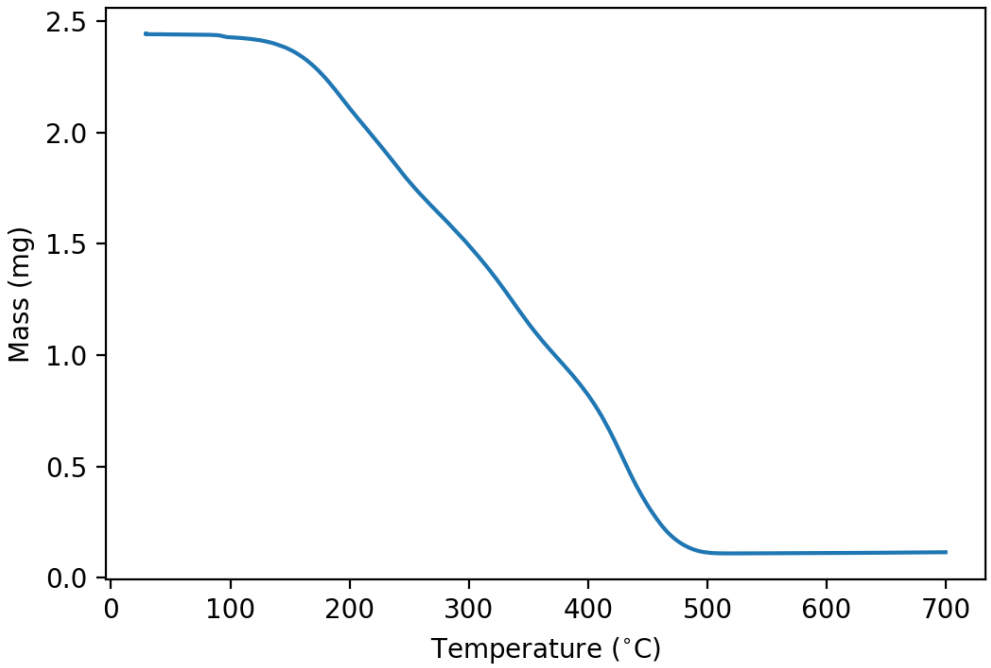

Figure 2.12: Thermogram demonstrating remaining mass of sodium chloride after all polymer was oxidised to gaseous form.

been demonstrated that all sulfur polymers are able to be fully decomposed into gases at temperatures above 500 ° C.[50] Therefore, when the polymer matrix was placed into a thermogravimetric analyser (TGA) under a flow of air, all polymer will degrade into gases above 500 °C. Sodium chloride will, however, be unaffected by this process. It follows that the residual mass in this case will be sodium chloride. This was checked *via* X-ray diffraction. However, the detection limits for pXRD and DSC are quite similar (0.5%-5%) depending on the instrument.[71] An example of a TGA thermogram is shown below, in Figure 2.12.

It can be seen that there are two distinct regions in the thermogram displayed in Figure 2.12. The first decomposition occurs just above 200 ° C. This is often attributed to the decomposition of long sulfur chains in the polymer. As these polymer chains decompose into sulfates, there is a remaining carbonaceous region.

The carbonaceous decomposition begins at 500 °C. It is interesting to note that there is a slow intermediary decomposition phase in this thermogram. This is most likely an artefact of the high heating rate of the TGA, and could be removed by decreasing the rate of heating. Interestingly, research has demonstrated that this carbonaceous region is still

somewhat enriched (10-20 %) with sulfur, and has applications[42].

The final part of the thermogram is the residual mass. This has been demonstrated to be sodium chloride *via* pXRD. It can be seen here that the residual mass for a porous polymer generated from perillyl alcohol, a diene used in this research, is around 2.001%.

Crosslinker	**Residual Sodium Chloride** (% wt)
poly[S-*ran*-(perillyl alcohol)]	2.001
poly[S-*ran*-(1,3-diisopropenylbenzene)]	0.9807
poly[S-*ran*-(farnesol)]	7.430
poly(S-*ran*-(dicyclopentadiene)]	4.565

Table 2.1: Residual sodium chloride masses when placed in a TGA under a gas flow of air heating at a ramp rate of 10 ° C per minute, holding at 700 °C for half an hour

Table 2.1 demonstrates the variation in residual salt masses for the polymers. There is a relatively large difference in residual sodium chloride for the polymers. This is attributable to the occurrence of regions of occlusion. It is possible that during the curing process, entire regions of sodium chloride become entombed with polymer. This polymer is then insoluble, and impermeable to water. This makes the sodium chloride impossible to remove.

As may be seen, it is possible to include and almost completely remove sodium chloride from an inverse vulcanisation reaction. This has been demonstrated by the use of crystalline detection (pXRD), and thermogravimetric means (TGA). However, it has been stated that this generates a porous network. This, however, has not been proven. In the following section 'Structure and properties' characterisation of the porous polymer will be explored. Following this, there will be exploration into characterisation of the polymer itself, before an exploration of the applications of porous polymers produced in this regard.

2.5 Structure and Properties

This section has been split into two subsections that are mostly characterisations of the porous network, and polymeric material itself. While the previous sections has been concerned with the characterisation of the process of forming a porous inverse vulcanised polymer, this section is concerned with the porous sulfur polymer formed.

Textural Characterisation

Characterisation of macroporous materials is limited in that the main method for textural characterisation of porous materials is considered to be mercury porosimetry. Textural characteristics are those that relate to the surface area and the porosity that results from the suprastructure of a material.[72]

Mercury porosimetry works under the principle that liquid mercury is a non-wetting fluid. No matter the surface — disregarding those reactive — mercury will exhibit a high degree of inter-facial tension. This is because in mercury the cohesive forces that exist between the atoms are much greater than the adhesive forces between mercury atoms and the adhering surface.[73] Therefore, by exerting an external pressure on a sample submerged in liquid mercury, a degree of intrusion will be experienced by the sample.

Smaller pores require a greater force of intrusion. By modelling pores as cylinders, it is possible to generate a pore size distribution for a given sample.[74] Naturally, however, not all pores are cylindrical and this is a limitation of the technique.

Furthermore, in some sample, exertion of a high degree of external pressure can begin to deform the sample. When the sample becomes mechanically deformed, it will no longer provide the correct response to generate a pore size distribution. It has been argued that even in the case that deformation occurs, mercury porosimetry can still yield viable results.[75]

Despite these facts, mercury porosimetry is the only technique that can be used to characterise the textural properties of a macroporous material. Figure 2.13 demonstrates the graph that is obtained upon processing the data that is obtained from this type of experiment. From Figure 2.13 it can be seen that there are a large amount of pores in the 5-12.5 μm region. There are also some smaller pores centred around the 1 μm region, with a very small spike in the region that is apparent for microporosity. These micropores were not evident when a N_2 isotherm was performed. As mercury porosimetry is more sensitive to porosity in this region, this data was discarded as an artefact.

Table 2.2 displays properties collected from the mercury intrusion experiment. The first of which is the pore area, it can be seen that the pore area is 15.891 $m^2 g^{-1}$. This pore area is more commonly known as the *specific surface area*.

The intrusion volume is another property that is gleaned from the mercury intrusion experiment. This value is more widely known as the *specific free volume* of the sample.

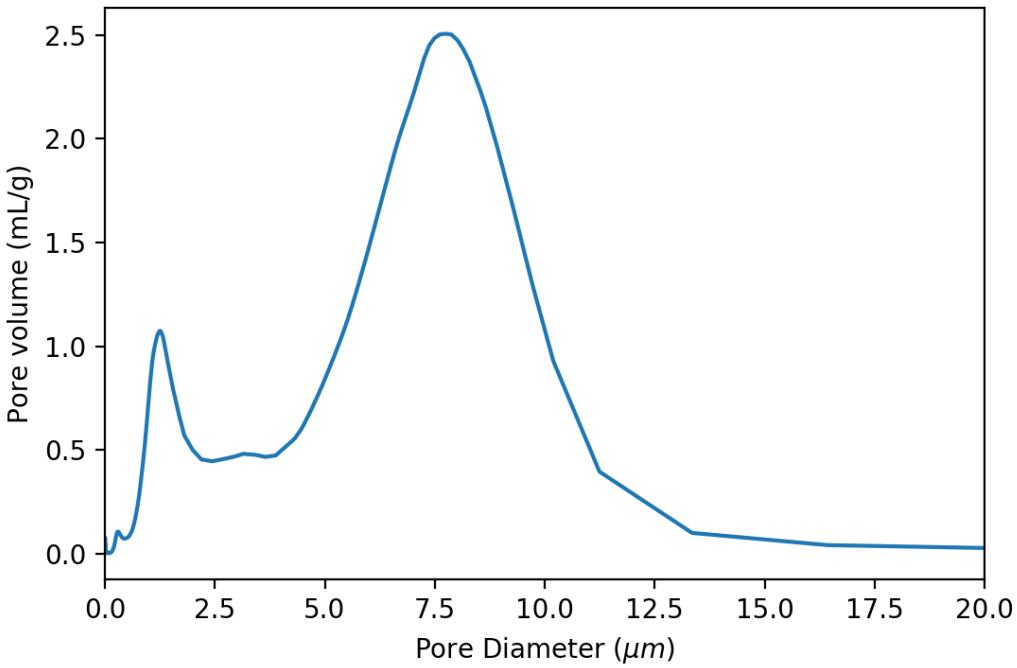

Figure 2.13: Graph generated from mercury porosimetry results. (S-DCPD) It can be seen that there is a large amount of pores responsible for the free volume in the sample in the 7.5 μm region, with a small amount of pores that are smaller, and a large amount of larger pores

The physical presentation of the intrusion volume is simply the summation of the volumes of the pores that are contained within the sample.

The bulk density should be considered as the density of the object as a whole, therefore, it would be lower than that of pure, non-porous polymer. The skeletal density is the density of the 'skeleton' of the porous area, in the case of a composite material this could be considered indeed to be the average density of many components. However, as the 'skeleton' is pure polymer, it is the density of the polymer.

Compressibility is a property that is not widely implemented in the field of polymer chemistry. However, it is often used in an industrial setting for investigations into the physical characteristics of coal and derivatives.[76,77] Searches of the literature return very little information. It is a property that is resultant of the theories that are encapsulated in the field of fluid dynamics. It is related to the ability of a material to deform. Of the most common materials, the material with a compressibility value that is most similar to this porous S-DCPD is glass.[78]

Overall, quantitative characterisation of textural information was performed by mer-

Property	Value
Pore Area	15.891 m^2g^{-1}
Intrusion Volume	1.25 mL g^{-1}
Average Pore Diameter	0.30420 μm
Bulk Density	0.5092 gcm^{-3}
Skeletal Density	1.3258 gcm^{-3}
Compressability	0.446 GPa

Table 2.2: Table summarising the properties that were extracted via *use of an intrusion experiment. (S-DCPD) It should be noted that many of the important textural properties, and several unrelated, were discovered through these techniques*

cury porosimetry. This technique is not widely employed in the field of polymer chemistry, but provides a number of insights into the properties of produced materials such as: density, pore area, pore volume, and compressibility of the produced material. In the following pages, discussion of the morphological characteristics of the produced polymer will be explored.

Morphological Characterisation

Morphological characterisation of porous materials is often performed using microscopy. Of the many branches of microscopy, the one that is the most applicable for macroporous materials is SEM. Optical microscopy would also be an acceptable form of analysis, but would lack the depth of field that is possible with electron microscopy. Transmission electron microscopy would most likely damage the sample, due to the high acceleration voltages that are employed in the excitation and transport of electrons through the sample.

Previous discussion highlighted that four separate organic cross-linking agents would be explored in the fabrication of macroporous sulfur polymers: 1,3-diisopropenylbenzene, farnesol, perillyl alcohol, and dicyclopentadiene. While their involvement in the research has sparsely been highlighted in the preceding pages owing to their lack of importance in the formation of a porogen; the following chapters will begin to describe some subtle morphological differences that result from their employment in the formation of a porous polymer.

It can be seen from Figure 2.14 that while the overarching morphological characteristics persist regardless of the choice of cross-linking agents; there are subtle difference in the smaller shapes that are present. These are most likely due to several factors: overall extent of reaction, viscosity profile of the polymerisation, and even the mechanism of reaction.

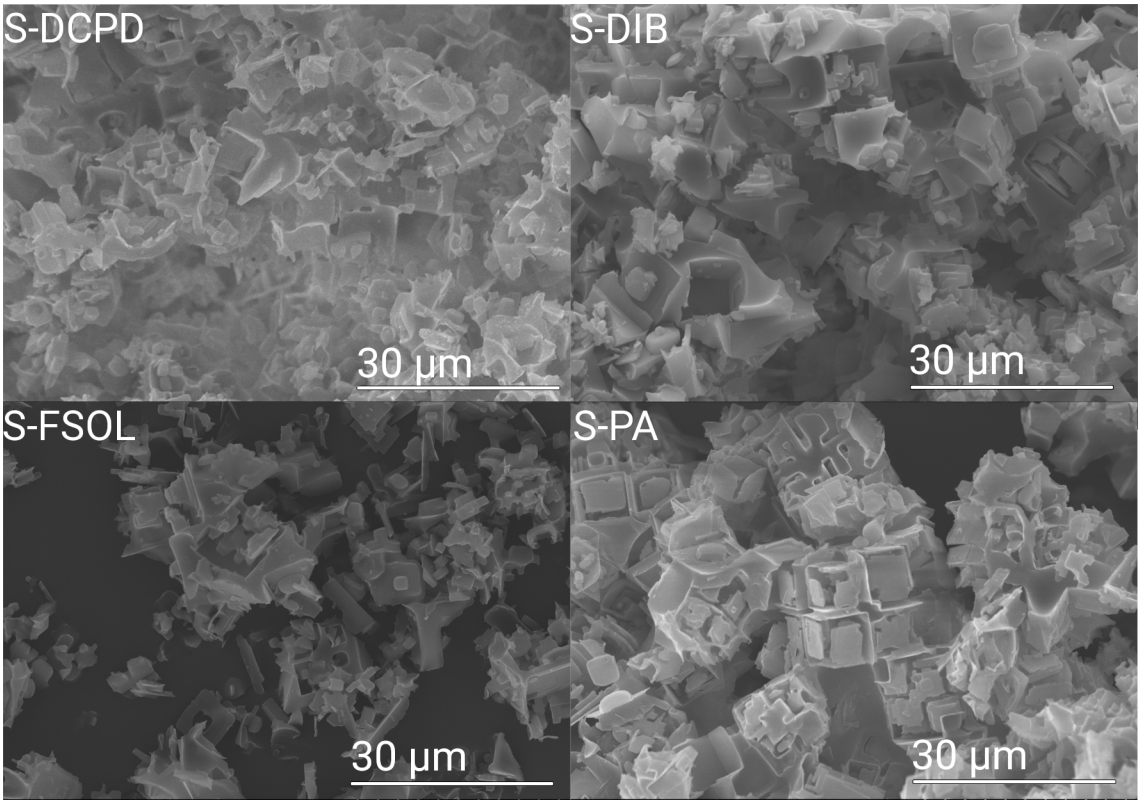

Figure 2.14: SEM micrographs showing the morphology induced by the salt templating process on the fabircation of porous sulfur polymers

A particularly interesting example would be the result of the fabrication of porous poly[S-*ran*-(perillyl alcohol)]. This fabrication attempt produced granules of porous material, a few millimetres in diameter, whereas all others produced a monolith.

This formation of granules is most likely due to the formation of a fraction of low M_w species that are liquid, and unable to hold the higher M_w species together, resulting in the physical degradation of the monolith into smaller pieces.

Overall, it would be prudent to say that the textural and morphological characterisation of the porous polymers provided a degree of agreement. It is possible to measure the pore throat size using imaging software, or a ruler and a calculator. These sizes demonstrated *via* SEM agree with the throat sizes demonstrated in the intrusion experiments. In the following section there will be discussion of the characteristics of the produced material, its thermal stability, and chemical properties.

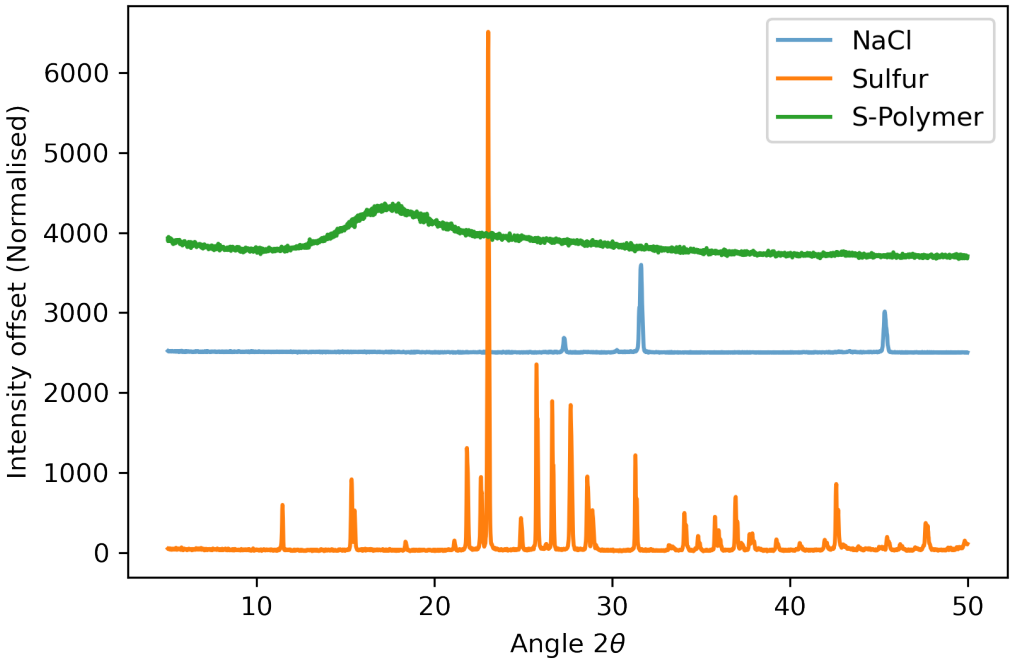

Figure 2.15: pXRD pattern demonstrating the crystalline reflection of monoclinic crystalline sulfur; body centred cubic sodium chloride; and amorphous polymer

Polymer Characterisation

While polymers produced in this body of research have been previously reported, none had been subjected to the process of using a porogen to direct their curing shape. Therefore, characterisation was performed to verify and cross-reference with results that had been previously reported in the literature to confirm successful polymerisation.

Firstly, analysis of sulfur, sodium chloride, and the polymer matrix itself was performed. This analysis allowed for the verification that there was no crystalline sulfur, or crystalline sodium chloride contained within the sample.

(Figure 2.15) displays the previously discussed powder patterns. The peaks in the pattern arise from the constructive interference of incident monochromatic X-rays on a sample. From these incident X-Rays, it is often possible to infer the molecular structure of a material. However, as sulfur polymers are entirely amorphous it is only possible to confirm the *absence* of crystallinity, and the presence of crystalline S_8 would confirm incomplete polymerisation.

Sulfur polymers are highly cross-linked, solid state materials. They have a demonstrable lack of crystallinity as polymers, and this is owing to their cross-linked nature. The

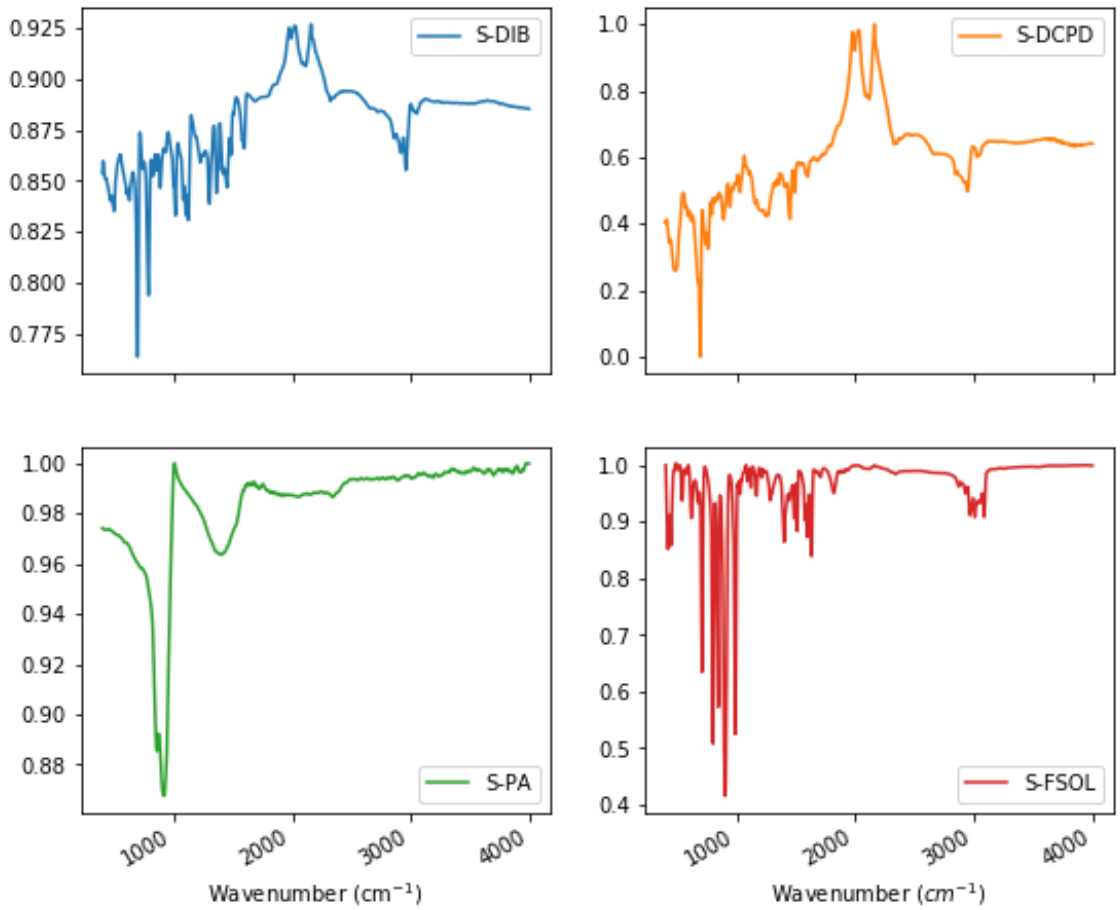

Figure 2.16: FTIR spectra of S-DIB (top left), S-DCPD (top right), S-PA (bottom left), S-FSOL (bottom right)

impurities that are being detected are, however, crystalline. This crystallinity is hence diagnostic of either incomplete reaction of sulfur, or improper removal of sodium chloride. As we can see only an amorphous 'hump' that arises from the short range order in the sample, we know that there is no remaining crystalline sulfur, and sodium chloride.

Given the insolubility demonstrated by these materials, it is often impossible to get meaningful solution based nuclear magnetic resonance (NMR) spectra, and hence information on the precise chemical environments in the polymers. It is, however, possible to garner information regarding the chemical functionality by the use of Fourier transformation infra-red spectroscopy (FT-IR). Typical FT-IR spectra are demonstrated in (Figure 2.16).

In (Figure 2.16) it is possible to see the reduction of the absorptions that are resultant of the C-H stretch (3280-3340 cm^{-1}), and C=C stretch(2190-2260 cm^{-1}). These features disappear as the reaction progresses, and sulfur radically adds across the ends of the double

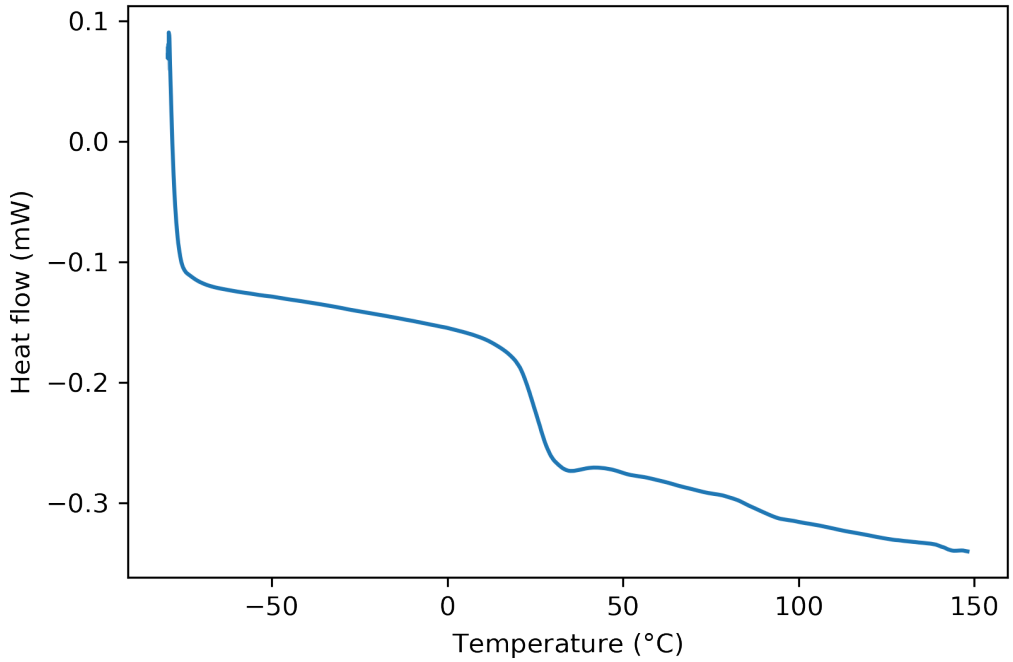

Figure 2.17: Thermogram produced when porous S-DCPD is analysed using a DSC, retaining a clear T_g that is centred around 35.7 textdegreeC

bonds. Interestingly, it would be expected that peaks for thiols would be found in this FT-IR, however, they are not seen. Thiols are usually located at 2584–2598 cm^{-1}. This is most likely due to the weak nature of the stretch itself.[79] The materials all exhibited spectrographs that are similar to previously reported literature.[30,50,58]

S-S, C-S, and S-H bonds should be visible in Raman spectroscopy, however, it was found that upon employment of Raman spectroscopy it was not possible to acquire a spectrum on the instruments available. This was due to the fact that the sample exhibited a strong degree of fluorescence, that obscured the spectrum. It should be possible to suppress the fluorescence of the samples when irradiated by the laser beam by changing the emitted wavelength to a non-standard wavelength that does not excite the material. It is also possible to use Kerr gating. However, access to equipment that is capable of doing these types of experiments is limited.

Differential scanning calorimetry (DSC) was performed on the polymers as a purely diagnostic technique. This was to determine if the polymer itself had been affected during the polymerisation reaction on the surface of the sodium chloride. A resultant thermogram from this type of experiment is displayed in Figure 2.17.

Sample	%C	%H	%N	%S
Porous S-DIB	42.6	4.3	0	52.5
Porous S-Farnesol	31.4	4.2	0	63.0
Porous S-Perillyl Alcohol	38.4	4.9	0	53.0
Porous S-DCPD	38.0	3.9	0	57.5

Table 2.3: Table summarising the results of CHNS analysis of the porous sulfur polymers produced in this study

It can be seen in Figure 2.17 that only one thermal transition is visible (37.5 °C), and this is a second order transition. This is most likely a glass transition, and is in line with other T_g's reported in the literature but is not as high.[1,58,69,80] This is likely due to the lower processing temperatures compared to the work of Parker *et al.* It can be assumed in this sense, that the thermal properties of the polymer produced are in line with that of previously reported polymers in the literature. It can also be assumed that the use of a solid-phase porogen did not affect the formation of the polymeric network.

CHNS revealed that the produced polymers compositions were somewhat different from the feedstock elements. (Table **??**) Across the board, there was found to be an enrichment of sulfur.

Overall, it can be seen through the use of pXRD, FT-IR, DSC, and even TGA that the polymers produced are comparable to those previously reported in the literature.[58,69] Characterisation of a sulfur polymer is a difficult process, requiring techniques and inferences that are not usually required when analysing other polymeric species. This is owing to their amorphous, insoluble nature.

However, despite this and owing to work set out previously, the chemical characteristics of sulfur polymers are becoming clearer every day. Work performed in this chapter is able to demonstrate that the polymers are amorphous, demonstrating their cross-linked nature. It is able to show the disappearance of the C=C stretch in FT-IR and the appearance of the C-S stretch. This infers the creation of the chemical cross-links. DSC was used to determine the T_g, a property that is exhibited by polymeric materials. Elemental analysis revealed that there is minimal to negligible loss of sulfur, or carbon cross-linker during the polymerisation process.

To conclude, a porous sulfur polymer was produced *via* a sodium chloride porogen. It was then characterised, and found to be consistent with prior literature values. The novel characterisation of the textural properties was performed by mercury porosimetry

and the morphological properties by SEM. In the following section, the applications of macroporous sulfur polymers will be explored.

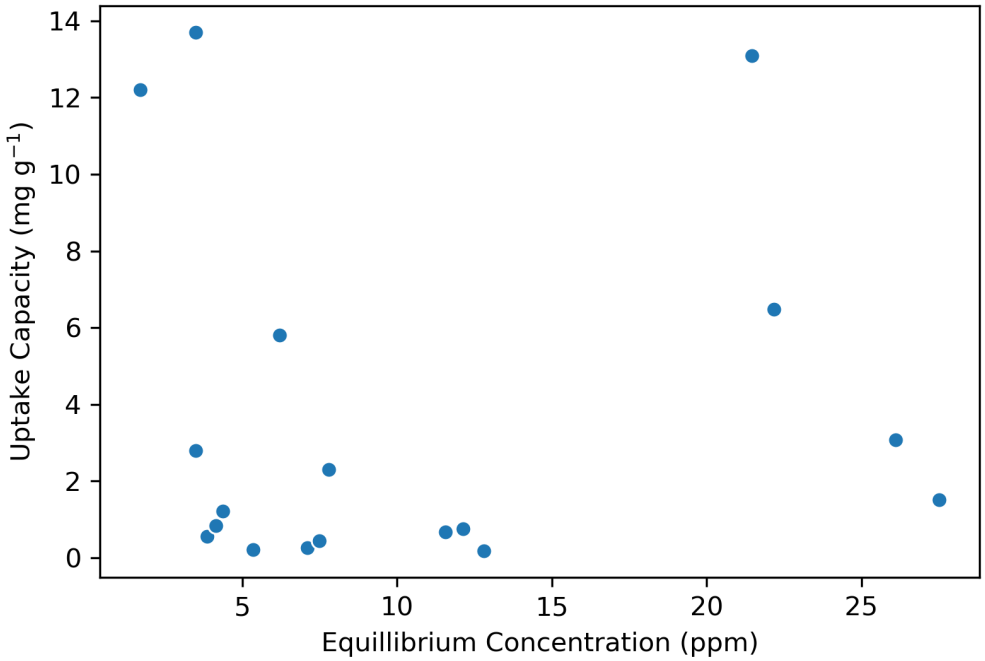

Figure 2.18: Accumulated experiments into the applicability of utilising a Langmuir isotherm on small amounts of porous S-DCPD. The graph illustrates the error in the experimental methodology by displaying a set of seemingly pseudo-random observations with no clear correlation.

2.6 Applications

2.6.1 Mercury Capture

As previously discussed, one of the applications of sulfur polymers is their use as a water remediation agent. Sulfur is a soft Lewis acid and will favourably form adducts with soft Lewis bases. Such a Lewis base is mercury, and this is a particular concern for human health. This, however, was discussed in great detail in the introduction. For a more complete discussion, refer back to there.

Initial, static tests of the absorption capacity of macroporous sulfur polymers were promising. However, the results of more thorough experiments were not as fruitful. Many repeat experiments were performed to assess the viability of a trend in the uptake of mercury. It was, however, found that this was almost impossible. (Figure 2.18) demonstrates an example of an attempt at obtaining an absorption isotherm for the material.

It can be seen in (Figure 2.18) that the material absorbs an apparently pseudo-random amount of mercury. Initially, it was believed that this was due to the poor wettability of

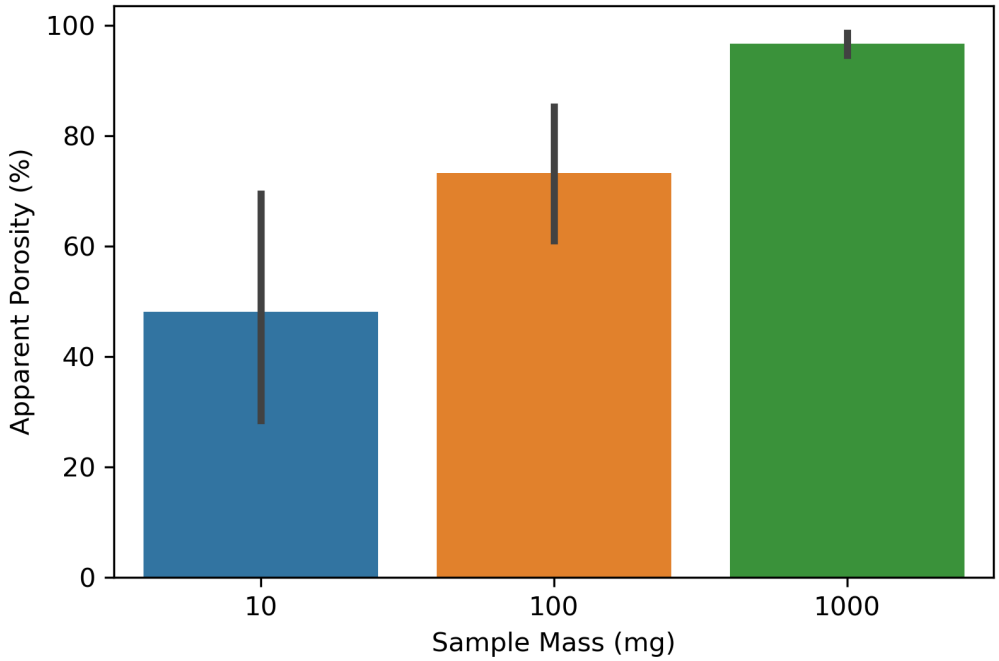

Figure 2.19: Bar plot demonstrating the effect of sample mass on the apparent porosity in salt templated samples. A larger sample mass demonstrates a higher degree of apparent porosity in the sample. This is likely due to small scale inhomogeneity.

the polymer. However, after successfully completely wetting the polymer by evacuation of gas and subsequent submersion in water, it was found that the polymer was still displaying the same effect.

Another hypothesis worked around the idea that there was a degree of inhomogeneity of the porous network within the polymer at the macroscale. This is explained as if there is a region of no porosity on the microscale, this could affect the apparent porosity when small amounts of material are measured. By increasing the amount of sample measured, it would negate these effects. This was confirmed by the measurement of the porosity of the samples. Briefly, this test was performed by taking advantage of the Archimedes principle.[81] It was found that smaller ($<$ 100 mg) masses of polymer were particularly susceptible to this effect of in-homogeneity, and the effect was not noticeable at larger sample masses. The black lines illustrate the error in apparent porosity in the sample. It can be seen that as the sample mass increases, the error in apparent porosity can be seen to decrease. (Figure 2.19)

This turned out to be the reason that the mercury tests were inconsistent, and when a

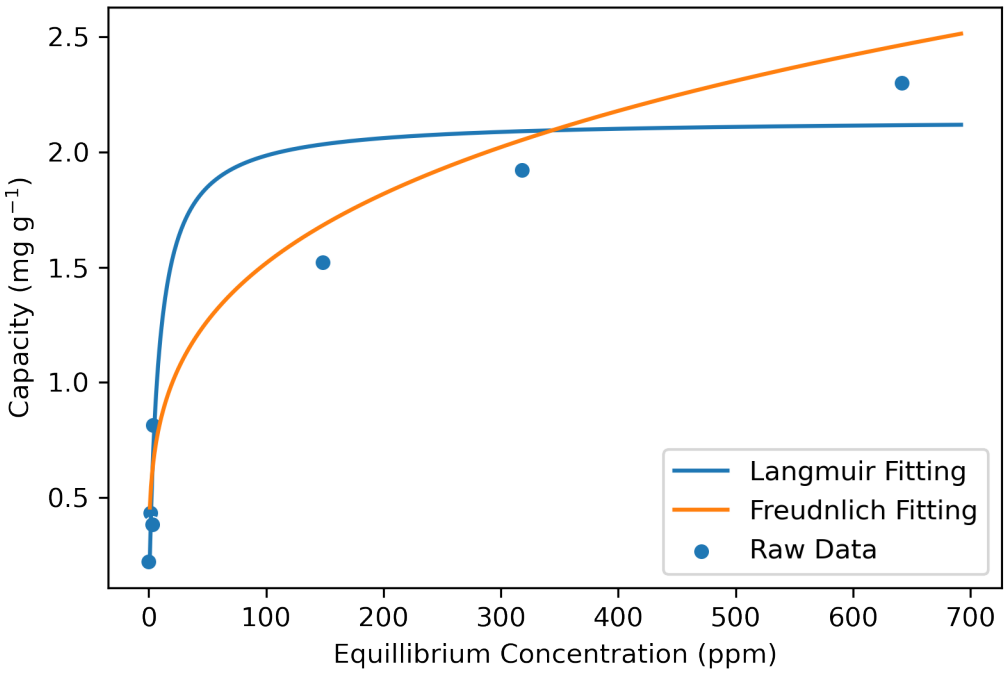

Figure 2.20: Absorption isotherm of $HgCl_2$ by the produced porous polymer. Whilst it was found that the Freundlich model provided a better fit (orange) the Langmuir fitting was statistically significant enough to provide information on the saturation capacity of the material.

larger sample mass was used in the mercury absorption experiment a consistent isotherm was produced. For a complete description, the procedure is documented in the methods section. This isotherm was fitted to the Langmuir model, and it was found that the capacity of the material for mercury (II) chloride was 2.27 mg g^{-1}. For a more in depth discussion of the fitting, please refer to the methods section. (Figure 2.20) This was the highest reported capacity for a pure sulfur polymer, and as of writing is still the highest. (12 August 2020)

Further research was performed into the behaviour of the material when absorbing mercury from a stable base, acid and neutral solution. It was found that the solution was basic, the capacity of the material was highest. This implies an underlying detail regarding the mechanism of absorption, which is that the site of ion exchange is acidic. With the assumption that the binding site is resultant of a sulfur atom, it would be most sensible to assume that the exchange site is a thiol. However, it was not possible to detect any thiolic vibrations in the FT-IR spectrum of the sample.This is likely due to the fact that the characteristic absorption of the thiol (S-H stretch) is very weak. Combined with

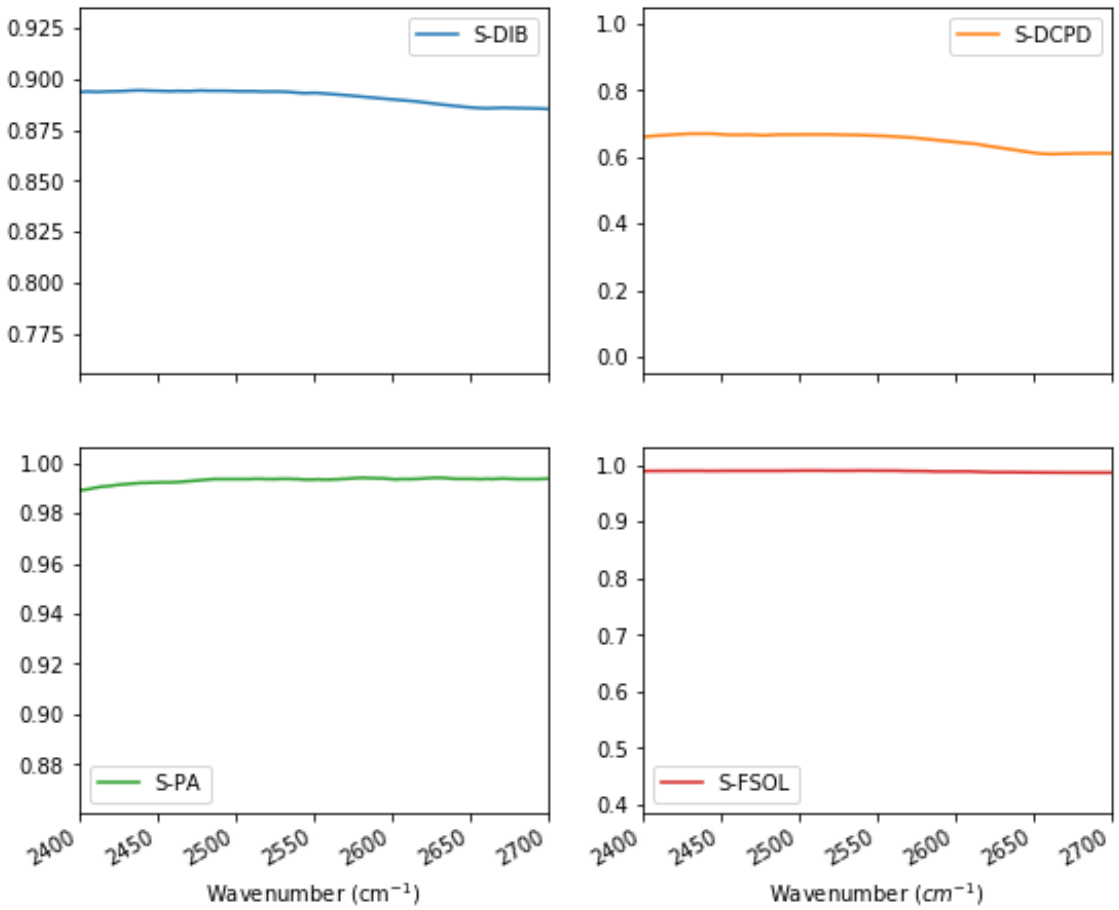

Figure 2.21: FTIR Spectrum of S-DIB (top left), S-DCPD (top right), S-PA (bottom left), S-FSOL (bottom right) with the x-axis (wave number) demonstrating the expected region for a thiol vibration and the absence of any signal

the inherent IR-transparency of the polymers produced, analysis by this means becomes difficult.

Further experiments investigated kinetics of absorption of mercury from solution by the polymer. It was found that the kinetics of absorption fit well to a second order mechanism. The regression of the fit was found to be 0.995. This type of fitting provides evidence that the mechanism is chemisorption based. This further backs the evidence that an acidic ion exchange reaction is occurring. (Figure 2.22)

In conclusion, it was found that the macroporous polymers produced in this research are a viable and cost-effective agent for the removal of mercury from solution. It was found that the mechanism of capture is most likely that of ion-exchange from an acidic sulfurous site (such as a thiol). This conclusion was made on the basis of chemisorbtion which was indicative of a formed chemical bond between the absorbent and Hg^{2+}. The greater performance of the material for absorbing $HgCl_2$ in a basic buffer indicates that

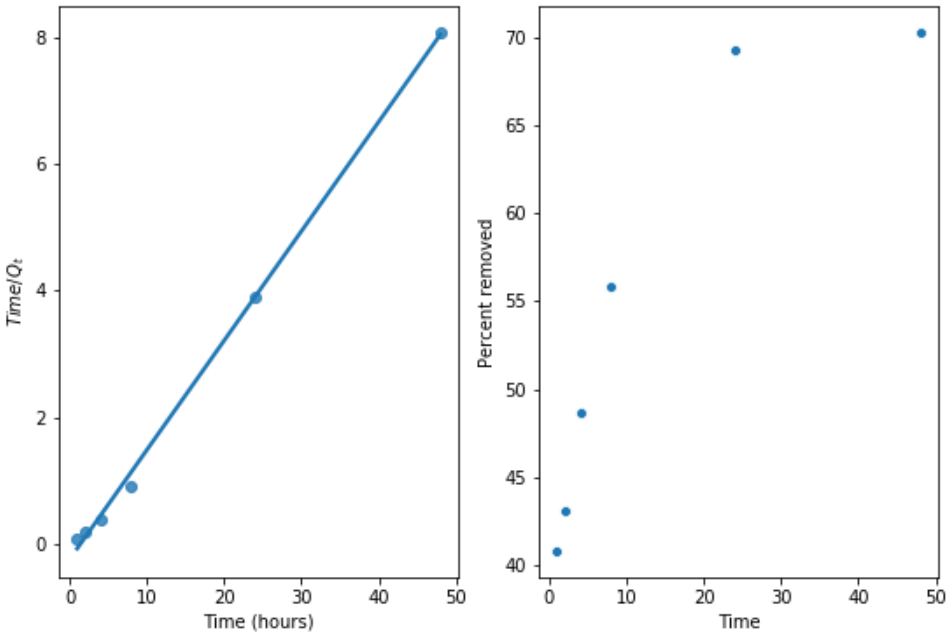

Figure 2.22: Second order fitting of the kinetics of removal of Hg^{2+} from solution by porous S-PA produced via salt templating over the course of 50 hours. (left) Raw unfitted kinetics experiment for the absorption of Hg^{2+} from solution by a produced porous polymer S-PA over the course of 50 hours from a 20 ppm solution.

the site was acidic. The data was not gathered with ease and the research was fraught with issues. Whilst this section of the research is a small fraction of the work carried out in this thesis, it took a lot of time to complete. However, given the results that were produced, it was definitely worth the time inputted.

2.6.2 Oil-Water Separation

As previously discussed in Chapter 1, oil-water separation is another potential application for sulfur polymers. Sulfur polymers are generally — but not totally — hydrophobic. This property limits their effectiveness in water remediation, but recent research is demonstrating that it is possible to tune this hydrophobicity. Nonetheless, it is possible to use this property to generate porous polymers that are able to selectively absorb oil from an oil-water interface.

In the case of the polymers generated in this study, toluene was used as an immiscible phase with water. In this system, the toluene rests above the water and an interface is formed. Upon introduction of the porous polymer to the system, the toluene is absorbed into the porous structure, leaving just the water behind.

It was found that the porous S-DCPD was able to absorb its own weight in toluene before saturation was reached. Furthermore, this was indicated by the removal of the red stained toluene. Sadly, however, research in this area was published in far more detail for a very similar material before it was possible to generate a more complete study.[82]

2.7 Conclusions

This chapter has demonstrated the work that was performed in the preparation of porous thiopolymer matrices. The work has resulted in the publication of two research articles. In one, the work was an initial demonstration of the method to the wider research community. The second research article was a more thorough analysis of the synthesis, properties, and applications of the produced materials.

Since publication, 6 further papers utilising techniques that were developed as a result of this work- at the time of writing — have been published in the area clearly demonstrating the useful nature of the work to the wider research community.[1,43,45,83] Furthermore, it was the first implementation of a porous sulfur polymer that demonstrated interconnectivity in its porosity.

To refer back to the initial aims of the chapter, we can confirm the meeting of those aims. Firstly, generation of a macroporous polymer was performed. This was confirmed by the employment of techniques such as FTIR, DSC, and pXRD to confirm the polymeric nature of the produced material. The porosity was confirmed by the employment of techniques such as mercury porosimetry and SEM. By confirming the porosity using techniques such as SEM, and mercury porosimetry the second aim of the chapter was met: the textural and morphological characteristics of the material were confirmed.

Finally, the interactions of the material with $HgCl_2$ were performed using the equipment that was available at the time. In this, the aims of the research were met and the absorption of mercury was performed and characterised.

Future research would look to further decrease the pore size of the produced materials. Mesoporous sulfur polymers would be the next step in this process, however, for a pure polymer no such material has been generated.

2.8 Materials & Methods

Sulfur (S_8, sublimed powder, reagent grade, 99.5%, Brenntag UK Ireland. Toluene ($\geq$ 98%) KBr (99.999 %), Sodium chloride (99.99%) and ethanol (99.5%) were obtained from Fischer scientific Ltd., Perillyl Alcohol ($\geq$ 95%), Dicyclopentadiene ($\geq$ 95%), Farnesol ($\geq$ 95%), and 1,3-diisopropenylbenzene ($\geq$ 97%) were obtained from Sigma Aldritch. All chemicals were used without further purification.

2.8.1 Procedure for Generation of a Sodium Chloride Porogen

Using Humidity Fusion

Sodium chloride (10 g, 0.171 mol) was placed into a silicone mould. The mould was then placed into a humidity controlled oven and left for 24 hours at 90% absolute humidity. After removal from oven, the sodium chloride porogen was placed in an oven at 373.15 K for 24 hours to dry. Upon removal, a solid, porous template of sodium chloride was formed.

Using Antisolvent Precipitation

A saturated solution of sodium chloride in water was prepared by addition of excess sodium chloride (500 g, 8.56 mol) into distilled water contained in a 500 mL Erlenmeyer flask. A magnetic stirrer bar was placed into the flask, and onto a magnetic stirrer. The mixture was allowed to stir for 24 hours at ambient temperature (295.15 K) and was then filtered to remove undissolved sodium chloride.

Note: The following section is written for a 50 mL : 50 mL antisolvent precipitation process. For differing ratios, the volumes of solutions of sodium chloride and ethanol should be altered accordingly

50 mL of ethanol was charged into a 200 mL Erlenmeyer flask. A magnetic stirring bar was placed into the flask, and the flask placed on a magnetic stirring plate. The stirring speed was set to be 1200 rpm. 50 mL of saturated sodium chloride was slowly (10 mL per minute) added to the ethanol. Upon addition precipitant sodium chloride was observed as a white suspension. After all sodium chloride solution was charged into the ethanol, the mixture was left to stir for ten minutes.

The mixture was then filtered through a glass frit equipped with a Whyman No. 10 filter paper. Upon removal of all liquid, a solid, moist monolith of sodium chloride remained.

The monolith was carefully removed from the filtration apparatus and placed in an oven for 24 hours at 373.15 K to dry. Upon removal from the oven, a solid, porous monolith of sodium chloride was formed.

2.8.2 Procedure for Generation of Porous Polymer

Note: The polymer used in this synthesis was S-DCPD, however the process may be applied to any polymer system used in inverse vulcanisation reactions. Observations of the reaction course may differ slightly wherein a differing organic crosslinker is used

Sulfur (5 g, 0.156 mol) and DCPD (5 g, 0.0378 mol) were weighed into a 40 mL vial. A magnetic stirring bar was also added to the vial. The vial was then placed into an aluminium heating block on a stirring plate with heating capability. The thermocouple was set to equilibrate at 432.15 K. Initially the sulfur and DCPD formed two separate phases, but after 5 minutes formed a single light yellow phase. After 5 minutes, the colour of the reaction began to darken and a slight increase in viscosity was noted. Subsequently, the reaction mixture turned an opaque black colour and a large increase in viscosity was noted. The solution was, at this point, removed from the heating block and poured carefully onto a sodium chloride porogen.

The composite was then placed into an oven at 413.15 K for 12 hours. Upon removal from the oven, the composite was allowed to cool in air. When cooled, the monolith was lightly ground in a mortar and pestle to particle sizes of approximately 5 mm. These pieces were then placed into an extraction thimble and were Soxhlet extracted with distilled water for 24 hours.

2.8.3 Absorption Experiment of Polymer

Analysis of removal of mercury

Porous sulfur polymer monoliths were broken apart into approximately 1 g chunks in a mortar and pestle. was added to a 12 mL centrifuge tube. To the centrifuge tube, 12 mL of the desired concentration of mercury chloride in water was added.

The solution was then placed on a device that rotated the tubes for 24 hours at 60 rpm. After 24 hours, the liquid was carefully poured out of the tube and into a syringe equipped with a 0.44 μm filter. The filtered liquid was weighed, and nitric acid added such that 10% of the final solution was nitric acid.

Stabilised solutions were then analysed on an Agilent 5110 ICP-OES spectrometer to elucidate the remaining concentration of mercury.

Fitting of Langmuir Isotherm

The Lanmguir model was fitted to the data using Origin Pro 9 using the Levenberg-Marquardt algorithm. Parameters for the curve were then used to plot the line using the Python library seaborn. The equation used was:

$$Q_e = \frac{K_\mathrm{D}\, C_e}{1 + K_\mathrm{D}\, C_e} \tag{2.1}$$

Where K_D is the affinity constant, Q_m is the saturation capacity and C_e is the equilibrium concentration.

Relevant technical details

Firstly, it is important to note that nitric acid was added to the liquid upon separation from polymer. Nitric acid acts as a stabilising agent for aqueous solutions of $HgCl_2$. While this may leave questions about the validity of the existence of $HgCl_2$ in wastewater streams, they are undoubtedly existent. Often in wastewater streams inherent acidity, and other matrix effects, will stabilise the $HgCl_2$ in solution.

Secondly, it is important for any person wishing to repeat this type of experiment to understand that there is a 'carry over' effect. When a solution of $HgCl_2$ is run through an ICP-OES the mercury may absorb onto the surface of the tubes that are used to carry the fluid through the system. This may be mitigated by several precautions. The first of which is to ensure that no solution of $HgCl_2$ that exceeds 20 ppm is allowed to run through the system. In the case where it is suspected that the concentration exceeds 20 ppm the solution should first be diluted and worked back from to find the original concentration.

Thirdly, and finally, in between runs on the ICP-OES the system must be flushed with a 10 mL solution of 10 % HNO_3, this will usually remove any residual $HgCl_2$ that remains in the system piping. Other researchers have employed a variety of methods such as using an internal standard of Hf, or a cysteine complexation solution, however HNO_3 works perfectly. Whilst these details are not standard, it is the author's hope that to provide use and save potentially incorrect results for the reader that hopes to replicate said results.

Oil-Water Seperation

Porous S-DCPD (1 g) produced *via* salt templating with a template generated from 90% volume ethanol and 10% saturated sodium chloride solution was placed in a recrystallising basin that contained 20 mL of distilled water and 5 mL of toluene stained with 1 mg of oil red dye. The polymer was placed onto the oil layer and allowed to soak for 5 minutes. The polymer was then removed from the mixture and gently dried with tissue paper and reweighed.

2.8.4 Instrumental

Scanning Electron Microscopy (SEM)

SEM imaging of the porous materials was achieved using a Hitatchi S-4800 cold Field Emission Scanning Electron Microscope (FE-SEM) operating in combined scanning and transmission modes. The samples were prepared by adhering 1mm chunks of porous polymer to an adhesive carbon tab. Imaging was conducted at a working distance of 8 mm with an acceleration voltage of 3 kV. Micrographs were generated using a combination of upper and lower detectors.

Powder X-ray diffraction

pXRD was aquired using a PANalytical X'Pert PRO diffractometer with Cu-$K_{\alpha 1+2}$ radiation operating in transmission geometry. The X-Rays were of 1.54 Å. Samples were prepared by grinding in a mortar and pestle until a fine powder presented. The samples were placed into a fine layer (0.5 mm) over a shallow well.

Thermogravimetric Analysis (TGA)

TGA was conducted in platinum pans using a TA Instruments Q5000IR analyser with an automatic vertical overhead thermobalance. The samples were heated at 5 °C min^{-1} to 900 °C under nitrogen. Samples were prepared by finely grinding materials in a mortar and pestle and weighing to approximately 1 mg.

Differential Scanning Calorimetry (DSC)

Thermograms were conducted in a TA Instruments Q200 DSC under nitrogen flow. Heating and cooling rates were set to 5 °C min^{-1} on a heat/cool/heat cycle with maximum temperature of 160 °C and minimum temperature of -60 °C. Samples were prepared by grinding in a mortar and pestle and subsequently weighing approximately 5 mg of sample into a pan which was then hermetically sealed in a press.

Fourier-transform infrared spectroscopy (FTIR)

FTIR was performed on a Bruker ALPHA II. Samples were ground with dry KBr in a mortar and pestle. Samples were initially trialled at 50 wt% material and 50 wt% KBr and pressed using a 2 tonne hydraulic press with a 2 mm die. Samples were adjusted based on the signal strength by regrinding the produced pellet and either adding or subtracting more polymer to the reground sample. It was found that between 60-90% of polymer was required to produce a readable spectrum.

Bibliography

(1) S. Petcher, D. J. Parker and T. Hasell, *Environmental Science: Water Research & Technology*, 2019, DOI: 10.1039/c9ew00477g.

(2) F. M. D'itra, in *Fourth Symposium on our Environment*, Springer Netherlands, 1991, pp. 165–182.

(3) P. Zuddas, G. Cao, A. Concas, C. Ardau, A. Cristini, P. Zuddas and G. Cao, *Elsevier*, 2017, DOI: 10.1016/j.chemosphere.2005.08.024.

(4) F. Pagnanelli, E. Moscardini, V. Giuliano and L. Toro, *Environmental Pollution*, 2004, **132**, 189–201.

(5) N. Alba, S. Gassó, T. Lacorte and J. Baldasano, *Journal of the Air & Waste Management Association*, 1997, **47**, 1170–1179.

(6) T. Astrup, H. Mosbæk and T. Christensen, *Waste Management*, 2006, **26**, 803–814.

(7) G. Conway, *Unwelcome Harvest: Agriculture and Pollution*, 2013, 1–5.

(8) B. Moss, *Phil. Trans. R. Soc. B*, 2008, **363**, 659–666.

(9) A. Prakash Sharma and B. D. Tripathi, *Environmental Monitoring and Assessment*, 2008, **138**, 31–39.

(10) D. H. Klein and P. Russell, *Environmental Science and Technology*, 1973, **7**, 357–358.

(11) P. Holmes, K. James and L. Levy, *Science of The Total Environment*, 2009, **408**, 171–182.

(12) L. Zhang and M. Wong, *Environment International*, 2007, **33**, 108–121.

(13) R. Kessler, *Environ. Health Perspect.*, 2013, **121**, A304–9.

(14) J. Wang, X. Feng, C. W. Anderson, Y. Xing and L. Shang, *Journal of Hazardous Materials*, 2012, **221-222**, 1–18.

(15) K. H. Telmer and M. M. Veiga, in *Mercury Fate and Transport in the Global Atmosphere: Emissions, Measurements and Models*, Springer US, 2009, pp. 131–172.

(16) P. Chu and D. B. Porcella, *Water, Air, & Soil Pollution*, 1995, **80**, 135–144.

(17) W. K. H. Hogland, *Journal of Environmental Quality*, 1994, **23**, 1364–1366.

(18) P. Grange, *Catalysis Reviews–Science and Engineering*, 1980, **21**, 135–181.

(19) J. K. C. Nduka, O. E. Orisakwe, L. O. Ezenweke, T. E. Ezenwa, M. N. Chendo and N. G. Ezeabasili, *The Scientific World Journal*, 1900, **8**, 931839.

(20) G. Wen, J. J. Schoenau, S. P. Mooleki, S. Inanaga, T. Yamamoto, K. Hamamura, M. Inoue and P. An, Journal of Plant Nutrition and Soil Science, 2003, vol. 166, pp. 54–60.

(21) W. Moeller and K. Winkler, *Journal of the Air Pollution Control Association*, 1968, **18**, 324–325.

(22) H. N. Madon and R. F. Strickland-Constable, *Industrial and Engineering Chemistry*, 1958, **50**, 1189–1192.

(23) R. G. Pearson, *Journal of the American Chemical Society*, 1963, **85**, 3533–3539.

(24) G. C. Vezzoli and R. J. Zeto, *Inorganic Chemistry*, 1970, **9**, 2478–2484.

(25) W. J. Chung, J. J. Griebel, E. T. Kim, H. Yoon, A. G. Simmonds, H. J. Ji, P. T. Dirlam, R. S. Glass, J. J. Wie, N. A. Nguyen, B. W. Guralnick, J. Park, Á. Somogyi, P. Theato, M. E. Mackay, Y. E. Sung, K. Char and J. Pyun, *Nature Chemistry*, 2013, **5**, 518–524.

(26) J. J. Griebel, N. A. Nguyen, A. V. Astashkin, R. S. Glass, M. E. Mackay, K. Char and J. Pyun, *ACS Macro Letters*, 2014, **3**, 1258–1261.

(27) B. Leutner and L. Diehl, *Manufacture of sulfur concrete*, 1977.

(28) M. P. Crockett, A. M. Evans, M. J. Worthington, I. S. Albuquerque, A. D. Slattery, C. T. Gibson, J. A. Campbell, D. A. Lewis, G. J. Bernardes and J. M. Chalker, *Angewandte Chemie - International Edition*, 2016, **55**, 1714–1718.

(29) S. J. Tonkin, C. T. Gibson, J. A. Campbell, D. A. Lewis, A. Karton, T. Hasell and J. M. Chalker, *Chemical Science*, 2020, **11**, 5537–5546.

(30) D. J. Parker, S. T. Chong and T. Hasell, *RSC Advances*, 2018, **8**, 27892–27899.

(31) J. A. Smith, S. J. Green, S. Petcher, D. J. Parker, B. Zhang, M. J. H. Worthington, X. Wu, C. A. Kelly, T. Baker, C. T. Gibson, J. A. Campbell, D. A. Lewis, M. J. Jenkins, H. Willcock, J. M. Chalker and T. Hasell, *Chemistry – A European Journal*, 2019, **25**, 10433–10440.

(32) P. Anastas and N. Eghbali, *pubs.rsc.org*, DOI: 10.1039/b918763b.

(33) Z. Deng, A. Hoefling, P. Theato and K. Lienkamp, *Macromolecular Chemistry and Physics*, 2018, **219**, 1700497.

(34) J. A. Smith, R. Mulhall, S. Goodman, G. Fleming, H. Allison, R. Raval and T. Hasell, *ACS Omega*, 2020, **5**, 5229–5234.

(35) H. Kim, J. Lee, H. Ahn, O. Kim and M. J. Park, *Nature Communications*, 2015, **6**, DOI: 10.1038/ncomms8278.

(36) A. Hoefling, D. T. Nguyen, P. Partovi-Azar, D. Sebastiani, P. Theato, S. W. Song and Y. J. Lee, *Chemistry of Materials*, 2018, **30**, 2915–2923.

(37) J. J. Griebel, R. S. Glass, K. Char and J. Pyun, *Progress in Polymer Science*, 2016, **58**, 90–125.

(38) S. Namnabat, J. J. Gabriel, J. Pyun and R. A. Norwood, Organic Photonic Materials and Devices XVI, ed. C. E. Tabor, F. Kajzar, T. Kaino and Y. Koike, SPIE, 2014, vol. 8983, p. 89830D.

(39) J. J. Griebel, S. Namnabat, E. T. Kim, R. Himmelhuber, D. H. Moronta, W. J. Chung, A. G. Simmonds, K.-J. Kim, J. van der Laan, N. A. Nguyen, E. L. Dereniak, M. E. Mackay, K. Char, R. S. Glass, R. A. Norwood and J. Pyun, *Advanced Materials*, 2014, **26**, 3014–3018.

(40) J. J. Griebel, N. A. Nguyen, S. Namnabat, L. E. Anderson, R. S. Glass, R. A. Norwood, M. E. Mackay, K. Char and J. Pyun, *ACS Macro Letters*, 2015, **4**, 862–866.

(41) L. E. Anderson, T. S. Kleine, Y. Zhang, D. D. Phan, S. Namnabat, E. A. LaVilla, K. M. Konopka, L. Ruiz Diaz, M. S. Manchester, J. Schwiegerling, R. S. Glass, M. E. Mackay, K. Char, R. A. Norwood and J. Pyun, *ACS Macro Letters*, 2017, **6**, 500–504.

(42) J.-S. M. Lee, D. J. Parker, A. I. Cooper and T. Hasell, *Journal of Materials Chemistry A*, 2017, **5**, 18603–18609.

(43) M. Mann, J. E. Kruger, F. Andari, J. McErlean, J. R. Gascooke, J. A. Smith, M. J. Worthington, C. C. McKinley, J. A. Campbell, D. A. Lewis, T. Hasell, M. V. Perkins and J. M. Chalker, *Organic and Biomolecular Chemistry*, 2019, **17**, 1929.

(44) M. Thielke, L. Bultema, D. Brauer, B. Richter, M. Fischer, P. Theato, M. W. Thielke, L. A. Bultema, D. D. Brauer, B. Richter, M. Fischer and P. Theato, *Polymers*, 2016, **8**, 266.

(45) A. D. Tikoalu, N. A. Lundquist and J. M. Chalker, *Advanced Sustainable Systems*, 2020, **4**, 1–9.

(46) A. M. Abraham, S. V. Kumar and S. M. Alhassan, *Chemical Engineering Journal*, 2018, **332**, 1–7.

(47) M. Worthington, R. Kucera, J. C. G. Chemistry and u. 2017, *pubs.rsc.org*.

(48) T. Hasell, D. J. Parker, H. A. Jones, T. McAllister and S. M. Howdle, *Chemical Communications*, 2016, **52**, 5383–5386.

(49) W. L. Murphy, R. G. Dennis, J. L. Kileny and D. J. Mooney, *Tissue Engineering*, 2002, **8**, 43–52.

(50) D. J. Parker, H. A. Jones, S. Petcher, L. Cervini, J. M. Griffin, R. Akhtar and T. Hasell, *Journal of Materials Chemistry A*, 2017, **5**, 11682–11692.

(51) N. A. Lundquist, M. J. Worthington, N. Adamson, C. T. Gibson, M. R. Johnston, A. V. Ellis and J. M. Chalker, *RSC Advances*, 2018, **8**, 1232–1236.

(52) M. J. H. Worthington, C. J. Shearer, L. J. Esdaile, J. A. Campbell, C. T. Gibson, S. K. Legg, Y. Yin, N. A. Lundquist, J. R. Gascooke, I. S. Albuquerque, J. G. Shapter, G. G. Andersson, D. A. Lewis, G. J. L. Bernardes and J. M. Chalker, *Advanced Sustainable Systems*, 2018, **2**, 1800024.

(53) Z. Ma, C. Gao, Y. Gong and J. Shen, *Journal of Biomedical Materials Research - Part B Applied Biomaterials*, 2003, **67**, 610–617.

(54) J. Courtois, E. Byström and K. Irgum, *Polymer*, 2006, **47**, 2603–2611.

(55) B. T. Smith, A. Lu, E. Watson, M. Santoro, A. J. Melchiorri, E. C. Grosfeld, J. J. van den Beucken, J. A. Jansen, D. W. Scott, J. P. Fisher and A. G. Mikos, *Acta Biomaterialia*, 2018, **78**, 341–350.

(56) E. Chevalier, D. Chulia, C. Pouget and M. Viana, *Fabrication of porous substrates: A review of processes using pore forming agents in the biomaterial field*, 2008.

(57) M. M. Coleman, J. R. Shelton and J. L. Koenig, *Industrial and Engineering Chemistry Product Research and Development*, 1974, **13**, 154–166.

(58) X. Wu, J. A. Smith, S. Petcher, B. Zhang, D. J. Parker, J. M. Griffin and T. Hasell, *Nature Communications*, 2019, **10**, 1–9.

(59) F. Mansour, S. Waheed, B. Paull and F. Maya, *Journal of Separation Science*, 2019, **43**, DOI: 10.1002/jssc.201900876.

(60) A. Tipton, B. Lu and P. V. Cleemput, *Method of porogen removal from porous low-k films using UV radiation*, tech. rep., 2007.

(61) *Preparation of macroporous biodegradable PLGA scaffolds for cell attachment with the use of mixed salts as porogen additives - Lin - 2002 - Journal of Biomedical Materials Research - Wiley Online Library.*

(62) J. Kim, M. J. Yaszemski and L. Lu, *Three-Dimensional Porous Biodegradable Polymeric Scaffolds Fabricated with Biodegradable Hydrogel Porogens*, tech. rep.

(63) J. Akella, S. N. Vaidya and G. C. Kennedy, *Physical Review*, 1969, **185**, 1135–1140.

(64) R. T. Tran, E. Naseri, A. Kolasnikov, X. Bai and J. Yang, *Biotechnology and Applied Biochemistry*, 2011, **58**, 335–344.

(65) X. Liang, Y. Qi, Z. Pan, Y. He, X. Liu, S. Cui and J. Ding, *Materials Chemistry Frontiers*, 2018, **2**, 1539–1553.

(66) G. Eshel, G. Levy, U. Mingelgrin and M. Singer, *Soil Science Society of America Journal*, 2004, **68**, 736–743.

(67) J. Nývlt, *Journal of Crystal Growth*, 1968, **3-4**, 377–383.

(68) S. P. Pinho and E. A. Macedo, *Journal of Chemical & Engineering Data*, 2005, **50**, 29–32.

(69) D. J. Parker, H. A. Jones, S. Petcher, L. Cervini, J. M. Griffin, R. Akhtar and T. Hasell, *Journal of Materials Chemistry A*, 2017, **5**, 11682–11692.

(70) G. Gittens, *Journal of Colloid and Interface Science*, 1969, **30**, 406–412.

(71) J. A. Newman, P. D. Schmitt, S. J. Toth, F. Deng, S. Zhang and G. J. Simpson, *Anal. Chem.*, 2015, **87**, 10950–10955.

(72) R. L. Burwell, *Pure and Applied Chemistry*, 1976, **46**, 71–90.

(73) R. Gido and A. Koestel, *Mercury Wetting and Non-Wetting Condensing Research*, tech. rep., 1963.

(74) H. M. Rootare, in *Advanced Experimental Techniques in Powder Metallurgy*, Springer US, 1970, pp. 225–252.

(75) G. W. Scherer, D. M. Smith and D. Stein, *Journal of Non-Crystalline Solids*, 1995, **186**, Proceedings of the Fourth International Symposium on Aerogels, 309–315.

(76) Z. Li, D. Liu, Y. Cai, Y. Yao and H. Wang, *Energy Exploration and Exploitation*, 2015, **33**, 809–826.

(77) Y. H. Li, G. Q. Lu and V. Rudolph, *Particle and Particle Systems Characterization*, 1999, **16**, 25–31.

(78) P. Vinet, J. Ferrante, J. H. Rose and J. R. Smith, *Journal of Geophysical Research*, 1987, **92**, 9319.

(79) In, *Interpreting Infrared, Raman, and Nuclear Magnetic Resonance Spectra*, ed. R. A. Nyquist, Academic Press, San Diego, 2001, pp. 65–83.

(80) J. S. M. Lee, D. J. Parker, A. I. Cooper and T. Hasell, *Journal of Materials Chemistry A*, 2017, **5**, 18603–18609.

(81) L. Mwaikambo, M. A. J. o. m. science and u. 2001, *researchportal.bath.ac.uk*.

(82) M. J. Worthington, R. L. Kucera, I. S. Albuquerque, C. T. Gibson, A. Sibley, A. D. Slattery, J. A. Campbell, S. F. Alboaiji, K. A. Muller, J. Young, N. Adamson, J. R. Gascooke, D. Jampaiah, Y. M. Sabri, S. K. Bhargava, S. J. Ippolito, D. A. Lewis, J. S. Quinton, A. V. Ellis, A. Johs, G. J. Bernardes and J. M. Chalker, *Chemistry - A European Journal*, 2017, **23**, 16219–16230.

(83) A. M. Abraham, S. V. Kumar and S. M. Alhassan, *Chemical Engineering Journal*, 2018, **332**, 1–7.

Chapter 3

Mesoporous Thiopolymers

3.1 Abstract

Much of the work presented in this chapter has been adapted from: 'Mesoporous knitted inverse vulcanised polymers'

Elemental sulfur is generated in large quantities when crude oil is refined. This elemental sulfur has limited use other than the production of sulfuric acid and other, more limited, commodity chemicals. Recently, attention in research has directed to the formation of 'inverse vulcanised' polymers. These polymers are formed from elemental sulfur and small molecule alkenes. Research has demonstrated these polymers make excellent sorbents, however, they lack high specific surface areas which are important for sorbent capacity. Herein, we report the first mesoporous polymer generated using inverse vulcanised polymers. We explore the generated polymers' properties as a sorbent.

3.2 Introduction

Elemental sulfur is produced in large quantities resulting from the hydrodesulfurisation of crude oil.[1,2] The main application of this side product of oil refining is in the manufacture of sulfuric acid.[3] Despite the ubiquity of sulfuric acid in modern industrial processing, there is still a large excess of sulfur produced.[4] In 2013 Pyun *et al.* demonstrated that it is possible to form high sulfur content polymers from elemental sulfur and 1,3-diisopropenylbenzene, in a process named 'inverse vulcanisation'.[3]

Since the publication of Pyun's seminal paper, there have been many other papers that have explored the applications of the polymers produced in this process: energy[5–7], optics[3,8–10], water remediation[11–18], antimicrobials[19,20], coatings[17,21], oil-water separation[14,22,23], thermal insulation[18], gas purification[18] and agriculture[24]. Many of these applications benefit from porosity, however to date there have only been a few methods explored for the incorporation of porosity into inverse vulcanised polymers.

The first method exploited was demonstrated by Hasell *et al.*, in which they demonstrated the use of supercritical carbon dioxide ($scCO_2$), to generate a closed cell macroporosity.[25] The foamed polymer was then used to absorb mercury chloride ($HgCl_2$) from aqueous solution. It was found that the polymer had a higher capacity for $HgCl_2$ than elemental sulfur. The second method was first demonstrated by Parker *et al.*, they demonstrated the use of a sacrificial sodium chloride porogen (pNaCl) to include connected macroporosity.[26] Further research performed in this area has focused on either more foaming or templating methods.[13,27,28]

One of the most explored applications of porous sulfur polymers is their application in the remediation of mercury contaminated water.[13,29,30] Mercury is a persistent and hazardous water pollutant.[31,32] Sulfur containing materials are particularly suitable for the remediation of mercury contaminated water owing to the soft-soft lewis acid base interaction that exists between the two elements.[33] In order to fully realise the potential of sulfur polymers more effective means of generating porosity must be explored, and one potential route to this is using the hypercrosslinking reaction first reported by Dvankov *et al.* in the 1970's.[34] In the hypercrosslinking reaction aryl rings are reacted with di, or trihaloalkanes to produce a highly cross-linked network via S_NAr.[35] These types of reactions produce polymers with interesting characteristics, such as the ability to swell in solvents

that are expected to be non-solvating.[34,36] This is due to their highly strained polymer network, and the creation of micropore channels that develop around solvent molecules. There is evidence that these materials also have applications in water remediation.[37]

Herein, we report the first attempt at applying this type of "knitting" reaction to inverse vulcanised polymers.

3.3 Aims

In order to limit the scope of the research to that which is attainable and sensible, the following research aims were set at the beginning of the research:

- Investigate the applicability of the hypercrosslinking reaction to soluble sulfur polymers.
- Characterise the textural and morphological properties of the produced material.
- Characterise the interactions of the materials with metal centres in aqueous solution.

3.4 Approaches

3.4.1 Considerations

Inverse vulcanised polymers have been synthesised with a large variety of alkenes.[21,26,38–41] Many of these alkenes produce polymers when reacted with elemental sulfur, however, there are not a lot of alkenes that react with sulfur to produce a polymer with the physio-chemical properties that are required for a hyper-crosslinking reaction. In the following paragraphs there will be discussion on these requirements but to summarise: firstly it must be soluble or able to swell in solvent, secondly and the polymer must contain an aryl ring.

As previously mentioned, the chosen polymer must be soluble or able to swell in solvent. For ease of implementation, solubility is preferred. A degree of solubility has been demonstrated in many sulfur polymers, however, ideally the polymer would be completely soluble in the chosen solvent. Chloroform was chosen as the solvent because it has been previously demonstrated that it is possible to hypercrosslink materials with chloroform as both the solvent, and cross-linker.[42,43] This highly simplifies the chemistry in the process. In the literature, there has been a myriad of demonstrations of inverse vulcanised polymers that possess this property, such as: S-Limonene[11], S-Perillyl Alcohol[15], S-Squalene[15], S-Styrene[39], and S-DIB[3].

Of these polymers, there is a requirement for an aryl ring to be incorporated into the polymer backbone. This aryl ring is required in order to access the Friedel-Crafts chemistry that is required to create the cross-links. Therefore, all polymers previously mentioned other than S-Styrene and S-DIB are not useful for this purpose. Of the two remaining, S-Styrene is the obvious choice, as the polymer possesses a higher solubility owing to its low degree of crosslinking. The proposed reaction scheme that was implemented is demonstrated below (Figure 3.1)

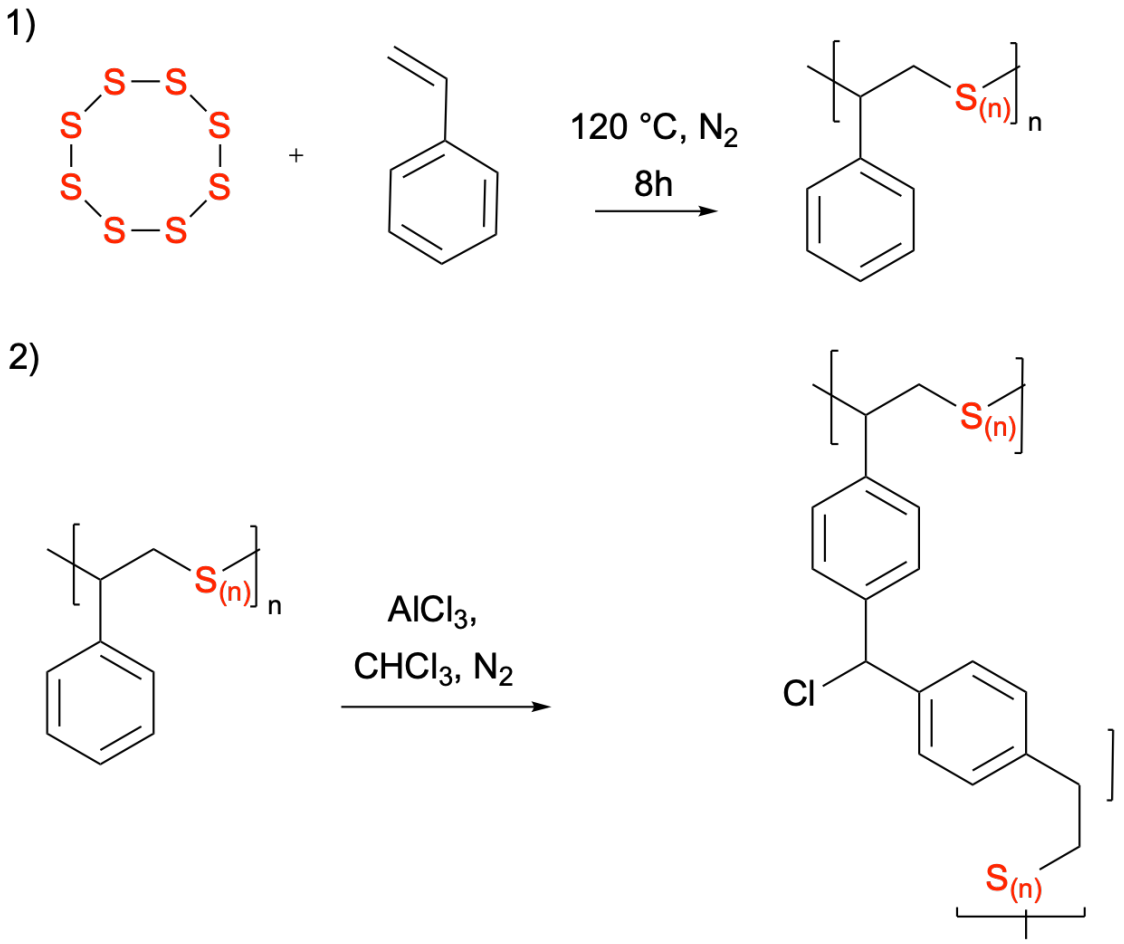

Figure 3.1: Reaction scheme for the generation of a mesoporous inverse vulcanised polymer through post synthetic crosslinking under stirring. Briefly, sulfur and styrene were mixed and heated at 130 °C under nitrogen to polymerise in step one, before $AlCl_3$ and chloroform were added, at 50 °C to induce crosslinking in the second step.

Given the relatively niche scope of the reaction process in terms of potential alkenes, the considerations that were necessary to make were quite small. However, there was one final consideration to take into account when designing the reaction process and that was the choice of catalyst. It has been demonstrated that $FeCl_3$ is the most active of the hypercrosslinking catalysts.[44] However, when initially trialled no solid, insoluble polymer was observed. This contrast with the products of the $AlCl_3$ catalyst, wherein an intractable powder was formed.

In conclusion, required properties for the precursor polymer were analysed, and a polymer selected that fit these requirements. Whilst the scope could have been extended by exploring other solvents, crosslinkers, and even sulfur polymers, it was decided to explore the viability of the reaction first. Furthering on from this, a more fundamental study into the properties of the produced polymers was performed, in lieu of a large synthetic scope.

3.5 Structure and Properties

3.5.1 Textural Characterisation

Previously, discussion of the characterisation of macroporous materials revolved around the use of mercury porosimetry. Whilst this technique is capable of measuring pore sizes as low as 30 nm, it is not able to measure smaller pore sizes.[45] The literature demonstrates that the porosity of materials produced using similar methods to the one employed in this study often contain pores smaller than 30 nm.[35] Therefore, mercury porosimetry would be a poor fit for characterisation of the sample generated in the study.

Another technique that is more widely employed is gas sorption. This technique is able to determine pore sizes that are much smaller (<50 nm).[46] The following paragraphs will present a brief description of the technique, so the unfamiliar reader is able to appreciate in an approximate sense how the technique functions.

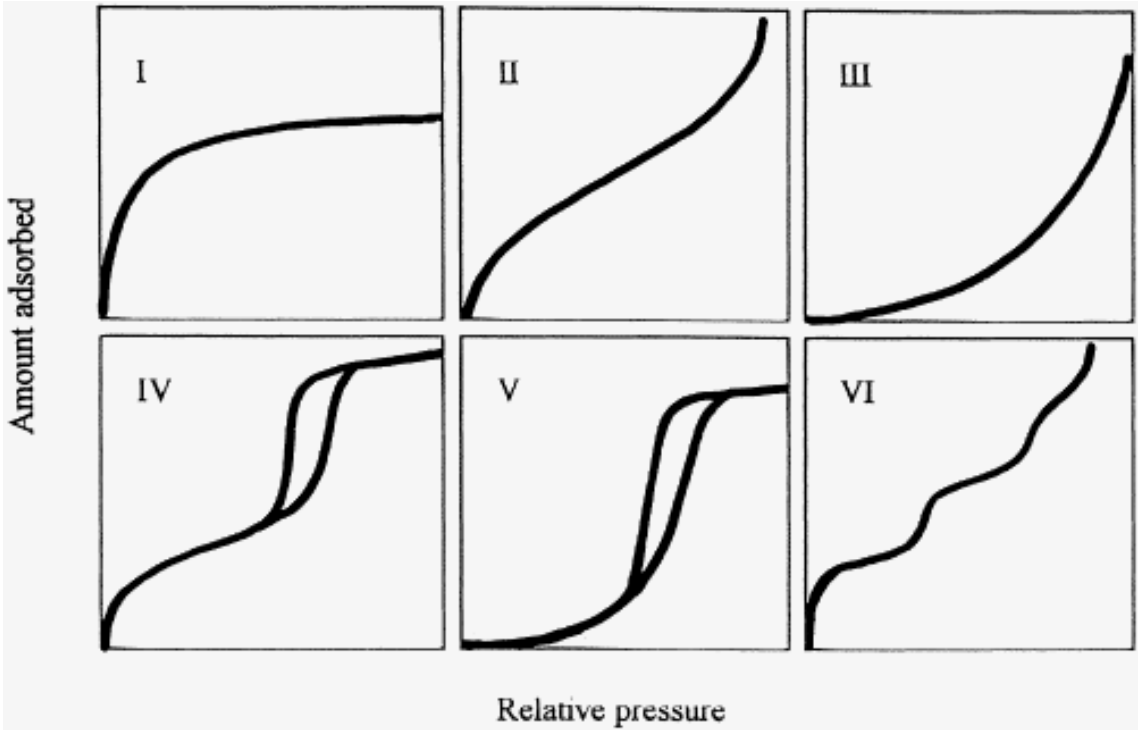

Figure 3.2: IUPAC defined isotherm types. Each isotherm is characteristic of a certain material type. Adapted from: https://doi.org/10.1016/S0001-8686(98)00044-X

In gas sorption, a monolayer of a chosen gas (usually nitrogen) is allowed to form on an evacuated sample at the boiling point of the chosen gas. The interactions that cause these monolayers to form are grouped under the blanket term: 'physisorption'.[47] The most

important characteristic of physisorption is that the binding interaction does not alter the chemical structure of the adsorbate. The main interaction that drives physisorption is the Van der Waals (or the London dispersion force) interaction.[47]

The information that is gathered in the gas sorption experiment is the quantity of adsorbed gas. This is measured as a function of the 'dosed' (injected gas) gas. When the dosed gas is plotted as a function of the adsorbed gas an adsorption isotherm is produced. Of these isotherms, IUPAC defines there to be 6 types (Figure 3.2).

Once an isotherm is gathered, a data reduction method is chosen to extract the porosity information for the sample. The most well known is the BET method, this uses a model developed by Brunauer, Emmet, and Teller to determine the surface area of a material.[48] Of particular importance to the material generated in this study is the BJH method developed by Barrett, Joyner, and Halenda.[49] This method allows for calculation of pore size distributions at the mesopore and macropore level. There are many other methods for the determination of porosity using gas sorption, and there are many volumes of literature on the topic.[50]

To conclude, gas sorption is a complicated but powerful technique for the elucidation of information on the porosity of a porous material. Therefore, it was decided that it would be used to study the porosity of the material SHCP-01.

Having discussed the theory of gas sorption to a limited extent, it is now possible to assess the porosity of SHCP-01. This material was generated from a 70 % weight sulfur styrene copolymer in excess of crosslinker, chloroform. Further synthetic detail is in the method section. Figure 3.3 displays the gas sorption isotherm of SHCP-01.

The type of isotherm generated by the material is somewhat ambiguous. It contains features of a type V isotherm (hysteresis), however the shape of the isotherm is reminiscent of type III. Referring back to 3.2 the SHCP-01 isotherm bares characteristics of both. It is likely that the material is a mixed material. Given the disordered structure of the material, this is likely. The isotherm was characteristic of a material that possessed mesoporosity. The hysteresis loop was caused by the mesopores filling with nitrogen condensate. When this isotherm was subject to the methods developed by Barrett, Joyner, and Halenda it was possible to generate a pore-size distribution as shown in (Figure 3.4).

As demonstrated in (Figure 3.4) a majority of the pores in the sample were located in the 5-10 nm region. However, pore sizes are detectable all the way to 40 nm. These types

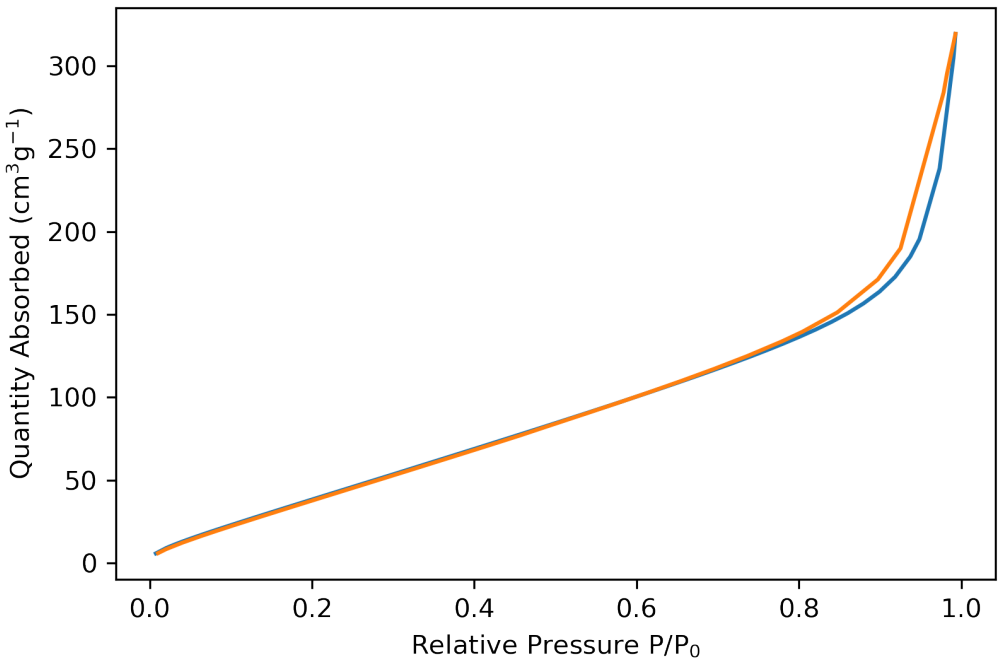

Figure 3.3: Gas sorption plot for produced porous polymer sample SHCP-01, where the blue line is the absorption cycle and the orange line is the desorption cycle.

of distributions are characteristic of polymer samples with high degrees of crosslinking.[51]

The BET surface area that was calculated for the material was 236 m^2g^{-1}. Given the pore size distribution and the surface area that was produced, it was likely that the materials produced are unlike Davankovs' hypercrosslinked polystyrenes.[44] These materials possessed unique structures that imbued them with non-classical physical properties. The materials were found to both possess rubbery and glassy properties at the same time. However, these properties seem to not exhibited by SHCP-01. This was likely due to two key reasons:

- The sulfur rank imparts a high degree of rotational freedom to the polymers, lowering the internal strain of the polymer.
- Complex processes in the reaction process are likely to oxidise the sulfur chains.

Whilst the second point was concerning in terms of producing a cleanly hypercrosslinked polymer, it was somewhat of a boon for absorption of mercury. Whilst the ideal reaction would produce a high surface area material, oxidation of the sulfur rank would however produce more chelating groups for water remediation. Previous research has demonstrated

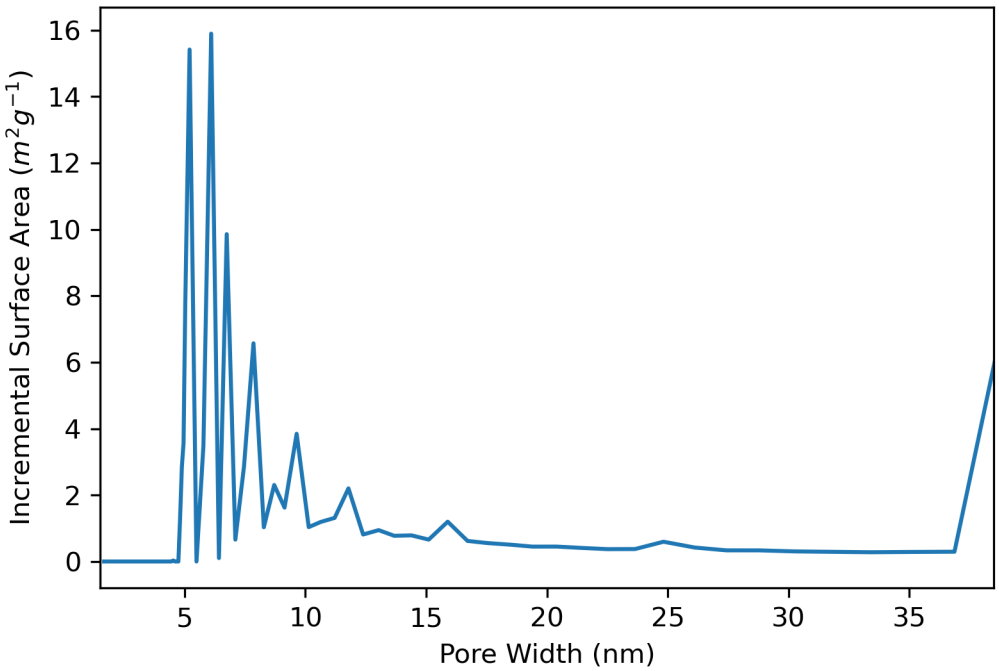

Figure 3.4: The pore size distribution of porous polymer SHCP-01, that was generated by applying several methods to the characteristic isotherm

that long S-S chains are not participatory in absorption. Evidence for oxidation of sulfur rank was discovered in the FT-IR of the sample. (Figure (3.12)

In conclusion, gas sorption was able to provide information about the textural properties of material SHCP-01. It was found that the material possessed a high degree of mesoporosity, but no microporosity. Macroporosity was also observed in the isotherm, but was more clearly visible in the SEM.

3.5.2 Morphological Characterisation

As discussed in the previous chapter, morphology of porous materials is usually analysed using electron microscopy. Of these techniques, the main two are transmission electron microscopy (TEM) and scanning electron microscopy (SEM). TEM is generally higher resolution, but also utilizes a higher acceleration voltage. These high energy electrons are more likely to decompose the material. Therefore, SEM was chosen as the technique for morphological analysis of SHCP-01.

Figure 3.5 displays two micrographs that were produced from SHCP-01 when viewed under a Tescan SEM. It can be seen from (a) which is a micrograph with a field of view

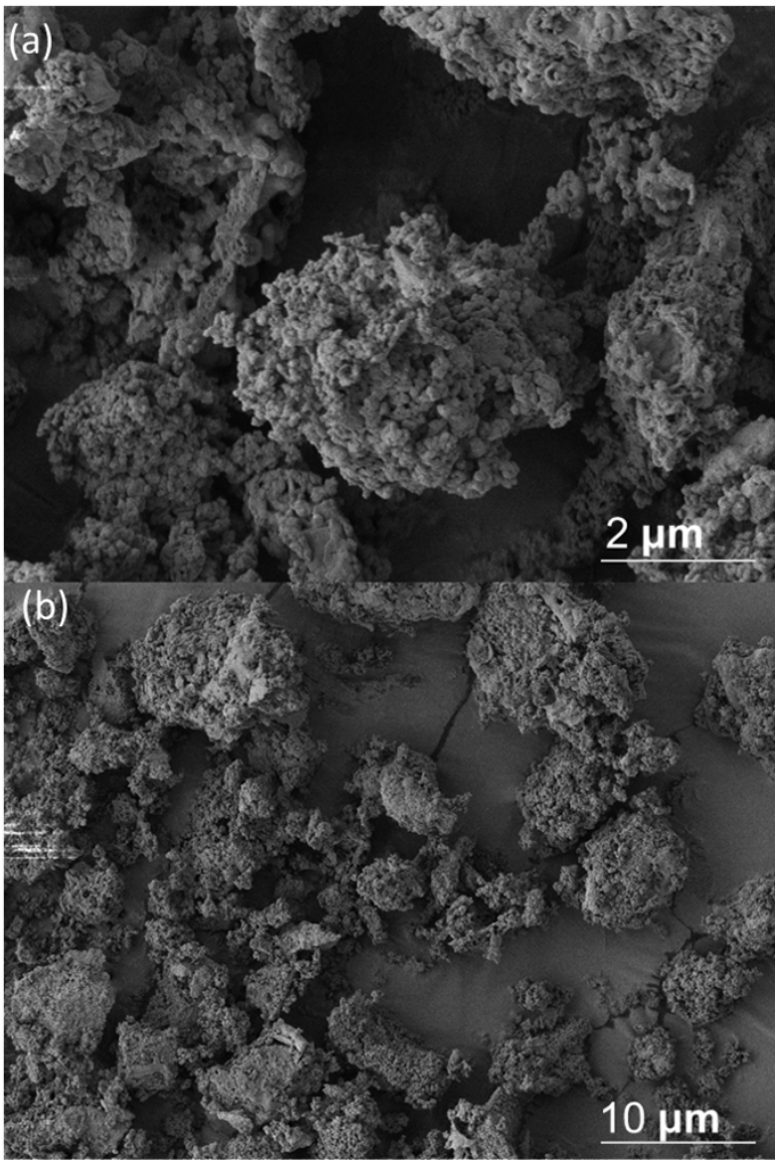

Figure 3.5: (a) 10 um FOV micrograph of SHCP-01 demonstrating the cauliflower like morphology of the particle in detail (b) 50 um FOV micrograph of SHCP-01 showing the irregular particle morphology and broad particle size range

(FOV) of 500 μm that the morphology is that of particles with an irregular shape. It is likely that as the polymer precipitated from solution during the crosslinking process it began to form an extended network, but due to the action of the stirrer the network was mechanically broken and hence the irregular particles.

It has been demonstrated in the literature that sometimes particulates are formed in the crosslinking of polymers.[52–54] However, these particles are almost unanimously spherical in nature. The spherical nature is generated because surface tension renders the most energetically favourable shape.

In (Figure 3.5b) a 50 μm FOV micrograph is visible. In this micrograph, the substruc-

ture of the irregular particles is more visible. The substructure displays the makeup of the irregular suprastructure as being constructed from smaller spheres. These spheres are likely the initial precipitant of a polymer gel that is highly cross-linked and retained the porosity in the solid state.

To conclude, the SEM revealed the morphology of the powdered SHCP-01 as irregular particles constructed from a much smaller polymeric sphere. It is likely that the mesoporosity that is generated, and detected by gas sorption experiments, is resultant from the packing of these spheres.

3.5.3 Polymer Characterisation

S-Styrene

Polymers produced in the process of inverse vulcanisation have undergone extensive characterisation.[55] Much of the characterisation that is used in the structural elucidation of inverse vulcanised polymers is also useful to the same elucidation in SHCP-01. This is a result of the shared physiochemical properties of SHCP-01 and inverse vulcanised polymers: insoluble, amorphous, and mainly comprised from sulfur.

Initial investigation into the chemical characteristics of SHCP-01 warranted investigation into S-Sty, the precursor. S-Sty was produced as first reported by Zhang *et al.*[56] A highly viscous yellow fluid was produced. The fluid was able to flow at higher temperatures (>30 °C), and be poured and cooled into a solid block and reheated to a liquid *ad infinitum*. This is demonstrated in Figure 3.6, in which the two melt cast forms of poly[s-(*ran*)-styrene] are demonstrated.

Despite previous reports, in which the authors claimed that the polymer was a fluid, it was found that the properties of the polymer were that of a shape persistent solid albeit with a low melting temperature. It is likely that the anaerobic synthesis lowered the degree of chain transfer and increased the molecular weight, imparting a higher melting transition to the material.

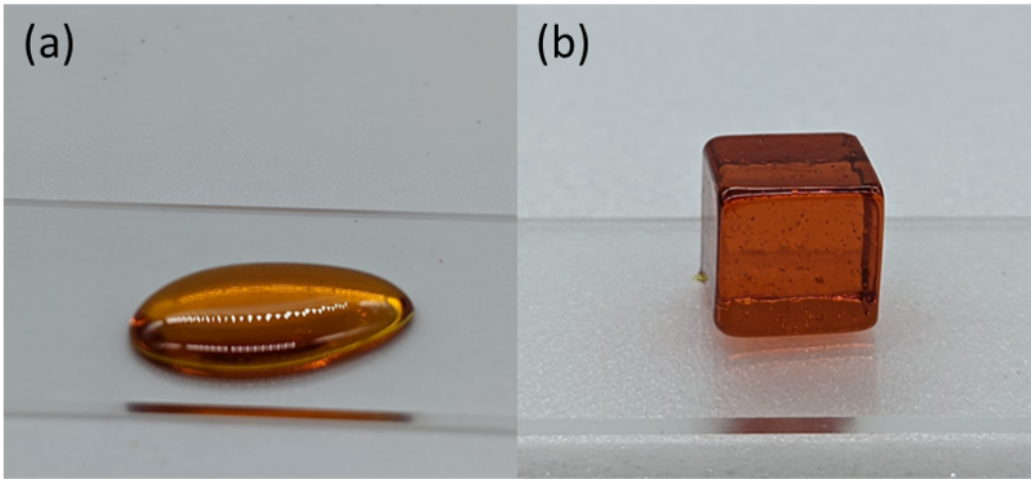

*Figure 3.6: (a) poly[s-(*ran*)-styrene] having been melted and poured onto a glass side (b) poly[s-(*ran*)-styrene] having been melted and cast into the shape of a freestanding cube*

Previous work performed with alkenes such as: 1,3-divinylbenzene[57], dicyclopentadiene,[58] farnesol[15], and farnesene[15] has demonstrated molecules with more than one alkene

to prevent melt processability. This is because the bifuncionality of the alkene promotes heavy crosslinking. However, styrene contains a single alkene functionality. Therefore, it would be sensible to assume that a linear polymer would result from this polymerisation reaction.

It was found that along with the melt transition of S-Styrene, there was a degree of solution processability, further hinting at the linear nature of the produced polymer. It was found that S-Styrene had a solubility of 10.7 mg L^{-1} in chloroform. The discovery of the solubility of S-Styrene in organic solvents allowed for use of gel permeation chromatography (GPC). The GPC trace for S-Styrene is demonstrated in Figure 3.7. From this trace it was calculated that the M_n, M_w values for S-Styrene were as demonstrated below in (Table 3.1).

Polymer Property	**Value**
M_n	105
M_w	3074
M_w/M_n	29.144

Table 3.1: Summary of the information gathered when the polymer is analysed using gel permeation chromatography

Furthermore, it was possible to perform ^{1}H NMR of the sample of S-Styrene, in deuterated chloroform. The NMR experiment confirmed the consumption of alkene within the polymer (peaks centred around 4.6, 5.8, 6.3 ppm), indicating a successful synthesis.(3.8) Previous work has indicated that the polymerisation mechanism of S-Styrene is complex, and likely proceeds *via* several mechanisms.[56]

Further analysis *via* pXRD demonstrated a lack of crystallinity in the produced polymer. Figure 3.9 demonstrates the pXRD pattern for elemental sulfur (orange) and S-Sty (green). The absence of crystalline S_8 in the pattern for S-Sty indicates consumption of elemental sulfur.

DSC was used to investigate the thermal properties of S-Styrene. (Figure 3.10) demonstrates the thermal transitions of S-Styrene, there are no observable thermal transitions that are apparent in the thermal analysis of elemental sulfur. Figure 3.10 also demonstrates the T_g of S-Styrene (-25.6 °C). The glass transition is a thermal transition that is only found in polymeric materials.

FTIR revealed a reduction of the C=C-H stretch at 900-920 cm^{-1} which indicates successful reaction of the C=C bond. This was complemented by a reduction in the

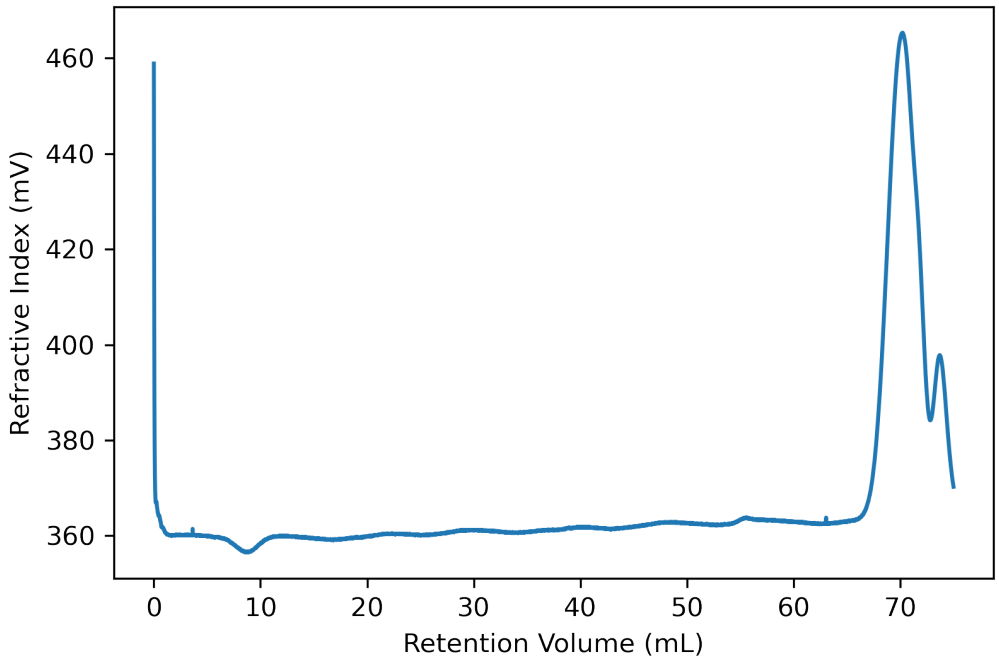

Figure 3.7: GPC trace of S-Sty demonstrating the low potential molecular weight of the produced polymer. It is likely that GPC is a poor technique for sulfur polymers as the standard that polymers are compared against is polystyrene which is chemically very different to a sulfur based polymer

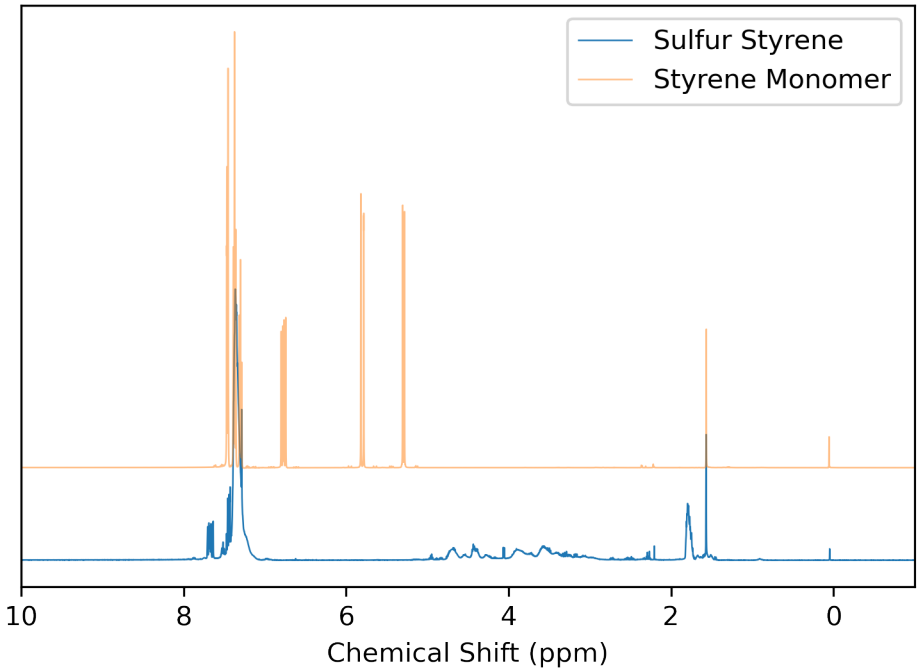

Figure 3.8: ^{1}H NMR of S-Styrene copolymer produced by reacting elemental sulfur and styrene at 135 °C.

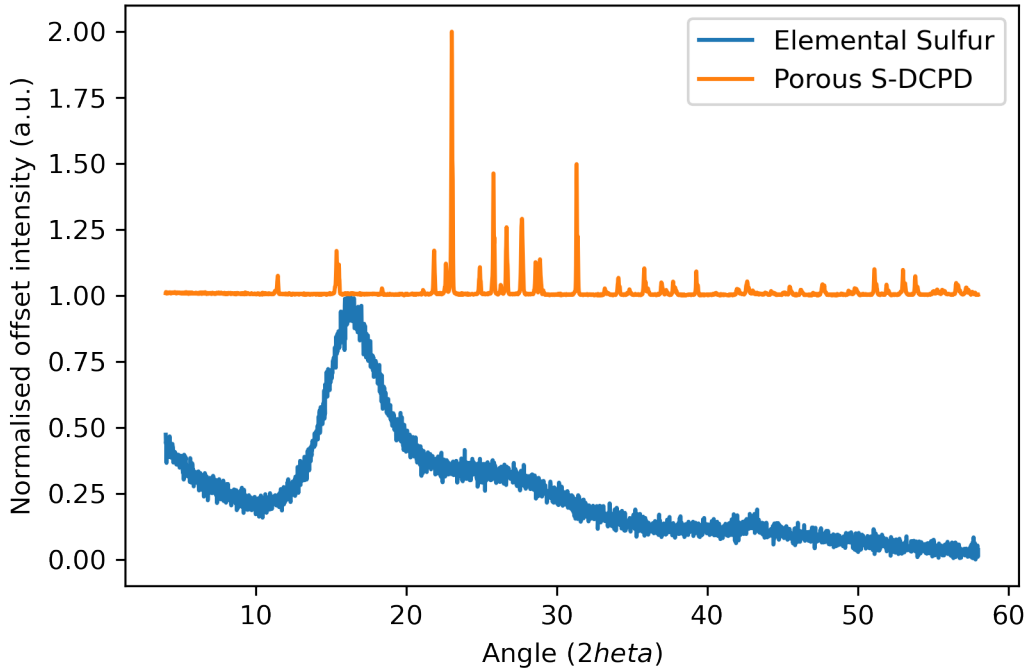

Figure 3.9: pXRD pattern of S-Styrene illustrating the amorphous nature of the produced material by lack of crystalline reflections in the diffraction pattern

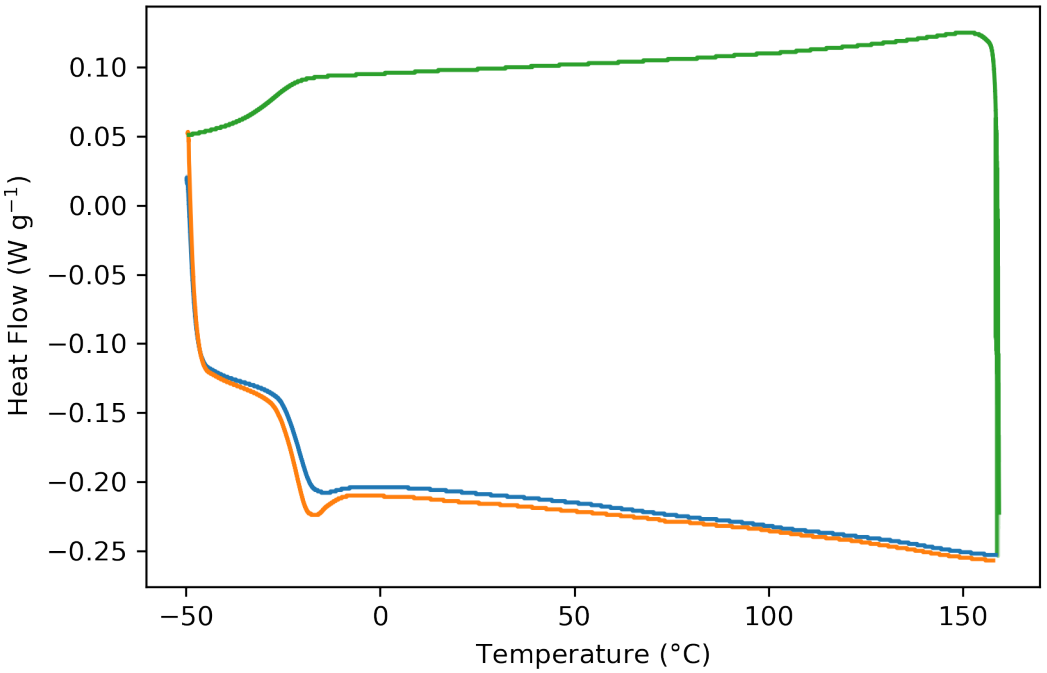

Figure 3.10: Plot demonstrating the results of a differential scanning calorimetry experiment of S-Styrene with a glass transition temperature centred around -25.6 °C that is consistent with literature values.[59]

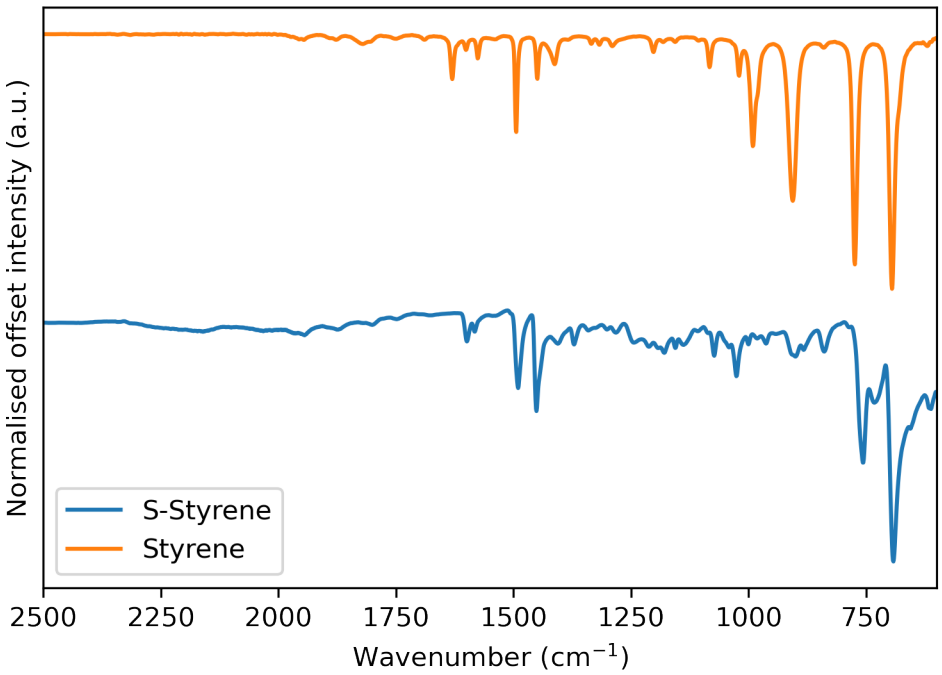

Figure 3.11: FTIR of S-Sty and the Styrene monomer

intensity of the C=C stretch at 985-1000 cm^{-1}, furthering the evidence for reaction of the C=C bond.

Finally, elemental analysis confirmed that the final composition of the polymer reflected that of it's predicted elemental composition. The analysed elemental composition was given as: (C: 26.72,H: 2.14,S: 70.71). The remaining elements present in the sample are likely to be trace amounts of catalyst, or oxygen from oxidation of the polymer during synthesis.

In conclusion, poly[s-(ran)-styrene] was successfully synthesised from elemental sulfur, and styrene in a bulk polymerisation process. The reaction was performed successfully at a 50 g scale with a 99.81 % yield. Successful polymerisation was inferred by comparing and contrasting with previously reported literature and readily available characterisation techniques. Further work in this section will address the product of the hypercrosslinking reaction (SHCP-01) and its chemical properties.

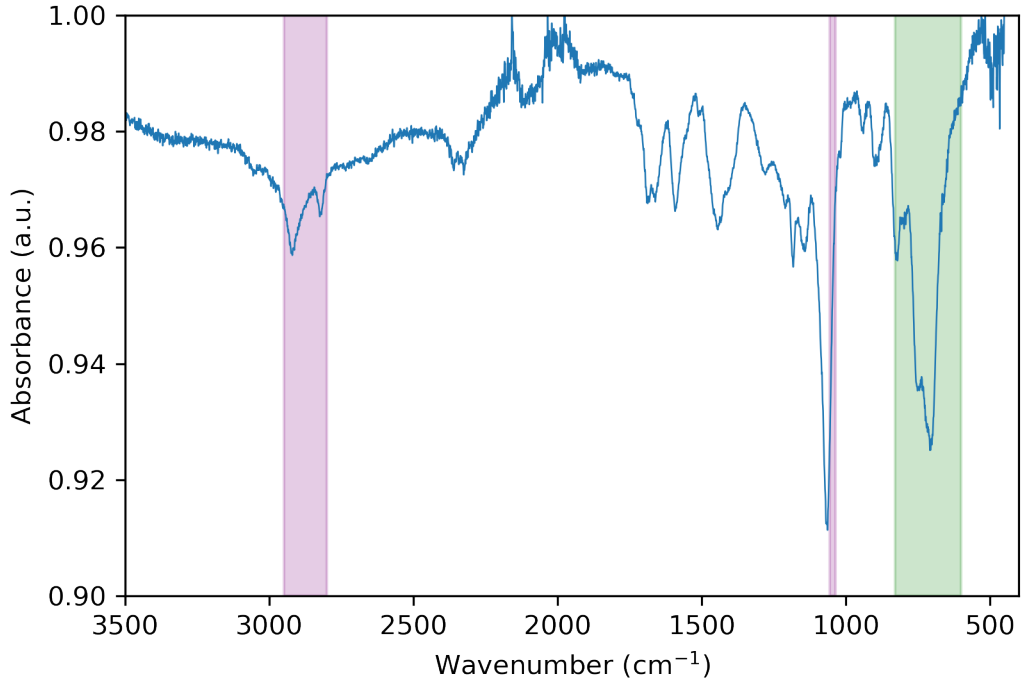

Figure 3.12: FTIR of SHCP01 demonstrating the inclusion of a C-Cl stretch that is indicative of the success of the reaction

SHCP01

As SHCP-01 was entirely novel, the characterisation first involved exploring the properties of the material. Given the produced material was insoluble and as such, techniques such as solution based NMR were ruled out. Solid state techniques such as: FT-IR, PXRD, DSC, elemental analysis, and TGA were, however, available for use in the characterisation of SHCP-01.

The FTIR of SHCP-01 produced the spectrum shown above. (Figure 3.12) There were several peaks that unveiled characteristics of the produced material. Firstly, the strong and broad band present at 600-830 cm^{-1} is characteristic of a C-Cl stretch. This is likely to be the result of the formed bridges between styrenes, which will have a remaining Cl. (green) There is also the aromatic C-H stretch highlighted. (purple)

Finally, elemental analysis confirmed that the final composition of the polymer reflected that of its predicted elemental composition. (C: 37.23% H: 2.48% S: 51.50%). There is a significant (20 %) decrease in the sulfur content. This is likely a result of the inclusion of the chloroform crosslinking units. pXRD (Figure 3.13) demonstrates a completely amorphous material. This is evidenced by the lack of crystalline reflections that the material would

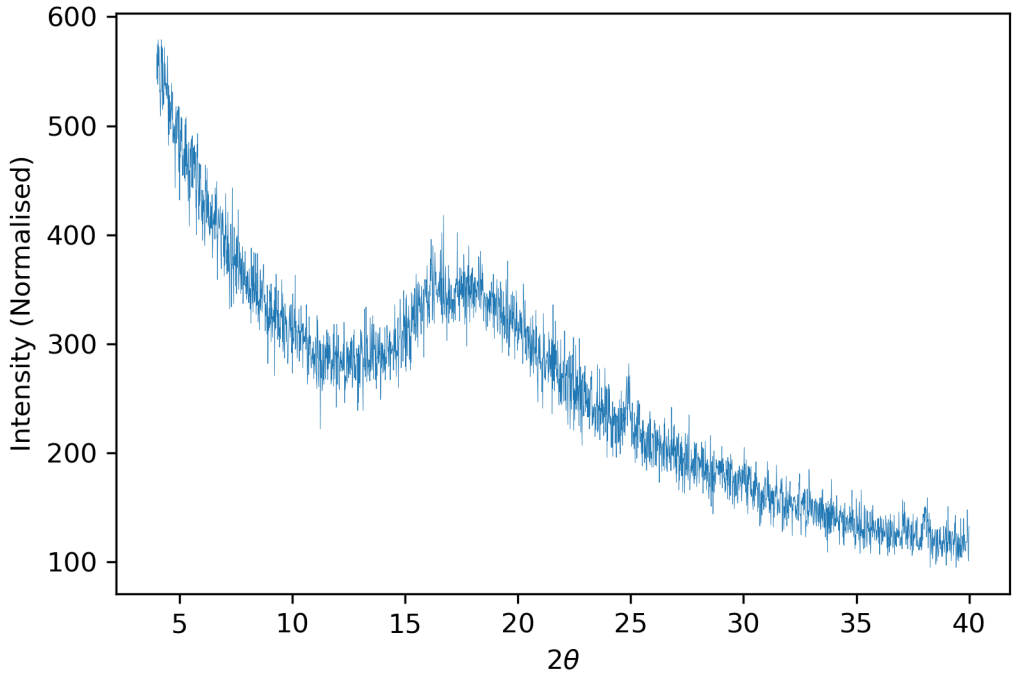

Figure 3.13: pXRD pattern for SHCP-01 demonstrating the lack of crystalline reflections in the material confirming the amorphous nature of the produced polymer

produce if it had any crystalline areas. The reflections would manifest as sharp peaks, however, they are absent. The lack of crystallinity is in fact supporting of the claim that the material is hypercrosslinked, as cross-linked materials are often not crystalline.

Thermogravimetric analysis (TGA) demonstrated the thermal stability of the material. The thermogram demonstrated that the material had a sharp decomposition at around 200 °C. This type of decomposition is characteristic of polymer with high sulfur content.

DSC was more complicated for SHCP-01. On the initial run of the DSC, it appeared that the thermogram produced was featureless. Sometimes when a material is highly cross-linked it may not exhibit a glass transition. This can be because there is a theoretical glass transition, but it lies above the decomposition temperature of the produced material.

It is also possible that the glass transition is very weak, and in this case it is possible to make the glass transition more pronounced by increasing the ramp rate during the DSC experiment.[60] In order to explore this, we increased the ramp rate to 30 °C per minute. The results of this are demonstrated in Figure 3.16. In this, a faint transition can be seen at 111.3 °C. If the transition was a glass transition, it would be slightly shifted higher as a result of the increased temperature ramp rate.

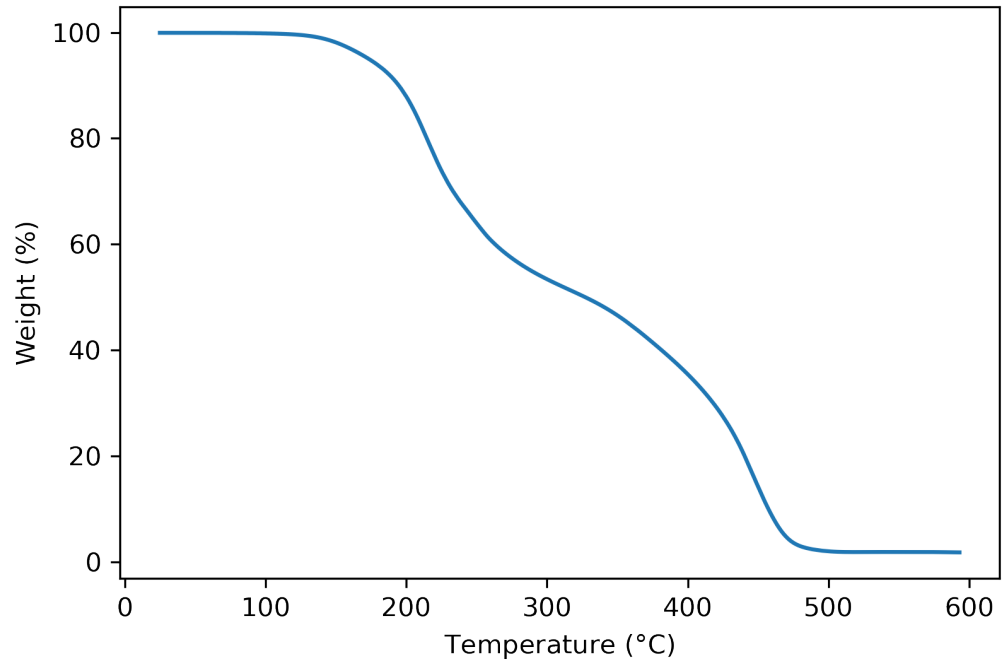

Figure 3.14: Thermogravimetric analysis of SHCP-01 showing the onset of decomposition just after 200 °C in air.

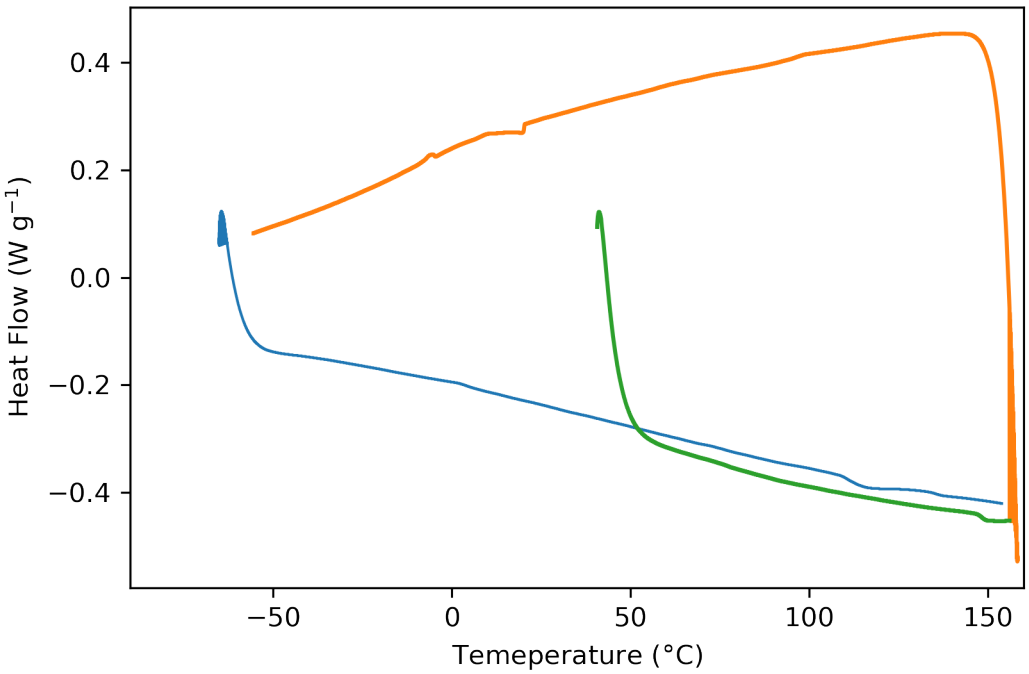

Figure 3.15: Thermogram of SHCP-01. A faint glass transition temperature can be observed at 111.3 °C. Initial heating (green), cooling cycle (orange), second heating cycle (green)

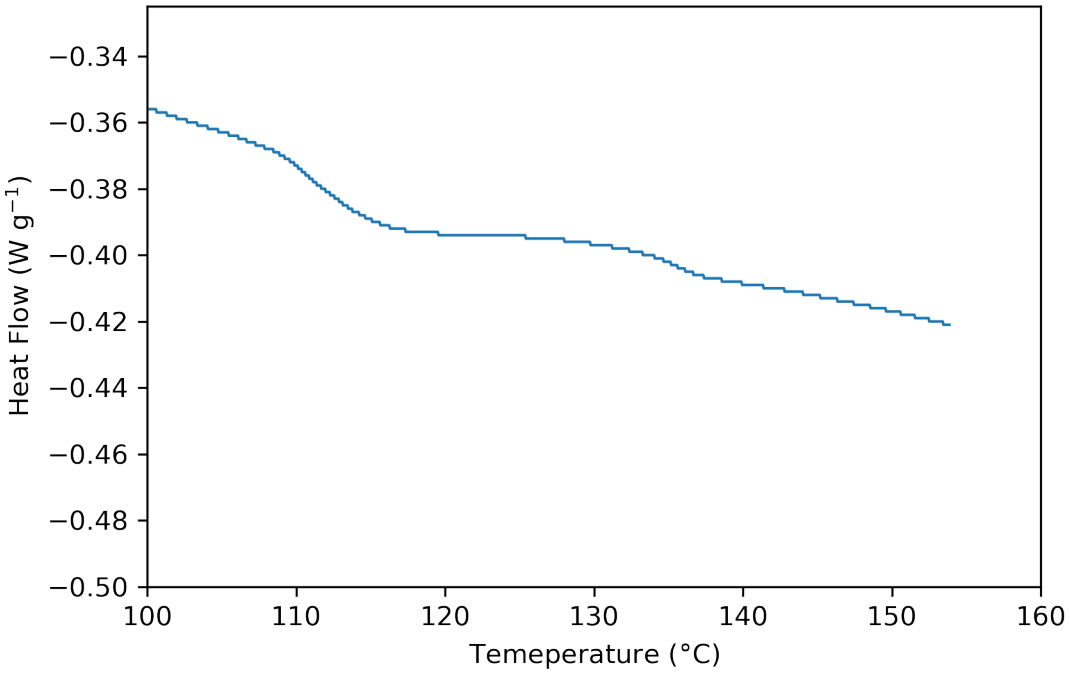

Figure 3.16: Results of a DSC experiment with the ramp rate increase to 30 °C a minute. The thermogram displayed here is merely a x-axis (temperature) limited expression of (Figure 3.15)

3.6 Applications

3.6.1 Ion-Exchange

Mercury is a potent environmentally present neurotoxin.[61] It is present in several chemical forms: $HgCl_2$, MeHgCl, $HgMe_2$, and others.[61,62] Some of the mercury is resultant from natural phenomena like geological activity, but a large portion of the pollution comes from anthropological sources.

A large source of environmental mercury is anthropological in origin, there is a large drive to remove mercury from the environment. One such 'drive' was the introduction of the Minimata convention in 2017.[63] 128 countries pledged to lower their mercury emissions by 2021.

Whilst there are large scale efforts to lower mercury emissions, there is a lack of high-performing sorbents for mercury. The current industrial standard for the removal of mercury from solution is styrene/DVB copolymers functionalised with thiouronium chelating groups.

However, despite being the industrial standard, these filters are still not rated for production of drinking water (NSF/ANSI Standard 61). The only method that is rated NSF/ANSI Standard 61 is ultrafiltration, a high energy inefficient process.

As previously discussed, sulfur and sulfur containing functionalities often possess a high affinity for mercury and its compounds.[64] It has been previously demonstrated that sulfur polymers are capable of high-affinity absorption of mercury from solution.[65]

When discussing the characteristics of ion-exchange resins, it is important to consider two key factors. The first and often most quoted value is the capacity of the ion-exchange resin. This capacity value is the maximum amount of substance (usually in mg) per g of ion-exchange resin.[66] The larger the number, the more substance the ion-exchange resin is able to absorb.

Secondly, and potentially more importantly, is the K_d value. This is often known loosely as the 'affinity' value.[67] A higher K_d results in a 'steeper' initial part of the absorption isotherm. What this translates into is the ability of the material to reduce the concentration of a substance at a low concentration. For compounds of mercury, this is especially important because mercury is incredibly toxic, no matter the concentration.[32]

Previous attempts utilising sulfur polymers for the removal of mercury from solution

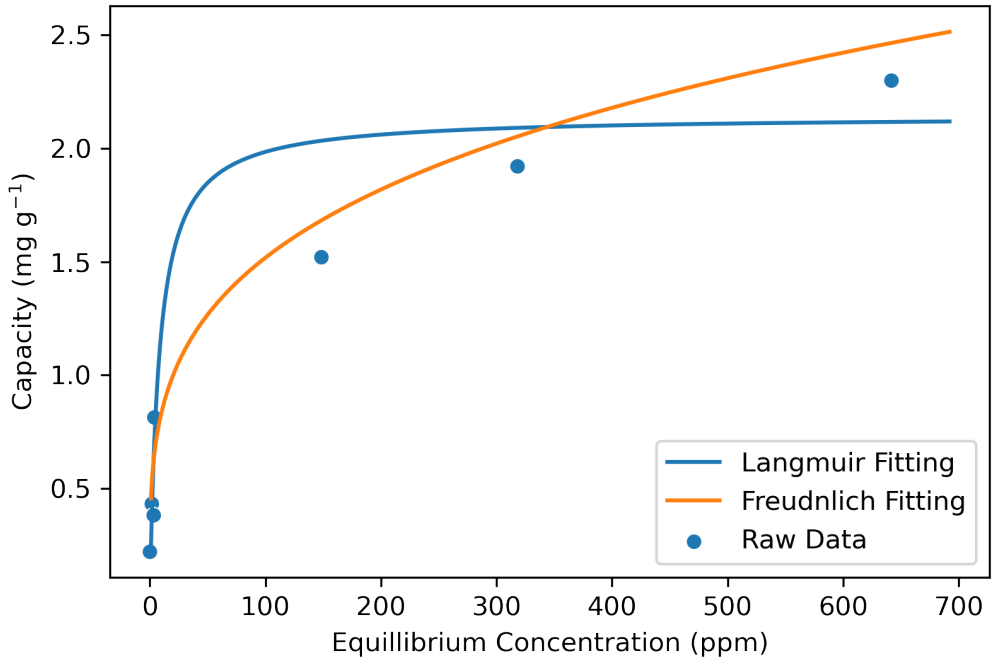

Figure 3.17: The results of an isotherm experiment on the salt templated material (S-PA) produced in Chapter 2. It can be seen that the Freundlich isotherm was a better fit. However, the Lanmguir fitting was also within acceptable limits (R^2 = 0.92).

have been met with varying degrees of success. For the 'pure' polymers, it is often found that a high affinity low capacity material is produced.[11,65,68,69] Materials like these are often lacking an isotherm, as it is impractical to generate isotherms at low concentrations. Some attempts have, however, been made. In 2019 Petcher *et al.* demonstrated that a salt porogen allowed for generation of macroporosity in pure sulfur polymer.[27] This polymer was fitted to a Langmuir isotherm and it was found that the capacity was 2.27 mg g^{-1}. The affinity (K_D) was 0.12 L mg^{-1}. (Figure 3.17).

In Figure (3.17) the characteristics for a low capacity, mid-affinity material can be seen (porous, salt templated S-DCPD). The low asymptote demonstrates the low capacity of the material, and the tangent to the y-axis demonstrates the affinity of the material. In figure 3.18 the isotherm for a high affinity, high-capacity material can be seen. This is evidenced by the characteristic 'sticking' of the line to the y-axis until quite a high value is obtained.

When SHCP-01 was tested for its characteristic absorption isotherm for $HgCl_2$ the results were good. Figure 3.18 displays the results of the experiment investigating this

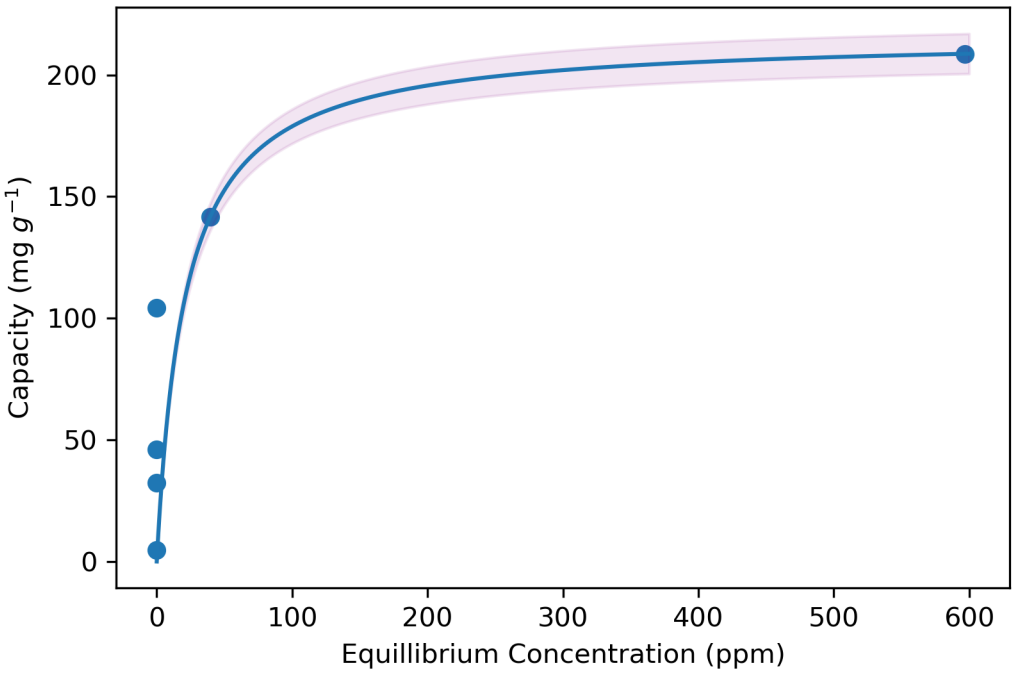

Figure 3.18: Graph demonstrating the results of a Hg^{2+} isotherm for porous polymer SHCP-01, with an overlay of a line fitting of the Langmuir model of absorption. The y-error is displayed as the shaded region surrounding the line.

characteristic. It can be seen that there is a high affinity, qualitatively, by the shape of the line. The calculated K_D for this line was 0.48. The calculated capacity for this line was 215.9 mg g^{-1}.

The capacity of the material was 215.9 mg g^{-1}. When compared to the industrial standard (activated carbon) it is 1.3 times higher.[70] When compared to the wider literature, the value is in the mid-range. However, part of the value of the material is in the cost. Considering the manufacture of the material was performed under ambient conditions, with commonly and cheaply available reagents, SHCP-01 is a fit for purpose material.

The K_D found was one of the highest reported in the literature. It is likely that this is owing in parts to the high sulfur content of the material, incorporating a large amount of chelating groups in the final material. It is this property that sets the material apart from others.

The high K_D value warranted further investigation, and to this end the sample was tested for its selectivity vs. competing metal ions and its capability to utilise its high affinity for mercury ions. The experiment involved the testing of the material in a simulated contaminated river water containing a large variety of metal ions at ppb range

concentrations.

Figure 3.19 demonstrates the results of this experiment. It can be seen that metal ions such as Se, Sc, Ni and others were completely unsequestered by the material but with complete removal of mercury from the solution. This is a particular boon for the material, as selectivity is key in design of ion-exchange materials. If it was desired that a material takes all metal ions out of solution, activated carbon would be the obvious choice. Often, this is not the case - especially in situations such as in drinking water or in purification of chlor-alkali brine for electrolysis.

Whilst the selectivity and affinity of the material were excellent, there was a final question in regard to SHCP-01's efficacy in a real world scenario. This was SHCP-01's ability to remove organomercury from solution. In real-world applications, methylmercury and its derivatives are often present, and these species interact differently than $HgCl_2$.

Dimethylmercury is a particularly potent neurotoxin and would be a model molecule for testing. However, it is too dangerous to use practically in a laboratory setting. Therefore, methylmercury chloride was used as a substitute in its stead. Whilst methylmercury chloride is ionic in character, it possesses some apolarity of dimethylmercury and is actually more common in the environment.

In order to limit exposure and use of methylmercury chloride, which is in itself incredibly toxic (LD50 39.6 mg kg^{-1} in rats[71]) it was decided to perform a simple single test at a low concentration. Table 3.2 demonstrates that the removal efficiency of methylmercury chloride from solution by SHCP-01 was 100 %. The blank solution was acquired from distilled water, the control solution was the distilled water spiked with methylmercury chloride, and the SHCP-01 filtered sample was the control filtered by SHCP-01. It can be seen that the material SHCP-01 removed all mercury from the sample.

Sample Name	**Hg Concentration (ppm)**
Blank	0.02
SHCP-01 Filtered	0.02
Control	11.45

Table 3.2: Table demonstrating the Hg concentrations of a blank sample, a sample filtered by SHCP-01 and a control sample.

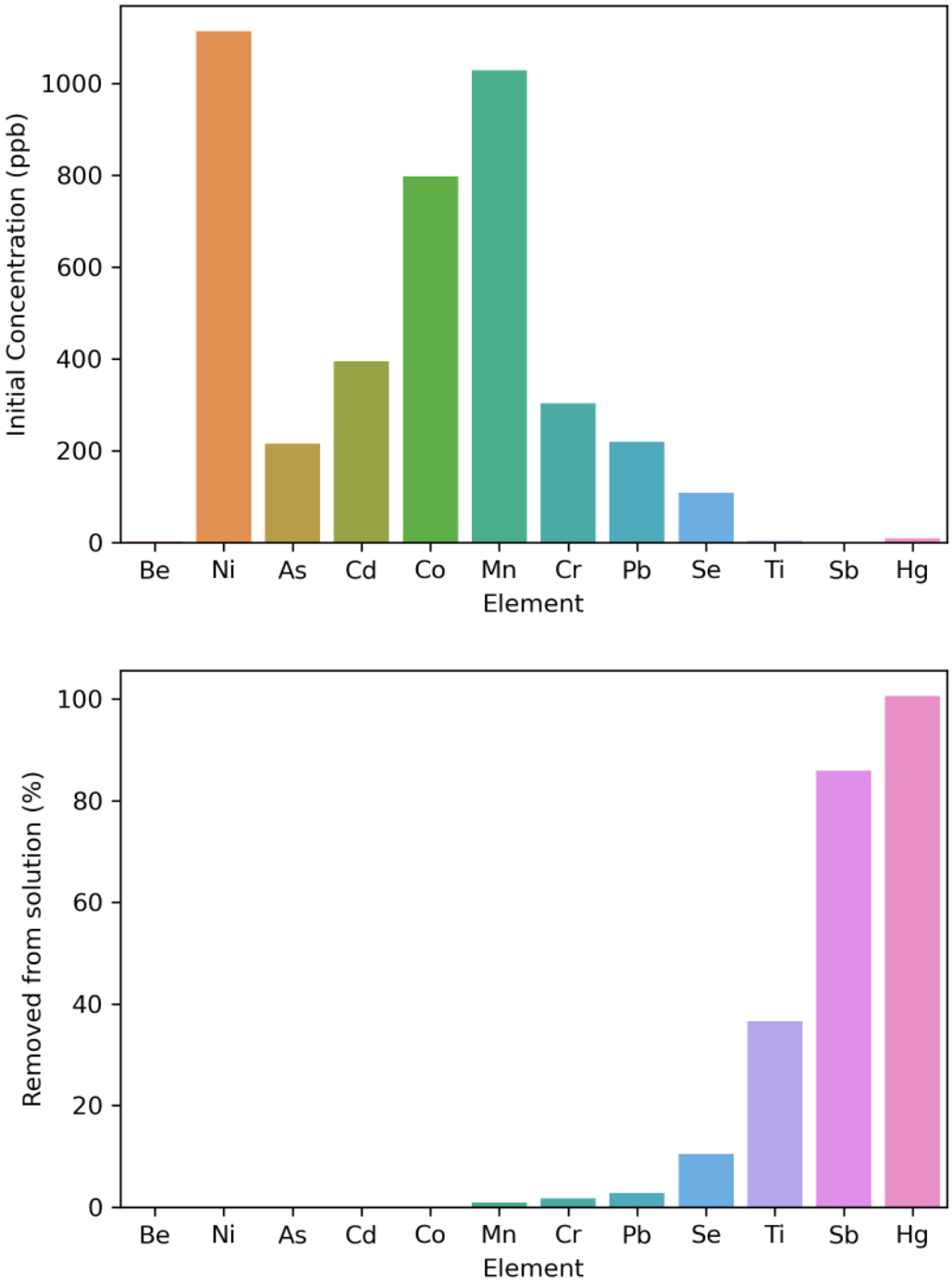

Figure 3.19: (top) Bar chart demonstrating the concentrations of metal ions present in a sample of polluted river water (bottom) Bar chart illustrating the percentage of metal ions removed from the river water by SHCP-01. It can be seen from the charts that the material is highly selective for mercury and antimony.

Overall, it was found that SHCP-01 was a promising candidate for sequestration of a wide variety of Hg(II) compounds from solution. It was found that SHCP-01 was able to sequester mercury from solution at a variety of concentrations, demonstrating its universality in the process. Furthermore, it was demonstrated that SHCP-01 was able to purify and selectively remove Hg from solution in a simulated real-world scenario.

3.7 Conclusions

At the outset of this project, three key aims were created. The first of which was to investigate the applicability of the hypercrosslinking process to soluble sulfur polymers. In that respect, the aim has been met. Whilst the scope of the study was niche, the method development of the process was quite complex.

Whilst the original hypercrosslinked polystyrenes exhibited non-classical properties that were the result of their highly strained internal structure, these properties were not reflected in the thiopolymer analogue. This is likely due to the inherent lability of the S-S bond. It is likely that such properties would be replicable in a thiopolymer.

The second aim was to investigate the textural and morphological properties of the resultant polymer, and to that extent the researches aims were met. It was found that the produced polymer had a cauliflower like morphology and a specific surface area of 236.04 m^2g^{-1}. Therefore, whilst the extreme levels of porosity that are exhibited in the original resins reported by Dvanakov *et al.* are not reproduced, a large increased in surface area was demonstrated.

The final aim of the research was to investigate the produced polymer, SHCP-01, in the removal of mercury from solution. This was thoroughly investigated and multiple forms, strengths, and matrices were investigated. ($HgCl_2$, MeHgCl and unknown mixed solutions) This research solidified the generalist nature of the polymer to many forms of aqueous mercury.

No research is ever fully complete, and in that regard there are several key avenues of potential further research in these polymers. To that end, it would be possible to investigate the kinetics of mercury removal from solution. Furthermore, it would be possible to investigate the applicability of these polymers for the removal of gaseous mercury.

Overall, however, it would be safe to conclude that the research was a success. A soluble sulfur polymer was subjected to the hypercrosslinking reaction conditions. Thereafter, it was characterised and found to possess an extraordinarily high surface area of 236.04 m^2g^{-1} and also a high sulfur content over 50 %. This type of material is an important discovery in the field of sulfur polymers, as until now no inverse vulcanised polymer has been found to possess an appreciable surface area.

3.8 Materials & Methods

Sulfur (S_8, sublimed powder, reagent grade, 99.5%, Brenntag UK Ireland. Chloroform ($\geq$ 98%) KBr (99.999 %), MeHgCl (1000 ppm) were obtained from Fischer scientific Ltd., Styrene (99%), $CDCl_3$ (99.8%), $FeCl_3$ (97%), $HgCl_2$ (99.999%, trace metals basis) were obtained from Sigma Aldritch. All chemicals were used without further purification.

3.8.1 Synthetic

Synthesis of poly[s-(*ran*)-styrene]

Sulfur (S_8, 14.000 g, 0.05458 mol) and Styrene ($C_6H_5CH{=}CH_2$, 6 g, 0.057609 mol) were placed in a 250 mL round bottom flask with a cross shaped magnetic stirrer bar. The round bottom flask was equipped with a rubber septum and placed under nitrogen flow. The round bottom flask was then placed into an aluminium heating block thermostatted at 100 °C for 20 minutes. After the 20 minutes had passed, the temperature was increased to 130 °C for 8 hours. Affording a viscous, insoluble yellow fluid. The sample was then allowed to cool and stored.

Hypercrosslinking of poly[s-(*ran*)-styrene] to produce SHCP-01

poly[s-(ran)-styrene] (2 g) was placed into a dry 250 mL round bottom flask and 50 mL of dry chloroform was added (an excess). The solution was heated to 50 °C to soften the poly[s-(ran)-styrene] and was stirred using a magnetic stirrer. After a suspension had formed, $AlCl_3$ (2 g, 0.01499 mol) was added. Immediately, a colour change was observed to a deep orange, which darkened with time. After 2 hours had passed, the remaining $AlCl_3$ was quenched with MeOH and stirring. The resultant black powder was filtered and washed with MeOH once, then $CHCl_3$ once. The resultant dark powder was then Soxhlet extracted with MeOH, and then $CHCl_3$ to afford a brown powder. Yield was recorded as 56.4%.

3.8.2 Applications Testing

$HgCl_2$ Isotherm

$HgCl_2$ (1.3520 g, 4.98 mmol) was weighed into a 1 L volumetric flask. The volumetric flask was subsequently filled to the 1 L line with distilled water and capped. The flask was inverted until all visble $HgCl_2$ powder had dissolved. The flask was then left for 24 hours and inverted another 20 times to ensure complete dissolution.

From this stock solution a series of diluted solutions were prepared: 1 ppm, 5 ppm, 10 ppm, 20 ppm, 50 ppm, 100 ppm, 200 ppm, 400 ppm, 800 ppm.

From each solution, 10 mL was dispensed into a 10 mL polypropylene centrifuge tube. To the tube, SHCP-01 (10 mg) was added. To ensure proper dispersal in the medium, the tubes were agitated and placed on a rotator for 24 hours.

After the allotted time had passed the solutions were filtered through 440 μm nylon syringe filters to remove the filtrate. The solutions were then prepared for ICP-OES. In the case of solution strength potentially greater than 20 ppm, the solutions were diluted by 1000 times prior to analysis to prevent carry over effects in analysis.

Fitting of Langmuir Isotherm

The Lanmguir model was fitted to the data using Origin Pro 9 using the Levenberg-Marquardt algorithm. Parameters for the curve were then used to plot the line using the Python library seaborn. The equation used was:

$$Q_e = \frac{K_\mathrm{D}\, C_e}{1 + K_\mathrm{D}\, C_e} \tag{3.1}$$

Where K_D is the affinity constant, Q_m is the saturation capacity and C_e is the equilibrium concentration.

MeHgCl Static Test

MeHgCl (1000 ppm, 2.5 mL) was pipetted into a 250 mL volumetric flask. The flask was then filled until the line. This yielded a 10 ppm MeHgCl solution.

10 mL of the 10 ppm MeHgCl solution was pipetted into a 10 mL polypropylene centrifuge tube. To this solution, SHCP-01 (10 mg) was added. The solution was agitated and left on a stirring rack for 24 hours.

Upon removal from the stirring rack, the solution was filtered through a 440 μm nylon syringe filter. The solution was then submitted for ICP-OES.

Simulated industrial waste testing

Certified reference material (10 mL) was pipetted into a 10 mL polypropylene centrifuge tube. To this tube, SHCP-01 (10 mg) was added. The solution was agitated and left on a stirring rack for 24 hours.

Upon removal from the stirring rack, the solution was filtered through a 440 μm nylon syringe filter. The solution was submitted for ICP-MS.

3.8.3 Instrumentation

Scanning Electron Microscopy (SEM)

SEM was conducted by adhering a carbon tab to a 12 mm SEM stud. Powders were dispersed onto the adhesive tab and imaged in a Tescan S800G. Imaging was conducted at a working distance of 5 mm with an electron acceleration of 1.5 eV and a beam current of 28 pA. Samples were prepared by dispersing dry powder onto an adhesive carbon tab.

Gel Permeation Chromatography (GPC)

The molecular weight of the poly[s-(*ran*)-styrene] was determined by gel permeation chromatography (GPC) using a Viscotek system comprising a GPCmax (degasser, eluent and sample delivery system), and a TDA302 detector array, using chloroform as eluent.

Powder X-ray Diffraction (PXRD)

pXRD was aquired using a PANalytical X'Pert PRO diffractometer with Cu-$K_{\alpha 1+2}$ radiation operating in transmission geometry. The X-Rays were of 1.54 Å. Samples were prepared by grinding in a mortar and pestle until a fine powder presented. The samples were placed into a fine layer (0.5 mm) over a shallow well.

Thermogravimetric Analysis (TGA)

TGA was conducted in platinum pans using a TA Instruments Q5000IR analyser with an automatic vertical overhead thermobalance. The samples were heated at 5 °C min^{-1} to 900 °C under nitrogen. Samples were prepared by finely grinding materials in a mortar and pestle and weighing to approximately 1 mg.

Differential Scanning Calorimetry (DSC)

Thermograms were conducted in a TA Instruments Q200 DSC under nitrogen flow. Heating and cooling rates were set to 5 °C min^{-1} on a heat/cool/heat cycle with maximum temperature of 160 °C and minimum temperature of -60 °C. Samples were prepared by grinding in a mortar and pestle and subsequently weighing approximately 5 mg of sample into a pan which was then hermetically sealed in a press.

Fourier-transform infrared spectroscopy (FTIR)

FTIR was performed on a Bruker ALPHA II. Samples were ground with dry KBr in a mortar and pestle. Samples were initially trialled at 50 wt% material and 50 wt% KBr and pressed using a 2 tonne hydraulic press with a 2 mm die. Samples were adjusted based on the signal strength by regrinding the produced pellet and ether adding or subtracting more polymer to the reground sample. It was found that between 60-90% of polymer was required to produce a readable spectrum.

^{1}H NMR

Solution NMR was recorded in deuterated chloroform using a Bruker Advance DRX (400 MHz) spectrometer at a concentration of 25 mg mL^{-1}

Bibliography

(1) P. Grange, *Catalysis Reviews*, 1980, **21**, 135–181.

(2) R. Steudel, *Elemental Sulfur and Sulfur-Rich Compounds I*, Springer, Berlin, Heidelberg, 2003, p. 166.

(3) W. J. Chung, J. J. Griebel, E. T. Kim, H. Yoon, A. G. Simmonds, H. J. Ji, P. T. Dirlam, R. S. Glass, J. J. Wie, N. A. Nguyen, B. W. Guralnick, J. Park, Á. Somogyi, P. Theato, M. E. Mackay, Y. E. Sung, K. Char and J. Pyun, *Nature Chemistry*, 2013, **5**, 518–524.

(4) M. Worthington, R. Kucera, J. C. G. Chemistry and u. 2017, *pubs.rsc.org*.

(5) A. Hoefling, D. T. Nguyen, P. Partovi-Azar, D. Sebastiani, P. Theato, S. W. Song and Y. J. Lee, *Chemistry of Materials*, 2018, **30**, 2915–2923.

(6) F. Wu, S. Chen, V. Srot, Y. Huang, S. K. Sinha, P. A. van Aken, J. Maier and Y. Yu, *Advanced Materials*, 2018, **30**, 1–8.

(7) J. J. Griebel, R. S. Glass, K. Char and J. Pyun, *Progress in Polymer Science*, 2016, **58**, 90–125.

(8) S. Namnabat, J. J. Gabriel, J. Pyun and R. A. Norwood, Organic Photonic Materials and Devices XVI, ed. C. E. Tabor, F. Kajzar, T. Kaino and Y. Koike, SPIE, 2014, vol. 8983, p. 89830D.

(9) J. J. Griebel, S. Namnabat, E. T. Kim, R. Himmelhuber, D. H. Moronta, W. J. Chung, A. G. Simmonds, K.-J. Kim, J. van der Laan, N. A. Nguyen, E. L. Dereniak, M. E. Mackay, K. Char, R. S. Glass, R. A. Norwood and J. Pyun, *Advanced Materials*, 2014, **26**, 3014–3018.

(10) T. S. Kleine, N. A. Nguyen, L. E. Anderson, S. Namnabat, E. A. Lavilla, S. A. Showghi, P. T. Dirlam, C. B. Arrington, M. S. Manchester, J. Schwiegerling, R. S. Glass, K. Char, R. A. Norwood, M. E. Mackay and J. Pyun, *ACS Macro Letters*, 2016, **5**, 1152–1156.

(11) M. P. Crockett, A. M. Evans, M. J. Worthington, I. S. Albuquerque, A. D. Slattery, C. T. Gibson, J. A. Campbell, D. A. Lewis, G. J. Bernardes and J. M. Chalker, *Angewandte Chemie - International Edition*, 2016, **55**, 1714–1718.

(12) N. A. Lundquist, M. J. Worthington, N. Adamson, C. T. Gibson, M. R. Johnston, A. V. Ellis and J. M. Chalker, *RSC Advances*, 2018, **8**, 1232–1236.

(13) A. D. Tikoalu, N. A. Lundquist and J. M. Chalker, *Advanced Sustainable Systems*, 2020, **4**, 1–9.

(14) M. J. Worthington, R. L. Kucera, I. S. Albuquerque, C. T. Gibson, A. Sibley, A. D. Slattery, J. A. Campbell, S. F. Alboaiji, K. A. Muller, J. Young, N. Adamson, J. R. Gascooke, D. Jampaiah, Y. M. Sabri, S. K. Bhargava, S. J. Ippolito, D. A. Lewis, J. S. Quinton, A. V. Ellis, A. Johs, G. J. Bernardes and J. M. Chalker, *Chemistry - A European Journal*, 2017, **23**, 16219–16230.

(15) D. J. Parker, S. T. Chong and T. Hasell, *RSC Advances*, 2018, **8**, 27892–27899.

(16) J. S. M. Lee, D. J. Parker, A. I. Cooper and T. Hasell, *Journal of Materials Chemistry A*, 2017, **5**, 18603–18609.

(17) X. Wu, J. A. Smith, S. Petcher, B. Zhang, D. J. Parker, J. M. Griffin and T. Hasell, *Nature Communications*, 2019, **10**, 647.

(18) A. M. Abraham, S. V. Kumar and S. M. Alhassan, *Chemical Engineering Journal*, 2018, **332**, 1–7.

(19) J. A. Smith, R. Mulhall, S. Goodman, G. Fleming, H. Allison, R. Raval and T. Hasell, *ACS Omega*, 2020, **5**, 5229–5234.

(20) Z. Deng, A. Hoefling, P. Theato and K. Lienkamp, *Macromolecular Chemistry and Physics*, 2018, **219**, 1700497.

(21) J. M. Scheiger, C. Direksilp, P. Falkenstein, A. Welle, M. Koenig, S. Heissler, J. Matysik, P. A. Levkin and P. Theato, *Angewandte Chemie International Edition*, 2020, **59**, 18639–18645.

(22) N. A. Lundquist, M. J. Sweetman, K. R. Scroggie, M. J. Worthington, L. J. Esdaile, S. F. Alboaiji, S. E. Plush, J. D. Hayball and J. M. Chalker, *ACS Sustainable Chemistry and Engineering*, 2019, **7**, 11044–11049.

(23) M. J. H. Worthington, C. J. Shearer, L. J. Esdaile, J. A. Campbell, C. T. Gibson, S. K. Legg, Y. Yin, N. A. Lundquist, J. R. Gascooke, I. S. Albuquerque, J. G. Shapter, G. G. Andersson, D. A. Lewis, G. J. L. Bernardes and J. M. Chalker, *Advanced Sustainable Systems*, 2018, **2**, 1800024.

(24) M. Mann, J. E. Kruger, F. Andari, J. McErlean, J. R. Gascooke, J. A. Smith, M. J. Worthington, C. C. McKinley, J. A. Campbell, D. A. Lewis, T. Hasell, M. V. Perkins and J. M. Chalker, *Organic and Biomolecular Chemistry*, 2019, **17**, 1929.

(25) T. Hasell, D. J. Parker, H. A. Jones, T. McAllister and S. M. Howdle, *Chemical Communications*, 2016, **52**, 5383–5386.

(26) D. J. Parker, H. A. Jones, S. Petcher, L. Cervini, J. M. Griffin, R. Akhtar and T. Hasell, *Journal of Materials Chemistry A*, 2017, **5**, 11682–11692.

(27) S. Petcher, D. J. Parker and T. Hasell, *Environmental Science: Water Research & Technology*, 2019, DOI: 10.1039/c9ew00477g.

(28) H. K. Lin, Y. S. Lai and Y. L. Liu, *ACS Sustainable Chemistry and Engineering*, 2019, **7**, 4515–4522.

(29) L. A. Limjuco, H. T. Fissaha, H. Kim, G. M. Nisola and W.-J. Chung, *ACS Applied Polymer Materials*, 2020, DOI: 10.1021/acsapm.0c00725.

(30) M. Thielke, L. Bultema, D. Brauer, B. Richter, M. Fischer, P. Theato, M. W. Thielke, L. A. Bultema, D. D. Brauer, B. Richter, M. Fischer and P. Theato, *Polymers*, 2016, **8**, 266.

(31) F. M. D'itra, in *Fourth Symposium on our Environment*, Springer Netherlands, 1991, pp. 165–182.

(32) T. W. Clarkson and L. Magos, *Critical Reviews in Toxicology*, 2006, **36**, 609–662.

(33) R. G. Pearson, *Journal of the American Chemical Society*, 1963, **85**, 3533–3539.

(34) V. Davankov, M. T. R. Polymers and u. 1990, *researchgate.net*, 1990, DOI: 10.1016/S0166-526X(11)56009-X.

(35) S. Xu, Y. Luo and B. Tan, *Macromolecular Rapid Communications*, 2013, **34**, 471–484.

(36) N. Fontanals, J. Cortés, M. Galià, R. M. Marcé, P. A. Cormack, F. Borrull and D. C. Sherrington, *Journal of Polymer Science, Part A: Polymer Chemistry*, 2005, **43**, 1718–1728.

(37) B. Li, H.-K. Luo, L. Liang, B. Tan, F. Su and H.-K. Luo, *Elsevier*, 2018, DOI: 10.1016/j.micromeso.2010.08.023.

(38) Y. Zhang, N. G. Pavlopoulos, T. S. Kleine, M. Karayilan, R. S. Glass, K. Char and J. Pyun, *Journal of Polymer Science Part A: Polymer Chemistry*, 2019, **57**, 7–12.

(39) Y. Zhang, J. J. Griebel, P. T. Dirlam, N. A. Nguyen, R. S. Glass, M. E. Mackay, K. Char and J. Pyun, *Journal of Polymer Science Part A: Polymer Chemistry*, 2017, **55**, 107–116.

(40) P. Yan, W. Zhao, B. Zhang, L. Jiang, S. Petcher, J. A. Smith, D. J. Parker, A. I. Cooper, J. Lei and T. Hasell, *Angewandte Chemie International Edition*, 2020, anie.202004311.

(41) J. C. Bear, W. J. Peveler, P. D. McNaughter, I. P. Parkin, P. O'Brien and C. W. Dunnill, *Chemical Communications*, 2015, **51**, 10467–10470.

(42) H. Gao, L. Ding, H. Bai, L. L. ChemSusChem and u. 2017, *Wiley Online Library*.

(43) L. Ding, H. Gao, F. Xie, W. Li, H. Bai and L. Li, *Macromolecules*, 2017, **50**, 956–962.

(44) M. Tsyurupa and V. Davankov, *Reactive and Functional Polymers*, 2006, **66**, 768–779.

(45) H. M. Rootare, in *Advanced Experimental Techniques in Powder Metallurgy*, Springer US, 1970, pp. 225–252.

(46) K. S. W. Sing, *Pure and Applied Chemistry*, 1985, **57**, 22–22.

(47) M. Thommes, K. Kaneko, A. V. Neimark, J. P. Olivier, F. Rodriguez-Reinoso, J. Rouquerol and K. S. Sing, *Pure and Applied Chemistry*, 2015, **87**, 1051–1069.

(48) W. G. McMillan and E. Teller, *The Journal of Physical Chemistry*, 1951, **55**, 17–20.

(49) E. P. Barrett, L. G. Joyner and P. P. Halenda, *Journal of the American Chemical society*, 1951, **73**, 373–380.

(50) S. Lowell, J. E. Shields, M. A. Thomas and M. Thommes, *Characterization of porous solids and powders: surface area, pore size and density*, Springer Science & Business Media, 2012, vol. 16.

(51) B. P. Santora, M. R. Gagné, K. G. Moloy and N. S. Radu, *Macromolecules*, 2001, **34**, 658–661.

(52) R. Arshady, *Colloid & Polymer Science*, 1992, **270**, 717–732.

(53) S. Shen, E. D. Sudol and M. S. El-Aasser, *Journal of Polymer Science Part A: Polymer Chemistry*, 1994, **32**, 1087–1100.

(54) C. M. Tseng, Y. Y. Lu, M. S. El-Aasser and J. W. Vanderhoff, *Journal of Polymer Science Part A: Polymer Chemistry*, 1986, **24**, 2995–3007.

(55) Y. Zhang, J. J. Griebel, P. T. Dirlam, N. A. Nguyen, R. S. Glass, M. E. Mackay, K. Char and J. Pyun, *Journal of Polymer Science, Part A: Polymer Chemistry*, 2017, **55**, 107–116.

(56) Y. Zhang, J. J. Griebel, P. T. Dirlam, N. A. Nguyen, R. S. Glass, M. E. Mackay, K. Char and J. Pyun, *Journal of Polymer Science, Part A: Polymer Chemistry*, 2017, **55**, 107–116.

(57) W. J. Chung, J. J. Griebel, E. T. Kim, H. Yoon, A. G. Simmonds, H. J. Ji, P. T. Dirlam, R. S. Glass, J. J. Wie, N. A. Nguyen, B. W. Guralnick, J. Park, Á. Somogyi, P. Theato, M. E. Mackay, Y. E. Sung, K. Char and J. Pyun, *Nature Chemistry*, 2013, **5**, 518–524.

(58) D. J. Parker, H. A. Jones, S. Petcher, L. Cervini, J. M. Griffin, R. Akhtar and T. Hasell, *Journal of Materials Chemistry A*, 2017, **5**, 11682–11692.

(59) Y. Zhang, J. J. Griebel, P. T. Dirlam, N. A. Nguyen, R. S. Glass, M. E. Mackay, K. Char and J. Pyun, *Journal of Polymer Science Part A: Polymer Chemistry*, 2017, **55**, 107–116.

(60) G. Wang and I. R. Harrison, *Thermochimica Acta*, 1994, **231**, 203–213.

(61) K. H. Telmer and M. M. Veiga, in *Mercury Fate and Transport in the Global Atmosphere: Emissions, Measurements and Models*, Springer US, 2009, pp. 131–172.

(62) P. Chu and D. B. Porcella, *Water, Air, & Soil Pollution*, 1995, **80**, 135–144.

(63) R. Kessler, *Environ. Health Perspect.*, 2013, **121**, A304–9.

(64) R. G. Pearson, *Journal of the American Chemical Society*, 1963, **85**, 3533–3539.

(65) T. Hasell, D. J. Parker, H. A. Jones, T. McAllister and S. M. Howdle, *Chemical Communications*, 2016, **52**, 5383–5386.

(66) K. K. Choy, J. F. Porter and G. McKay, *Journal of Chemical and Engineering Data*, 2000, **45**, 575–584.

(67) Y. L. C. and, S. A. Physicochemical and u. 2006, *Elsevier*.

(68) M. P. Crockett, A. M. Evans, M. J. Worthington, I. S. Albuquerque, A. D. Slattery, C. T. Gibson, J. A. Campbell, D. A. Lewis, G. J. Bernardes and J. M. Chalker, *Angewandte Chemie - International Edition*, 2016, **55**, 1714–1718.

(69) A. M. Abraham, S. V. Kumar and S. M. Alhassan, *Chemical Engineering Journal*, 2018, **332**, 1–7.

(70) P. Hadi, M. H. To, C. W. Hui, C. S. K. Lin and G. McKay, *Aqueous mercury adsorption by activated carbons*, 2015.

(71) F. M. Lin, M. Malaiyandi and C. R. Sierra, *Bull Environ Contam Toxicol*, 1975, **14**, 140–148.

Chapter 4

Thiopolymer Catalysis

4.1 Abstract

The following abstract was adapted from the research article on which a large portion of this chapter was based upon.

Inverse vulcanisation has enabled the creation of stable polymers that are derived from elemental sulfur, an unwanted by-product of the petrochemical refining process. Whilst the process doesn't require solvents, possesses high atom economy, and doesn't require initiators, the chemistry and applications are limited by the physiochemical properties of the cross linkers. Often, cross linkers are unable to be used as their boiling points are too low or simply will not react with elemental sulfur. Here, we report the catalysis of inverse vulcanisation. The catalysts are cheap and readily available and have been found to improve the properties of the produced polymers, increase yield, reduce reaction temperature and even reduce the emissions of dangerous H_2S gas. Furthermore, catalysis of inverse vulcanisation has been found to allow cross linkers that were previously unreactive to react with elemental sulfur.

4.2 Author Contributions

The work that is reported in this chapter was part of a larger, contiguous body of work centred around catalysis of inverse vulcanised polymers. The work was originally conceived by T. Hasell, and initial experiments and catalytic screening were performed by X. Wu. All work that was performed into subsequent investigations into the properties of produced polymers, synthetic work and experiments into rate acceleration were performed by myself, J. Smith and B. Zhang in equal parts. All the authors involved in the process were informed of the inclusion of data from the shared pool of work into this thesis and were happy for it to be included.

4.3 Introduction

Note: The work documented in this chapter was performed as a part of a larger body of work reported here: https://doi.org/10.1038/s41467-019-08430-8

The inverse vulcanisation process, first reported by Chung *et al.* in 2013 generated an entire field of research.[1] Whilst the polymers produced had a myriad of applications, such as: optics[2–4], battery materials[5,6], ion-exchange resins[7–16], fertiliser composites[17] among others, the polymers had several undesirable reaction characteristics that left scope for improvement. One of these was the high temperature of reaction (>159 °C), this limited the scope of the process. Another was the release of toxic H_2S gas.[18]

Lowering the temperature of reaction for inverse vulcanisation would save in energetic demands for synthesis, and even potentially improve the properties of the produced polymers. For this to be realised a catalyst would have to be investigated. In this chapter the investigation of potential targets for catalysis of inverse vulcanisation will be explored, the properties of the produced polymers synthesised investigated, and finally, quantification of the catalysed reaction profile. Furthermore, investigation of a catalyst for inverse vulcanisation would potentially open the inverse vulcanisation to temperatures <159°C, something that is not generally possible.

There are exceptions to the previous statement. Styrene[5], 2-ethylidene-5- norbornene[19], 4-vinylanilline[20] and others are able to undergo polymerisation reactions below this temperature. However, in a general sense the statement is still correct as low temperature reactions suffer from issues such as: production of oligomeric species and incomplete conversion of starting materials.[5,21]

In contrast, high-temperature (> 159°C) reactions suffer from issues such as: H_2S production, precursor evaporation, auto acceleration and the homopolymerisation of elemental sulfur.[22] Discovery of suitable catalysts for these types of reactions would mitigate the disadvantages of low temperature reactions and further reduce the chance of from which that high temperature reactions also suffer.

In doing so, it would be possible to further solidify the potential of inverse vulcanised reactions in an industrial setting by improving the possibility of scalability. It would also be possible to explore cross linkers that are currently impossible to copolymerise with sulfur due to low boiling points and high volatility.

In conclusion, development of a catalyst for inverse vulcanisation would potentially remove several barriers that prevent the scaling of the reaction to industrial levels, such as: H_2S production, high energy requirements, and low reaction scope. The following section will aim to discuss accelerators in the rubber industry, which are chemically similar to the targets for a catalyst for the inverse vulcanisation process. These molecules were chosen to investigate because of the chemical similarities between inverse vulcanisation and conventional vulcanisation.

4.3.1 Accelerators in the Rubber Industry

Vulcanisation was pioneered in the 1830s by Charles Goodyear.[23] However, the commercial and industrial use of vulcanised rubber was limited heavily by the fact the vulcanisation with sulfur alone is an incredibly slow and inefficient process.[24] Differences between catalysts and accelerators for the purpose of this work are likely to be somewhat unimportant as the end result is often indistinguishable.

However, despite this, it is important to first define the difference between a catalyst and accelerator. According to the IUPAC Gold Book, which references an older document concerning IUPAC recommendation from 1993 a catalyst is:

"A substance included in the solvent to increase the rate of transfer without affecting the position of equilibrium. The term accelerator may also be used, but kinetic synergist is not recommended."[25]

Modern (unofficial) usage has resulted in the term accelerant taking on the meaning of something that is not extractable after reaction completion. However, most of this is inconsequential and the reaction promoters that are explored in this text will be referred to interchangeably as catalysts and accelerators.

In the 1880s, the first semblance of a catalyst for the vulcanisation of rubber was discovered, almost 50 years after the initial discovery.[26] Research into molecules that are capable of performing as catalysts is still underway even today. Interestingly, the mechanistic designation of the pathways in which these molecules operate are often vague. This is due to the difficulty in analysing these types of reaction. Products are generally insoluble and amorphous, owing to their crosslinked nature. Therefore, common laboratory techniques such as solution based NMR and XRD are unavailable for the elucidation of reaction intermediates and products.

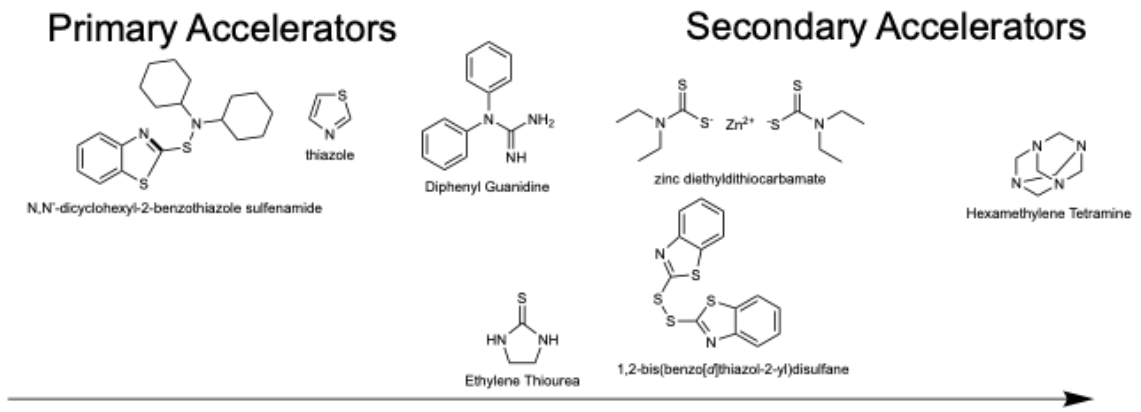

Figure 4.1: Diagram illustrating several accelerators, empirically ordering them in terms of their primary/secondary characteristics across a spectrum with the left side being entirely primary in character and the right being entirely secondary in character

Many of the effects that accelerators used in the rubber industry have on the vulcanisation process have not been investigated in the new field of inverse vulcanisation. The work in this chapter focuses on the initial application of commonly used vulcanisation accelerators in the inverse vulcanisation reaction as catalysts.

In order to explain the choices made in this work, it is important to explore the classes of compounds that are available in vulcanisation. Primary accelerators are classes of compounds based upon functionalities like thiazoles and sulfenamindes.[27] These compounds slow the curing, and improve the physical properties of the product, such as the hardness or the T_g. In this body of work, these types of accelerator were disregarded as the investigation objectives were centred around increasing the rate of reaction. A surprising result was found in that even though primary accelerators were not investigated, the physical properties improved regardless.

Secondary accelerators such as thiurams and dithiocarbamates are used to increase the speed of the vulcanisation reaction. Therefore, this class of accelerant is of greater relevance to the objectives of this body of work. Examples of both types of accelerators are displayed in (Figure 4.1). Whilst entirely empirical, the diagram gives a roundabout idea of the accelerator classes. Not all accelerators are exclusively in a single class, which is seemingly contradictory. Hexamethylene tetramine is an example of an accelerator that is used exclusively as a secondary accelerator, and as such is to the far right of the diagram. Ethylene thiourea is used as both and is more towards the centre.

It is fairly common that accelerators can share the characteristics of both types of

accelerator, something that increases the reaction speed is likely to improve the physical properties of the resultant rubber.[24] How this improvement in properties for rubber would translate to inverse vulcanised polymers is to be explored in this body of work.

There are many key parameters that must be fulfilled in the design of catalysts/accelerators for vulcanisation reactions. One of the most important characteristics that must be able to be fulfilled is solubility in molten rubber. Without solubility, the catalyst will not disperse well. This is well known in the rubber industry and is often referred to as 'sulfur bloom'.[28] A parallel could be drawn in the inverse vulcanisation reaction by looking at the solubility of the catalyst in liquid sulfur.

A second key characteristic that the chosen catalyst must have is the stability at the required operating temperature. This is likely to transfer quite well to the inverse vulcanisation process, as temperatures are somewhat comparable to the traditional vulcanisation.

A third characteristic is the cure rate, this is important in the rubber industry as it determines things such as 'scorch', which is the production of product that is insoluble in rubber. Localised production of this scorch can cause the final rubber product to possess weakened mechanical properties.

There are many other parameters that could be considered such as the stability and potential toxicity of the accelerator, decomposition products of the accelerator, the cure cycle and many more. However, many of these properties are researched and developed in house, and are trade secrets, so information is difficult to gather on the topic or are subject to patents.

In conclusion, catalysis in the rubber industry is a heavily researched area. There are many characteristics and subsets of catalysts that have been developed and effect the resultant rubber in different ways. Specialist terms such as scorch and sulfur bloom were covered. Whilst the area of rubber accelerants is heavily researched, it would be safe to assume a large portion of the findings are not available to the public, as the information produced from the research would be commercially sensitive. Therefore, it is only possible to work with what is available in the public domain.

4.4 Aims

In order to limit the scope of the research to that which is attainable and sensible, the following research aims were set at the beginning of the research:

- Screen several potential targets for the acceleration of the inverse vulcanisation reaction using time to gel as an indication of the rate of reaction increase
- Use the catalyst that produced the greatest increase in reaction rate to investigate the effect of rate increase across a series of cross linkers that have been previously reported and some that have not
- Characterise the produced materials and compare the properties of the produced polymer with that of a sample that had not been synthesised with an accelerator
- Use the information found to discuss potential mechanistic pathways for the acceleration

4.5 Approaches

Catalytic Screening

Many reactions with elemental sulfur will proceed at elevated temperature with no underlying issues at all. Examples of this have been demonstrated with DCPD[29], DIB[1], rapeseed oil[10], and others.[14,30,31] However, some cross linkers are not able to react with elemental sulfur. One of these cross linkers is ethylene glycol dimethacrylate (EGDMA). A graphical representation of this alongside several other examples is demonstrated in (Figure 4.2).

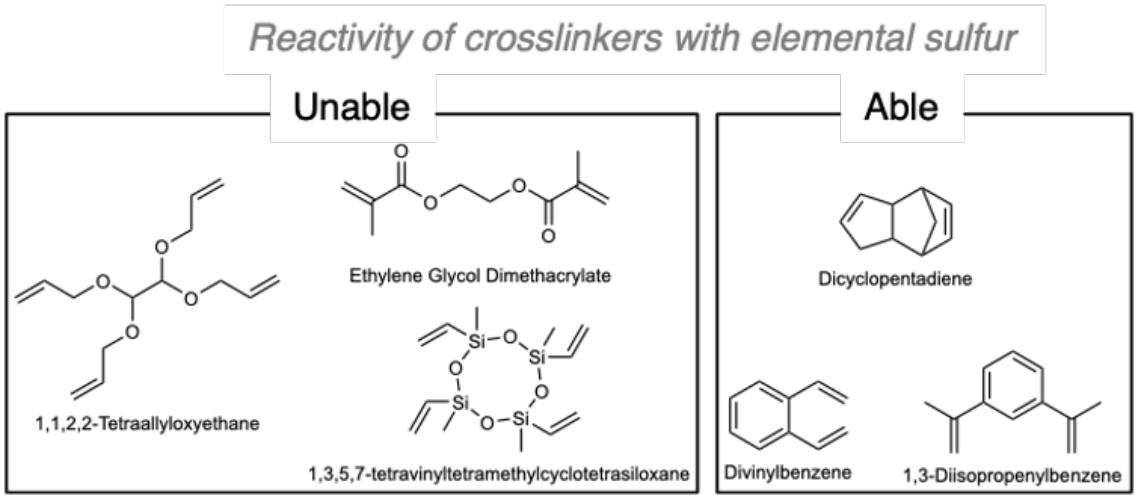

Figure 4.2: Graphic displaying cross linkers that are able to react with sulfur at an elevated temperature to form a polymer, and cross linkers that are not able to do this. Polymers that are unable to react include 1,1,2,2-tetrallylethoxyethane, ethylene glycol dimethacrylate, 1,3,5,7-tetravinyltetramethylcyclotetrasiloxane. Polymers that are able to react include dicyclopentadiene, divinylbenzene, and 1,3-diisopropenylbenzene

Given that EGDMA was unable to form a polymer with elemental sulfur under typical reaction conditions, we hypothesised that a suitable accelerator would facilitate this process and began the process of screening reactions to evaluate whether this would work. Table 4.1 demonstrates the result of this. The catalysts were chosen by drawing inspiration from catalysts used in the rubber industry, as previously discussed.

The catalytic screening was performed by reacting EGDMA with elemental sulfur at 135°C, and observing the products of reaction. In many cases, no homogeneous product was observed. This was usually a mixture of elemental sulfur and partially homopolymerised EGDMA. The produced materials were then analysed by pXRD to determine if any crystalline sulfur remained in the mixture.

As shown in Table 4.1, it appears that the metal centre had very little effect on the

overall reaction progress, and the inclusion of a diethyldithiocarbamate ligand had a marked effect on reaction progression. Interestingly, this result overlap with the findings of the rubber industry, in which thiuram derivatives are prominent secondary accelerators.

However, in contrast to the previous point, it was found that ZnO did not have any appreciable effect on the reaction progress with EGDMA. In the rubber industry, ZnO is a common accelerator. This may be that ZnO had limited solubility in the system, or even just is inert to the reaction conditions. To explore this effect fully, it would be necessary to see if there is any increase in reaction rate in a system that it works with. This was not explored further in this work.

Potential Accelerator	**Reaction products**	**Completed Reaction?**
Copper (II) Chloride	Yellow dispersion	No
Zinc (II) Chloride	Yellow dispersion	No
Iron (II) Chloride	Yellow-green dispersion	No
Copper (II) Oxide	Dark yellow dispersion	No
Zinc (II) Oxide	Yellow Dispersion	No
Elemental Zinc	Yellow Dispersion	No
Thiram	Yellow inhomogeneous solid	Partial
Zinc (II) Staerate	Orange Dispersion	Partial
Zinc (II) Diethyldithiocarbamate	Dark red solid	Yes
Iron (II) Diethyldithiocarbamate	Dark red solid	Yes
Cobalt (II) Diethyldithiocarbamate	Dark red solid	Yes
Copper (II) Diethyldithiocarbamate	Dark red solid	Yes
Nickel (II) Diethyldithiocarbamate	Dark brown solid	Yes
Sodium (I) Diethyldithiocarbamate	Dark red solid	Yes

Table 4.1: Table displaying a comprehensive list of potential catalysts trialled in this research their reaction products and assessment of completion of reaction

As previously mentioned, the criteria for a successful reaction was determined by the absence of crystalline reflections of elemental sulfur when the produced material was analysed *via* pXRD. An absence of crystalline reflections often confirms the consumption of elemental sulfur in the inverse vulcanisation and has significant precedent in the literature as a 'spot check'.[29] The results of performing pXRD on the produced materials that were resultant from varying the catalysts is displayed in Figure 4.3.

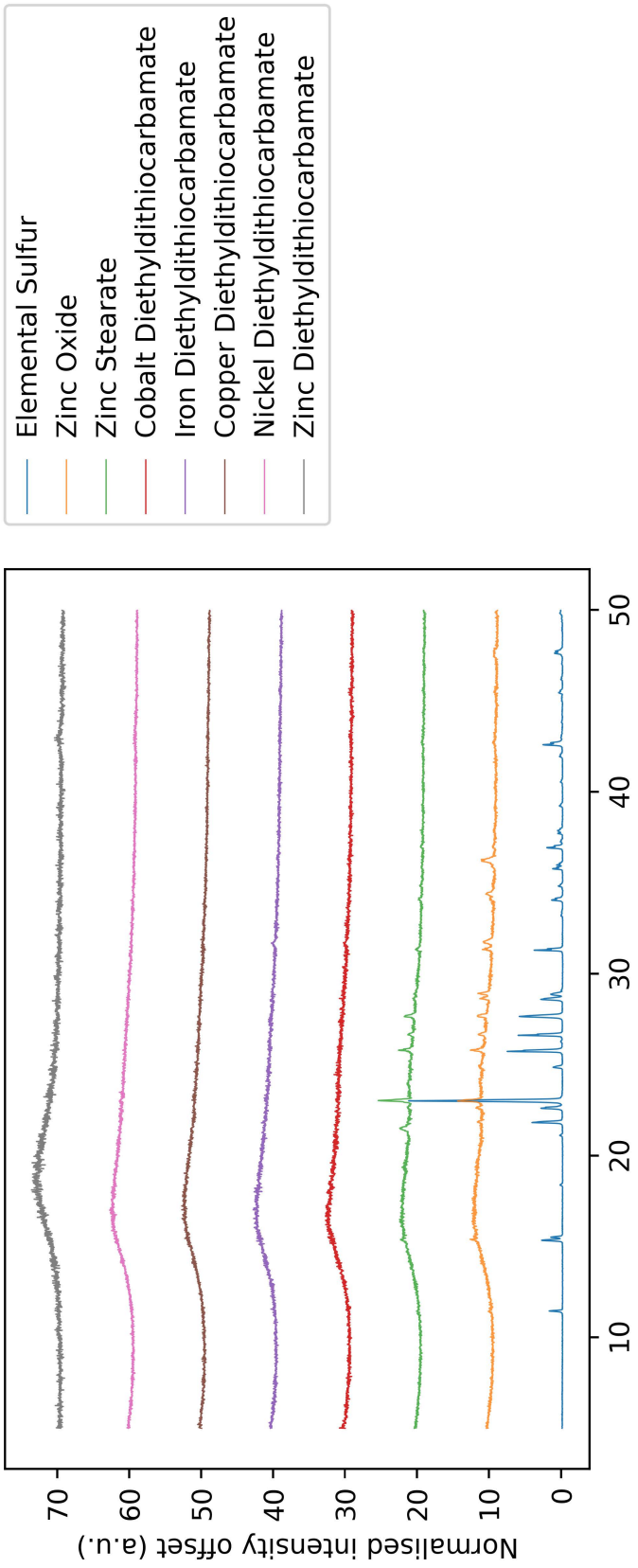

Figure 4.3: pXRD patterns of reaction products utilising differing catalytic agents in the inverse vulcanisation process.

It can be seen in Figure 4.3 that there are no peaks attributable to the crystalline reflections of sulfur in the samples in Table 4.1 that were classified as successful reactions in Table 4.1. There is just a large, broadened hump that is attributable to the amorphous nature of the materials. This hump is usually attributed to the combined interference of short range order present with an amorphous material. In certain materials such as the ZnO and zinc stearate there are crystalline reflections. These same crystalline reflections are present in the control sample. (sulfur)

It is possible that the thiocarbamate moiety plays a large role in the acceleration of the reaction. This is likely due to previously discussed similarities in the structure of industrial accelerants. Out of the tested catalysts, the best performing was sodium (I) diethyldithiocarbmate. However, in the reaction with EGDMA the reaction began to show characteristics of autoacceleration. There was a noticeable foaming, that is often characteristic of reactions that are close to autoaccelerating. For the purposes of the study it was important that the chosen accelerant had a wide operational temperature range, therefore zinc (II) diethyldithiocarbamate was chosen. It is likely that this effect was observed because the mass percentage of the diethyldithiocarbmate ligand was higher in the overall molecule.

4.6 Structure and Properties

4.6.1 Proposed mechanistic pathway

In spite of the many years that vulcanisation has been practised in an industrial setting, there is very little understanding of how the reaction proceeds. The reaction is complex, difficult to analyse and remains controversial in discussions regarding its mechanistic pathway even today.[32]

Conventional vulcanisation could proceed *via* a radical mechanism or an ionic mechanism.[32–34] In the radical mechanism, the S-S bond would undergo homolytic fission to produce a radical pair of sulfur atoms and in heterolytic fission an ion pair. (Figure 4.4) This process is dependent on the temperature to which the sulfur is heated. Generally speaking it has been demonstrated that sulfur undergoes homolytic fission at temperatures greater than 159°C, this is generally referred to as the 'floor temperature'.[35,36] At temperatures above 230°C sulfur will undergo heterolytic fission.[37]

Figure 4.5 demonstrates some of the groups that are potentially formed in the inverse vulcanisation process. There is literature that suggests these groups form in the vulcanisation process, which is very similar. Furthermore, it is likely that there are many more groups formed in the reaction that are not detectable in the final polymer.

Hence, it can be seen why it becomes difficult to draw any conclusions on potential mechanistic pathways that the catalyst provides. The complexity of the process is very high, and even the rubber industry has poor understanding of what is happening on a molecular scale. Therefore, so much understanding has been empirically derived.

Because the reaction is so complex, it could be easier to split the reaction into some key stages:

- Melting of inert sulfur and formation of polysulfides
- Reaction of polysulfides with alkene

As previously discussed, the first stage of the inverse vulcanisation reaction begins with the ring opening of elemental sulfur. This ring opening forms diradical sulfur chains. The first issue that was commonly encountered was the miscibility of the reaction feedstock.

Some cross linkers used such as: EGDMA, Trivinylcyclohecane (TVCH), trans, trans,cis-1,5,9-cyclododecatriene (TCCD) demonstrated poor miscibility with liquid sul-

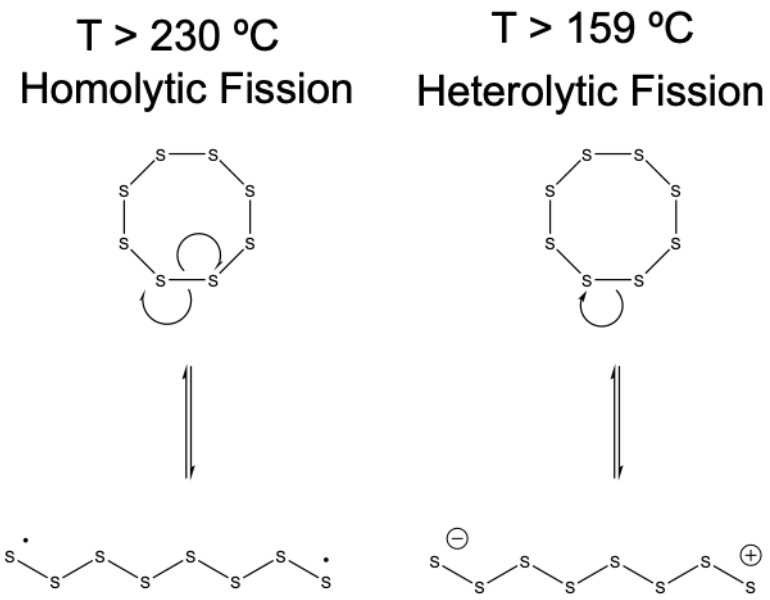

Figure 4.4: Schematic illustrating the homolytic and heterolytic fission of elemental sulfur

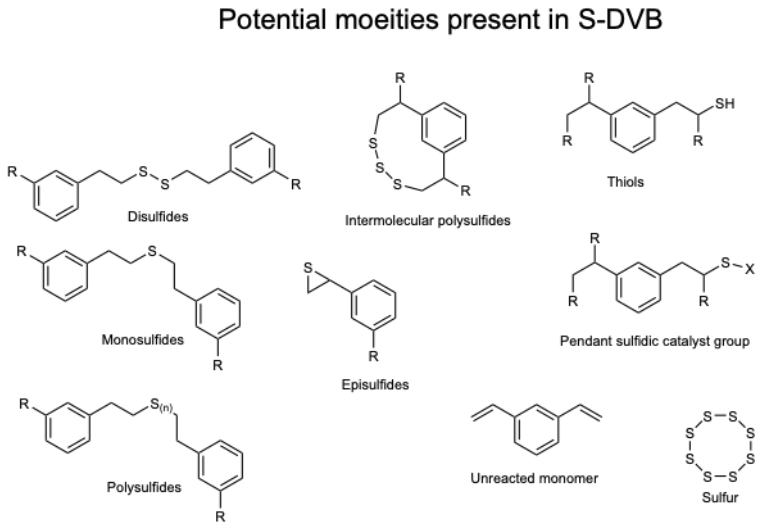

Figure 4.5: Diagram illustrating potential groups that are formed during the inverse vulcanisation reaction. Many groups are likely to form in very small quantities

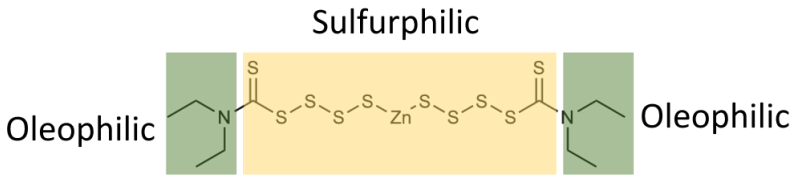

Figure 4.6: Diagram demonstrating the proposed 'sulfurphilic' and oleophilic regions of the zinc diethyldithiocarbamate intermediates produced during the catalysed inverse vulcanisation reaction

fur. However, upon inclusion of zinc diethyldithiocarbamate (ZnD) it was noted that a suspension formed. This suspension was noted among many of the cross linkers that were previously unable to react with liquid sulfur because of poor miscibility. Therefore, it would be fair to assume that a portion of the action of the catalyst could be attributed to a phase transfer like mechanism allowing the polysulfides to effectively solubilise into the cross linker, or vice-versa. (Figure 4.6)

Secondly, and equally important, is the formation of polysulfides. It has been recorded in the literature that the S-S bond in elemental sulfur is able to undergo homolytic fission above 159°C. This is not the full story, in fact this is an equilibrium. Some estimates put the amount of fissile sulfur at 1% is 159°C, with smaller amount existing below this temperature, and more existing at higher temperatures.

It has been suggested that zinc polysulfides form, and these zinc polysulfides are able to form at lower temperatures and more favourably than the 'bare' polysulfides that result from a purely thermal fission of the S-S bond. If this is the case, then it would not be out of the question to assume that the ZnD is accelerating the reaction by increasing the amount of available sulfur radicals for reaction.[26]

It could also be possible that these zinc complexed polysulfides are more easily able to react with alkenes. In this sense, the reaction is being catalysed in more than one way.[26]

These reasons for catalysis of vulcanisation are, however, non-specific and general in nature. Furthermore, all prior specifics regarding the mechanism have been discussed in the context of vulcanisation. Inverse vulcanisation is a different, albeit similar, process. A great portions of the literature surrounding inverse vulcanised polymers discusses an addition across a double bond *via* a radical addition reaction.[31,38–42] In almost direct disagreement to this there has been reports of generation of H_2S gas which suggests hydrogen abstraction.[43–46]

However, the field of inverse vulcanisation is still in its early stages. As a result of this,

much research is yet to be performed on inverse vulcanised polymers and their mechanism alone is yet to be elucidated. It would be unwise to make any strong suggestions as to the definitive mechanism of these polymerisation reactions without having any supporting evidence.

In conclusion, the difficulty and controversy surrounding the vulcanisation mechanistic pathway was introduced and discussed and contrasted with the inverse vulcanisation pathway. This was then combined with some initial observations into the catalysis of sulfur polymers. No strong suggestions for the catalytic pathway were made due to the difficulty in analysing reaction products. The following sections will discuss several noted effects the catalyst had on the production of the polymers, such as reduced H_2S emission, an increased rate of reaction and even an increase in the yield of the polymer. Attempts at rationalising these observations will be made.

4.6.2 Reduced H_2S emission

Evolution of H_2S during the inverse vulcanisation process has been noted almost as early as the first paper published on inverse vulcanisation. The first definitive recognition of the release of this toxic gas was reported by Yagci *et al.* in 2013.[45] In their experiment, they bubbled the effluent gas stream from an inverse vulcanisation reaction with polybenzodioxanes through a solution of lead nitrate and observed a precipitant of lead sulfide in the collecting flask.

The implication of this finding was quite large in scope. Initially, it highlighted a potential hazard in the inverse vulcanisation process. It also highlighted a potential issue in the scaling of the inverse vulcanisation reaction, that this obstacle must be overcome in order to produce inverse vulcanised polymers on a larger scale, or even to equip reactors with scrubbing mechanisms for the affluent gas stream. Environmental H_2S pollution remains a serious problem.[47]

One final implication was that at some point in the reaction process, hydrogen was being abstracted from a crosslinking molecule in the reaction medium. One of the initial suggestions for the mechanistic source was a process known as hydrogen abstraction, in which a free radical is able to remove a hydrogen radical from a substrate leaving a radical centre on the centre from which it was abstracted. The role that hydrogen abstraction plays in inverse vulcanisation is not yet clear, but some discussion has been put forward in previous sections.

It was decided to measure the effect of ZnD catalyst on the production of H_2S in inverse vulcanisation reactions. Figure 4.7 demonstrates the gas produced during the inverse vulcanisation reaction of cross linkers: Limonene, DCPD, DVB, and DIB. As can be seen in Figure 4.7 there is a clear trend in the reduction of evolved H_2S gas during the reaction when ZnD is included in the reaction mixture.

It was noted that up to a reduction of 700% in H_2S gas emission was produced in the reactions in which ZnD was used. This was a significant improvement upon the initial reaction conditions. This reduction in release of harmful gas opened the process to potential scale-up reactions and was the first time such a reduction had been reported.

To conclude, the inclusion of ZnD catalyst into the inverse vulcanisation reaction significantly and effectively lowered the amount of H_2S gas produced in the reaction. This could be due to the lowered temperature, or even due to differences in the mechanism .

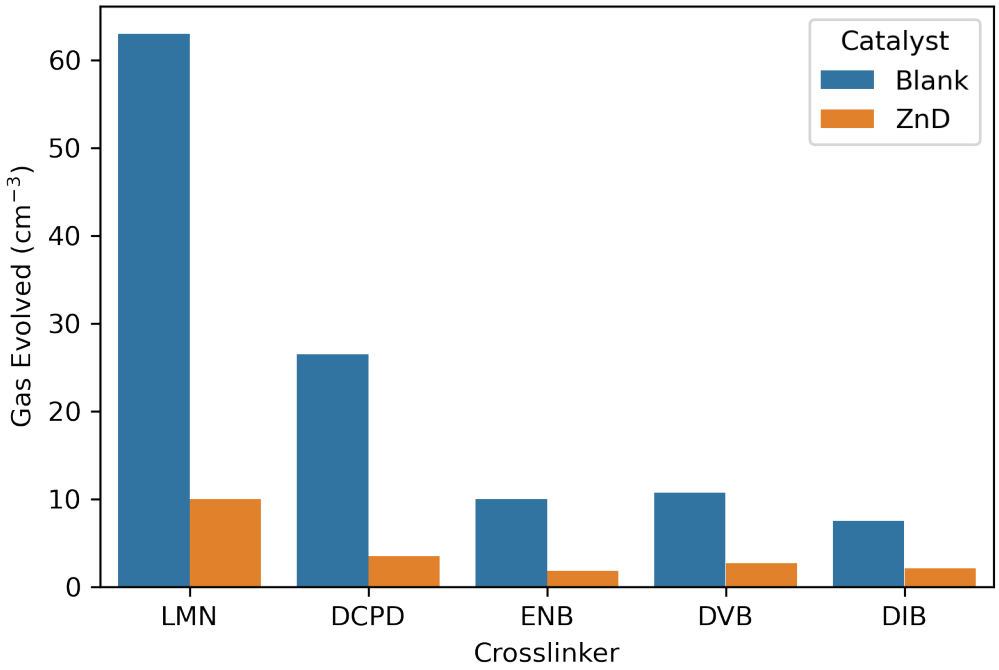

Figure 4.7: Results of an experiment that looked into the production of H_2S gas in the inverse vulcanisation reaction. It can be seen that the inclusion of a catalyst lowered the amount of H_2S produced across all cross linkers tested in the study (Limonene, DCPD, ENB, DVB, DIB)

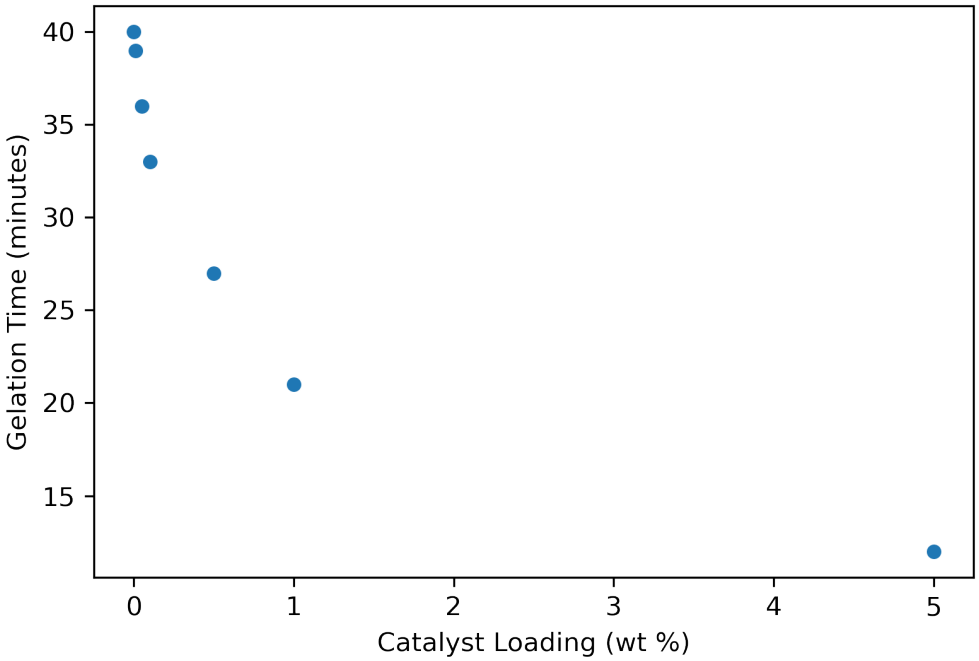

Figure 4.8: Graph demonstrating the reduced time to gelation for a 10 g reaction between equal masses of elemental sulfur and DIB with varying loadings of ZnD catalyst

4.6.3 Increased rate of reaction

One of the most important measurable qualities of a catalyst, and often the overall point in the use of a catalyst, is the effect the catalyst has on the rate of reaction. In order to get a rough idea of the effectiveness of the catalyst, it was decided to measure this effect. By measuring the time taken to gel for different loading of catalyst, it would be possible to get an idea of the relationship between catalyst loading and rate of reaction. The reaction that was chosen for the study was the reaction between elemental sulfur and DIB.

Figure 4.8 demonstrates the effect of increase of time to gelate vs. the wt % loading of ZnD into the reaction feedstock. In this instance, the gelation time is taken to be the time for the magnetic stirring bar to stop stirring due to the viscosity increase. It can be seen that as the wt % of ZnD is increased in the reaction feedstock, the time to solidification of the subsequent copolymer decreases in a non-linear fashion.

Above 5 wt% loading, it was noted that the reaction tended to progress to a speed that was almost too fast. When reactions between bulk monomers progress too quickly, they are susceptible to the Tromsdorf-Norrish effect and are likely to suffer from extreme exotherms.[48] Therefore, it was decided to limit the reaction loading to 5 wt% for safety.

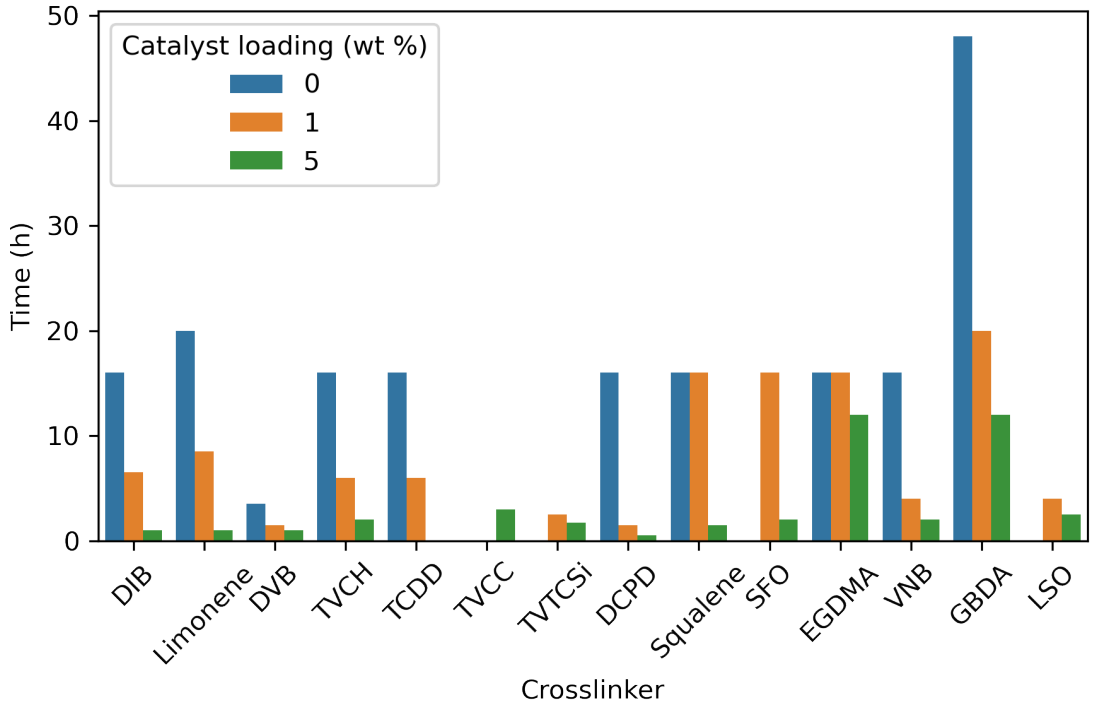

Figure 4.9: Bar chart demonstrating the increase in rate of reaction (inferred from time to form a homogeneous solution) for sulfur for a large range of cross linkers. Some set as 16 hours when given as a range

Given that the effect of the catalyst loading was noted for DIB it was decided to look at the effect that the catalyst loading had on the curing time for a series of cross linkers. The results of these experiments are summarised in Figure 4.9. It is evident that there was a decrease of time to gel across the board. The results, however, are not consistent in the sense that there is no proportional decrease across all cross linkers. This is understandable, given that the chemical groups contained within the different cross linkers are different and are likely to react differently.

Furthermore, as will be discussed in later sections there are some cross linkers where the time is actually 0, this is for the cross linkers that failed to produce a complete polymer.

In conclusion, it was found that the catalyst increased the rate of reaction exponentially for DIB when its wt % was increased. Further research determined that a series of cross linkers were further able to increase their rates of reaction with elemental sulfur by inclusion of a ZnD catalyst, and that the rate of reaction was not always exponential in increase.

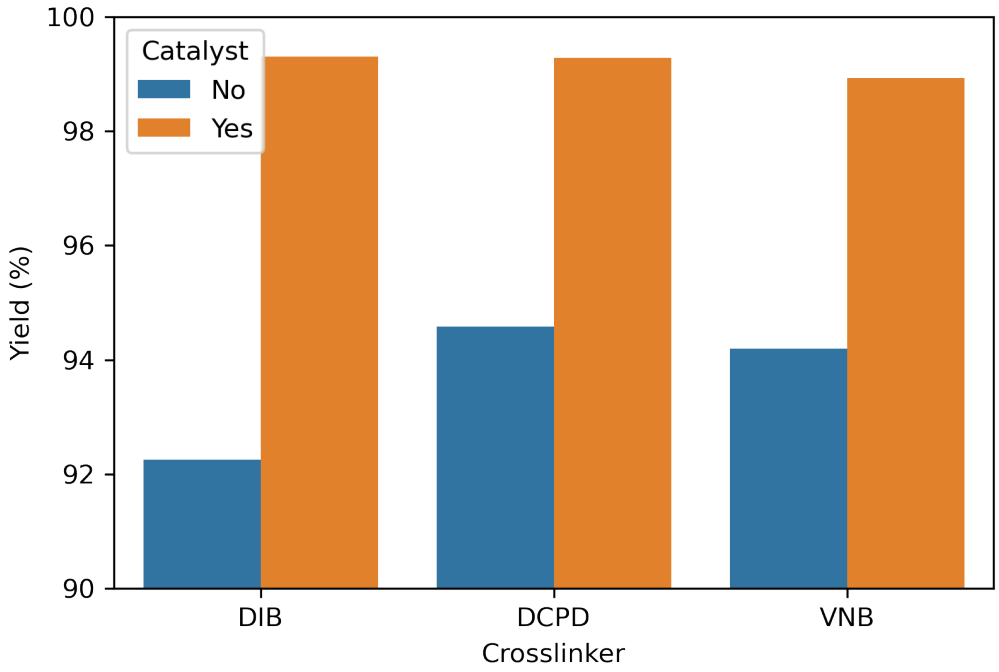

Figure 4.10: Bar chart demonstrating the increase in yield for a copolymerisation between elemental sulfur and DIB, DCPD or VNB with equal masses of sulfur and organic cross linker and 1% wt ZnD

4.6.4 Increased yields

Often, cross linkers used in the inverse vulcanisation process have boiling points that are comparable to the temperature of reaction. One of the results of this is that there is a significant, but nominal amount of material lost to evaporation during the course of the reaction. It was hypothesised that by adding ZnD to the reaction mixture, it would be possible to increase the yield of the reaction by lowering the amount of volatilised material during the reaction. By making the assumption that each system had a constant rate of evaporation, it leads that a quicker polymerisation would reduce the amount of evaporated volatile material. A further benefit of the increased yield would be a lowered emission during reaction.

As can be seen in (Figure 4.10) the yield of the reactions for DIB, DCPD and VNB increased with the inclusion of a 1% wt catalyst loading.

In the case of the copolymer formed by DIB and sulfur, it was found that the yield increased from 92.25% to 99.30%. This is a substantial increase in yield, and is most likely due to the aforementioned reasons. For DCPD and VNB, similar, but slightly lower

increases in yields were noted. (Figure 4.10)

In conclusion, it was found that inclusion of 1 wt% ZnD increased the yields of the inverse vulcansation reactions of S-DIB, S-DCPD, S-VNB to above 99% in each case. The increase in yield was attributed to a decreased rate of evaporation of monomer during the reaction. This is an important discovery in the field of sulfur polymers, as it brings the yield optimisation to near perfect numbers.

4.7 Applications

4.7.1 Previously Unreactive Cross linkers

EGDMA

Inverse vulcanised polymers are not universal. It is often impossible to form a copolymer from any selected cross linker and elemental sulfur. It is important that the cross linker has several key characteristics. The first of these is reactivity. An example of a reactive cross linker is DVB, upon mixing with sulfur a polymer will form in less than one hour. However, in the case of EGDMA this is not true. EGDMA will simply not react with elemental sulfur at temperatures above 159°C. If the reaction is performed, the result is elemental sulfur and cross linker intact in the vial. Figure 4.11 demonstrates this. At 0 wt% loading (left) the result of a reaction between EGDMA and elemental sulfur at 159°C for 24 hours is displayed. This yellow powder analyses as elemental sulfur.

Another possible reason for poor reactivity is poor miscibility with elemental sulfur. EGDMA is another great case of this, as EGDMA is very polar, it dissolves poorly into elemental sulfur which is apolar. Therefore, the initially weak reaction that results from elemental sulfur and EGDMA is further diminished by the poor reaction interface.

However, by inclusion of 1 wt% ZnD it is possible to react elemental sulfur with EGDMA to form a copolymer. As demonstrated in (Figure 4.11) a red copolymer results, (middle) that darkens when the catalyst loading is increased to 5 wt %. (right)

The resultant polymer is somewhat comparable in characteristics to S-DIB, a previously reported cross linker. It is a deep red, hard solid. However, in contrast to S-DIB S-EGDMA is completely insolube and possesses no soluble fraction even in organic solvents such as tetrahydrofuran or chloroform.

Confirmation of successful reaction was firstly elucidated by means of pXRD as discussed previously and demonstrated in Figure 4.3. However, this evidence is not complete in nature. In order to strengthen the evidence, analysis was performed by solid state ^{13}C NMR and FTIR. As can be seen in (Figure 4.12a) the evidence for the formation of C-S bonds is found at 25 ppm, with a complete loss of the C=C peaks that are present in the unmodified monomer at 125 ppm. For complete assignment, refer to appendix Figure A.34.

Further confirmation can be found in Figure 4.12b, wherein a FTIR spectrograph is

Figure 4.11: Photograph of produced polymer, S-EGDMA produced at different catalytic loadings: (left) 0 wt% (middle) 1 wt% (right) 5 wt%

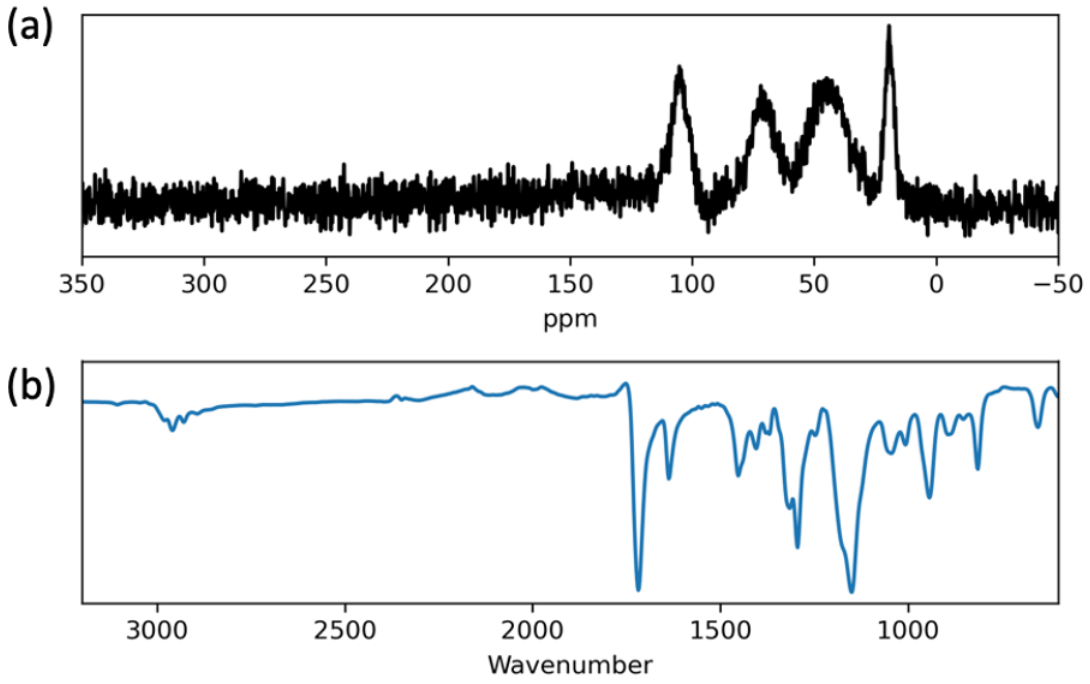

Figure 4.12: (a) ^{13}**C** *SS-NMR spectrum of S-EGDMA synthesised with 1 % ZnD catalyst and a 50:50 ratio of elemental sulfur and EGDMA (b) FTIR spectrum of S-EGDMA synthesised with 1 % ZnD catalyst and a 50:50 ratio of elemental sulfur and EGDMA.*

visible. The graph clearly demonstrates the reduction in intensity for the signal at 1650 cm^{-1}. Furthermore, there are reductions in the fingerprint region that correspond to the signals that are attributed to the C-H bending of alkene peaks. (650, 800, 950 cm^{-1}). Given this information, it can be concluded that there was a reaction with elemental sulfur and the alkenes.

Characterisation of the thermal properties of S-EGDMA was performed by employing DSC and TGA. The DSC (Figure 4.13) revealed a glass transition temperature of approximately 20°C, without much variation even when catalyst was used. The important part of this information, however, was not the value of the glass transition but the appearance of one.

When combined with the previously mentioned information that was gathered from the ^{13}C NMR and FTIR, it confirmed that a polymeric material was formed, and that the alkenes had reacted with sulfur. This, when combined with the insolubility of the final product, provided strong support to the claim a polymer was successfully generated, and the catalyst was working. It is important to note that when no catalyst was used, a melt transition for elemental sulfur was observed, confirming the presence of elemental sulfur in

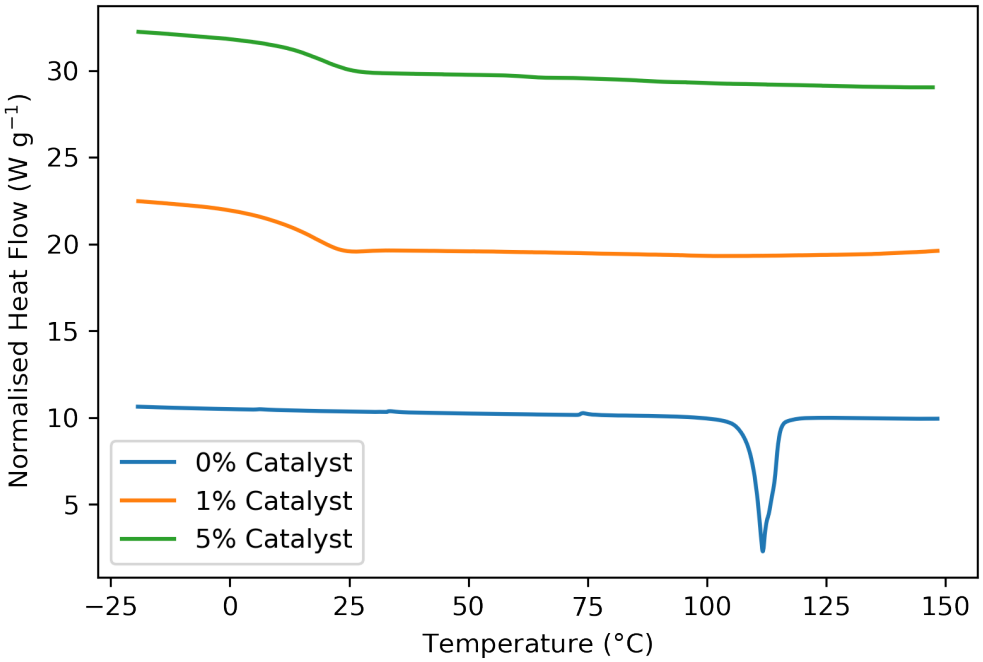

Figure 4.13: DSC of S-EGDMA on the final heating cycle at various catalytic loading wt percentages with the glass transition visible, and the 0 wt% sample clearly displaying a sulfur melt transition

the sample. In this case, the polymer had not formed.

Thermogravimetric analysis (Figure 4.14) of the polymer revealed a decomposition temperature of approximately 200 °C for the polymer, regardless of catalytic loading or even type of catalyst. However, given that previous experiments had revealed a lack of reaction for the ZnO catalyst, it seemed that TGA did not reveal a great deal of information regarding the process.

The information that this experiment provided was that the polymer produced had properties in line with the general class of inverse vulcanised materials, as most polymers produced this was exhibited a 5 % decomposition temperature at 200 °C.

The reason for the invariability in this is due to the fact that the first bonds to decompose under thermal action are likely to be the S-S bonds, as they have the smallest bond enthalpy in the system. After this, it is likely to be the C-S bond degradation. The remaining mass in the char is likely to be carbonaceous material, somewhat similar to that which has previously been produced at scale and reported by Lee *et al.*.[49]

In conclusion, it was found that the catalyst chosen was able to produce a copolymer with elemental sulfur with a cross linker that had previously been unable to form a copoly-

mer with sulfur. This opens the door to several potential crosslinking agents that were previously unable to be used due to poor reactivity.

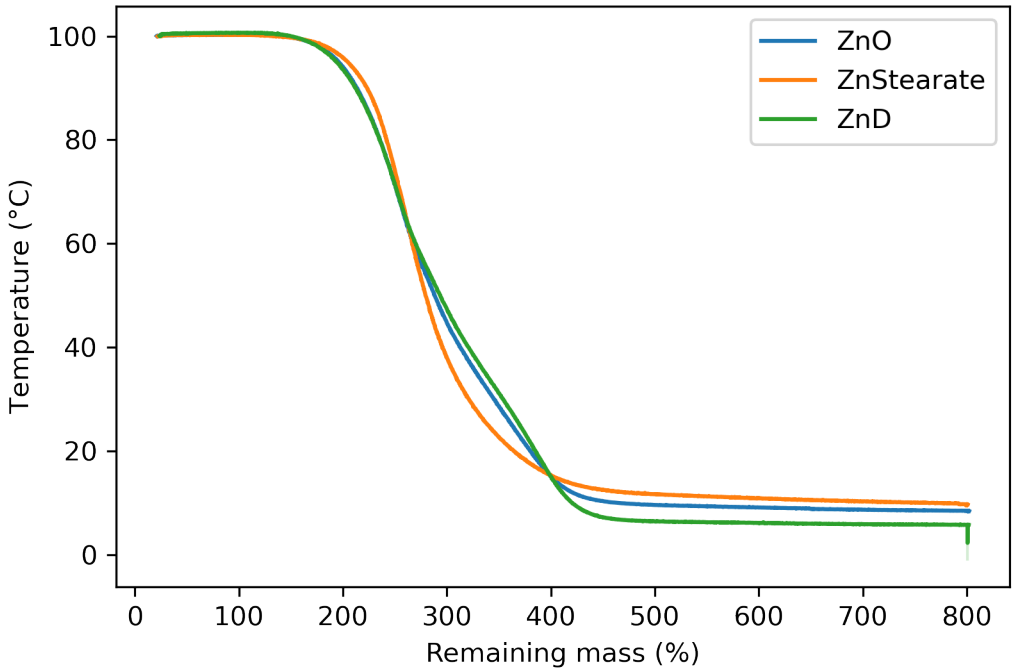

Figure 4.14: TGA of S-EGDMA demonstrating a decompoisition onset at 200°C, which is characteristic of inverse vulcanised polymers[50]

TVTSCi

Another example of a cross linker that had previously been unreported as reactive with elemental suflur was 1,3,5,7-tetravinyl tetramethyl cyclotetrasiloxane (TVTSCi). Initially, when TVTSci was mixed with elemental sulfur at an elevated temperature (135°C) a yellow dispersion formed. After 4 hours, it appeared that elemental sulfur had begun to condense on the top of the reaction vessel. After 24 hours, all that remained was elemental sulfur, and the TVTSCi had evaporated. It was concluded that the TVTSCi was unable to form a copolymer with sulfur uncatalysed. Solid state ^{13}C NMR revealed the formation of C-S bonds. (Appendix, Figure A.31)

Given that EGDMA was previously unreactive towards elemental sulfur under these conditions, but became reactive after inclusion of ZnD it was hypothesised that the chemical may facilitate the reaction. Upon performing the experiment, it was found that TVTSCi would not react at 135°C in the presence of ZnD. Furthermore, it would not react at 160°C in the presence of 1% ZnD. However, at 160°C and with 5% wt ZnD a polymer was successfully formed.

DSC revealed there was no elemental sulfur contained within the formed material. However, there were also no features to the thermogram. This type of behaviour is uncommon, but not unreported.

Thermogravimetric analysis (TGA) of TVTSCi revealed a thermogram typical of sulfur polymers. It was noted that there was an initial decomposition around 200°C, with a residual mass of char left at the end of the cycle.

In conclusion, it was found that TVTSCi was able to react with elemental sulfur under conditions that inverse vulcanisation typically undergoes. However, it was also found that the reaction was relatively slow in comparison to other cross linkers, required a higher temperature even with catalyst and also did not form a 'completely' cross-linked polymer. Further research in this area would perhaps centre around performing the reaction in a sealed pressure vessel, to allow access to increased temperatures without boiling the TVTSCi away.

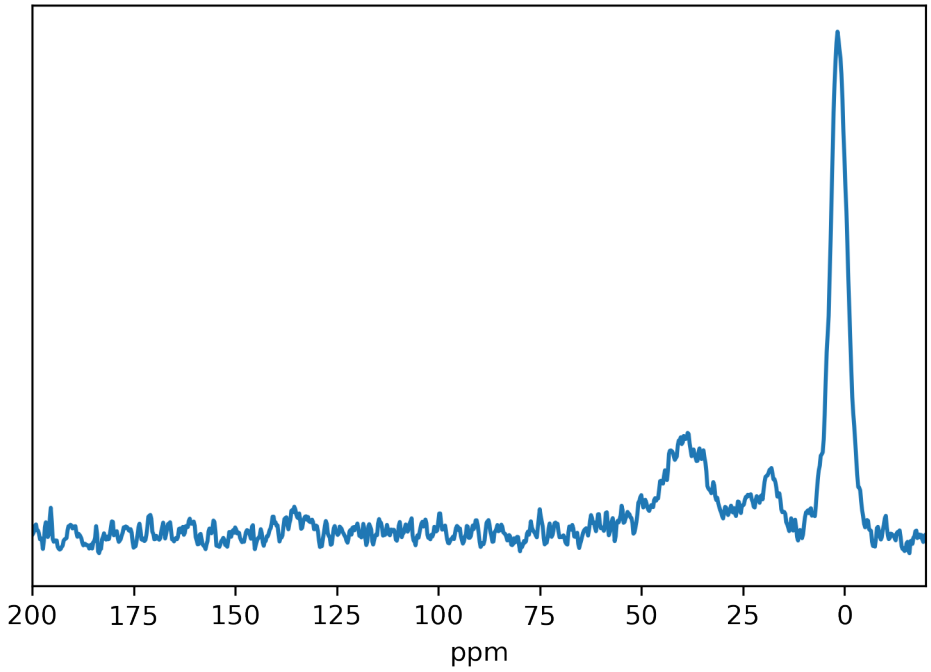

Figure 4.15: ^{13}C MAS solid state NMR of S-TVTSCi.

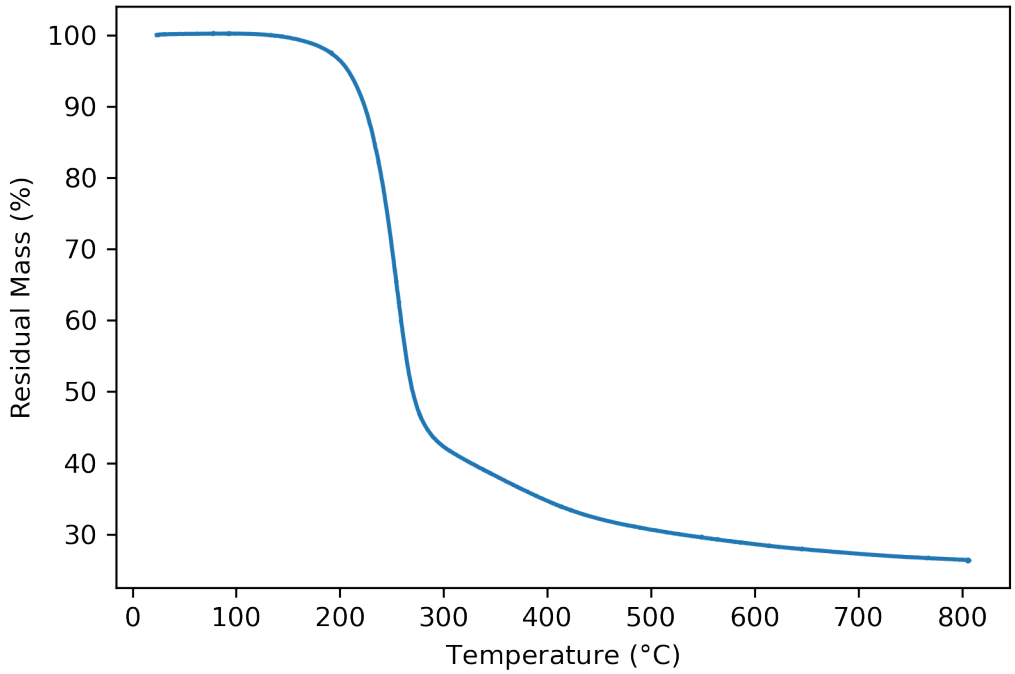

Figure 4.16: Thermogravimetric analysis of S-TVTSCi ran under nitrogen to 800 °C.

Glyoxal bis(diallylacetal)

Glyoxal bis(diallyacetal) GBDA is a multi-functional compound that is mainly used in thiol-ene click chemistry polymerisation for the synthesis of gels and other compounds. Upon initial reaction without catalyst, it was found that the reaction proceeded albeit extremely slowly. By the time a gel had formed, it was found that a large quantity of sulfur had sublimed onto the top of the reaction vial. Therefore, it was considered that the reaction was not viable without catalyst, as the reaction products involved a poor atom economy and conversion.

However, upon addition of zinc (II) diethyldithiocarbamate it was discovered that the reaction would gel after 2.5 hours. This decrease in time to gelate was over tenfold, a massive increase in rate of reaction (at 5% catalyst loading).

The ^{13}C SS NMR spectrum of the reaction between GBDA and sulfur was different in its appearance to that of many of the cross linkers that were tested in this body of research. GBDA showed discrete evidence for the formation of C-S bonds at 45 ppm. However, alongside the evidence for the formation of the C-S bonds, there were also resonances attributable to C=C bonds present in the sample. These were located at 120 and 150 ppm. It is likely that not all alkene bonds present in GBDA were reacting during the inverse vulcanisation process, even with catalyst. (Figure 4.17) For complete assignment refer to appendix, Figure A.30.

This incomplete consumption of C=C bonds during the reaction of elemental sulfur with GBDA is further confirmed when the sample is analysed using FTIR. (Figure 4.18) The FTIR spectrum shows that there is only the slightest reduction of the signal at 3100 cm^{-1}, which corresponds to C=C-H vibrations. There is also a slight decrease in the fingerprint region C-H bends (55, 900, 1000 cm^{-1}). Given that the uncatalysed sample took 49 hours to form a gel, this is relatively unsurprising. (Figure 4.9)

The thermogram that was produced when S-GBDA was run in the DSC, however, does show a slight glass transition. The transition, however, is very weak. The 0 wt% catalysed sample displayed a very large error (25°C) for the assessed T_g, which is uncharacteristic for the polymers produced in this reaction. When combined with the very slight glass transition that was observed, and the previous results that were obtained from NMR and FTIR, it is possible to conclude that the reaction progress was slow and inefficient.

Overall, the synthesis of S-GBDA should be considered to be successful. A polymer

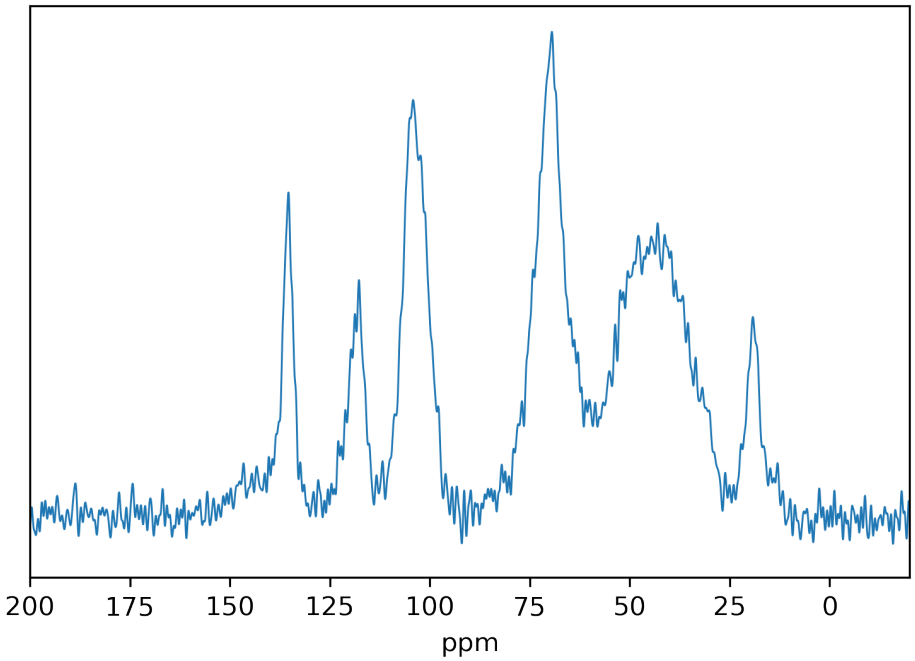

Figure 4.17: ^{13}C MAS solid state NMR of S-GBDA

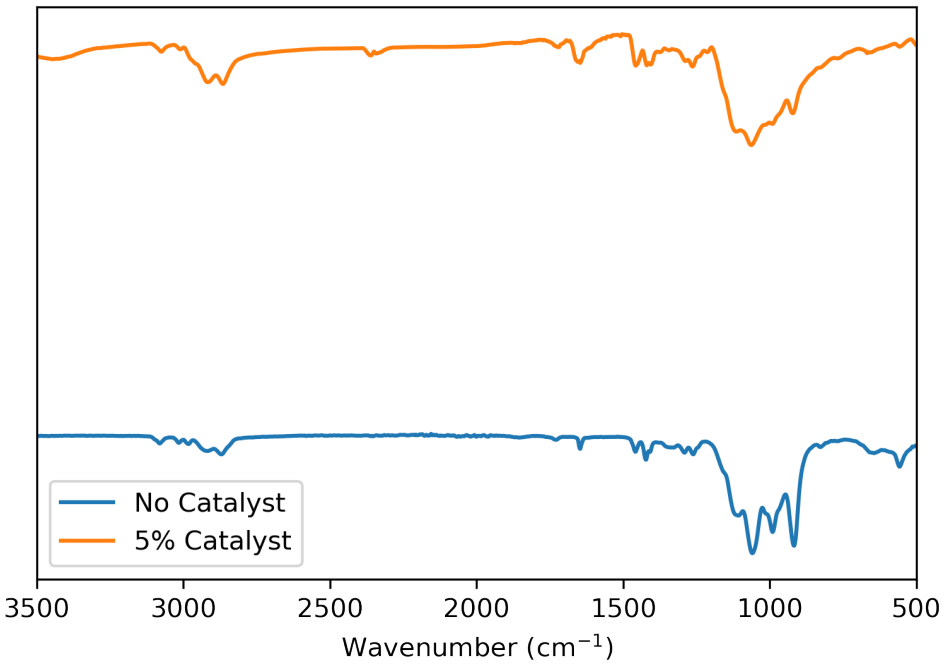

Figure 4.18: FTIR spectrum of the polymer produced from elemental sulfur and GBDA

was formed, and a portion of the double bonds reacted. However, of the cross linkers that were tested in this study, it was definitely the poorest in terms of its reactivity and polymer forming ability.

4.7.2 Improving qualities of previously reported polymers

As previously discussed, using a catalyst in the inverse vulcanisation reaction did indeed increase the rate of reaction. There are other effects produced when using a catalyst that are also worth discussing. One of the first properties that was noted in the produced polymer was a pronounced increase in glass transition for the produced polymers.

An example of this can be found in the bio-renewable cross linker squalene. Squalene is a renewable triterpene that was originally obtained from shark liver oil.[51] However, modern production utilises biosynthetic techniques to avoid using sharks.[51] Initial reports of the synthesis of sulfur and squalene found the polymer to have a glass transition of around 30°C.[14] This was confirmed by our own experiments. Figure 4.19 shows the differences in T_g's obtained when the concentration of catalyst is varied in the reaction feedstock.

As can be seen in Figure 4.19 increasing the concentration of zinc (II) diethyldithiocarbamate increased the glass transition of the resulting polymer. An increase of 5 wt % increased the glass transition of the produced polymer by, on average, 5°C. This increase in glass transition is likely due to the increased crosslinking of the polymer.

The increase in glass transition observed for S-Squalene when increasing the concentration of catalyst, zinc deithyldithiocarbamate, was noted universally among all tested samples. The increase in T_g for the tested samples from 0 wt % loading to 5 wt % loading is displayed below in (Figure 4.20).

The increase that is displayed in (Figure 4.20) is widely varied, and not consistent at all. However, to expect a uniformity in increase in such a diverse scope of substituents would be unrealistic. What is, however, noticeable is that the glass transition is increased across the board. A net increase means the extent of reaction increased.

S-Limonene

S-Limonene was a polymer that was first reported by Chalker *et al.*[52] It is a cyclic monoterpene produced in the citrus peel industry[53], and widely used in cosmetics[54]. The properties of the copolymer produced were that of a high viscosity fluid. The polymer was found to be able to remove mercury from water, but its lack of shape persistency made it undesirable for any practical use.

It was hypothesised that by using an appropriate catalyst, it would be possible to improve the physical properties of S-Limonene. The following section is a discussion on

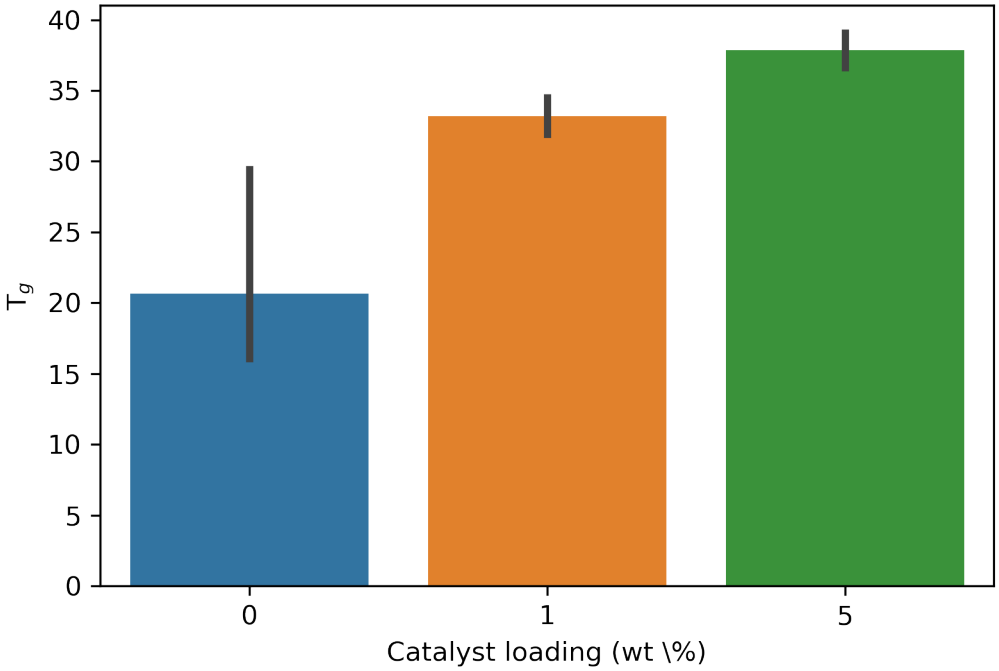

Figure 4.19: Graph illustrating the T_g of S-Squalene produced from equal masses of elemental sulfur and squalene whilst varying the mass of ZnD catalyst used in the synthesis of the polymer.

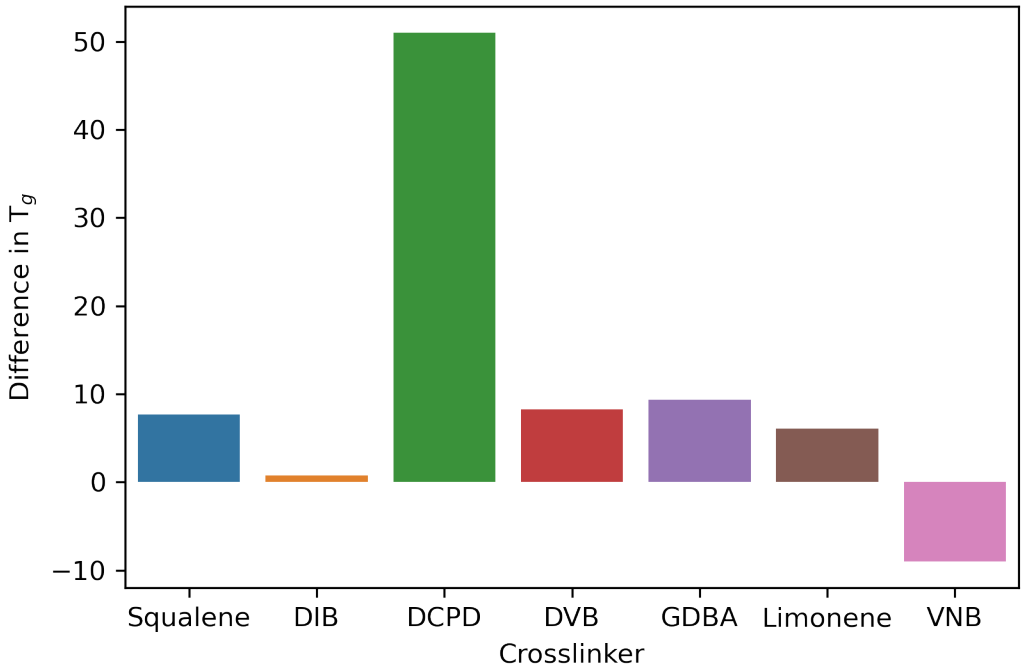

Figure 4.20: Average increase in glass transition as a function of a 5 % increase in catalytic loading for samples tested in this study.

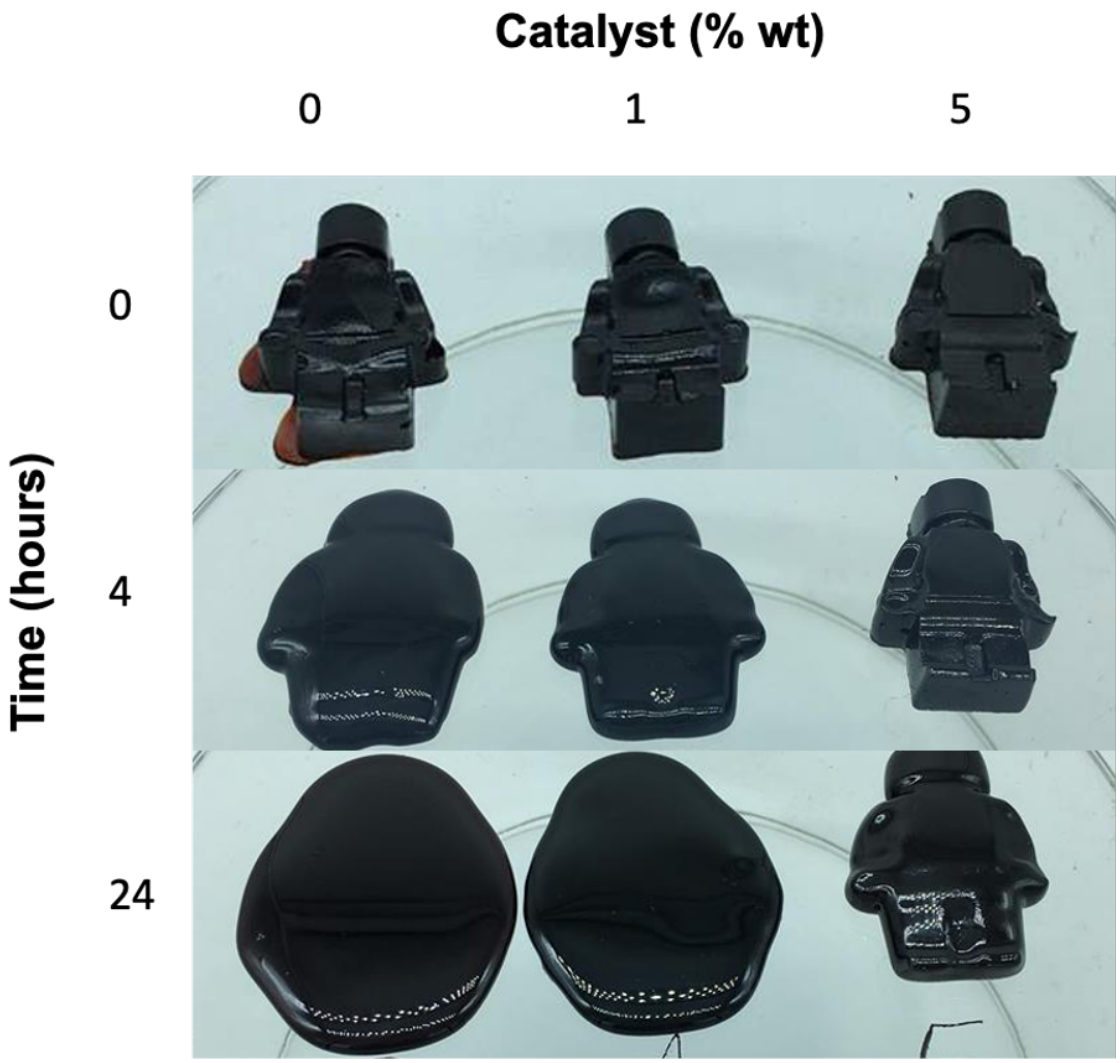

Figure 4.21: Figure demonstrating the improved shape persistency of S-Limonene when ZnD is added to the reaction feed. After 24 hours, the original moulded shape is held to a much better degree than without catalyst

the properties of the catalysed S-Limonene reaction and how the catalyst affected the resultant properties of the produced polymer.

The original synthetic procedure for S-Limonene was inefficient. The first step involved heating elemental sulfur with limonene for extended periods of time, and eventually distilling away unwanted small molecules under vacuum at high temperatures.

Initially, when reacting with 1 % catalyst it was found that the polymer gelled after a reduced time of 7 hours, from the original 20.[55] Furthermore, it was found that the vacuum distillation post reaction was not necessary. The polymer produced also had an increased degree of shape persistency, but was still noticeably tacky. Figure 4.21 demonstrates the increase in shape persistence.

As is evident in (Figure 4.21) the shape persistency increased an appreciable amount. After 4 hours the shape of the robot was the same as when initially cast with only deformation becoming apparent after 24 hours as opposed to the uncatalysed sample which had become noticeably deformed after 4 hours. This, yet again, could be attributed to a greater polymerisation efficiency in the final polymer.

Given that S-Limonene has always been fully soluble, it was hypothesised that the catalyst merely increased the molecular weight of the produced polymer. Therefore, gel permeation chromatography was employed to support this claim. Table 4.2 demonstrates the results of a GPC chromatogram of solutions of S-Limonene produced with various concentrations of catalyst. Interestingly, very little difference is noted between the samples. However, there is an increase in the polydispersity for the 5% sample. It could be that the 5% catalysed sample has a broader molecular weight distribution due to the presence of higher molecular weight components within the mixture.

	$\mathbf{M}_n$	$\mathbf{M}_w$	$\mathbf{M}_w/\mathbf{M}_n$
Limonene (0 wt%)	455	785	1.74
S-Limonene (1 wt%)	410	720	1.76
S-Limonene (5 wt%)	411	805	1.96

Table 4.2: Summary of the information gathered when S-Limonene produced in this study is analysed using gel permeation chromatography.

The DSC revealed that there was initially a decrease in the glass transition temperature of S-Limonene, at a 1% wt catalyst loading, with an increase when the loading was increased to 5% (Figure 4.22). This effect is not dissimilar to what was observed in GBDA. Given that limonene is susceptible to H-abstraction[9], it is likely that not all C=C were available for polymerisation. In this, it is not dissimilar to GBDA, which did not invoke all of its double bonds in polymerisation.

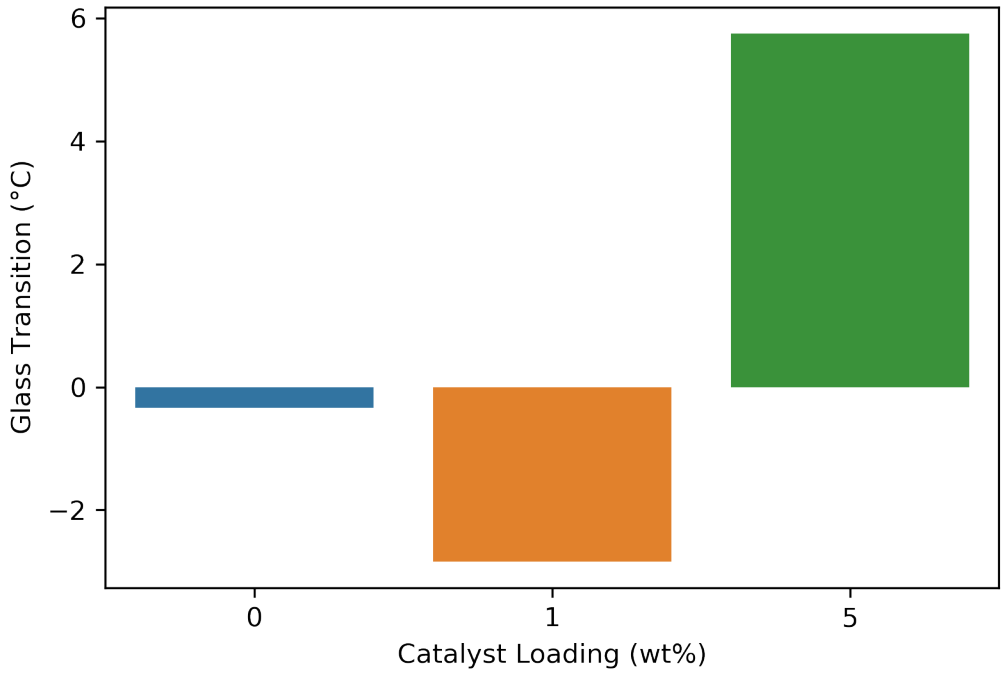

Figure 4.22: Bar plot showing the glass transitions of polymers produced from elemental sulfur and limonene utillizing varying amounts of ZnD catalyst in the process

S-DCPD

Dicyclopentadiene (DCPD) is a small molecule petrochemical produced in the cracking of naphtha.[56] S-DCPD was first reported by Parker *et al.* in 2016 by reaction of elemental sulphur with dicyclopentadiene at 160°C, followed by a curing step for 24 hours in an oven at 140°C.[50] In this work it was found that a black, insoluble polymeric material was formed. When the reaction feed was 50% sulfur and 50% DCPD, it was found that the T_g of the resultant polymer was 115.25°C. There was no elemental sulfur detected in the produced polymer, in the DSC thermogram or the pXRD pattern.

In the divergent work produced on the catalytic reaction between elemental sulfur and DCPD in the presence of ZnD the reaction time to the gel point was found to be 0.4 hours. DSC revealed the T_g to be approximately 90 °C at 5 wt% ZnD loading. This is actually a lowering of T_g in comparison to the previous report. However, the time for reaction was significantly reduced. It could be hypothesised that by increasing the reaction time further, the T_g would be higher. In a control experiment in this study, the uncatalysed sample was found to have a T_g much lower (Figure 4.23).

Figure 4.23 displays the differences in T_g's graphically. The higher T_g exhibited in the

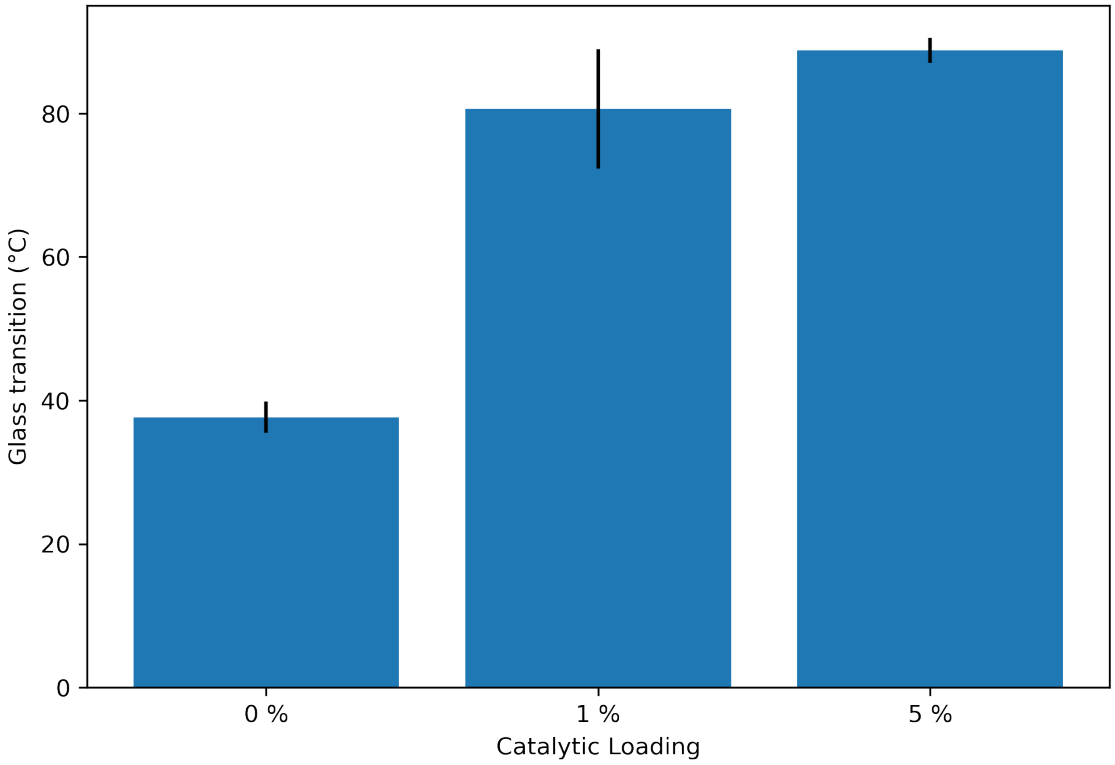

Figure 4.23: Bar chart demonstrating the increase in T_G when an increasing amount of ZnD catalyst is utilised in the synthesis of a S-DCPD polymer that comprises equal portions of elemental sulfur and DCPD

original work is liable to be the result of longer reaction times at higher temperatures. In the original work it was found that DCPD would not appreciably react with elemental sulfur to produce a cross-linked copolymer. It was, however, found that elemental sulfur would produce a linear polymer with DCPD.

With the exception of the T_g and the dramatic reduction in reaction time, there is not much difference in the physical properties of the produced polymers. This is, in part, due to the difficulty of obtaining analytical data on an insoluble, amorphous polymer.

In conclusion, it was found that inclusion of catalyst dramatically reduced the reaction time of elemental sulfur and DCPD. It was found that the produced polymer had a lower T_g than in the original study, but higher in a control study. All other physical characteristics were similar. Further experimentation would aim to recreate the initial conditions that Parker *et al.* employed but with the inclusion of ZnD to explore whether a T_g as high as they reported is able to be attained.

S-DVB

In 2016 Salman *et al.* demonstrated for the first time the copolymerisation of elemental sulfur with divinylbenzene (DVB). This work explored the applications of the produced materials (optics). Interestingly, the reaction was performed at 200°C. The material that was produced in their work was not a cross-linked polymer. It was found that the polymer was soluble in a variety of organic solvents including: chloroform, dichloromethane, 1,2-dichloroethane, and tetrahydrofuran. The authors did note that the polymerisation temperature was very close to the decomposition temperature of similarly produced materials. It was also interesting to note that the polymerisation temperature is approaching the heterolytic splitting temperature of sulfur. They also attempted to polymerise at temperatures as low as 180°C but found the produced materials were heterogeneous in nature.

It is likely that DVB has poor solubility in polymeric sulfur, and as a result a two phase system is formed at the lowered (>180°C) temperatures. Above 200°C it has been demonstrated that ionic sulfur predominates the reaction mixture, and likely increases the degree of hydrogen abstraction, lowering crosslinking. This does however leave the question of what a more 'traditional' (< 180°C) inverse vulcanisation reaction would appear. In the work explored in this chapter, it was found that at a lower temperature of 135°C elemental sulfur would react with DVB. The time to initial gelation was 2.5 hours. Upon addition of 5 wt % ZnD the reaction time until gelation shortened to 0.85 hours, comparable to the 0.16 hours of the first reported work but at a temperature 65°C lower.

Because of the almost uniquely high temperature of synthesis reported in the work by Salman *et al.*, the polymer properties are markedly different. For example, in Salman's work, the produced polymers (60 wt % S_8) are soluble and have a T_g of 11.93°C. In this work, it was found that a 50 wt % S_8 polymer had a T_g of 107°C. Whilst these two materials are not directly comparable as their composition is different, previous work has demonstrated that increasing sulfur content does not have such a drastic effect on T_g.[50]

In summary, it was found that there were differences in the properties of the produced copolymer of elemental sulfur and divinybenzene. Figure 4.24 demonstrates the effect of ZnD loading on the T_g of the produced polymer. It was found that in comparison to the original work, the polymer properties had improved by a large extent and even the extent of polymerisation had increased. This is supported by an increase in T_g and a decrease in solubility, which suggested an increase in extent of polymerisation.

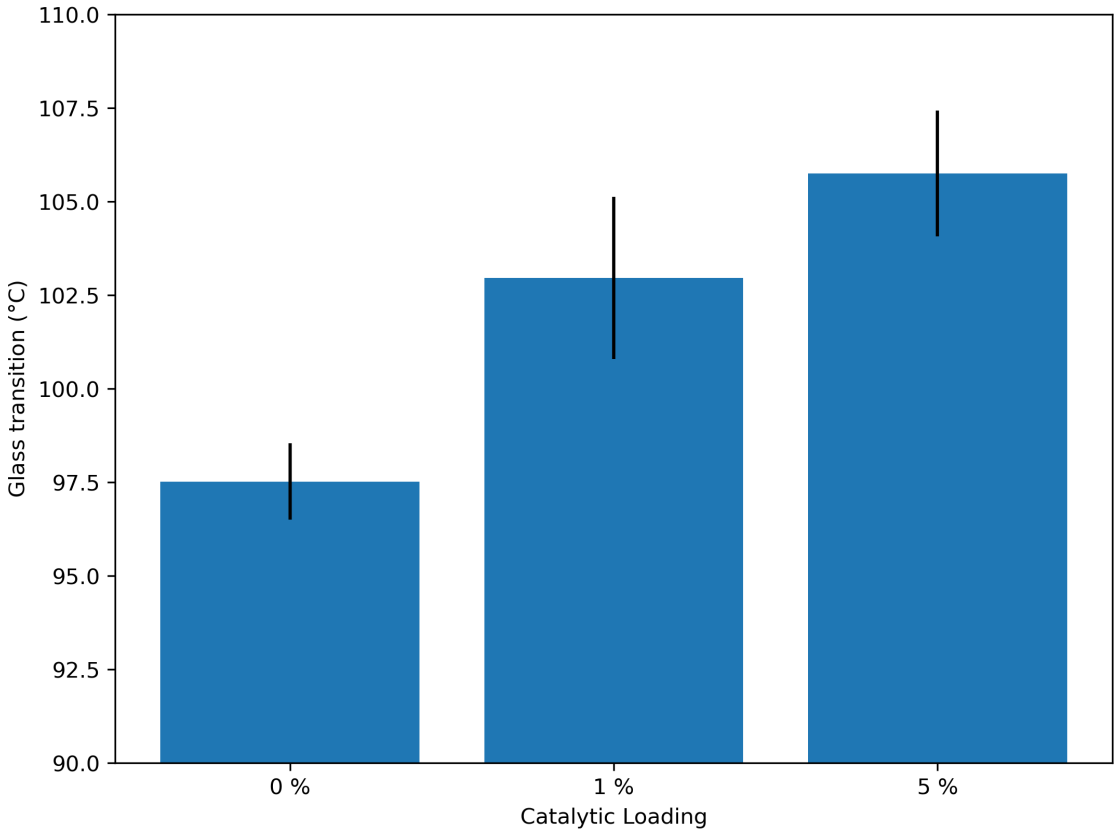

Figure 4.24: Bar plot demonstrating the increase in T_g of the S-DVB copolymer produced as a function of the catalytic loading.

S-Squalene

S-Squalene polymer was first reported by Parker *et al.* in 2018.[14] They demonstrated that it is possible to react elemental sulfur with squalene. Squalene is a triterpene that was originally obtained from shark liver oil. All reactions were performed at 175°C. Reactions were held at this temperature for between 5 and 20 minutes before being transferred to an oven for curing at 140°C for 18 hours. At the composition that was explored in this body of work, the investigators discovered that the T_g of the produced polymer was 14°C. There was a degree of solubility associated with the products of the reaction.

In comparison to the polymers produced in this body of work, it was found that the T_g of the S-Squalene copolymer benefited from the decrease in reaction temperature with the T_g actually increasing to 30°C at a lowered initial reaction temperature. Including 5% ZnD into the reaction feed increased the T_g two 37.5°C with almost double the originally reported T_g.

Overall, it was found that by including a catalyst, the properties of the copolymer produced by reaction of elemental sulfur and squalene were improved greatly.

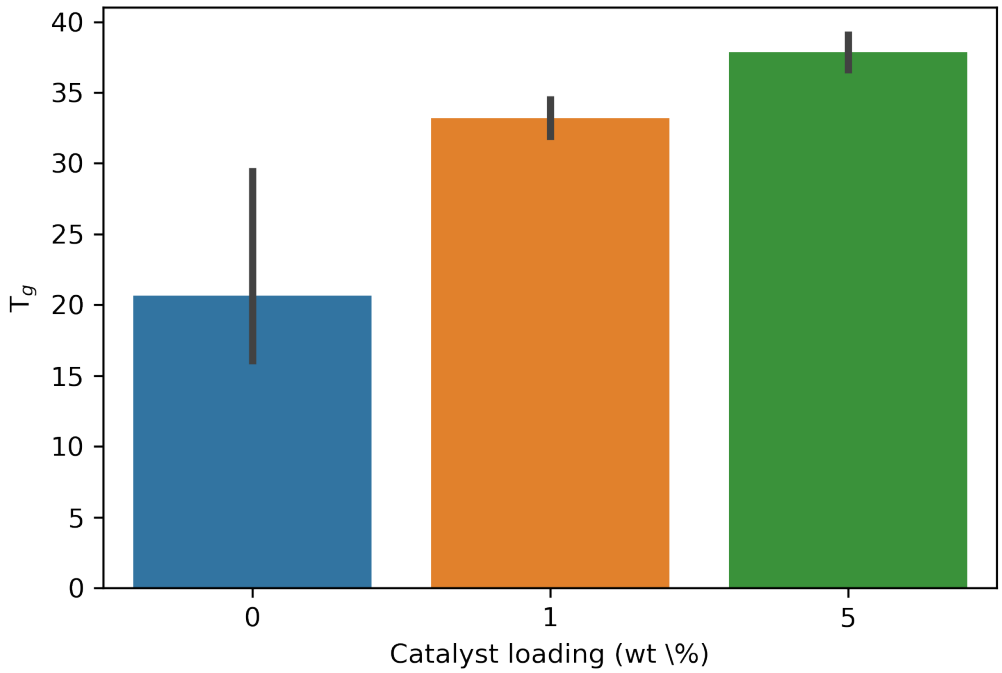

Figure 4.25: Bar plot demonstrating the increase in glass transition of a polymer produced from elemental sulfur and squalene. utilising varying amounts of ZnD catalyst. The black lines indicate the error in the measurement of the samples T_g

S-DIB

1,3-diiosopropenylbenzene (DIB) is isosteric to DVB, only differing in the substitution of one of its hydrogen centres for a methyl group. Its reaction with sulfur was the first to be reported as 'inverse-vulcanisation' and to this date remains one of the most important papers on inverse vulcanisation. First reported in 2013[57], the inverse vulcanisation reaction of elemental sulfur with DIB is a model inverse vulcanisation reaction.

The process for the formation of S-DIB is as simple as mixing elemental sulfur and DIB in a vial at 185°C for 8-10 minutes. Almost instantaneous vitrification occurs, and a stable polymer is formed, without a curing stage. The T_g reported was 17°C, with some solubility reported. The small degree of solubility was attributed by the authors to the formation of intramolecular loops (Figure 4.26) that were able to be extracted from the overarching cross-linked network.

In this body of work, it was found that despite the lower temperature of reaction (135°C) it was possible to achieve comparable levels of reaction speed (1 hour) with a loading of 5% ZnD. Furthermore, the polymer that was produced had a complete insolubility in all

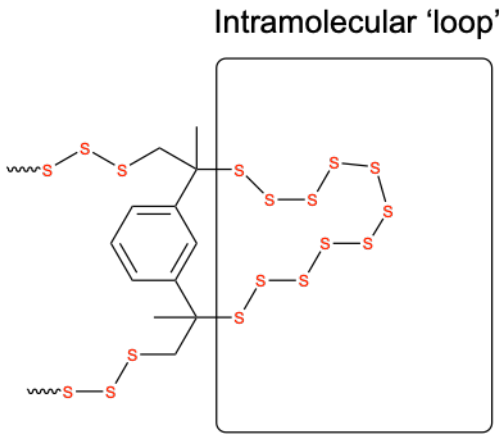

Figure 4.26: Scheme demonstrating the architecture of theorised intramolecular loops of sulfur first described by Chung et al.[57]

organic solvents that were tested in the previous study. Also, the T_g increased from 17°C to 36°C in a comparable sample. Interestingly, it was found that increasing the catalytic loading did not increase the T_g linearly. (Figure 4.27)

To conclude, it was found that by inclusion of a catalyst and lowering the reaction temperature the reaction speed of elemental sulfur and DIB decreased moderately, but a modification of produced polymer properties was observed. (Increase in T_g and lowering of solubility) This modification is likely to be the result of lowering the degree of chain transfer and increasing the extent of polymerisation in the polymerisation process.

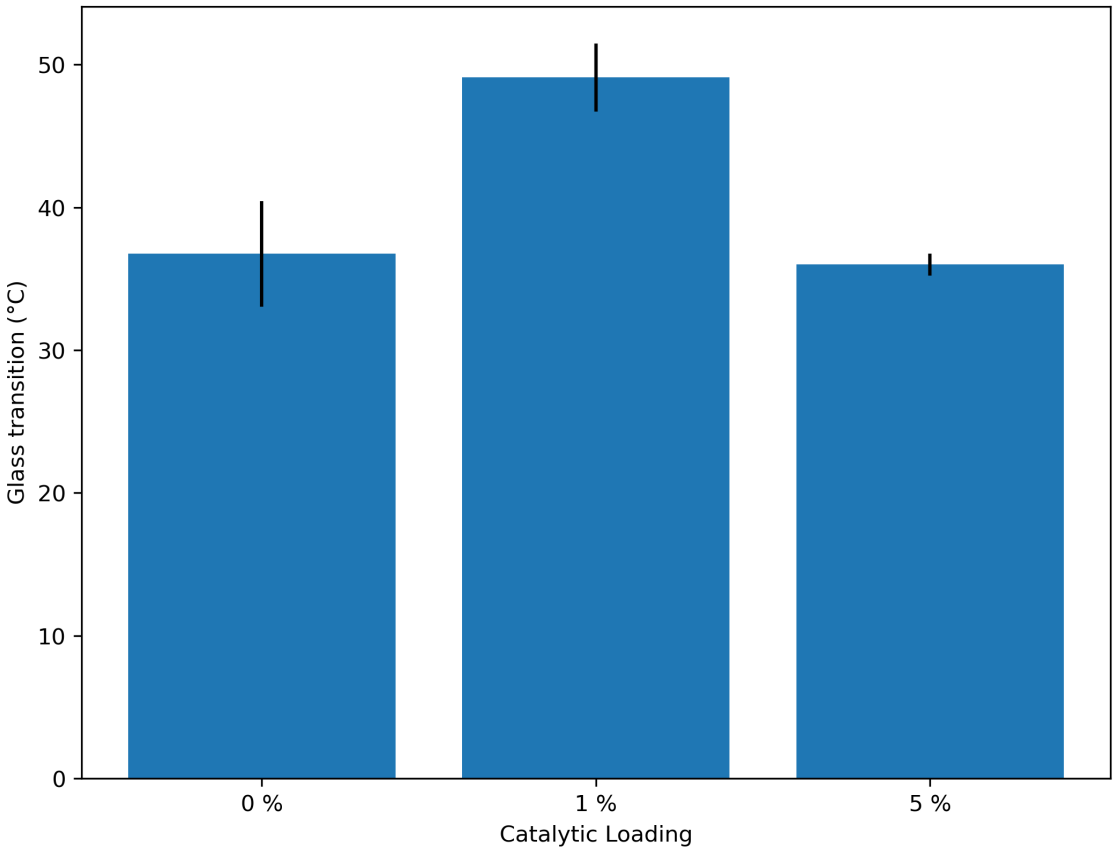

Figure 4.27: Bar plot demonstrating the T_g of S-DIB polymers produced when different loading's of catalyst were included in the reaction feed-stock.

4.7.3 Novel cross linkers able to be polymerised uncatalysed

In this body of work, a variety of cross linkers were tested for their reaction with elemental sulfur in the inverse vulcanisation process. It was found that some novel cross linkers were able to react even in the absence of a catalyst. Within this section, these cross linkers will be discussed.

S-TVCH

Trivinylcyclohexane (TVCH) is a comprised of a cyclohexane core with 3 hydrogen atoms (1,3,5) replaced by allyl groups. It is a highly reactive crosslinking component used in the manufacture of crosslinked polyethylene for packaging and ion-exchange resins.

Reactions with 0% ZnD were partially successful. Whilst it appeared that a reaction occurred, it was actually found that the majority of the TVCH had evaporated in the polymerisation process, resulting in a remaining black liquid at the bottom with sublimed sulfur at the top of the reaction vial. The reaction was considered to have successful, however it was impossible to find a glass transition for the produced material.

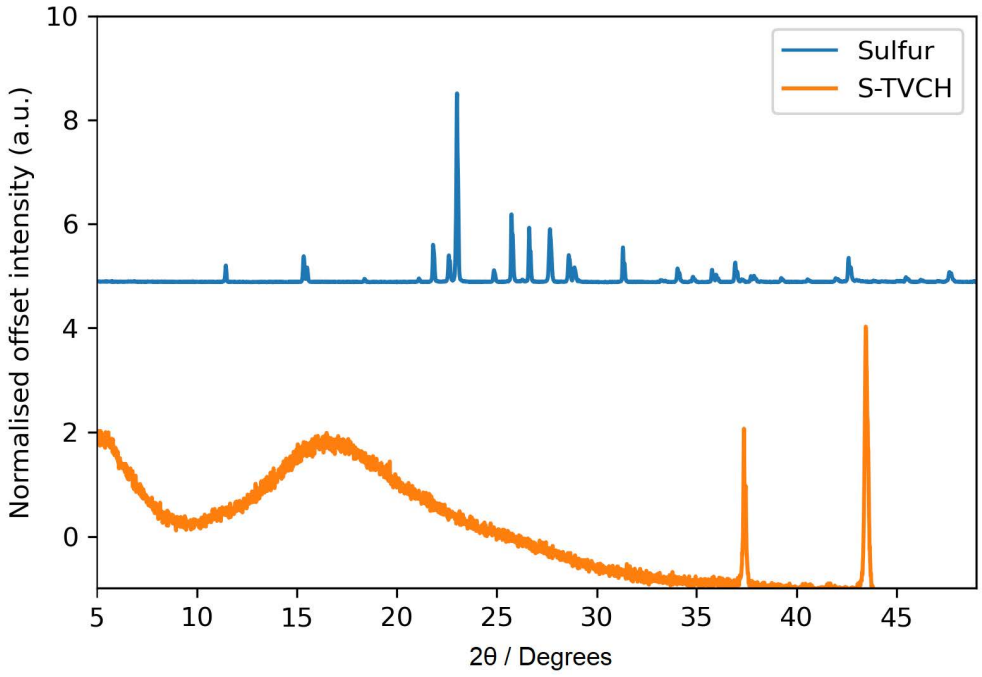

Figure 4.28: pXRD pattern comparing elemental sulfur with the polymer produced from elemental sulfur and trivinylcyclohexane

Initial confirmation of the reaction of was found by pXRD, as previously discussed pXRD reveals an absence of crystalline elemental sulfur in all samples. (Figure 4.28) In the polymer sample pXRD crystalline reflections were present for the aluminium sample holder.

DSC revealed that the sample that had a feedstock of 0% ZnD had no observable T_g with the samples of feeds 1% and 5% had T_g's of 37.1°C and 22.8°C respectively. (Figure 4.29)

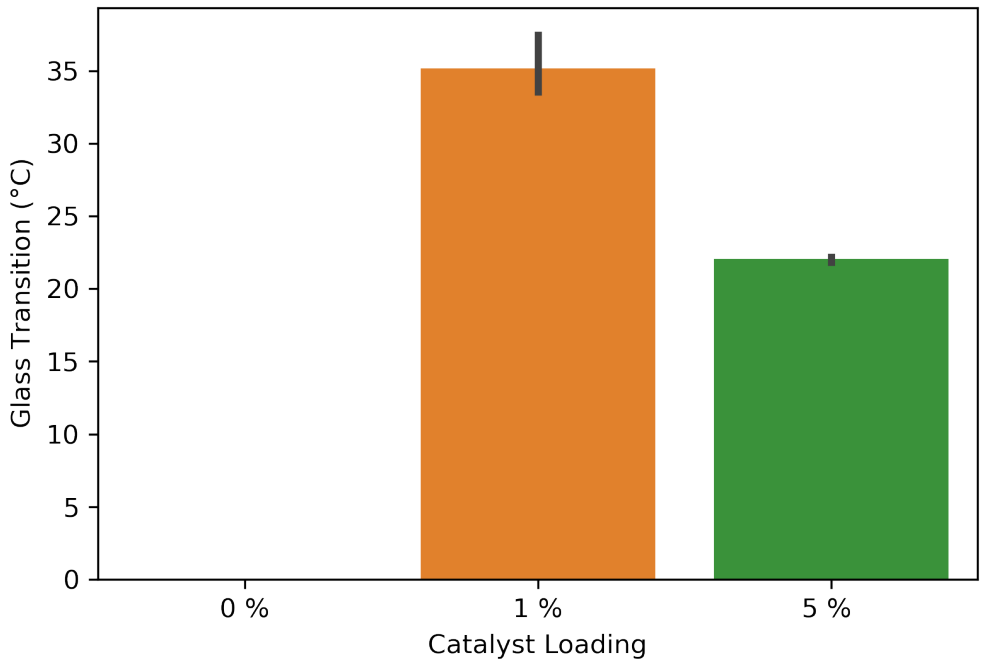

Figure 4.29: Comparison of the glass transition temepratures of S-TVCH when catalysed by varying amounts of ZnD. No glass transition was observed for the 0 wt% catalysed sample

FTIR (Figure 4.30) revealed that there was a significant reduction in the signal at 3100 cm^{-1}, which is the result of the C=C-H vibrations. The signals at 1750 cm^{-1} and 1650 cm^{-1} are also reduced in comparison to the control and are the result of inequivalent C=C vibrations. Furthermore, there were reductions in intensity of signals at 650, 900, and 1000 cm^{-1} which are characteristic of C=C-H bending modes.

TGA (Figure 4.31 revealed a thermal degradation that was typical of an inverse vulcanised polymer. A degradation onset of around 200°C, with a residual char mass at the end of the decomposition curve.

S-TVCH was almost unique in its ability to be solubilised in chloroform. As a result of

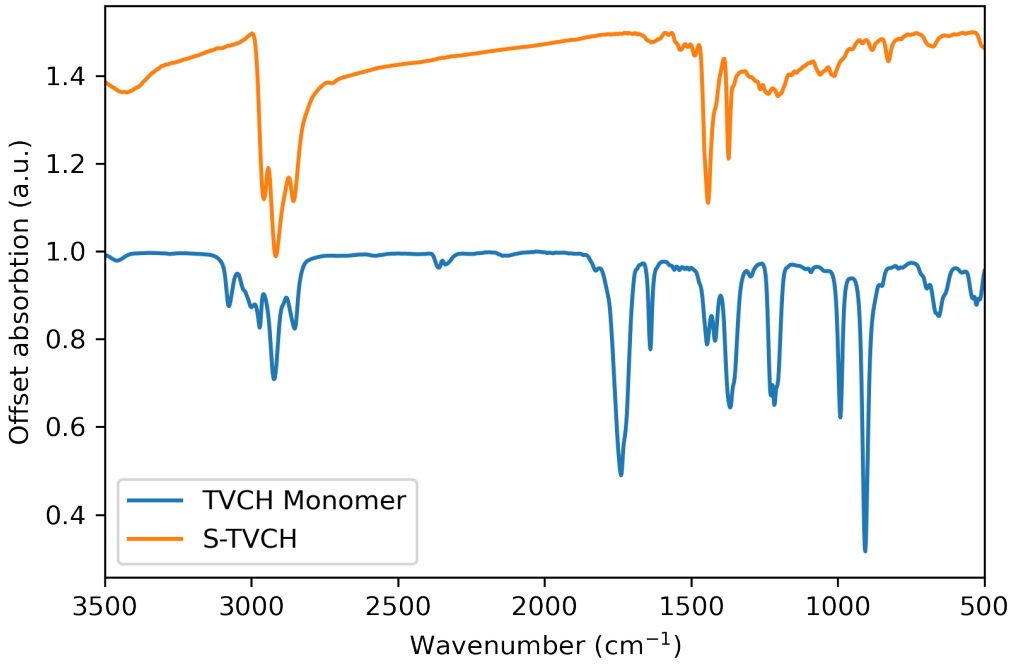

Figure 4.30: FTIR of the S-TVCH polymer (orange) and the TVCH monomer (blue)

this, the polymer was dissolved in $CDCl_3$ and a ^1H NMR spectrum was obtained. (Figure 4.32) The NMR confirmed the disappearance of the C=C-H resonance (4.95-5.2 ppm) and the new peaks present in the 3-4 ppm range may be the result of H-C-S resonances.

In conclusion, a new sulfur polymer was formed from elemental sulfur and TVCH. The resultant polymer was somewhat different from the usual crosslinked polymers that were obtained from inverse vulcanisation in its solubility. However, this was likely the result of a lowered degree of crosslinking efficiency. Future work would look at optimising the crosslinking of TVCH even further to produce a fully crosslinked polymer.

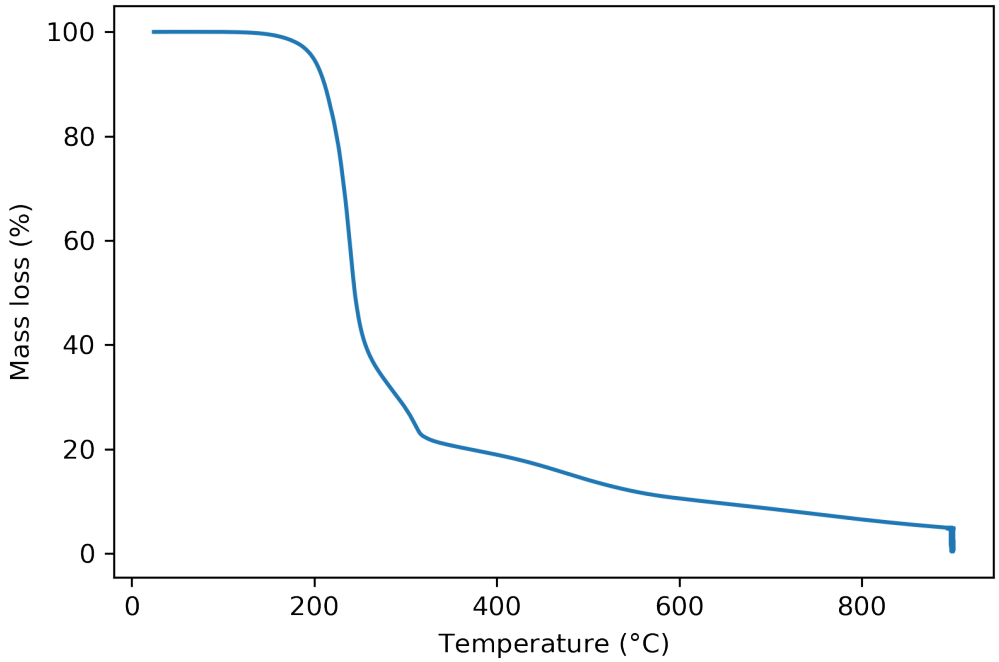

Figure 4.31: Decomposition curve for the S-TVCH polymer that comprised equal parts elemental sulfur and TVCH with 1 wt% ZnD. Sample was ran under nitrogen to 850°C

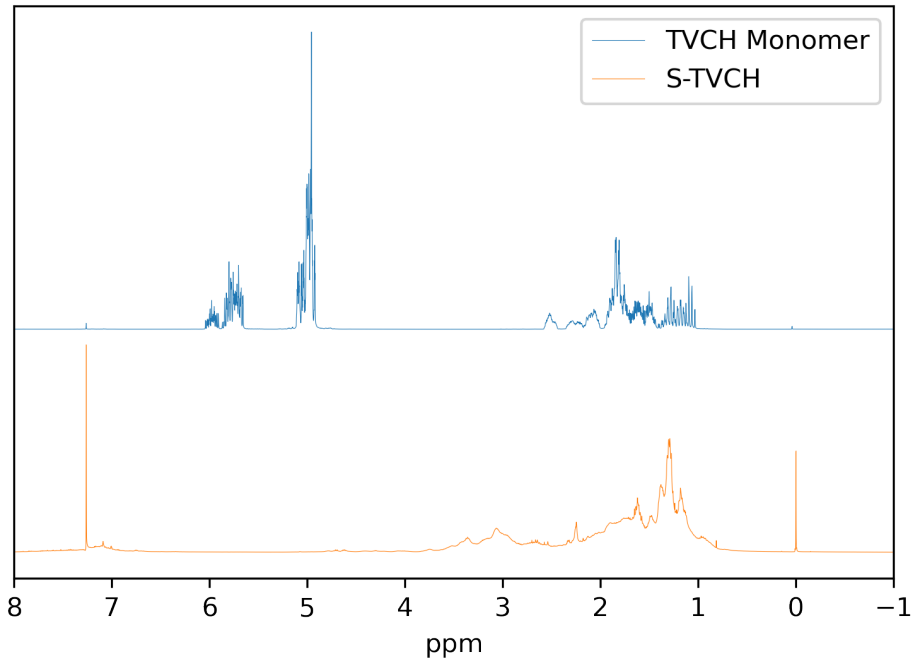

Figure 4.32: H NMR Spectrum TVCH

S-VNB

Vinylnorborene (VNB) is a small molecule diene that is used industrially to produce EPDM rubber, a synthetic rubber.[58] Because of its uses in the field of vulcanisation it is a potentially good fit for the inverse vulcanisation process. Furthermore, it is structurally similar to ethylene norborene a cross linker that was reported by Smith *et al.* in 2018.[19]

Initial reactions without the addition of ZnD required reaction times of over 12 hours. With the addition of 1% ZnD this time decreased to 5 hours, and finally with 5% ZnD the reaction time decreased to 2 hours.

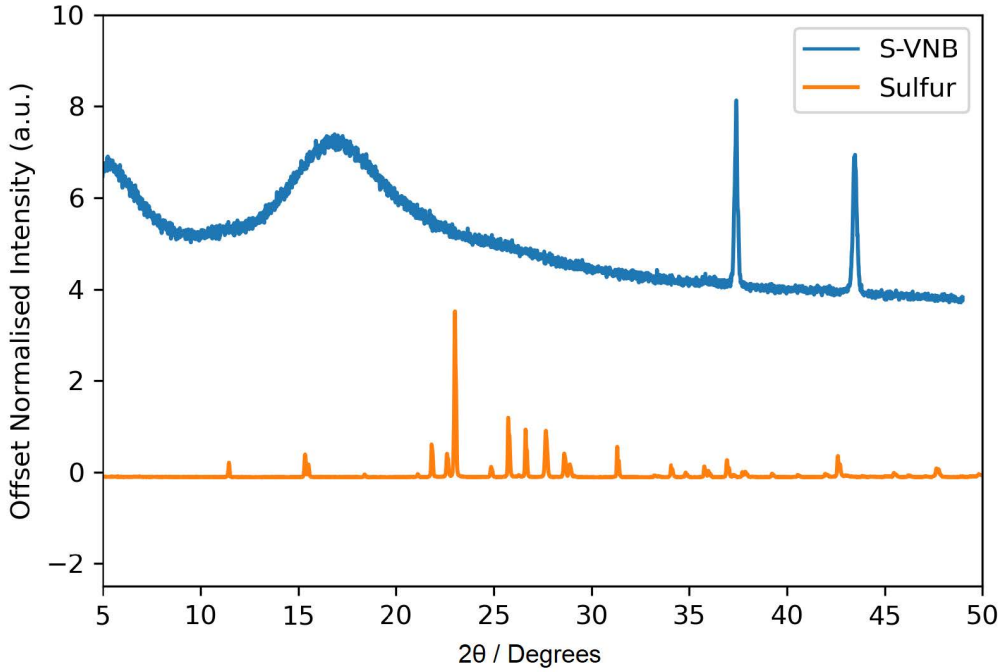

Figure 4.33: pXRD pattern obtained for the analysis of S-VNB comprised of equal wt% elemental sulfur and VNB monomer.

As previously performed for TVCH, VNB was confirmed to have reacted by the absence of the crystalline reflections of elemental sulfur through the use of pXRD. (Figure 4.33) Consumption of elemental sulfur is a positive indicator for a successful reaction but does not confirm the formation of a polymer. DSC revealed that the T_g of the produced uncatalysed sample was 109°C, rising as high as 112°C with 1% ZnD catalyst. It was noted that the T_g decreased when the ZnD loading was increased to 5% resulting in a T_g of 101°C.

FTIR of S-VNB revealed a reduction in the signal at 3100 cm^{-1}, which was characteristic of the C=C-H vibration. Further reductions were noted at 1750 cm^{-1} and 1600 cm^{-1},

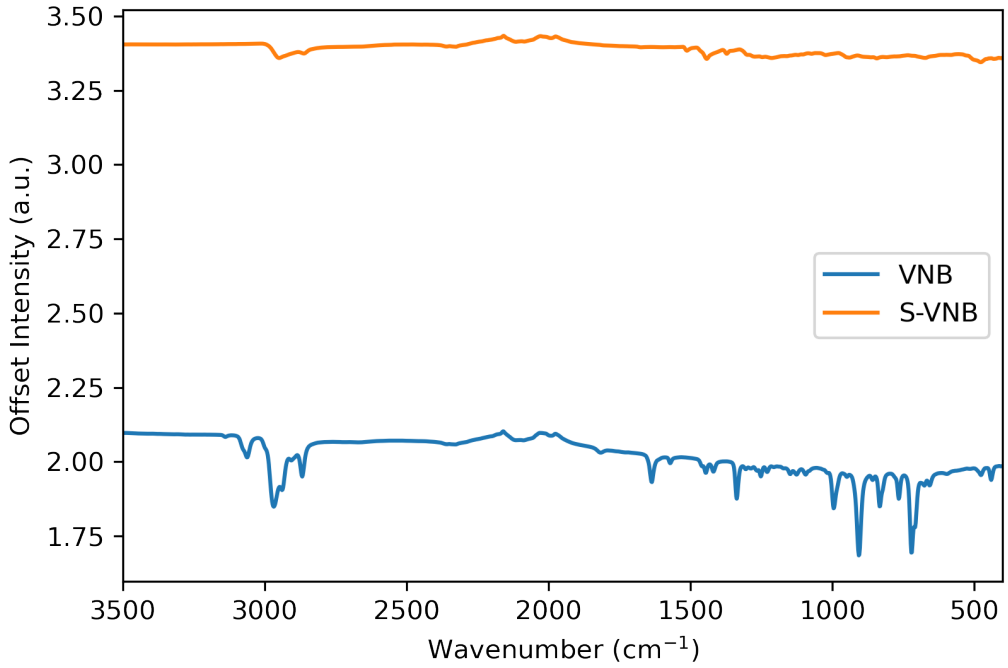

Figure 4.34: FTIR spectrum demonstrating the spectrum of S-VNB (orange) and VNB monomer (blue).

which were characteristic of the C=C vibrations. Finally, fingerprint signals characteristic of the C=C-H bending modes were reduced at 700, 900, and 1050 cm^{-1}, respectively. When combined with the previous data, the case for polymerisation becomes strong.

TGA revealed a decomposition profile that was typical of inverse vulcanised polymers with a decomposition temperature of 200°C. As previously discussed almost all sulfur polymers have the same decomposition profile that is a result of their similar chemical makeup. Initially, the S-S bonds decompose, followed by the C-S bonds, eventually leaving a carbanaceous material.

Finally, ^{13}C solid state NMR confirmed the formation of C-S bonds, reduction of C=C bonds and actually indicated some isomerisation of the molecule. For complete assignment refer to appendix, Figure A.32.

In conclusion, a polymer was formed from elemental sulfur and VNB. The polymer was found to be insoluble, and possess a relatively high T_g (>100°C). The polymerisation process was confirmed by TGA, FTIR and SS NMR.

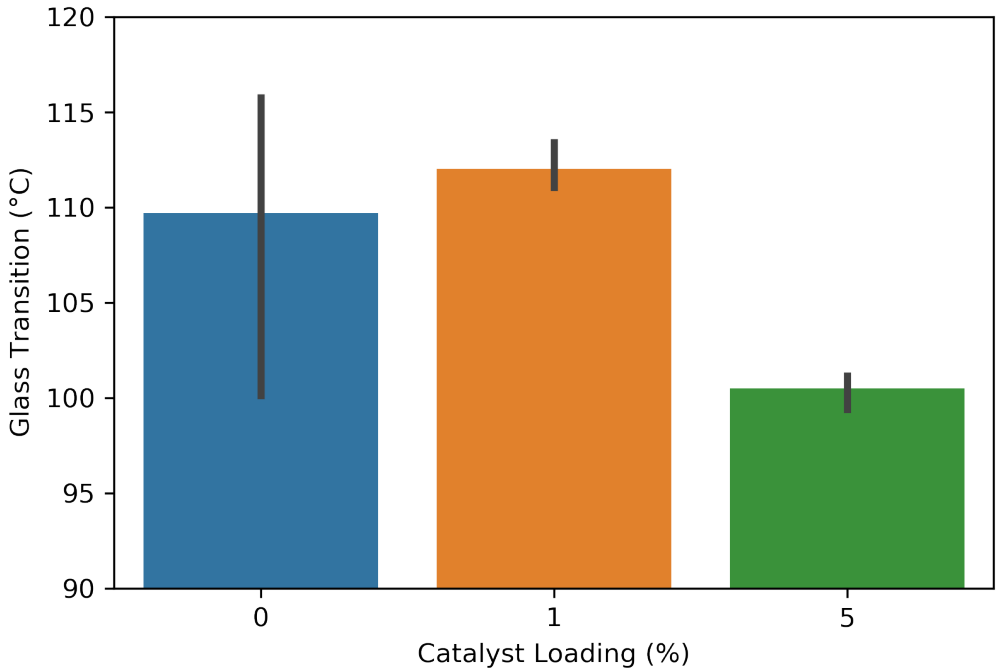

Figure 4.35: Bar graph demonstrating the difference in T_g of S-VNB with varying loadings of ZnD catalyst. The polymer comprised equal parts elemental sulfur and VNB. Reaction was run on a 10 g scale.

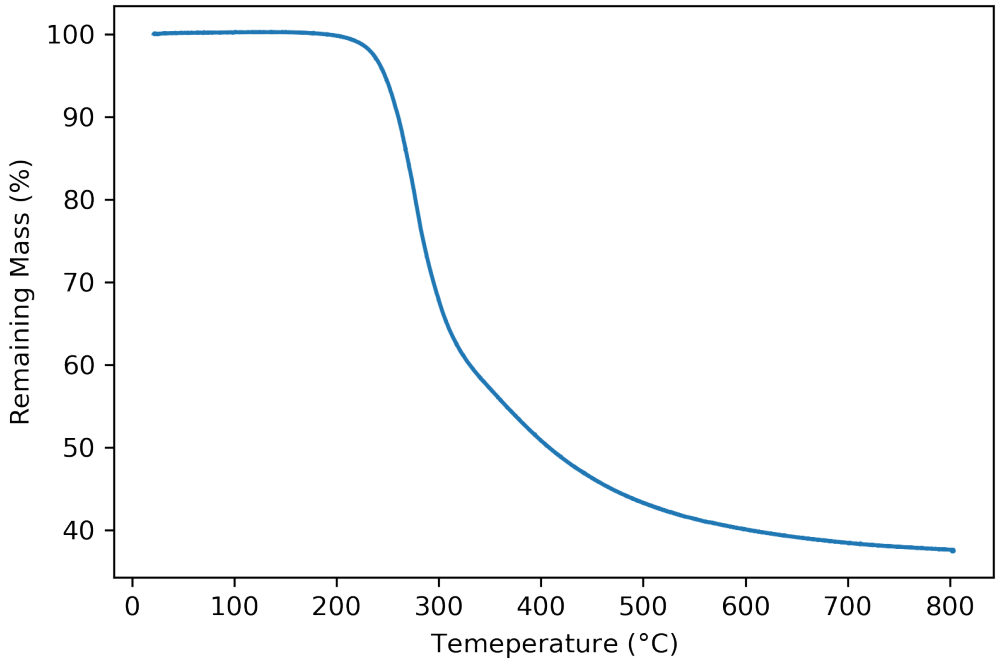

Figure 4.36: Decomposition curve for S-VNB comprised of equal parts elemental sulfur and VNB determined by weight. 1 wt% of ZnD catalyst was invcluded and the sample was heated to 800 °C under nitrogen.

S-CDTT

trans,trans,cis-1,5,9-cyclododecatriene (CDTT) is a small molecule olefin possessing 3 alkene groups. It is a chemical precursor used in the manufacture of nylon polymer, automotive products and other things. Because of the high degree of unsaturation, it was proposed as a potential candidate for the inverse vulcanisation process.

CDTT behaved similarly to the previously discussed cross linker, TVCH when reacted with elemental sulfur. When uncatalysed reaction products were of poor quality, with large amount of evaporated cross linker and sublimed sulfur on the reaction vessel. However, much like VNB, CDDT responded well to the inclusion of ZnD catalyst.

pXRD of the uncatalysed sample revealed the presence of elemental sulfur in the reaction product. However, inclusion of 1% wt ZnD ensured a successful reaction. The same was observed for the sample with 5% wt ZnD.

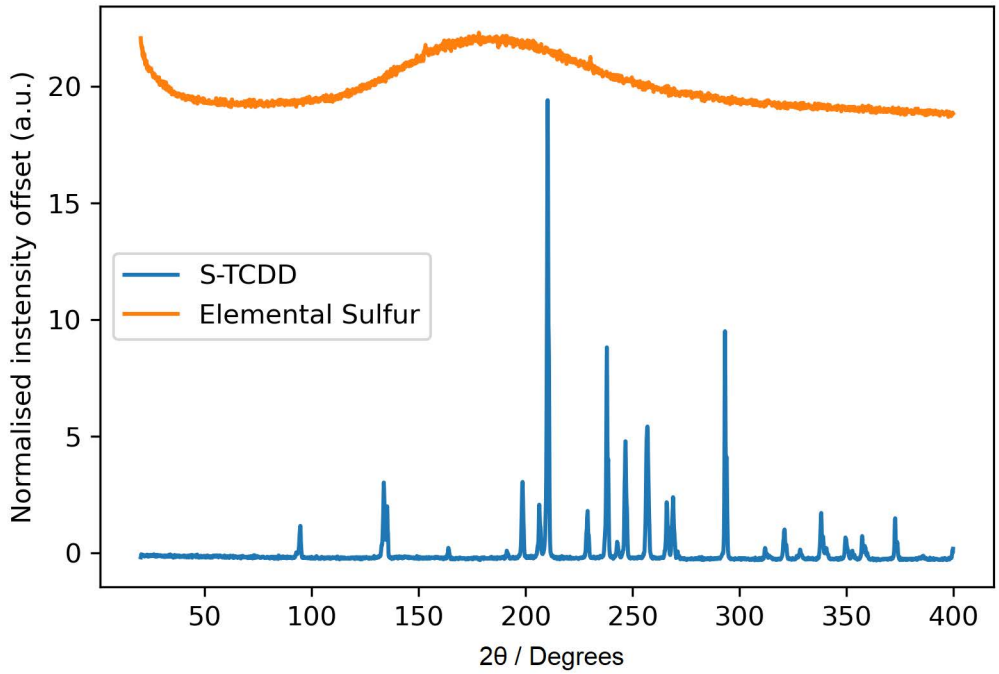

Figure 4.37: Offset lineplot of the results of pXRD analysis of the S-CDTT (blue) polymer vs elemental sulfur (orange)

The DSC of S-CDTT was more problematic than that of the other cross linkers. There was no detectable T_g for the samples with no ZnD and 5% wt ZnD. However, the sample with 1% wt ZnD produced a sample with a T_g of 35.1°C.

The FTIR of S-CDTT revealed a reduction in the signals at 3050 cm^{-1} and 1750 cm^{-1}.

These signals are typically resultant from the C=C and C=C-H vibrations, respectively. The alkene C=C-H bends that were located in the fingerprint region also showed a reduction in intensity. (600 cm^{-1}, 850 cm^{-1}, 950 cm^{-1}). Solid state ^{13}C NMR confirmed the formation of C-S bonds. For complete assignment, refer to appendix, Figure A.33. As with

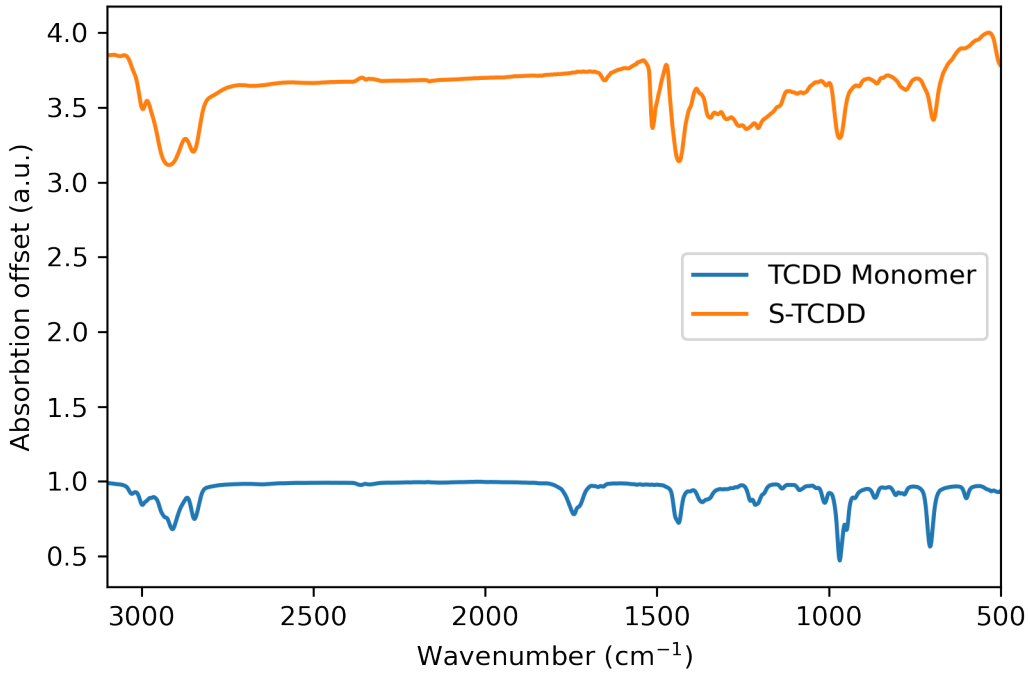

Figure 4.38: FTIR spectrum (offset) of TCDD monomer (blue) and S-TCDD polymer (orange)

previous cross linkers TVCH and VNB the thermal decomposition was typical of inverse vulcanised polymers, showing an onset of degradation just above 200 °C.

In conclusion, a sulfur polymer was formed from elemental sulfur and CDDT. The polymer synthesis was entirely successful for a 1% loading of ZnD but no T_g was detectable for the 0% loading and 5% loading of ZnD.

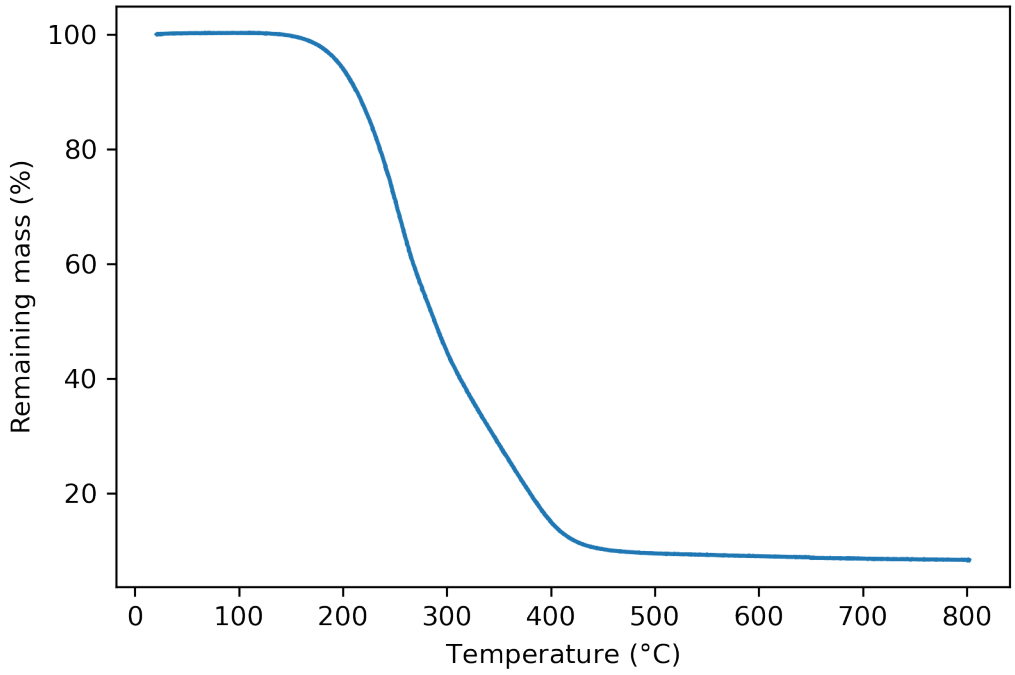

Figure 4.39: Results of a thermogravimetric analysis experiment on S-CDTT showing a decomposition offset after 200°C

4.8 Conclusions

In order to draw a conclusion about the work that was performed in this chapter, it would be appropriate to discuss the aims that were set at the beginning of the chapter. The first aim was concerning the screening of potential targets for the catalysis of the inverse vulcanisation reaction, using the gelation time as an indicator of the rate of reaction increase.

This target was met by the screening of a library of potential catalysts as listed in the section entitled 'Catalytic Screening' wherein 14 potential catalysts were screened. The gelation time was then used as a key indicator of the success of the catalyst for improving the rate of reaction in the catalysed process. Furthermore, it was used to graphically illustrate time to gelate as a function of the loading wt % of catalyst in the section entitled 'Structure and Properties'.

The catalyst that produced the greatest increase in rate of reaction was ZnD and this was used in a variety of cross linkers to examine the effects the catalyst had on the rate of reaction and the effect on the physical properties of the produced polymer.

The produced materials were then characterised to an appropriate degree, confirming the consumption of the alkenes and the appearance of a T_g which infers the formation of a polymeric network within the produced material.

Finally, the potential mechanistic pathway was discussed. In the sense of meeting the aims of the body of work it could be said that the work was a success. Catalysis is a difficult area of research, and when combined with the difficulty of analysis of cross-linked materials, there is a great scope for potential future experiments. Future work could look at using molecular models to explore the potential interactions between catalysts and elemental sulfur.

It would also be possible to explore more catalysts. The rubber industry has a massive amount of catalysts already in use that have not yet been investigated in the inverse vulcanisation reaction. It may be possible to design catalysts *ab initio* by selecting potential catalytic groups and building up a molecule from there.

4.9 Methods

4.9.1 Materials

Sulfur (S_8, sublimed powder, reagent grade, 99.5%, Brenntag UK Ireland. (Purchased in 25 kg bags), ethylene glycol dimethylacrylate (EGDMA, 98%, Alfa Aesar), glyoxal bis(diallyl acetal) (GBDA, Aldrich), trans,trans,cis-1,5,9-cyclododecatriene (CDDT, 98%, Alfa Aesar), 1,3,5,7-tetravinyltetramethylcyclotetrasiloxane (TVTCSi, 97%, Alfa Aesar), 1,2,4-trivinylcycohexane (TVCH, 98%, Fluorochem), dicyclopentadiene (DCPD >95%, TCI), 1,3-diisopropenylbenzene (DIB, 97%, Aldrich), divinylbenzene (DVB, 80%, Merck), (R)-(+)-limonene (97%, Aldrich), squalene (98%, Alfa Aesar), linseed oil (Aldrich), sodium diethyldithiocarbamate trihydrate (Alfa Aesar), copper diethyldithiocarbamate (TCI), nickel diethyldithiocaebamate (TCI), zinc diethyldithiocarbamate (97%, Aldrich), ZnO (Aldrich), zinc (Aldrich), $ZnCl_2$ (Aldrich), $FeCl_2$ (Aldrich), CuO (Aldrich), $CuCl_2$ (Aldrich), zinc stearate (Aldrich), 2-cyano-2-propyl benzodithioate (>97%, Aldrich), thiram (Aldrich), chloroform (Aldrich), and chloroform-d ($CDCl_3$,Cambridge Isotope Laboratories Inc.) were commercially available and used as received without any further purification. Iron diethyldithiocaebamate and cobalt diethyldithiocarbamate were both synthesized from sodium diethyldithiocarbamate following a method reported in the literature.

Table of explored reaction feeds

cross linker	cross linker mass (g)	Sulfur mass (g)	ZnD mass (g)
TVTSCi	5	5	0
TVTSCi	4.95	4.95	0.1
TVTSCi	4.75	4.75	0.5
CDDT	5	5	0
CDDT	4.95	4.95	0.1
CDDT	4.75	4.75	0.5
DCPD	5	5	0
DCPD	4.95	4.95	0.1
DCPD	4.75	4.75	0.5
DVB	5	5	0
DVB	4.95	4.95	0.1
DVB	4.75	4.75	0.5
DIB	5	5	0
DIB	4.95	4.95	0.1
DIB	4.75	4.75	0.5
EGDMA	5	5	0
EGDMA	4.95	4.95	0.1
EGDMA	4.75	4.75	0.5
GBDA	5	5	0
GBDA	4.95	4.95	0.1
GBDA	4.75	4.75	0.5
limonene	5	5	0
limonene	4.95	4.95	0.1
limonene	4.75	4.75	0.5
squalene	5	5	0
squalene	4.95	4.95	0.1
squalene	4.75	4.75	0.5
TVCH	5	5	0
TVCH	4.95	4.95	0.1
TVCH	4.75	4.75	0.5
VNB	5	5	0
VNB	4.95	4.95	0.1
VNB	4.75	4.75	0.5

Table 4.3: Table of explored reaction feeds.

4.9.2 Synthetic procedures for polymers

Synthesis of poly[sulfur-(*ran*)-TVTSCi]

TVTSCi (5 g, 0.0145 mol), sulfur (5 g, 0.156 mol) were weighed into a 10 mL glass vial and equipped with a 10 mm magnetic stirring bar. The vial was equipped with a B10 rubber septum and a needle inserted into the septum. The vial was placed into an aluminium heating block thermostatted to 135°C. Stirring was set to 800 rpm. After 10 minutes, the needle was removed and the mixture allowed to react until gelled. The reaction proceeded from a yellow cloudy bright yellow suspension that darkened over time to brown, and eventually black. If curing was desired, the reaction mixture was allowed to stand for a further 12 hours.

Synthesis of poly[sulfur-(*ran*)-CDDT]

cross linker (5 g, 0.0308 mol), sulfur (5 g, 0.156 mol) were weighed into a 10 mL glass vial and equipped with a 10 mm magnetic stirring bar. The vial was equipped with a B10 rubber septum and a needle inserted into the septum. The vial was placed into an aluminium heating block, thermostatted to 135 °C. Stirring was set to 800 rpm. After 10 minutes, the needle was removed and the mixture allowed to react until gelled. Whilst stirring, the colour darkened from a cloudy yellow to a dark brown over the course of reaction. If curing was desired, the reaction mixture was allowed to stand for a further 12 hours.

Synthesis of poly[sulfur-(*ran*)-DCPD]

cross linker (5 g, 0.0378 mol), sulfur (5 g, 0.156 mol) were weighed into a 10 mL glass vial and equipped with a 10 mm magnetic stirring bar. The vial was equipped with a B10 rubber septum and a needle inserted into the septum. The vial was placed into an aluminium heating block, thermostatted to 135 °C. Stirring was set to 800 rpm. After 10 minutes, the needle was removed and the mixture allowed to react until gelled. Initially, a clear, light yellow solution formed that darkened to black over time. If curing was desired, the reaction mixture was allowed to stand for a further 12 hours.

Synthesis of poly[sulfur-(*ran*)-DVB]

cross linker (5 g, 0.0384 mol), sulfur (5 g, 0.156 mol) were weighed into a 10 mL glass vial and equipped with a 10 mm magnetic stirring bar. The vial was equipped with a B10 rubber septum and a needle inserted into the septum. The vial was placed into an aluminium heating block, thermostatted to 135 °C. Stirring was set to 800 rpm. After 10 minutes, the needle was removed and the mixture allowed to react until gelled. Over the course of reaction, a light yellow solution formed that eventually became a gel, turning to a dark red. If curing was desired, the reaction mixture was allowed to stand for a further 12 hours.

Synthesis of poly[sulfur-(*ran*)-DIB]

DIB (5 g, 0.0316 mol), sulfur (5 g, 0.156 mol) were weighed into a 10 mL glass vial and equipped with a 10 mm magnetic stirring bar. The vial was equipped with a B10 rubber septum and a needle inserted into the septum. The vial was placed into an aluminium heating block, thermostatted to 135 °C. Stirring was set to 800 rpm. After 10 minutes, the needle was removed and the mixture allowed to react until gelled. Initially, a light yellow solution formed that turned to a clear red gel over time. If curing was desired, the reaction mixture was allowed to stand for a further 12 hours.

Synthesis of poly[sulfur-(*ran*)-(EGDMA]

EGDMA (5 g, 0.0252 mol), sulfur (5 g, 0.156 mol) were weighed into a 10 mL glass vial and equipped with a 10 mm magnetic stirring bar. The vial was equipped with a B10 rubber septum and a needle inserted into the septum. The vial was placed into an aluminium heating block, thermostatted to 135 °C. Stirring was set to 800 rpm. After 10 minutes, the needle was removed and the mixture allowed to react until gelled. If curing was desired, the reaction mixture was allowed to stand for a further 12 hours.

Synthesis of poly[sulfur-(*ran*)-glyoxal bis(diallyldiacetal]

GBDA (5 g, 0.0197 mol), sulfur (5 g, 0.156 mol) were weighed into a 10 mL glass vial and equipped with a 10 mm magnetic stirring bar. The vial was equipped with a B10 rubber septum and a needle inserted into the septum. The vial was placed into an aluminium heating block, thermostatted to 135 °C. Stirring was set to 800 rpm. After 10 minutes, the

needle was removed and the mixture allowed to react until gelled. Initially a cloudy yellow mixture formed that eventually formed a clear red gel. If curing was desired, the reaction mixture was allowed to stand for a further 12 hours.

Synthesis of poly[sulfur-(*ran*)-limonene]

Limonene (5 g, 0.0367 mol), sulfur (5 g, 0.156 mol) were weighed into a 10 mL glass vial and equipped with a 10 mm magnetic stirring bar. The vial was equipped with a B10 rubber septum and a needle inserted into the septum. The vial was placed into an aluminium heating block, thermostatted to 135 °C. Stirring was set to 800 rpm. After 10 minutes, the needle was removed and the mixture allowed to react until gelled. Initially a clear yellow solution formed that transitioned to a cloudy brown solution that then darkened over time. If curing was desired, the reaction mixture was allowed to stand for a further 12 hours.

Synthesis of poly[sulfur-(*ran*)-squalene]

Squalene (5 g, 0.0121 mol), sulfur (5 g, 0.156 mol) were weighed into a 10 mL glass vial and equipped with a 10 mm magnetic stirring bar. The vial was equipped with a B10 rubber septum and a needle inserted into the septum. The vial was placed into an aluminium heating block, thermostatted to 135 °C. Stirring was set to 800 rpm. After 10 minutes, the needle was removed and the mixture allowed to react until gelled. Initially a cloudy yellow solution formed that darkened to black over time. If curing was desired, the reaction mixture was allowed to stand for a further 12 hours.

Synthesis of poly[sulfur-(*ran*)-TVCH]

1,3,5-TVCH (5 g, 0.0308 mol), sulfur (5 g, 0.156 mol) were weighed into a 10 mL glass vial and equipped with a 10 mm magnetic stirring bar. The vial was equipped with a B10 rubber septum and a needle inserted into the septum. The vial was placed into an aluminium heating block thermostatted to 135 °C. Stirring was set to 800 rpm. After 10 minutes, the needle was removed and the mixture allowed to react until gelled. Initially a cloudy yellow solution formed that darkened over time. The suspension was not stable and required constant stirring. If curing was desired, the reaction mixture was allowed to stand for a further 12 hours.

Synthesis of poly[sulfur-(*ran*)-vegtable oil]

cross linker (5 g), sulfur (5 g, 0.156 mol) were weighed into a 10 mL glass vial and equipped with a 10 mm magnetic stirring bar. The vial was equipped with a B10 rubber septum and a needle inserted into the septum. The vial was placed into an aluminium heating block, thermostatted to 135 °C. Stirring was set to 800 rpm. After 10 minutes, the needle was removed and the mixture allowed to react until gelled. Initially a cloudy yellow solution formed that began to thicken very quickly, and a solid formed that looked inhomogeneous. If curing was desired, the reaction mixture was allowed to stand for a further 12 hours.

Synthesis of poly[sulfur-(*ran*)- 5-Vinyl-2-norbornene]

5-Vinyl-2-norbornene (5 g, the 0.0416 mol), sulfur (5 g, 0.156 mol) were weighed into a 10 mL glass vial and equipped with a 10 mm magnetic stirring bar. The vial was equipped with a B10 rubber septum and a needle inserted into the septum. The vial was placed into an aluminium heating block, thermostatted to 135 °C. Stirring was set to 800 rpm. After 10 minutes, the needle was removed and the mixture allowed to react until gelled. Initially a clear yellow solution formed that eventually gelled to a light yellow that darkened over time. If curing was desired, the reaction mixture was allowed to stand for a further 12 hours.

4.9.3 Instrumental Methods

Measurement of H_2S evolution during inverse vulcanisation reaction

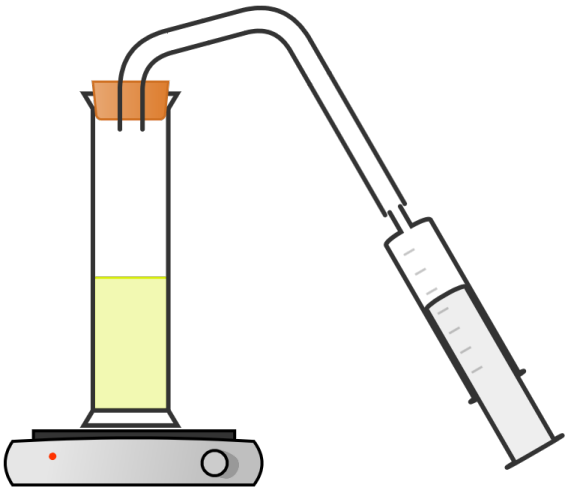

Figure 4.40: Schematic illustrating the gas collection experiments

The gas collection experiments are roughly described visually in Figure 4.40. In the experiment the desired ratio of cross linker, sulfur and ZnD were weighed into a 40 mL vial and this was subsequently placed into an aluminium heating block thermostatted to 135 °C. The mixture was pierced with a needle after 10 minutes to release any volatilised cross linker, and then the need was connected to some silicon tubing that was connected to a gas syringe. The reaction was run for 24 hours and the amount of gas released measured.

cross linker	cross linker mass (g)	Sulfur mass (g)	ZnD mass (g)
DIB	5	5	0
DIB	4.75	4.75	0.5
DCPD	5	5	0
DCPD	4.75	4.75	0.5
VNB	5	5	0
VNB	4.75	4.75	0.5

Table 4.4: Table demonstrating the amounts of cross linker, elemental sulfur and ZnD catalyst used in the H_2S collection tests

Gel Permeation Chromatography (GPC)

The molecular weight of the poly[s-(*ran*)-styrene] was determined by gel permeation chromatography (GPC) using a Viscotek system comprising a GPCmax (degasser, eluent and sample delivery system), and a TDA302 detector array, using chloroform as eluent.

Powder X-ray diffraction

pXRD was aquired using a PANalytical X'Pert PRO diffractometer with Cu-$K_{\alpha 1+2}$ radiation operating in transmission geometry. The X-Rays were of 1.54 Å. Samples were prepared by grinding in a mortar and pestle until a fine powder presented. The samples were placed into a fine layer (0.5 mm) over a shallow well.

Thermogravimetric Analysis (TGA)

TGA was conducted in platinum pans using a TA Instruments Q5000IR analyzer with an automatic vertical overhead thermobalance. The samples were heated at 5 °C min^{-1} to 900 °C under nitrogen. Samples were prepared by finely grinding materials in a mortar and pestle and weighing to approximately 1 mg.

Differential Scanning Calorimetry (DSC)

Thermograms were conducted in a TA Instruments Q200 DSC under nitrogen flow. Heating and cooling rates were set to 5 °C min^{-1} on a heat/cool/heat cycle with maximum temperature of 160 °C and minimum temperature of -60 °C. Samples were prepared by grinding in a mortar and pestle and subsequently weighing approximately 5 mg of sample into a pan which was then hermetically sealed in a press.

Fourier-transform infrared spectroscopy (FTIR)

FTIR was performed on a Bruker ALPHA II. Samples were ground with dry KBr in a mortar and pestle. Samples were initially trialled at 50 wt% material and 50 wt% KBr and pressed using a 2 tonne hydraulic press with a 2 mm die. Samples were adjusted based on the signal strength by regrinding the produced pellet and ether adding or subtracting more polymer to the reground sample. It was found that between 60-90% of polymer was required to produce a readable spectrum.

13C magic-angle spinning (MAS)

NMR spectra were performed on a Bruker Avance III operating at a ^{1}H Larmor frequency of 700 MHz, using a Bruker 4 mm HX probe. Chemical shifts were referenced using the CH3 resonance of solid alanine at 20.5 ppm (13C). A chemical shielding reference of 189.7 ppm was used, determined from a separate calculation on an optimized tetramethylsilane molecule.

^{1}H NMR

Solution NMR was recorded in deuterated chloroform using a Bruker Advance DRX (400 MHz) spectrometer. Samples were typically prepared by soaking excess sample in $CDCl_3$ for 24 hours when a low degree of solubility was exhibited. In samples of high solubility, 10-25 mg of sample was dissolved in 1 mL of $CDCl_3$

Bibliography

(1) W. J. Chung, J. J. Griebel, E. T. Kim, H. Yoon, A. G. Simmonds, H. J. Ji, P. T. Dirlam, R. S. Glass, J. J. Wie, N. A. Nguyen, B. W. Guralnick, J. Park, Á. Somogyi, P. Theato, M. E. Mackay, Y. E. Sung, K. Char and J. Pyun, *Nature Chemistry*, 2013, **5**, 518–524.

(2) S. Namnabat, J. J. Gabriel, J. Pyun and R. A. Norwood, Organic Photonic Materials and Devices XVI, ed. C. E. Tabor, F. Kajzar, T. Kaino and Y. Koike, SPIE, 2014, vol. 8983, p. 89830D.

(3) D. A. Boyd, V. Q. Nguyen, C. C. McClain, F. H. Kung, C. C. Baker, J. D. Myers, M. P. Hunt, W. Kim and J. S. Sanghera, *ACS Macro Letters*, 2019, **8**, 113–116.

(4) J. J. Griebel, S. Namnabat, E. T. Kim, R. Himmelhuber, D. H. Moronta, W. J. Chung, A. G. Simmonds, K.-J. Kim, J. van der Laan, N. A. Nguyen, E. L. Dereniak, M. E. Mackay, K. Char, R. S. Glass, R. A. Norwood and J. Pyun, *Advanced Materials*, 2014, **26**, 3014–3018.

(5) Y. Zhang, J. J. Griebel, P. T. Dirlam, N. A. Nguyen, R. S. Glass, M. E. Mackay, K. Char and J. Pyun, *Journal of Polymer Science Part A: Polymer Chemistry*, 2017, **55**, 107–116.

(6) A. Hoefling, D. T. Nguyen, P. Partovi-Azar, D. Sebastiani, P. Theato, S. W. Song and Y. J. Lee, *Chemistry of Materials*, 2018, **30**, 2915–2923.

(7) A. M. Abraham, S. V. Kumar and S. M. Alhassan, *Chemical Engineering Journal*, 2018, **332**, 1–7.

(8) S. Petcher, D. J. Parker and T. Hasell, *Environmental Science: Water Research & Technology*, 2019, DOI: `10.1039/c9ew00477g`.

(9) M. P. Crockett, A. M. Evans, M. J. Worthington, I. S. Albuquerque, A. D. Slattery, C. T. Gibson, J. A. Campbell, D. A. Lewis, G. J. Bernardes and J. M. Chalker, *Angewandte Chemie - International Edition*, 2016, **55**, 1714–1718.

(10) N. A. Lundquist, M. J. Worthington, N. Adamson, C. T. Gibson, M. R. Johnston, A. V. Ellis and J. M. Chalker, *RSC Advances*, 2018, **8**, 1232–1236.

(11) A. D. Tikoalu, N. A. Lundquist and J. M. Chalker, *Advanced Sustainable Systems*, 2020, **4**, 1–9.

(12) N. A. Lundquist, M. J. Sweetman, K. R. Scroggie, M. J. Worthington, L. J. Esdaile, S. F. Alboaiji, S. E. Plush, J. D. Hayball and J. M. Chalker, *ACS Sustainable Chemistry and Engineering*, 2019, **7**, 11044–11049.

(13) M. J. Worthington, R. L. Kucera, I. S. Albuquerque, C. T. Gibson, A. Sibley, A. D. Slattery, J. A. Campbell, S. F. Alboaiji, K. A. Muller, J. Young, N. Adamson, J. R. Gascooke, D. Jampaiah, Y. M. Sabri, S. K. Bhargava, S. J. Ippolito, D. A. Lewis, J. S. Quinton, A. V. Ellis, A. Johs, G. J. Bernardes and J. M. Chalker, *Chemistry - A European Journal*, 2017, **23**, 16219–16230.

(14) D. J. Parker, S. T. Chong and T. Hasell, *RSC Advances*, 2018, **8**, 27892–27899.

(15) J. S. M. Lee, D. J. Parker, A. I. Cooper and T. Hasell, *Journal of Materials Chemistry A*, 2017, **5**, 18603–18609.

(16) T. Hasell, D. J. Parker, H. A. Jones, T. McAllister and S. M. Howdle, *Chemical Communications*, 2016, **52**, 5383–5386.

(17) M. Mann, J. E. Kruger, F. Andari, J. McErlean, J. R. Gascooke, J. A. Smith, M. J. Worthington, C. C. McKinley, J. A. Campbell, D. A. Lewis, T. Hasell, M. V. Perkins and J. M. Chalker, *Organic and Biomolecular Chemistry*, 2019, **17**, 1929.

(18) R. O. Beauchamp, J. S. Bus, J. A. Popp, C. J. Boreiko, D. A. Andjelkovich and P. Leber, *Critical Reviews in Toxicology*, 1984, **13**, 25–97.

(19) J. A. Smith, X. Wu, N. G. Berry and T. Hasell, *Journal of Polymer Science Part A: Polymer Chemistry*, 2018, **56**, 1777–1781.

(20) Y. Zhang, N. G. Pavlopoulos, T. S. Kleine, M. Karayilan, R. S. Glass, K. Char and J. Pyun, *Journal of Polymer Science Part A: Polymer Chemistry*, 2019, **57**, 7–12.

(21) L. B. Blight, B. R. Currell, B. J. Nash, R. T. M. Scott and C. Stillo, *British Polymer Journal*, 1980, **12**, 5–11.

(22) X. Wu, J. A. Smith, S. Petcher, B. Zhang, D. J. Parker, J. M. Griffin and T. Hasell, *Nature Communications*, 2019, **10**, 647.

(23) A. Y. Coran, *Science and Technology of Rubber*, 2005, **17**, 321–366.

(24) H. L. Fisher, *Industrial and Engineering Chemistry*, 1939, **31**, 1381–1389.

(25) N. M. Rice, H. M. Irving and M. A. Leonard, *Pure and Applied Chemistry*, 1993, **65**, 2373–2396.

(26) T. WATANABE, *Journal of Synthetic Organic Chemistry, Japan*, 1978, **36**, 395–402.

(27) R. N. Datta, *Rubber curing systems*, iSmithers Rapra Publishing, 2002, vol. 12.

(28) E. Koczorowska, B. Jurkowska and B. Jurkowski, *Journal of Applied Polymer Science*, 1998, **69**, 1531–1536.

(29) D. J. Parker, H. A. Jones, S. Petcher, L. Cervini, J. M. Griffin, R. Akhtar and T. Hasell, *Journal of Materials Chemistry A*, 2017, **5**, 11682–11692.

(30) P. Yan, W. Zhao, B. Zhang, L. Jiang, S. Petcher, J. A. Smith, D. J. Parker, A. I. Cooper, J. Lei and T. Hasell, *Angewandte Chemie International Edition*, 2020, anie.202004311.

(31) J. M. Scheiger, C. Direksilp, P. Falkenstein, A. Welle, M. Koenig, S. Heissler, J. Matysik, P. A. Levkin and P. Theato, *Angewandte Chemie International Edition*, 2020, **59**, 18639–18645.

(32) M. Smith, *Handbook of Rubber Technology: Natural, Synthetic Rubber and Technology of Vulcanisation Vol. I (HB)*, CBS Publishers & Distributors, 2004.

(33) *The chemistry and physics of rubber-like substances; studies of the Natural Rubber Producers' Research Association. (Book, 1963) [WorldCat.org].*

(34) D. Dondi, A. Buttafava, A. Zeffiro, C. Palamini, A. Lostritto, L. Giannini and A. Faucitano, *European Polymer Journal*, 2015, **62**, 222–235.

(35) R. Steudel, S. Passlack-Stephan and G. Holdt, *ZAAC - Journal of Inorganic and General Chemistry*, 1984, **517**, 7–42.

(36) Q. Lian, Y. Li, K. Li, J. Cheng and J. Zhang, *Macromolecules*, 2017, **50**, 803–810.

(37) A. J. Parker and N. Kharasch, *Chemical Reviews*, 1959, **59**, 583–628.

(38) A. M. Abraham, S. V. Kumar and S. M. Alhassan, *Chemical Engineering Journal*, 2018, **332**, 1–7.

(39) M. W. Thielke, L. A. Bultema, D. D. Brauer, B. Richter, M. Fischer and P. Theato, *Polymers*, 2016, **8**, 266.

(40) J. Lim, J. Pyun and K. Char, *Recent approaches for the direct use of elemental sulfur in the synthesis and processing of advanced materials*, 2015.

(41) J. A. Smith, R. Mulhall, S. Goodman, G. Fleming, H. Allison, R. Raval and T. Hasell, *ACS Omega*, 2020, **5**, 5229–5234.

(42) H. Kang, H. Kim and M. J. Park, *Advanced Energy Materials*, 2018, **8**, 1–9.

(43) V. Kumar, S. Wadi, K. K. Jena, S. Z. Khawaja, K. Yannakopoulou, M. Fardis, G. Mitrikas, M. Karagianni, G. Papavassiliou and S. M. Alhassan, *ACS Publications*, 2018, **3**, 3330–3339.

(44) M. Arslan, B. Kiskan and Y. Yagci, *Scientific Reports*, 2017, **7**, DOI: `10.1038/s41598-017-05608-2`.

(45) M. Arslan, B. Kiskan and Y. Yagci, *Macromolecules*, 2016, **49**, 767–773.

(46) Y. Zhang, J. J. Griebel, P. T. Dirlam, N. A. Nguyen, R. S. Glass, M. E. Mackay, K. Char and J. Pyun, *Journal of Polymer Science Part A: Polymer Chemistry*, 2017, **55**, 107–116.

(47) E. Martínez-Ahumada, A. López-Olvera, V. Jancik, J. E. Sánchez-Bautista, E. González-Zamora, V. Martis, D. R. Williams and I. A. Ibarra, *Organometallics*, 2020, **39**, 883–915.

(48) T. J. Tulig and M. Tirrell, *Macromolecules*, 1982, **15**, 459–463.

(49) J. S. M. Lee, D. J. Parker, A. I. Cooper and T. Hasell, *Journal of Materials Chemistry A*, 2017, **5**, 18603–18609.

(50) D. J. Parker, H. A. Jones, S. Petcher, L. Cervini, J. M. Griffin, R. Akhtar and T. Hasell, *Journal of Materials Chemistry A*, 2017, **5**, 11682–11692.

(51) M. Tsujimoto, *Industrial and Engineering Chemistry*, 1920, **12**, 63–72.

(52) M. P. Crockett, A. M. Evans, M. J. Worthington, I. S. Albuquerque, A. D. Slattery, C. T. Gibson, J. A. Campbell, D. A. Lewis, G. J. Bernardes and J. M. Chalker, *Angewandte Chemie - International Edition*, 2016, **55**, 1714–1718.

(53) V. Negro, G. Mancini, B. Ruggeri, D. F. B. Technology and u. 2016, *Elsevier*.

(54) C. Ravichandran, P. Badgujar, ..., given=P Gundev - Food, giveni=P. G. F., *Elsevier*.

(55) X. Wu, J. A. Smith, S. Petcher, B. Zhang, D. J. Parker, J. M. Griffin and T. Hasell, *Nature Communications*, 2019, **10**, 1–9.

(56) G. MA, C. H. F. Chemicals, Specialty and u. 2004, *en.cnki.com.cn*.

(57) W. J. Chung, J. J. Griebel, E. T. Kim, H. Yoon, A. G. Simmonds, H. J. Ji, P. T. Dirlam, R. S. Glass, J. J. Wie, N. A. Nguyen, B. W. Guralnick, J. Park, Á. Somogyi, P. Theato, M. E. Mackay, Y. E. Sung, K. Char and J. Pyun, *Nature Chemistry*, 2013, **5**, 518–524.

(58) M. Van Duin, R. Orza, R. Peters and V. Chechik, Macromolecular Symposia, 2010, vol. 291-292, pp. 66–74.

Chapter 5

Conclusions

5.1 Conclusions and Future Work

5.1.1 Macroporous Sulfur Polymers

At the beginning of this thesis, in chapter 1 the section entitled 'project overview' discussed some of the aims that were to be met during the research I conducted during my PhD programme.

The first of these aims was to generate a macroporous sulfur polymer that was able to remove mercury from solution. The aims of this were met, and a macroporous sulfur polymer was synthesised and analysed. It was found that the polymer possessed a surface area of over 15 m^2g^{-1}, and had a capacity of 2.27 mg g^{-1} for $HgCl_2$. As of writing, there has not yet been an inverse vulcanised polymer produced in the same way with a higher mercury capacity.

Whilst the capacity is absolutely low, relatively speaking was a breakthrough in the field of inverse vulcanisation. The method was adapted and reused by several research groups. So in that sense, the investigation should be considered a success.

Future work in the field of macroporous sulfur polymers should look to concern itself with several key challenges:

- How small can the pore size be taken?
- Are there alternative porogens?
- Can the polymer surface be altered to improve the wettability of the polymer?

- Is it possible to combine the methods of generation macroporosity and mesoporosity to generate hierarchical porosity?

Whilst these challenges are not at all comprehensive, it is my feeling that addressing them would substantially improve the scope of application for macroporous sulfur polymers.

5.1.2 Mesoporous Sulfur Polymers

The second area of research to be discussed in terms of conclusions and future work is the mesoporous sulfur polymers. This work produced the highest surface area sulfur polymer that has been reported.

The surface area of SHCP-01 was 236 m^2 g^{-1}. Owing to its high surface area, SHCP-01 was able to remove large amounts of mercury chloride from solution. The capacity of SHCP-01 was reported as 215.9 mg g^{-1}, with an incredibly high K_D of 0.48. This high affinity, high capacity material is, at the time of writing, the highest capacity for a 'pure' sulfur polymer. This achievement comes with the caveat of a chemical modification or introduction of bridging groups on the phenyl rings.

Any future work in this area should concern itself with the following key challenges:

- Are there alternative ways of generating mesoporosity in sulfur polymers?
- Is it possible to control the porosity that is produced by the knitting method?
- Can this method be applied to any other sulfur polymers?

At the time of writing, this work is relatively new. It will be interesting to see how the method develops, and if any further methods or applications are developed.

In conclusion, the aims that were set out in the project aims were met and mesoporous sulfur polymers were produced. Future work has been addressed.

5.1.3 Catalysed Sulfur Polymers

In the project aims, a rather broad aim was stated in that an attempt would be made into understanding the mechanism of inverse vulcanisation. In hindsight, this was a rather optimistic aim.

However, it was possible to develop catalysts that made a small, but significant dent in the progress in this area. It was discovered that the conventional understanding that

the scission of the S-S bond above 159 °C was able to be circumvented and polymerisation reactions able to occur as low as 135 °C. Therefore, in this sense the project aim was not met but alternative and useful conclusions were drawn.

Future work in this area of research maybe should not concern itself with attempting to completely understand the mechanism of inverse vulcanisation which is highly complex and difficult to analyse, alternatively looking to make further 'small dents' of progress.

A highly challenging, but potentially profitable, area of research would be finding ways to conduct these polymerisations' below 100 °C. Below this temperature a range of solvent could be introduced into the polymerisation process and areas such as precipitation polymerisation could be explored.

Furthermore, it is possible that polymers with improved mechanical properties may be produced at lower temperatures. We demonstrated that at lower temperatures, better physical properties are developed.

In conclusion, a body of work on catalysis was produced. The work was highly successful, and has opened a whole avenue of potential research that may be tapped.

5.1.4 Overall Conclusions

Overall, it is my belief that the research I conducted as part of my PhD was a success. Whilst not all aims were met and not all research was completed, that is the nature of the research environment. I was able to produce several high quality pieces of research that I feel contributed to the body of knowledge of chemistry. Finally, I would like to take the time to thank anyone who has read my thesis in its entirety. It is my hope that it was an enjoyable experience.

Appendix A

Appendix

Testing the effectiveness of salt templated polymers Hg removal at different pH

3 100 mL buffer solutions were prepared for a basic, neutral and acidic condition. The concentration of buffer was maintained at 10 mmol. To the buffer solutions, 1.6 mL of stock was added to achieve a concentration of 63 ppm.

pH	**Percentage removed from 63 ppm Hg^{2+} solution (%)**
4.9	21.3
7	11.2
9.1	12.19

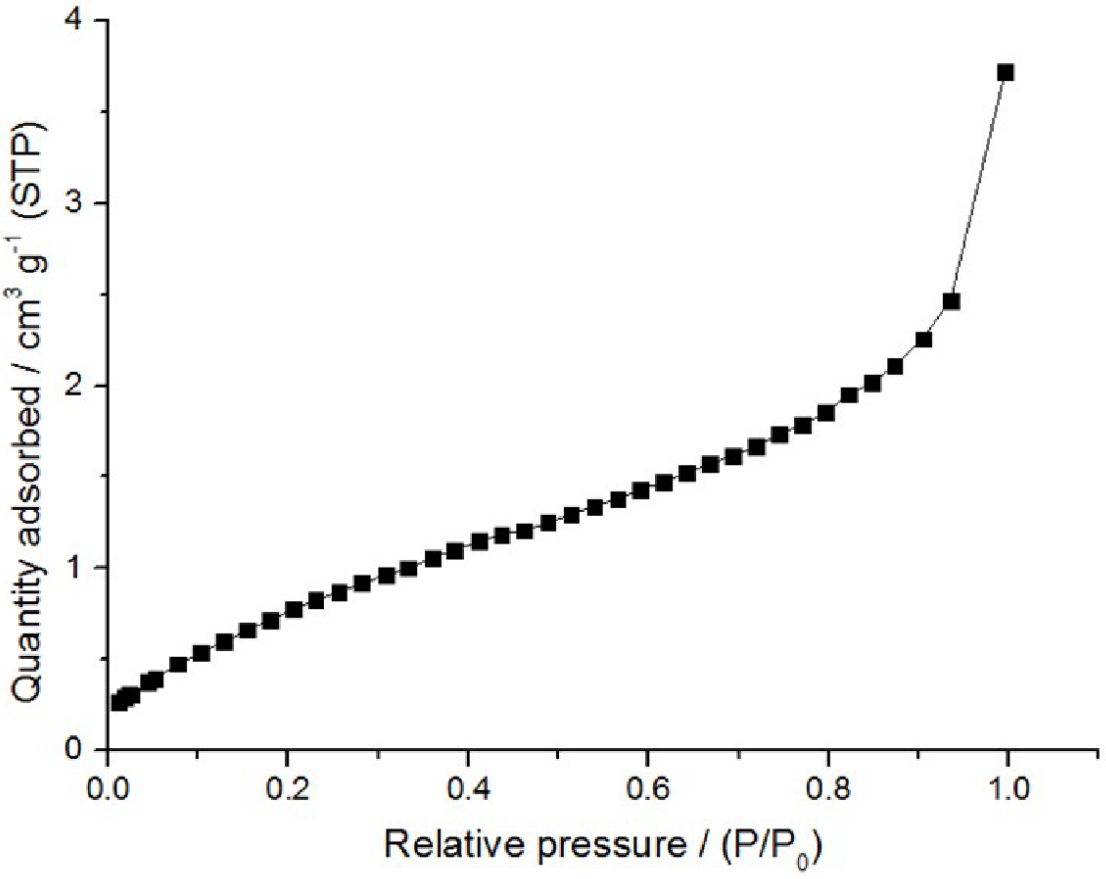

Figure A.1: N2 Isotherm demonstrating the apparent lack of micro and mesoposity in salt templated porous S-DCPD as described in Chapter 2.

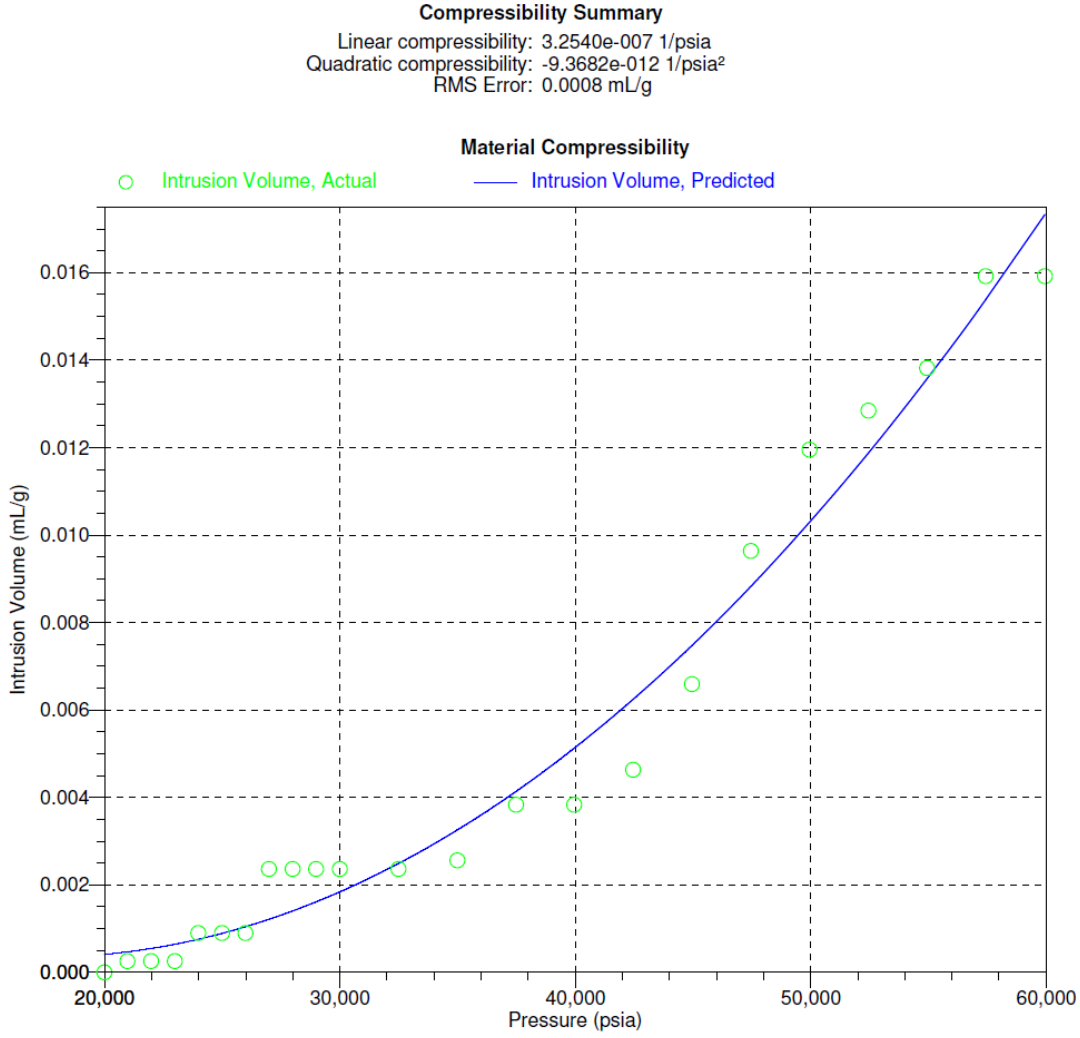

Figure A.2: (top) Summary of the compressibility of porous S-DCPD as described in Chapter 2 (bottom) Graph demonstrating the relationship between the pressure applied to salt templated S-DCPD and the resultant intrusion volume of elemental mercury into the sample.

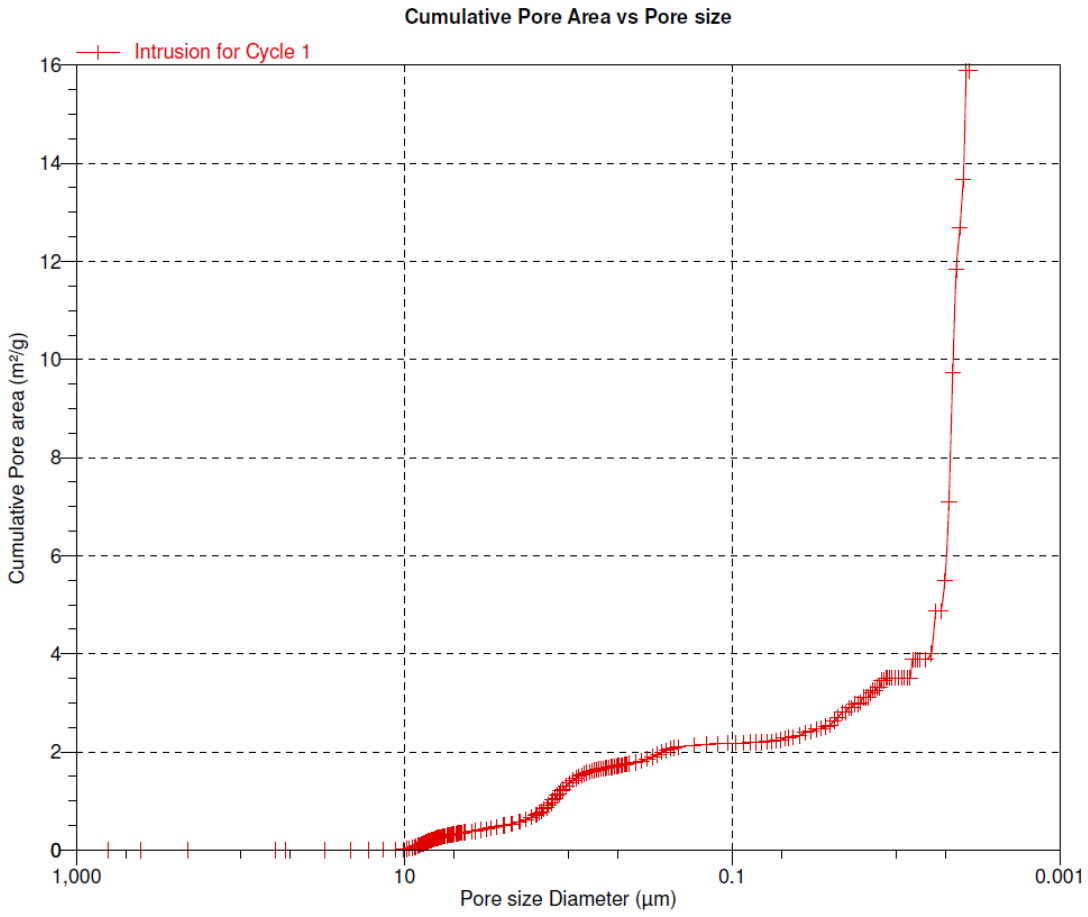

Figure A.3: Graph demonstrating the cumulative pore area of salt templated porous S-DCPD as described in Chapter 2 as a function of the pore size diameter as determined by mercury porosimetry.

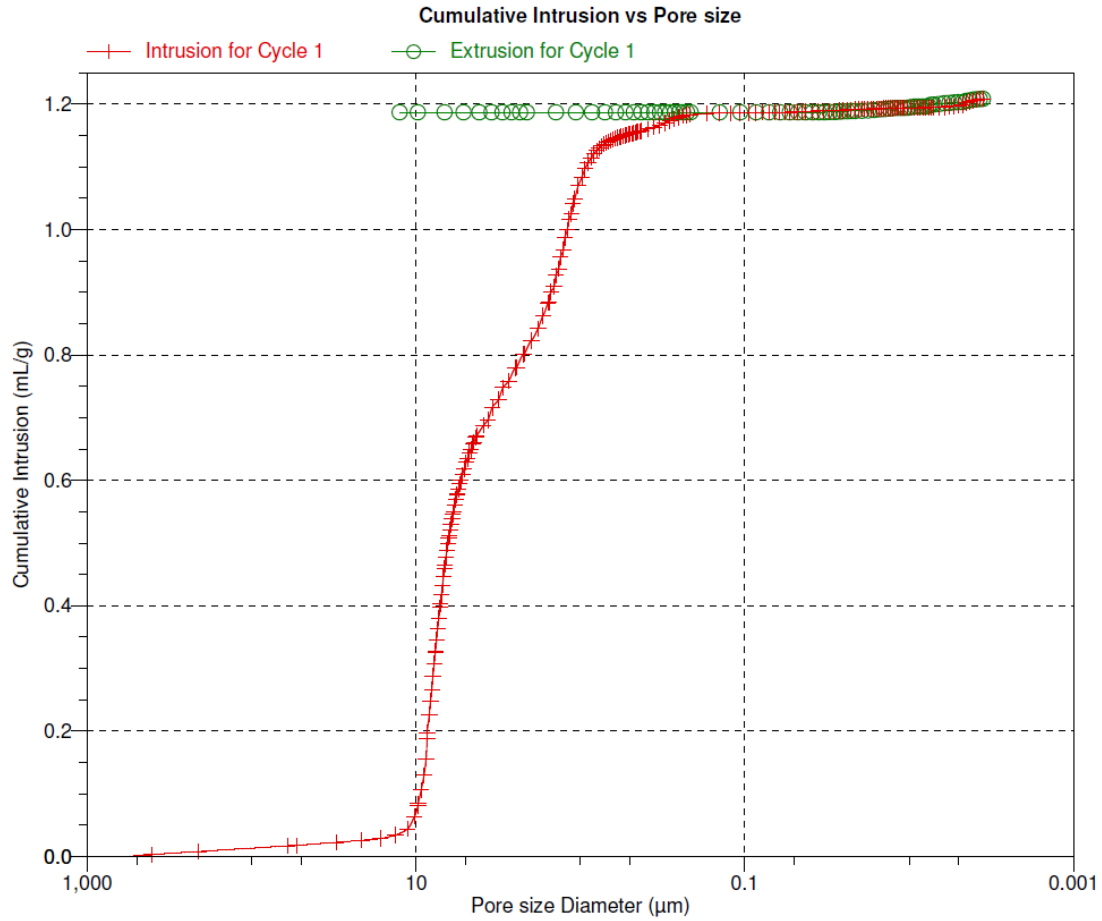

Figure A.4: Graph demonstrating the cumulative intrusion of elemental mercury into salt templated porous S-DCPD as described in Chapter 2 as a function of the pore size diameters present in the sample determined by mercury porosimetry.

Solvent	Solubility
Chloroform	Insoluble
Toluene	Insoluble
Dichloromethane	Insoluble
Tetrahydrofuran	Insoluble
DMSO	Insoluble
Water	Insoluble
Methanol	Insoluble
Ethanol	Insoluble

Figure A.5: Solubility of porous polymer SHCP-01 from Chapter 3 in various organic solvents and water.

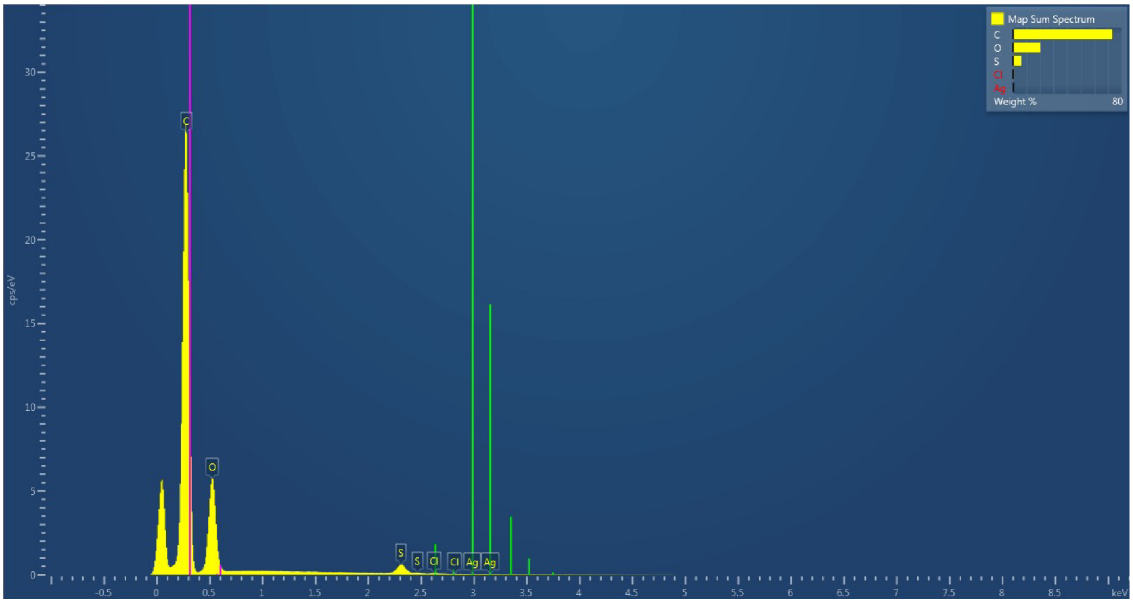

Figure A.6: EDS spectra of porous polymer SHCP-01 from Chapter 3 demonstrating the presence of Cl, S, C. Other elements are also present in small quantities as artefacts of the preparation of the sample (Ag, O)

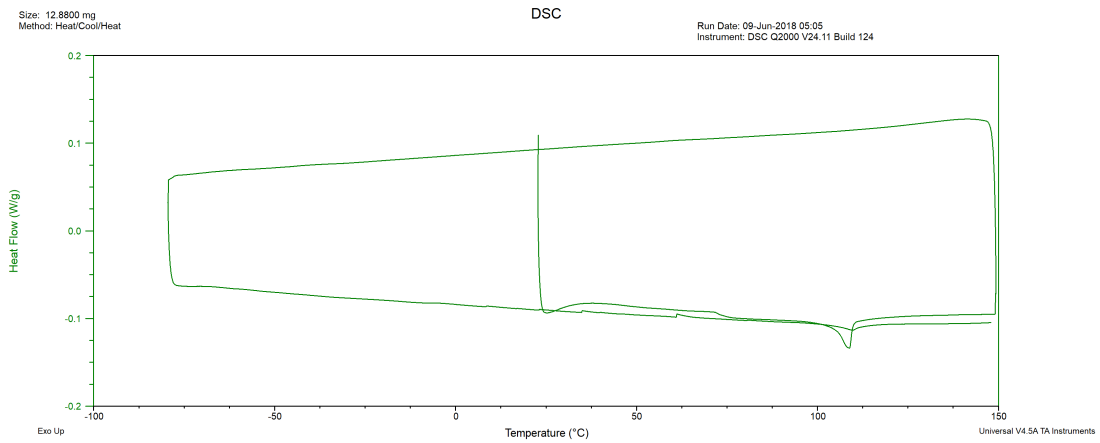

Figure A.7: Thermogram of S-TVTSCi as described in Chapter 4 (5% ZnD Loading, 47.5% Sulfur, 47.5% TVTSci)

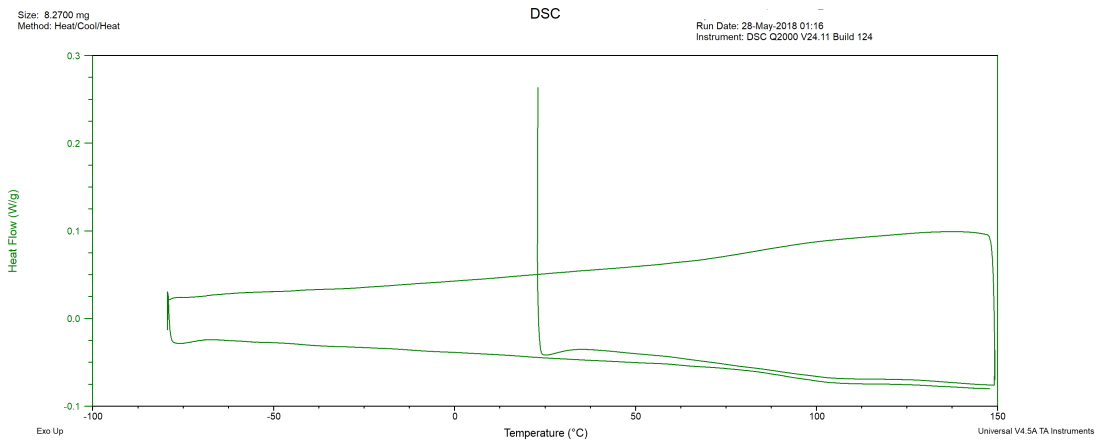

Figure A.8: Thermogram of S-DCPD as described in Chapter 4(1% ZnD Loading, 49.5% Sulfur, 49.5% DCPD)

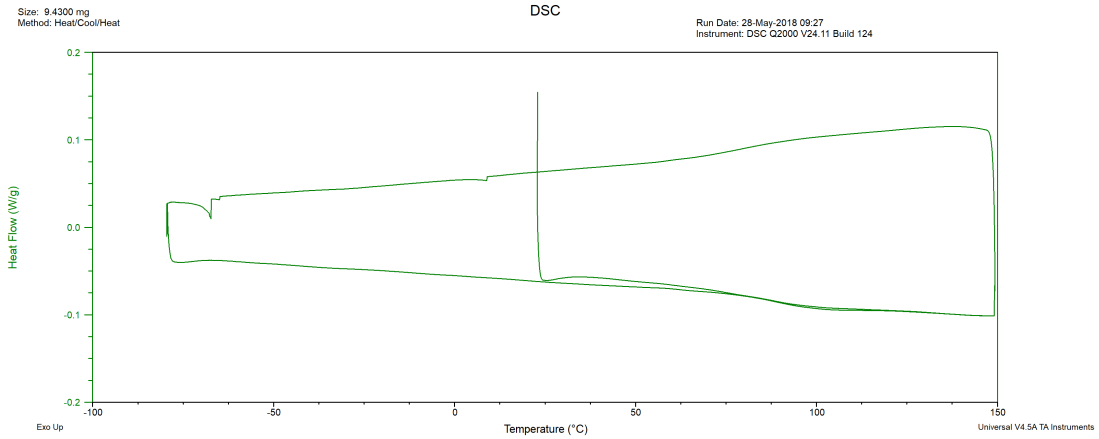

Figure A.9: Thermogram of S-DCPD as described in Chapter 4(5% ZnD Loading, 47.5% Sulfur, 47.5% DCPD)

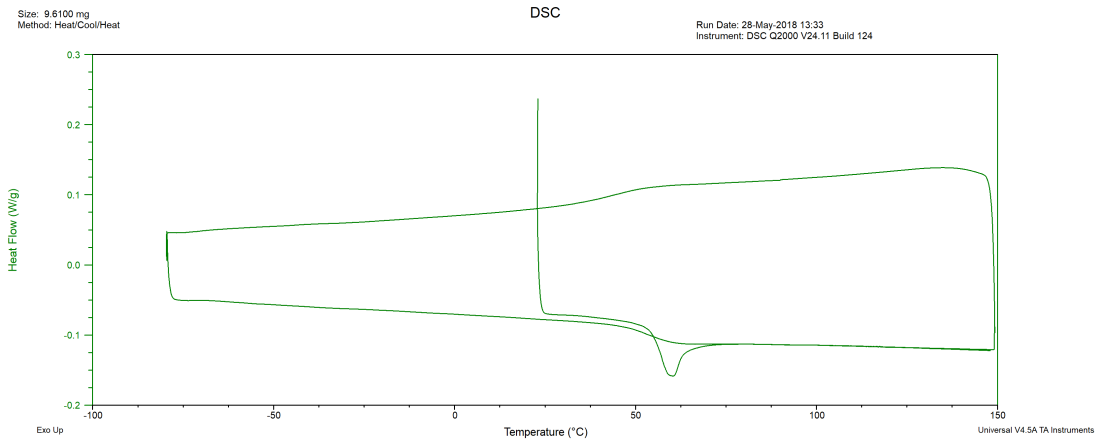

Figure A.10: Thermogram of S-DIB as described in Chapter 4(1% ZnD Loading, 49.5% Sulfur, 49.5% DIB)

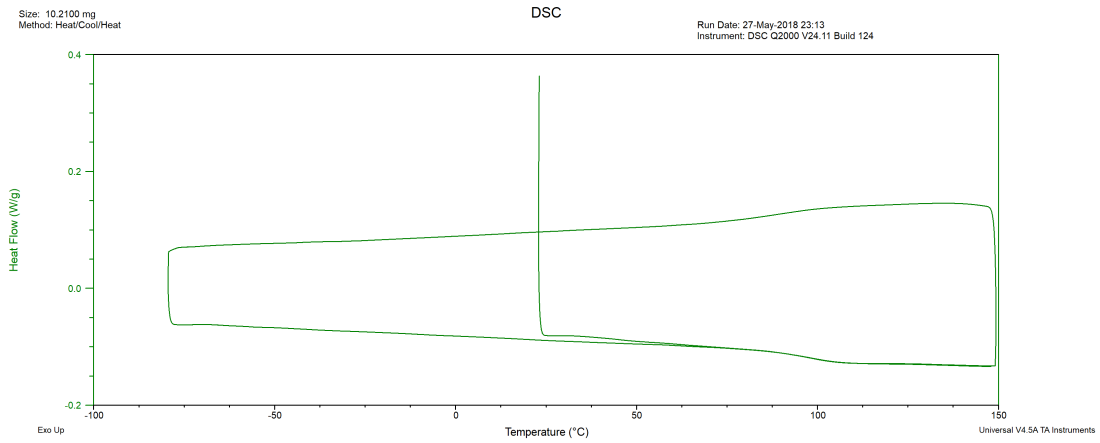

Figure A.11: Thermogram of S-DVB as described in Chapter 4(50% Sulfur, 50% DVB)

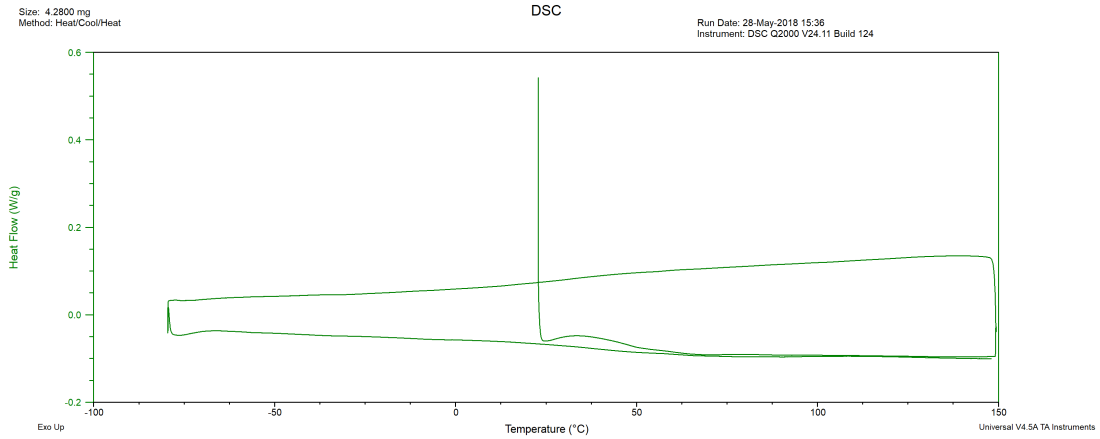

Figure A.12: Thermogram of S-DVB as described in Chapter 4(1% ZnD Loading, 49.5% Sulfur, 49.5% DVB)

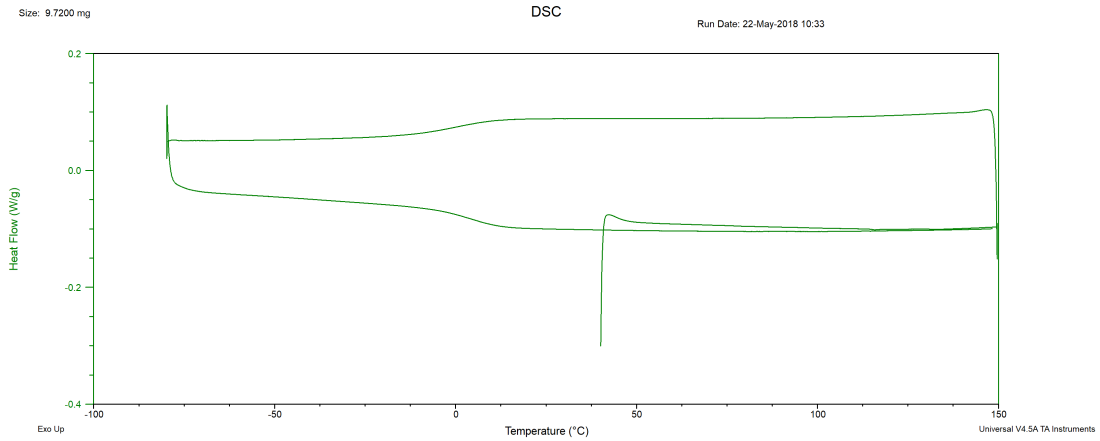

Figure A.13: Thermogram of S-EGDMA as described in Chapter 4(1% ZnD Loading, 49.5% Sulfur, 49.5% EGDMA)

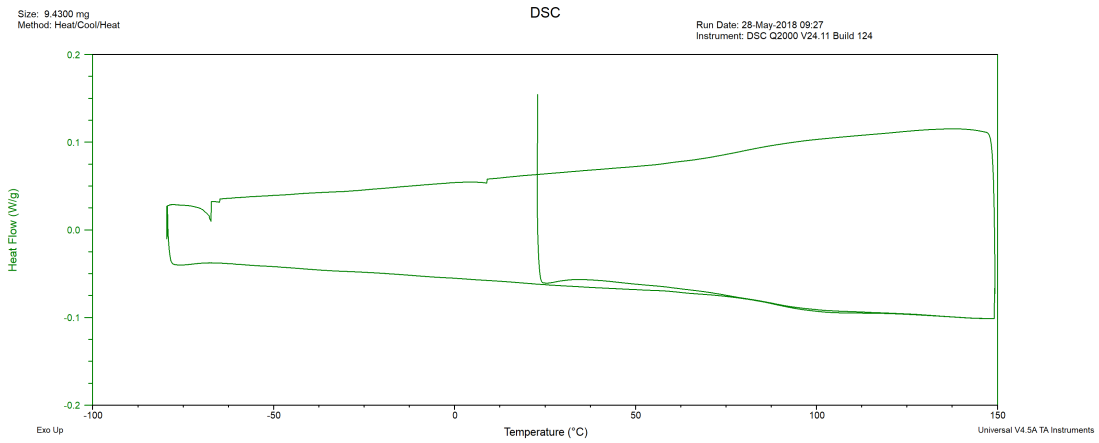

Figure A.14: Thermogram of S-EGDMA as described in Chapter 4(5% ZnD Loading, 47.5% Sulfur, 47.5% EGDMA)

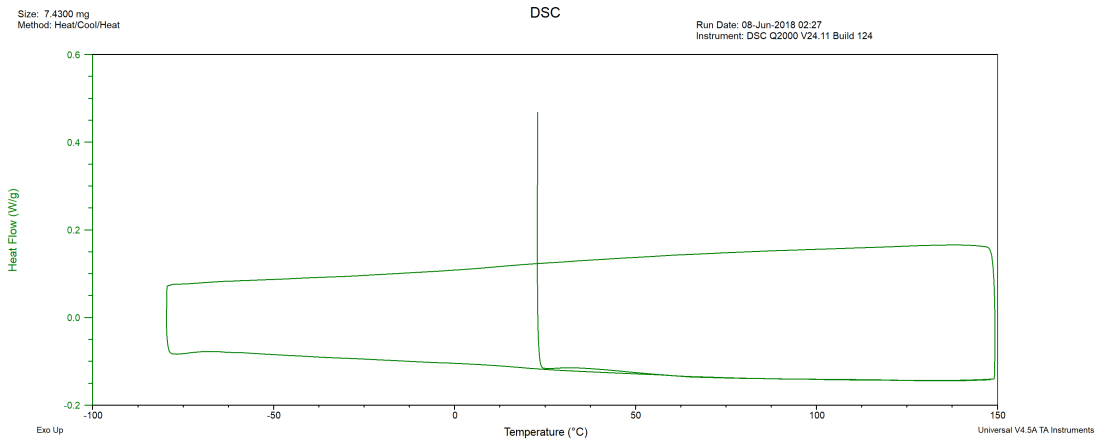

Figure A.15: Thermogram of S-GBDA as described in Chapter 4(50% Sulfur, 50% GBDA)

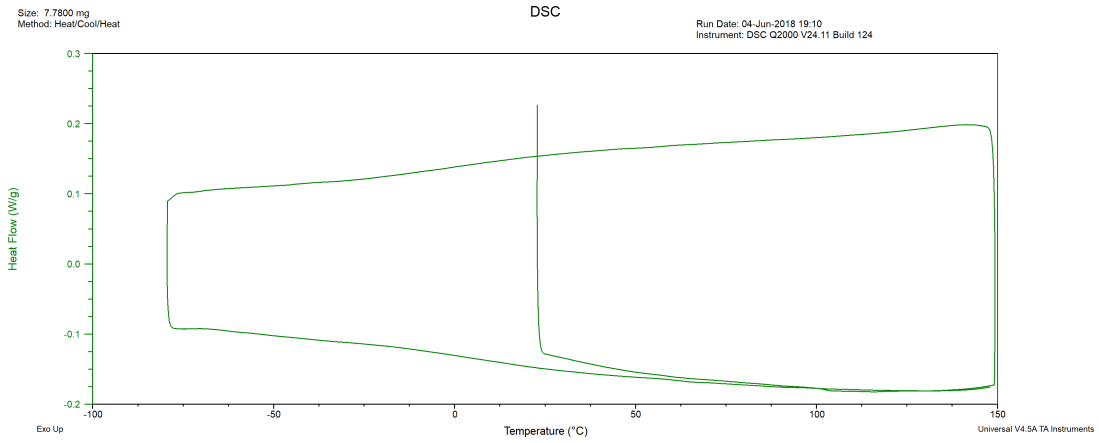

Figure A.16: Thermogram of S-GBDA as described in Chapter 4(1% ZnD Loading, 49.5% Sulfur, 49.5% GBDA)

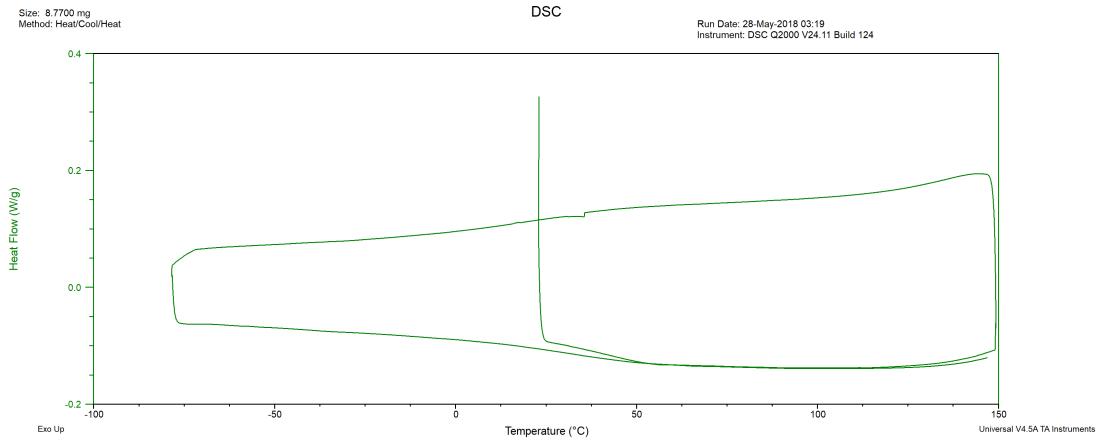

Figure A.17: Thermogram of S-GBDA as described in Chapter 4(5% ZnD Loading, 47.5% Sulfur, 47.5% GBDA)

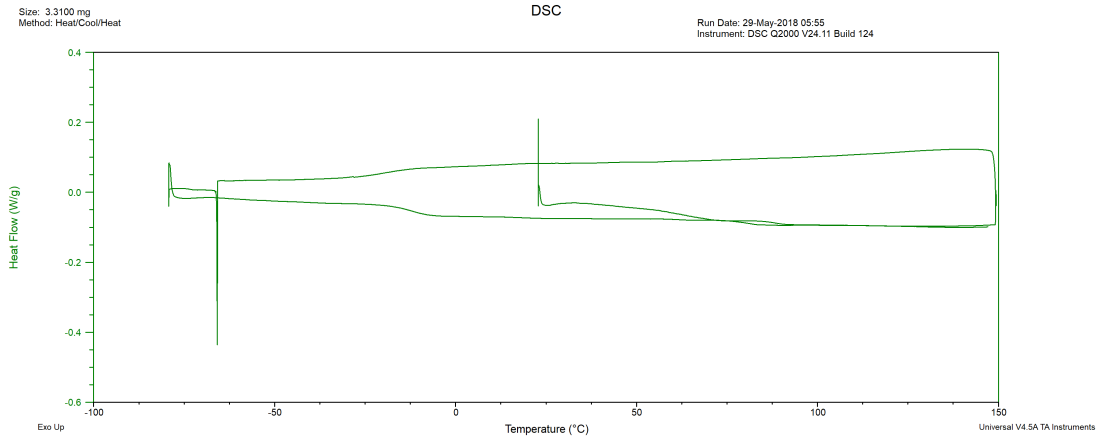

Figure A.18: Thermogram of S-Limonene as described in Chapter 4(50% Sulfur, 50% Limonene)

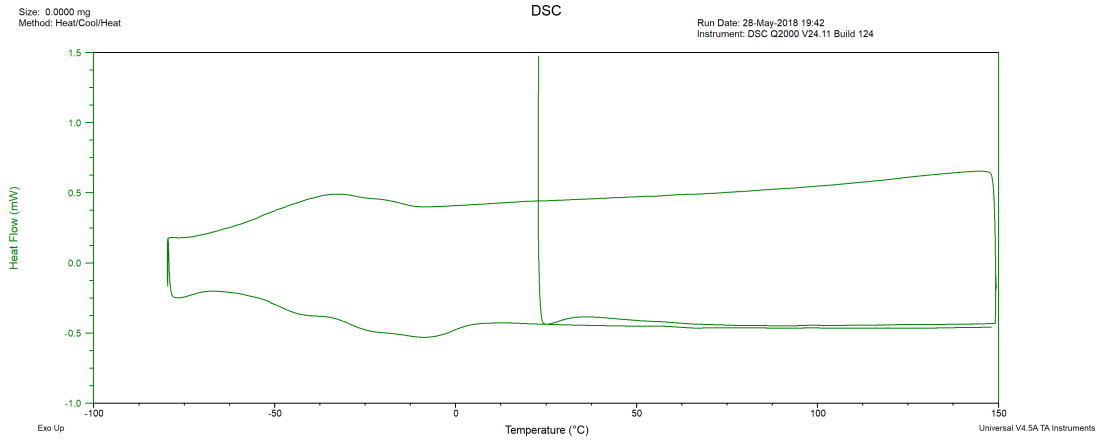

Figure A.19: Thermogram of S-Limonene as described in Chapter 4(1% ZnD Loading, 49.5% Sulfur, 49.5% Limonene)

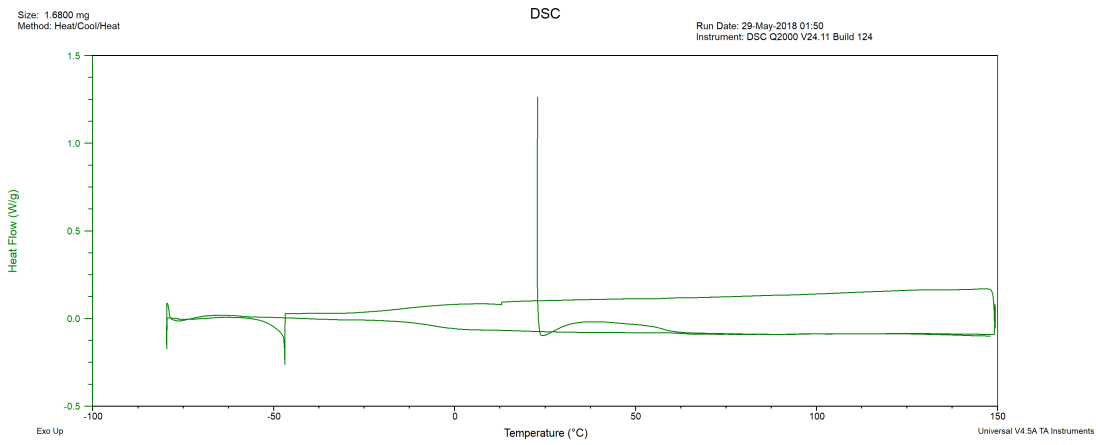

Figure A.20: Thermogram of S-Limonene as described in Chapter 4(5% ZnD Loading, 47.5% Sulfur, 47.5% Limonene)

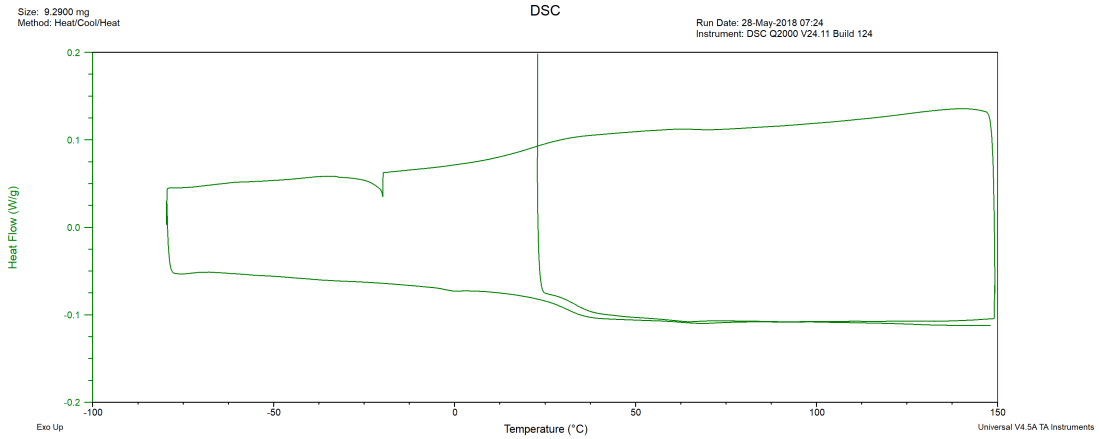

Figure A.21: Thermogram of S-Squalene as described in Chapter 4(50% Sulfur, 50% Squalene)

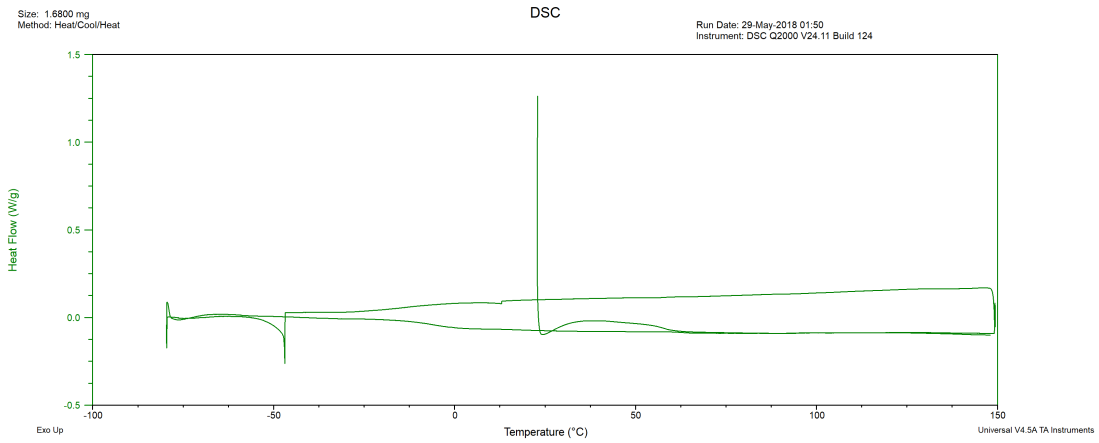

Figure A.22: Thermogram of S-Squalene as described in Chapter 4(5% ZnD Loading, 47.5% Sulfur, 47.5% Squalene)

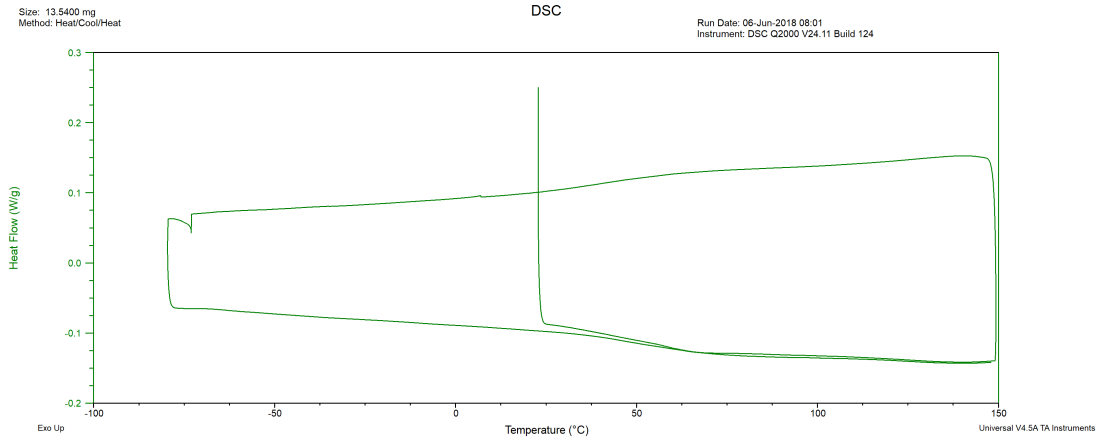

Figure A.23: Thermogram of S-CDTT as described in Chapter 4(50% Sulfur, 50% CDTT)

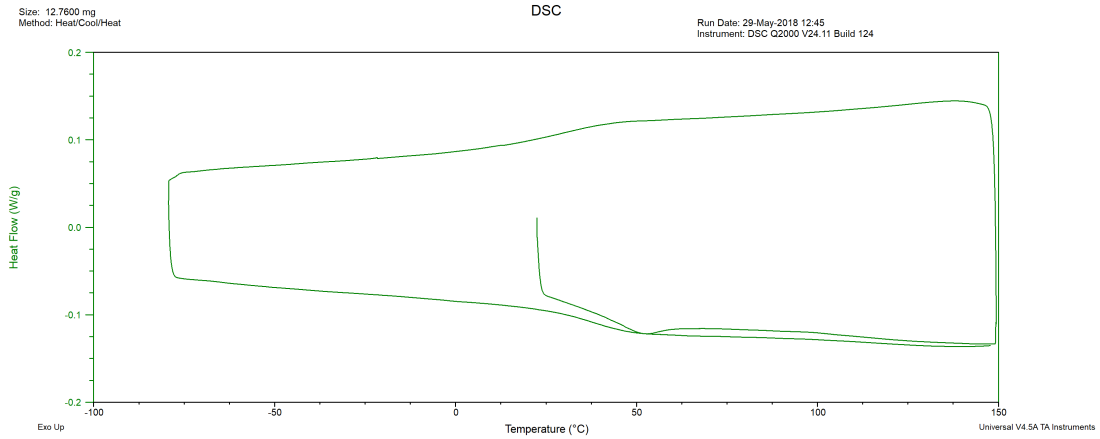

Figure A.24: Thermogram of S-CDTT as described in Chapter 4(1% ZnD Loading, 49.5% Sulfur, 49.5% CDTT)

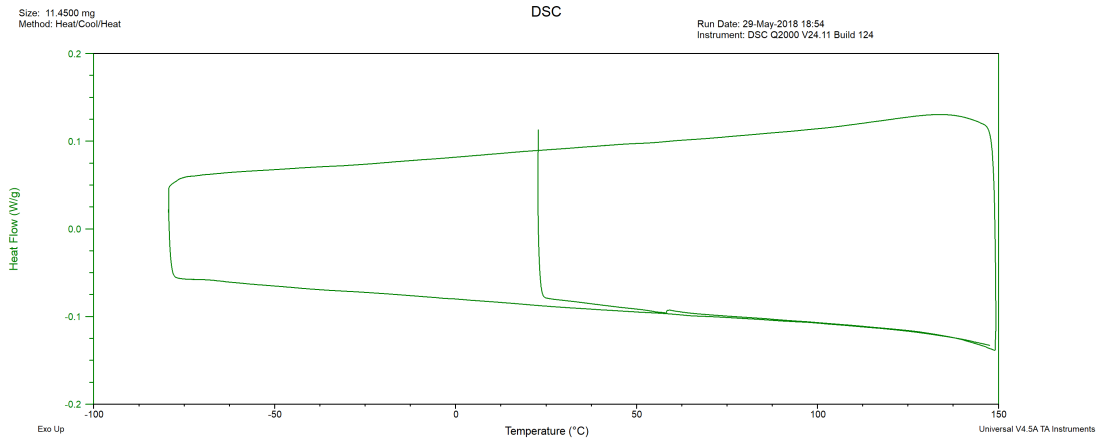

Figure A.25: Thermogram of S-CDTT as described in Chapter 4(5% ZnD Loading, 47.5% Sulfur, 47.5% CDTT)

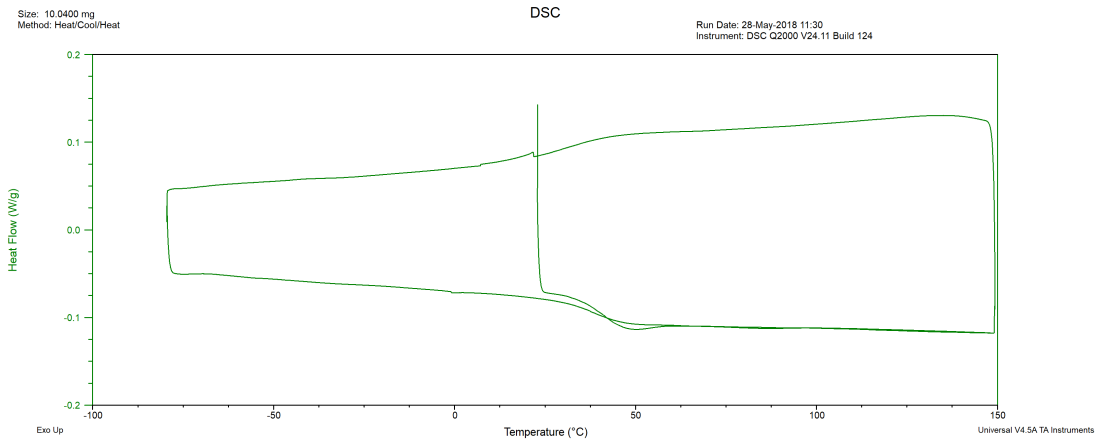

Figure A.26: Thermogram of S-TVCH as described in Chapter 4 (1% ZnD Loading, 49.5% Sulfur, 49.5% TVCH)

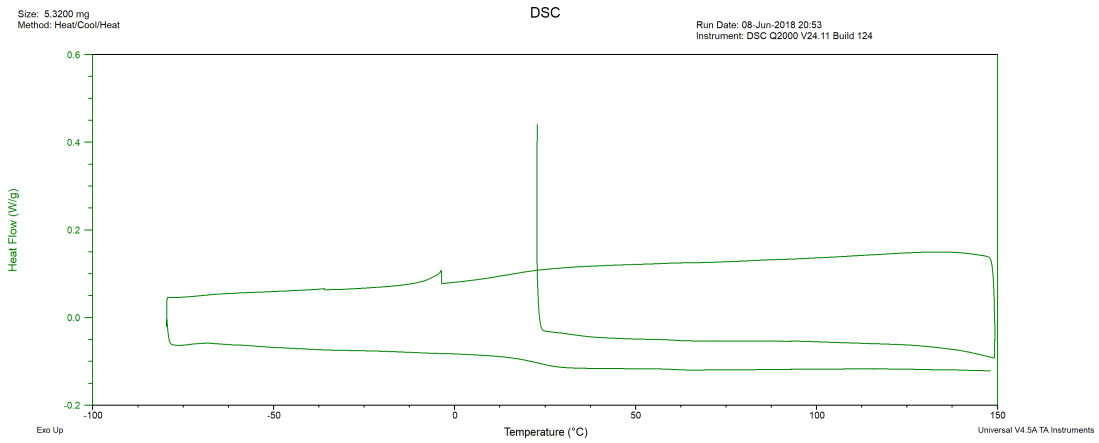

Figure A.27: Thermogram of S-TVCH as described in Chapter 4 (5% ZnD Loading, 47.5% Sulfur, 47.5% TVCH)

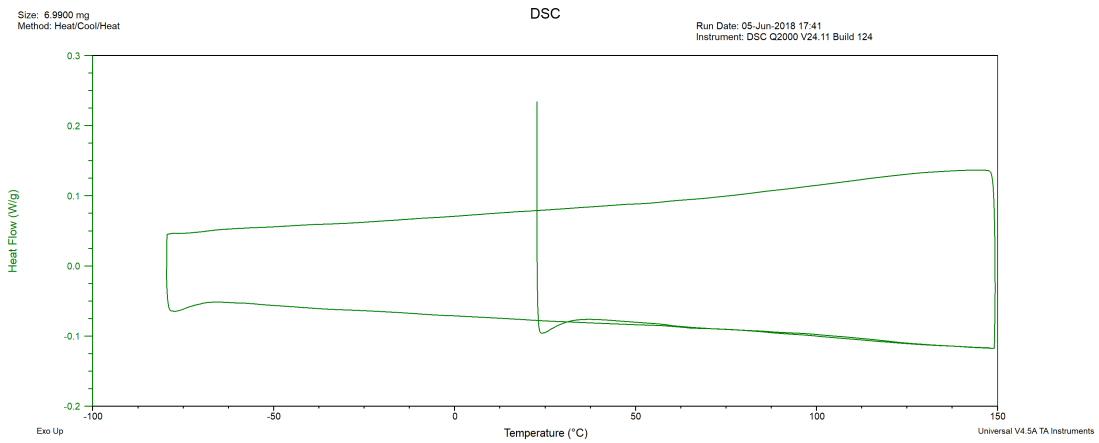

Figure A.28: Thermogram of S-VNB as described in Chapter 4(50% Sulfur, 50% VNB)

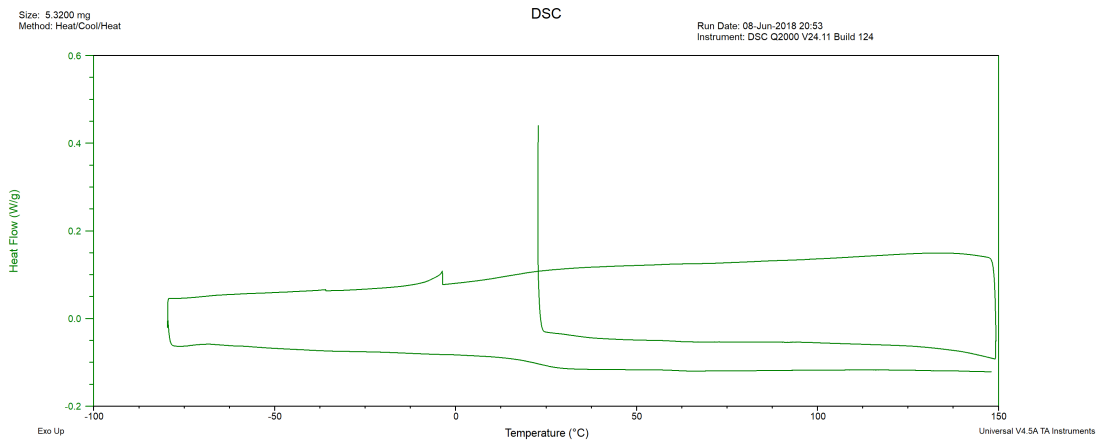

Figure A.29: Thermogram of S-TVCH as described in Chapter 4(5% ZnD Loading, 47.5% Sulfur, 47.5% VNB)

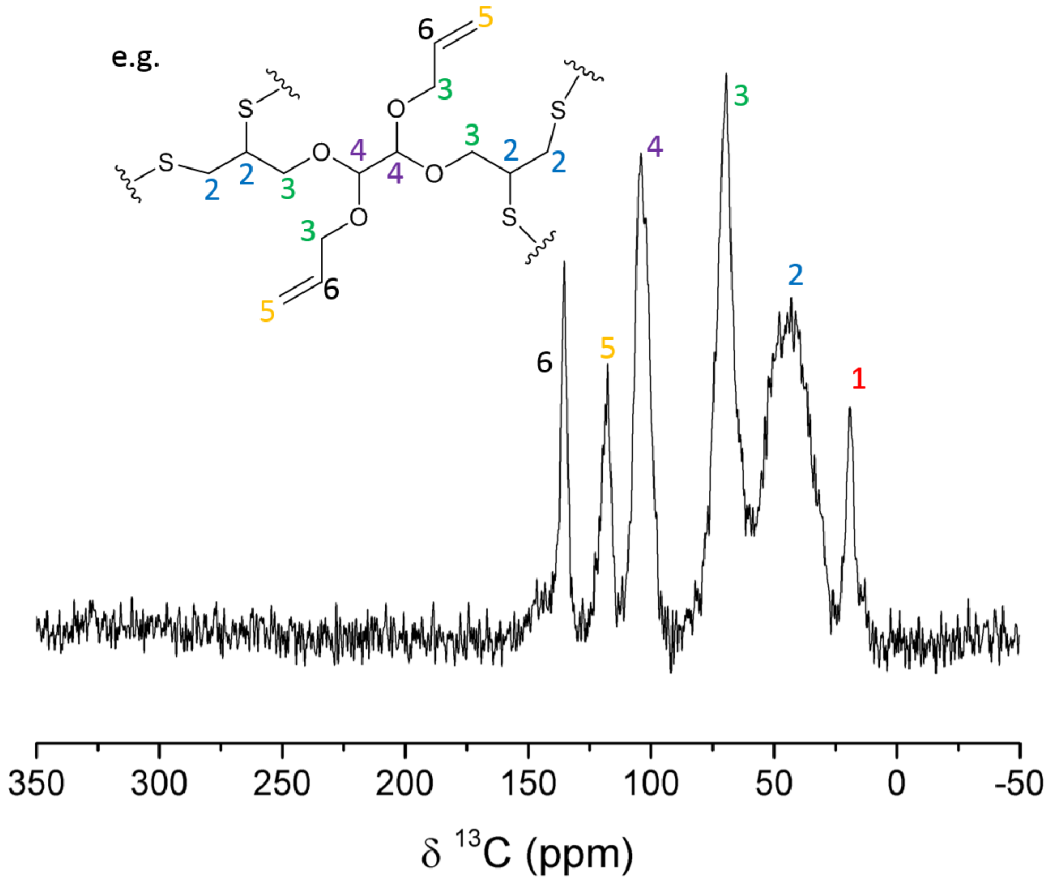

Figure A.30: Solid state ^{13}C NMR spectra of S-CDTT (49.5% Sulfur, 49.5% CDTT, 1% ZnD)

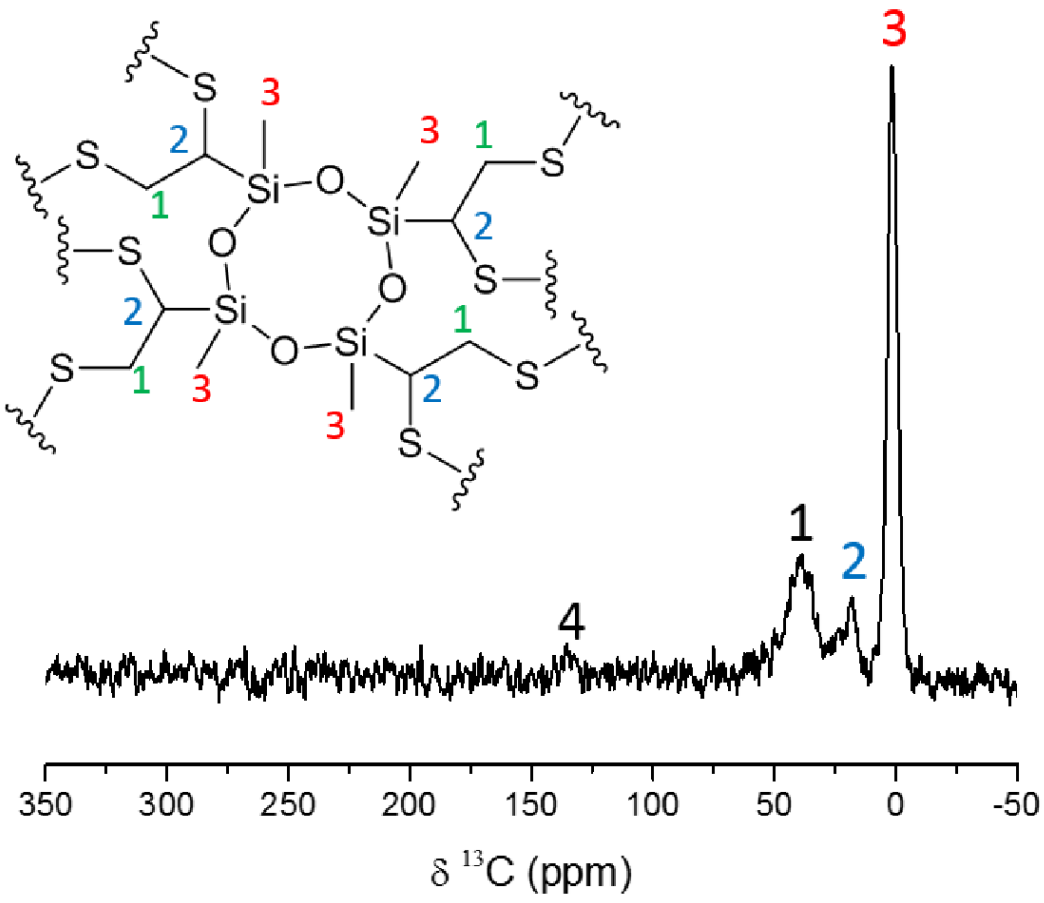

Figure A.31: Solid state ^{13}C NMR spectra of S-TVTCSi (49.5% Sulfur, 49.5% TVTCSi, 1% ZnD)

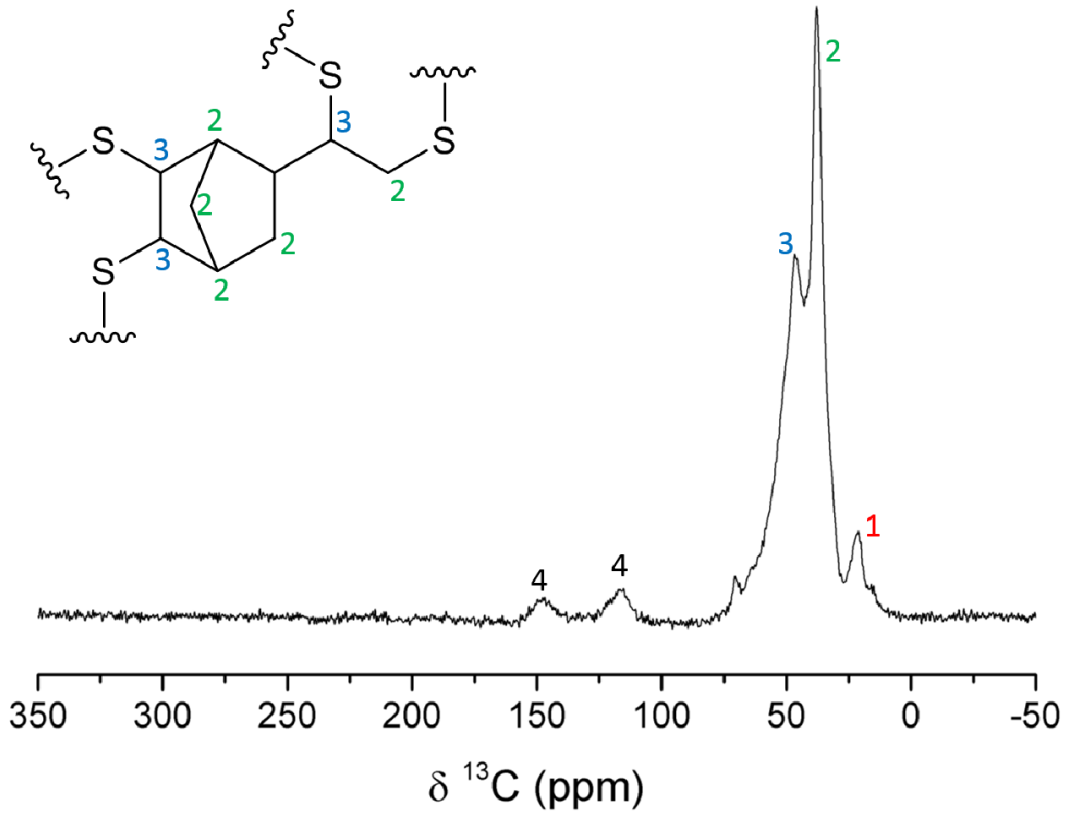

Figure A.32: Solid state ^{13}C NMR spectra of S-VNB (49.5% Sulfur, 49.5% VNB, 1% ZnD)

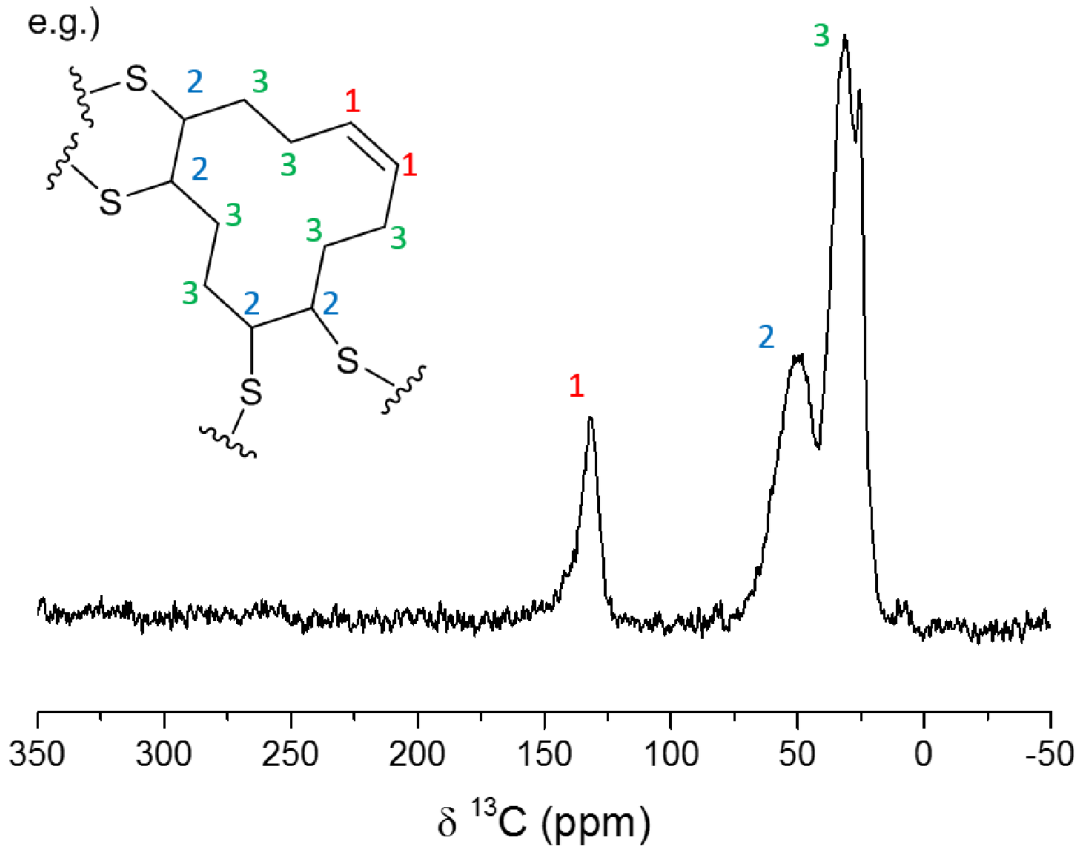

Figure A.33: Solid state ^{13}C NMR spectra of S-CDTT (49.5% Sulfur, 49.5% CDTT, 1% ZnD)

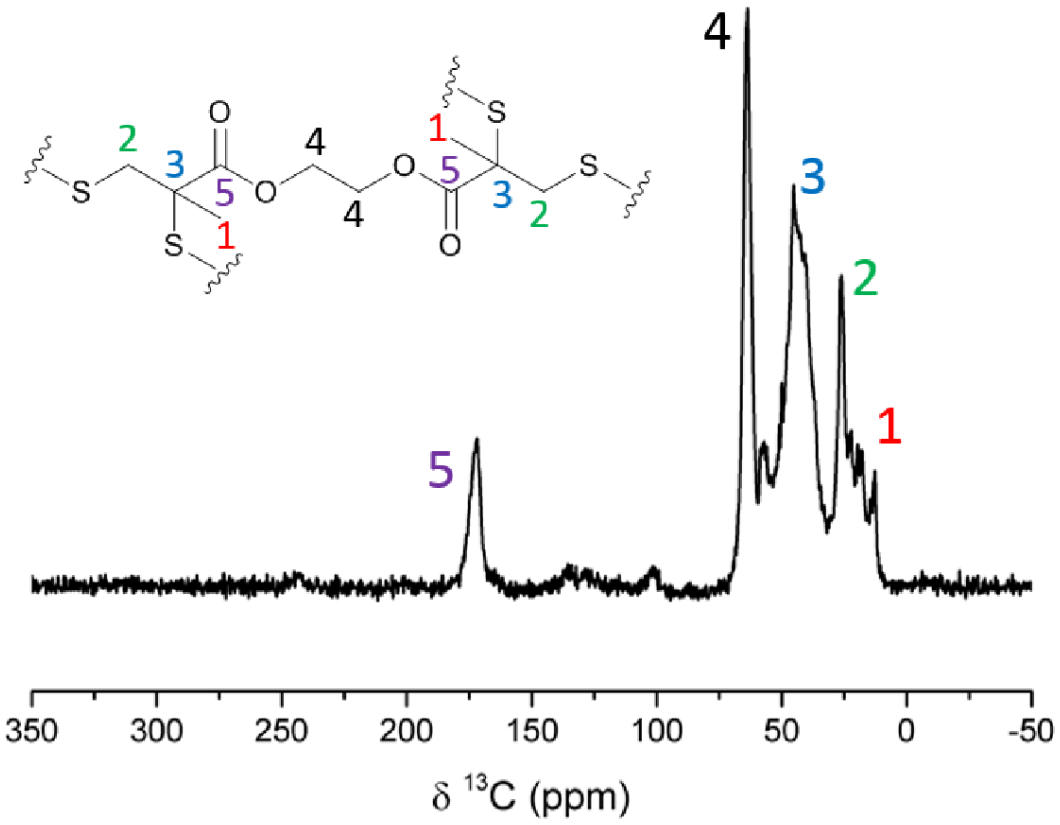

Figure A.34: Solid state ^{13}C NMR spectra of S-EGDMA (49.5% Sulfur, 49.5% EGDMA, 1% ZnD)